

CENTRAL LIBRARY
I.I.T., GUWAHATI
Acc. No. 13702
Date..... 25/11/98

621.47

50K/5

N 56



Four

Liquid Flat-Plate Collectors

A brief description of the liquid flat-plate collector has been given in Sec. 2.1, and its varied applications have been described in Sec. 2.2. These include water heating, space heating and cooling, and low-temperature cycles for power generation.

4.1 GENERAL

The basic parts that make up a conventional liquid flat-plate collector are (i) the absorber plate, (ii) the tubes fixed to the absorber plate through which the liquid to be heated flows, (iii) the transparent covers, and (iv) the insulated container. The main advantage of a flat-plate collector is that it utilizes both the beam and diffuse components of the solar radiation. In addition, because of its simple stationary design, it requires little maintenance. Its principal disadvantage is that because of the absence of optical concentration, the area from which heat is lost is large. As a result, the collection efficiency is generally low.

The liquid heated is generally water. However, sometimes mixtures of water and ethylene glycol are used if ambient temperatures below 0°C are likely to be encountered. The absorber plate is usually made from a metal sheet ranging in thickness from 0.2 to 1 mm, while the

tubes, which are also of metal, range in diameter from 1 to 1.5 cm. They are soldered, brazed, welded or pressure bonded to the bottom of the absorber plate with the pitch ranging from 5 to 12 cm. In some designs, the tubes are bonded to the top or are in-line and integrated with the absorber plate. The metal most commonly used, both for the absorber plate and the tubes, is copper. However, in India, because of the shortage of copper, other absorber plate-tube combinations have been successfully developed. These include aluminium sheets fixed to copper or galvanized steel tubes with a pressure bond, mild steel or galvanized steel sheets with galvanized steel tubes, and stainless steel sheets with built-in channels. The header pipes, which lead the water in and out of the collector and distribute it to the tubes, are made of the same metal as the tubes and are of slightly larger diameters (2 to 2.5 cm).

Plain or toughened glass of 4 or 5 mm thickness is the most favoured material for the transparent covers. The usual practice is to have one or two covers with spacings ranging from 1.5 to 3 cm.

The bottom and sides are usually insulated by mineral wool, rock wool or glass wool with a covering of aluminium foil and has a thickness ranging from 2.5 to 8 cm. The whole assembly is contained within a box which is tilted at a suitable angle. The collector box may be made of aluminium, steel sheet, or fibre glass.

The face areas of most commercially available collectors are around 2 m^2 , with the length (along the sloping direction) being usually larger than the width.

More details of the components used in collectors are given in IS 12933 (Part 2)*.

In the last few years, the use of plastic materials for the absorber plate, the tubes as well as the covers has increased. This is particularly true for applications involving lower temperatures up to 60 or 70°C. Initially plastics were not used because they degraded on exposure to sunlight. They also have low thermal conductivities and high coefficients of expansion as compared to metals. However, recent advances in polymer technology have resulted in the development of suitable plastic materials which can withstand long exposures to sunlight. Plastics have the advantages of being light in weight and easy to manufacture. They also cost less and require less energy input for their manufacture than metals like copper and aluminium. However, it has to be remembered that they generally originate from fossil fuels. As the volume of production of flat-plate collectors increases, the above

considerations of energy input and raw material origin will become increasingly important.

The present rate of production of liquid flat-plate collectors in the world, as well as in India, is low. However, it is increasing rapidly. About 200 000 m^2 have been installed in India in the 1980's. The typical cost of a good quality collector is about Rs 3500 per square metre. Installed costs of systems are usually about $1\frac{1}{2}$ times the above cost, since they include the cost of erection, piping and accessories.

4.2 PERFORMANCE ANALYSIS

We will now take up for detailed consideration the performance analysis of a liquid flat-plate collector. The analysis will first be done for a steady state situation* in which the liquid is flowing through tubes bonded on the under-side of the absorber plate. Later on, the results for other types of flat-plate collectors will be given and transient effects will be considered.

An energy balance on the absorber plate yields the following equation for a steady state

$$q_u = A_p S - q_l \quad (4.1)$$

in which

q_u = useful heat gain, i.e. the rate of heat transfer to the working fluid,

S = incident solar flux absorbed in the absorber plate,

A_p = area of the absorber plate,

q_l = rate at which heat is lost by convection and re-radiation from the top, and by conduction and convection from the bottom and sides.

From Sec. 3.7, the flux incident on the top cover of the collector is given by Eq. (3.33)

$$I_T = I_b r_b + I_d r_d + (I_b + I_d) r_r$$

Each of the terms in the above equation is multiplied by a term called the transmissivity-absorptivity product ($\tau\alpha$) in order to determine the flux S absorbed in the absorber plate. Thus,

$$S = I_b r_b (\tau\alpha)_b + [I_d r_d + (I_b + I_d) r_r] (\tau\alpha)_d \quad (4.2)$$

quasi-steady

in which,

τ = transmissivity of the glass cover system, the ratio of the solar radiation coming through after reflection at the glass interfaces and absorption in the glass to the radiation incident on the glass cover system.

α = absorptivity of the absorber plate.

$(\tau\alpha)_b$ = transmissivity-absorptivity product for beam radiation falling on the collector (defined in Sec. 4.4).

$(\tau\alpha)_d$ = transmissivity-absorptivity product for diffuse radiation falling on the collector.

The other terms have been defined in Chapter 3.

Thus, in order to evaluate q_u in Eq. (4.1), it is necessary to derive expressions for calculating the values of $(\tau\alpha)_b$, $(\tau\alpha)_d$ and q_l . This calculation will therefore be taken up in the sections which follow.

At this stage, it will be worthwhile to define two terms, the instantaneous collection efficiency and stagnation temperature. The instantaneous collection efficiency is given by

$$\eta_i = \frac{\text{Useful heat gain}}{\text{Radiation incident on the collector}} = \frac{q_u}{A_p I_T} \quad (4.3)$$

In the definition given in Eq. (4.3), the area of the absorber plate, A_p , is used in the denominator. Often the collector aperture area (A_a) or the collector gross area (A_g) is also used. The *collector aperture area* is the net opening in the topmost cover through which solar radiation is admitted into the collector, while the *collector gross area* is the area of the topmost cover (including the frame). A_a is usually about 10 to 15 per cent more than A_p , while A_g is about 15 to 20 per cent more than A_p .

If the liquid flow rate through the collector is stopped, there is no useful heat gain and the efficiency is zero. In this case, the absorber plate attains a temperature such that $A_p S = q_l$. This temperature is the highest that the absorber plate can attain and is sometimes referred to as the *stagnation temperature*. Knowledge of the stagnation temperature is useful as an indicator for comparing different collector designs. It also helps in choosing proper materials for construction of the collector.

It has been stated earlier (Sec. 3.6.3) that many solar processes occur at a relatively slow pace. As a result, the time base of an hour is often convenient. Thus Eq. (4.3) is also valid as an expression for calculating the hourly collection efficiency, if q_u is the useful heat gain in one hour (kJ/h) and I_T is the energy incident on the collector face in one hour ($\text{kJ/m}^2 \cdot \text{h}$).

4.3 TRANSMISSIVITY OF THE COVER SYSTEM

The transmissivity of the cover system of a collector can be obtained with adequate accuracy by considering reflection-refraction and absorption separately, and is given by the product form

$$\tau = \tau_r \tau_a \quad (4.4)$$

where τ_r = transmissivity obtained by considering only reflection and refraction

and τ_a = transmissivity obtained by considering only absorption.

4.3.1 Transmissivity Based on Reflection-Refraction

When a beam of light of intensity I_{bn} travelling through a transparent medium 1 strikes the interface separating it from another transparent medium 2, it is reflected and refracted (Fig. 4.1). The reflected beam has reduced intensity I_r and has a direction such that the angle of reflection is equal to the angle of incidence. On the other hand, the directions of the incident and refracted beams are related to each other by Snell's law which states that

$$\frac{\sin \theta_1}{\sin \theta_2} = \frac{n_2}{n_1} \quad (4.5)$$

where θ_1 = angle of incidence,

θ_2 = angle of refraction,

n_1, n_2 = refractive indices of the two media.

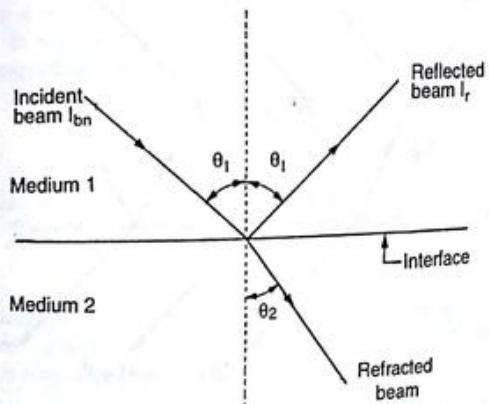


Fig. 4.1 Reflection and Refraction at the Interface of two Media

The reflectivity ρ ($= I_r/I_{bo}$) is related to the angles of incidence and refraction by the equations

$$\rho = \frac{1}{2}(\rho_I + \rho_{II})$$

$$\rho_I = \frac{\sin^2(\theta_2 - \theta_1)}{\sin^2(\theta_2 + \theta_1)} \quad (4.1)$$

$$\rho_{II} = \frac{\tan^2(\theta_2 - \theta_1)}{\tan^2(\theta_2 + \theta_1)} \quad (4.2)$$

ρ_I and ρ_{II} being the reflectivities of the two components of polarization.

For the special case of normal incidence ($\theta_1 = 0^\circ$), it can be shown that

$$\rho = \rho_I = \rho_{II} = \left(\frac{n_1 - n_2}{n_1 + n_2} \right)^2 \quad (4.3)$$

The transmissivity τ is given by an expression similar to that for ρ . Thus

$$\tau = \frac{1}{2}(\tau_{II} + \tau_{III}) \quad (4.4)$$

where τ_{II} and τ_{III} are the transmissivities of the two components of polarization.

Consider one of the components of polarization of a beam incident on a single cover. Because of the fact that there are two interfaces, multiple reflections and refractions will occur as shown in Fig. 4.2.

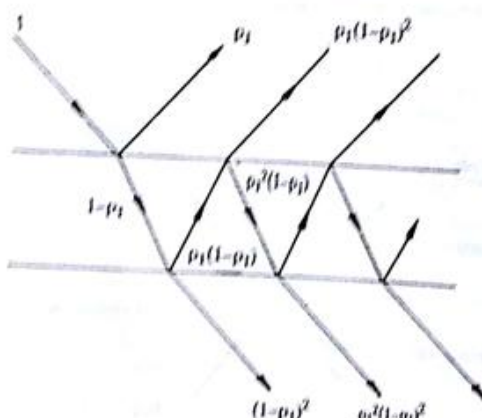


Fig. 4.2 Ray Diagram Showing Transmission Through a Single Cover Considering Reflection-Refraction Alone

Hence,

$$\begin{aligned} \tau_{II} &= (1 - \rho_{II})^2 + \rho_I^2(1 - \rho_{II})^2 + \rho_{II}^2(1 - \rho_{II})^2 + \dots \\ &= (1 - \rho_{II})^2(1 + \rho_I^2 + \rho_{II}^2 + \dots) \\ &= \frac{(1 - \rho_{II})^2}{1 - \rho_I^2} = \frac{1 - \rho_I}{1 + \rho_I} \end{aligned} \quad (4.10)$$

Similarly,

$$\tau_{III} = \frac{1 - \rho_{II}}{1 + \rho_{II}} \quad (4.11)$$

These results can be readily extended to a system of M covers for which it can be shown that

$$\tau_{II} = \frac{1 - \rho_I}{1 + (2M - 1)\rho_I} \quad (4.12)$$

$$\tau_{III} = \frac{1 - \rho_{II}}{1 + (2M - 1)\rho_{II}} \quad (4.13)$$

and

4.3.2 Transmissivity Based on Absorption

The transmissivity based on absorption can be obtained by assuming that the attenuation due to absorption is proportional to the local intensity (Bouger's law). Consider a beam of intensity I_{bo} incident normally on a transparent cover of thickness δ_c and emerging with an intensity I_I (Fig. 4.3). From Bouger's law

$$dI = -KI dx$$

where K is a constant of proportionality and is called the extinction coefficient. It will be assumed to have a value independent of wavelength. Integrating over the length traversed by the beam, we have

$$\tau_a = \frac{I_I}{I_{bo}} = e^{-KD_c} \quad (4.14)$$

In case the beam is incident at an angle θ_1 , the path traversed through the cover would be $(\delta_c / \cos \theta_2)$, where θ_2 is the angle of refraction. Then Eq. (4.14) gets modified to the form

$$\tau_a = e^{-KD_c \cos \theta_2} \quad (4.15)$$

The extinction coefficient K is a property of the cover material. Its value varies from about 5 to 25 m^{-1} for different qualities of glass. A low value is obviously desirable.

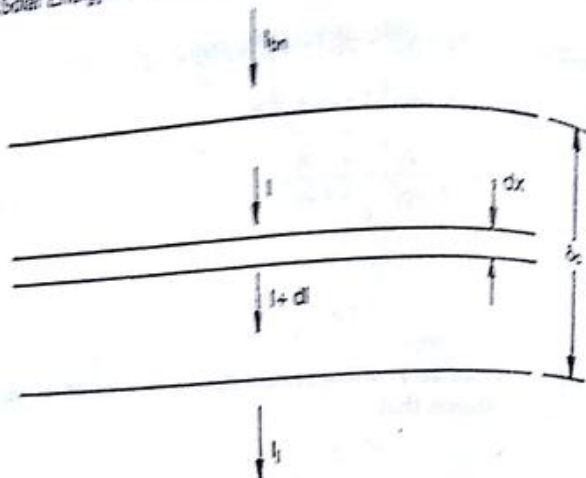


Fig. 4.3 Absorption in a Transparent Cover

Example 4.1

Plot the variation of τ_a , τ_o and τ with the angle of incidence for the following cover system

Material	:	Glass
Number of covers	=	3
Thickness of each cover	=	4 mm
Refractive index of glass relative to air	=	1.52
Extinction coefficient of glass	=	15 m ⁻¹

- The calculation is given in detail for one angle of incidence, viz. $\theta_1 = 15^\circ$

$$\text{Hence, } \theta_2 = \sin^{-1} [(\sin 15^\circ)/1.52] = 9.80^\circ$$

$$\rho_I = \frac{\sin^2 (9.80^\circ - 15^\circ)}{\sin^2 (9.80^\circ + 15^\circ)} = 0.047$$

$$\rho_{II} = \frac{\tan^2 (9.80^\circ - 15^\circ)}{\tan^2 (9.80^\circ + 15^\circ)} = 0.039$$

$$\tau_{rI} = \frac{1 - 0.047}{1 + (5 \times 0.047)} = 0.773$$

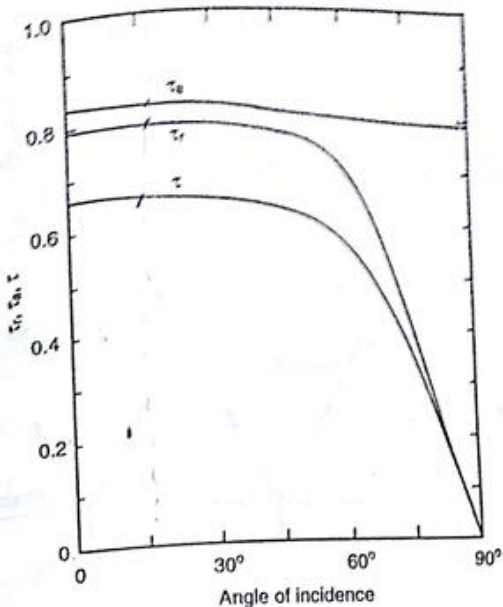
$$\tau_{rII} = \frac{1 - 0.039}{1 + (5 \times 0.039)} = 0.805$$

$$\tau_r = \frac{1}{2} (0.773 + 0.805) = 0.789$$

$$\tau_o = \exp [-(3 \times 15 \times 4 \times 10^3 \cos 9.80^\circ)] = 0.823$$

$$\tau = 0.789 \times 0.823 = 0.657$$

The transmissivities for other angles of incidence are obtained in a similar manner. Their variation with the angle of incidence is shown in Fig. 4.4. It will be seen that the values are essentially constant up to angles of incidence of 45° . Thereafter, the values drop rather sharply to zero as the angle of incidence increases to 90° .

Fig. 4.4 Example 4.1—Variation of τ_o , τ_a and τ with Angle of Incidence**4.3.3 Transmissivity for Diffuse Radiation**

The preceding considerations apply only to beam radiation. Calculation of the transmissivity of a cover system when diffuse radiation is incident on it presents some difficulty, because the radiation comes from many directions. The usual practice is to assume that the diffuse radiation is equivalent to beam radiation coming at an angle of incidence of 60° . This angle is arrived at by considering the variation of τ as seen in Fig. 4.4 and by assuming that the amount of diffuse radiation coming from all directions is the same.

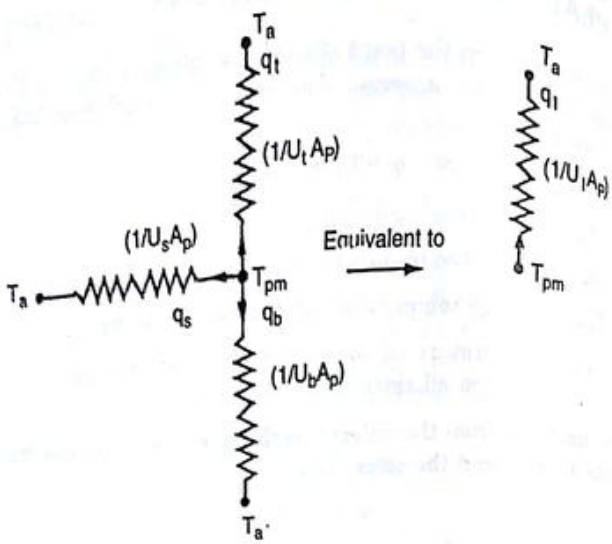


Fig. 4.6 Thermal Resistance Network Showing Collector Losses

and the absorber plate constitute a system of infinite parallel surfaces and that the flow of heat is one-dimensional and steady.* It is further assumed that the temperature drop across the thickness of the covers is negligible and that the interaction between the incoming solar radiation absorbed by the covers and the outgoing loss may be neglected. The outgoing re-radiation is of large wavelengths. For these wavelengths, the transparent cover will be assumed to be opaque. This is a very good assumption if the material is glass.

A schematic diagram for a two-cover system is shown in Fig. 4.7. In a steady state, the heat transferred by convection and radiation between (i) the absorber plate and the first cover, (ii) the first cover and the second cover, and (iii) the second cover and the surroundings must be equal. Hence,

$$\frac{q_t}{A_p} = h_{p-c1}(T_{pm} - T_{c1}) + \frac{\sigma(T_{pm}^4 - T_{c1}^4)}{\left(\frac{1}{\epsilon_p} + \frac{1}{\epsilon_c} - 1\right)} \quad (4.22)$$

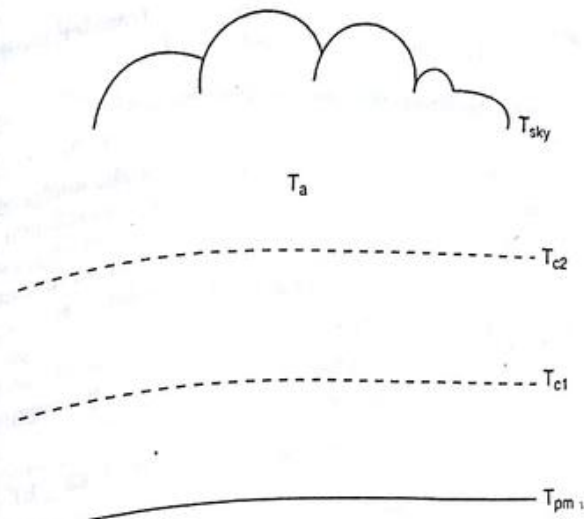


Fig. 4.7 Calculation of the Top Loss Coefficient

$$= h_{c1-c2}(T_{c1} - T_{c2}) + \frac{\sigma(T_{c1}^4 - T_{c2}^4)}{\left(\frac{1}{\epsilon_c} + \frac{1}{\epsilon_c} - 1\right)} \quad (4.23)$$

$$= h_w(T_{c2} - T_a) + \sigma\epsilon_c(T_{c2}^4 - T_{sky}^4) \quad (4.24)$$

where h_{p-c1} = convective heat transfer coefficient between the absorber plate and the first cover,

h_{c1-c2} = convective heat transfer coefficient between the first and second covers,

h_w = convective heat transfer coefficient between the top-most cover (in this case the second) and the surrounding air,

T_{c1}, T_{c2} = temperatures attained by the two covers,

T_{sky} = effective temperature of the sky with which the radiative exchange takes place,

ϵ_p = emissivity of the absorber plate for long wavelength radiation,

ϵ_c = emissivity of the covers for long wavelength radiation.

Equations (4.22), (4.23) and (4.24) constitute a set of three non-linear equations which have to be solved for the unknowns q_t, T_{c1} and T_{c2} . However, before this can be done it will be necessary to have some

*H.C. Hottel and B.B. Woertz, "Performance of Flat-Plate Solar-Heat Collectors". Trans. ASME, 64, 91 (1942).

$$U_b = \frac{k_i}{\delta_b}$$

where k_i = thermal conductivity of the insulation,
 δ_b = thickness of the insulation.

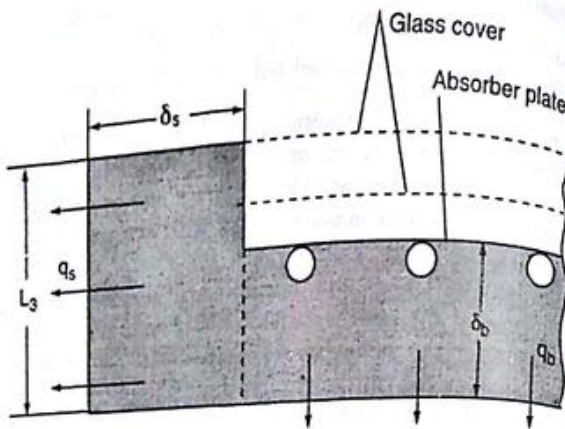


Fig. 4.8 Bottom and Side Losses from a Flat-plate Collector

4.5.3 Side Loss Coefficient

As in the case of the bottom loss coefficient, it will be assumed that the conduction resistance dominates and that the flow of heat is one-dimensional and steady. The one-dimensional approximation can be justified on the grounds that the side loss coefficient is always much smaller than the top loss coefficient.

If the dimensions of the absorber plate are $L_1 \times L_2$ and the height of the collector casing is L_3 , then the area across which heat flows sideways is $2(L_1 + L_2)L_3$. The temperature drop across which the heat flow occurs varies from $(T_{pm} - T_a)$ at the absorber plate level to zero both at the top and bottom. Assuming, therefore, that the average temperature drop across the side insulation is $(T_{pm} - T_a)/2$ and that the thickness of this insulation is δ_s , we have

$$q_s = 2L_3(L_1 + L_2)k_i \frac{(T_{pm} - T_a)}{2\delta_s} \quad (4.30)$$

Thus, from Eq. (4.20),

$$U_s = \frac{(L_1 + L_2)L_3 k_i}{L_1 L_2 \delta_s} \quad (4.31)$$

Example 4.2

Calculate the overall loss coefficient for a flat-plate collector with two glass covers with the following data:

Size of absorber plate	= 0.90 m \times 1.90 m
Spacing between plate and first glass cover	= 4 cm
Spacing between first and second glass cover	= 4 cm
Plate emissivity	= 0.92
Glass cover emissivity	= 0.88
Collector tilt	= 20°
Mean plate temperature	= 70°C
Ambient air temperature	= 24°C
Wind speed	= 2.5 m/s
Back insulation thickness	= 8 cm
Side insulation thickness	= 4 cm
Thermal conductivity of insulation	= 0.05 W/m-K

From Eq. (4.28),

$$T_{sky} = 297.2 - 6 = 291.2 \text{ K}$$

Substituting this value and the given values of T_{pm} , T_a , ϵ_p and ϵ_c in Eqs (4.22) to (4.24), we have

$$\frac{q_t}{A_p} = h_{p-c1}(343.2 - T_{c1}) + \frac{5.67 \times 10^{-8}(343.2^4 - T_{c1}^4)}{\left(\frac{1}{0.92} + \frac{1}{0.88} - 1\right)} \quad (4.32)$$

$$\frac{q_t}{A_p} = h_{c1-c2}(T_{c1} - T_{c2}) + \frac{5.67 \times 10^{-8}(T_{c1}^4 - T_{c2}^4)}{\left(\frac{1}{0.88} + \frac{1}{0.88} - 1\right)} \quad (4.33)$$

$$= h_{c1-c2}(T_{c1} - T_{c2}) + 4.455 \times 10^{-8}(T_{c1}^4 - T_{c2}^4)$$

and

$$\frac{q_t}{A_p} = h_w(T_{c2} - 297.2) + 5.67 \times 10^{-8} \times 0.88(T_{c2}^4 - 291.2^4) \quad (4.34)$$

$= h_w(T_{c2} - 297.2) + 4.990 \times 10^{-8}(T_{c2}^4 - 71.9061 \times 10^8)$

Equations (4.32) to (4.34) have to be solved for the unknowns (q_t/A_p) , T_{c1} and T_{c2} . For this, the values of n_{p-c1} , h_{c1-c2} and h_w are needed. Since these values depend upon T_{c1} and T_{c2} , a trial-and-error method becomes necessary.

Assume

$$T_{c1} = 325 \text{ K}$$

$$T_{c2} = 305 \text{ K}$$

We use the correlations (4.25) to calculate h_{p-c1} and h_{c1-c2} ,
correlation (4.27) to calculate h_w .

Calculation of h_{p-c1}

Mean temperature of air between plate and first cover

$$= \frac{343.2 + 325}{2} = 334.1 \text{ K}$$

At this temperature,*

$$k = 0.0291 \text{ W/m-K}$$

$$v = 19.06 \times 10^{-6} \text{ m}^2/\text{s}$$

$$Pr = 0.696$$

$$Ra_L \cos \beta = 9.81 \times \frac{1}{334.1} \frac{(343.2 - 325) \times 0.04^3}{19.06^2 \times 10^{-12}} \times 0.696 \cos 20^\circ$$

$$= 61544$$

Therefore,

$$Nu_L = 0.229(61544)^{0.252} = 3.6873$$

$$h_{p-c1} = \frac{3.6873 \times 0.0291}{0.04} = 2.683 \text{ W/m}^2\text{-K}$$

Calculation of h_{c1-c2}

Mean temperature of air between first and second cover

$$= \frac{325 + 305}{2} = 315 \text{ K}$$

Proceeding in a similar manner, we obtain

$$h_{c1-c2} = 2.803 \text{ W/m}^2\text{-K}$$

Calculation of h_w

Mean temperature of air between second cover and ambient

$$= \frac{305 + 297.2}{2} = 301.1 \text{ K}$$

At this temperature,

$$\rho = 1.173 \text{ kg/m}^3$$

$$C_p = 1.005 \text{ kJ/kg-K}$$

$$v = 15.80 \times 10^{-6} \text{ m}^2/\text{s}$$

$$Pr = 0.701$$

*Properties of air and water are given in Appendix 4.

Characteristic dimension

$$L^* = \frac{4A_c}{C_c} = \frac{4 \times (1.90 + 0.08)(0.90 + 0.08)}{2(1.90 + 0.08 + 0.90 + 0.08)}$$

$$= 1.311 \text{ m}$$

$$Re_L^* = \frac{2.5 \times 1.311}{15.80 \times 10^{-6}} = 0.2074 \times 10^6$$

From Eq. (4.27),

$$j = 0.86 \times (0.2074 \times 10^6)^{-1/2}$$

$$= 0.001888$$

Therefore,

$$h_w = 0.001888 \times 1.173 \times 1.005 \times 2.5 \times 10^3 \times (0.701)^{-2/3}$$

$$= 7.04 \text{ W/m}^2\text{-K}$$

After substituting these values into Eqs (4.32)–(4.34), we obtain the values of T_{c1} and T_{c2} which satisfy the equations. The calculation is shown in tabular fashion:

T_{c1} (K)	T_{c2} (K)	(q_i/A_p) from		
		Eq. (4.32)	Eq. (4.33)	Eq. (4.34)
325	305	174.8	167.6	127.9
326	307	165.7	160.7	153.4
326.4	307.4	162.0	161.1	158.6
326.5	307.6	161.1	160.4	161.1

The values of (q_i/A_p) in the last line of the table are reasonably close to each other. Therefore the average value of 160.9 W/m^2 is acceptable. Since the values of $T_{c1} = 326.5 \text{ K}$ and $T_{c2} = 307.6 \text{ K}$ are close to the original assumptions of 325 K and 305 K , it will not be necessary to repeat the calculations for h_{p-c1} , h_{c1-c2} and h_w with these new values. Therefore,

$$U_t = \frac{160.9}{(343.2 - 297.2)} = 3.50 \text{ W/m}^2\text{-K}$$

Using Eq. (4.29), bottom loss coefficient

$$U_b = \frac{0.05}{0.08} = 0.63 \text{ W/m}^2\text{-K}$$

From Eq. (4.31), side loss coefficient

$$U_s = \frac{(0.90 + 1.90) \times 0.16 \times 0.05}{0.90 \times 1.90 \times 0.04}$$

$$= 0.33 \text{ W/m}^2\text{-K}$$

Therefore, overall loss coefficient

$$U_t = 3.50 + 0.63 + 0.33 \\ = 4.46 \text{ W/m}^2\text{-K}$$

4.5.4 Empirical Equation for Top Loss Coefficient

From Example 4.2, it is clear that a tedious iterative calculation is required for obtaining the value of the top loss coefficient. Based on calculations for a large number of cases covering the entire range of conditions normally expected for flat-plate collectors, Klein* has developed the following convenient empirical equation for calculating the top loss coefficient.

$$U_t = \left[\left(\frac{C}{T_{pm}} \right) \left(\frac{T_{pm} - T_a}{M + f} \right)^{0.33} + \frac{1}{h_w} \right]^{-1} \\ + \left[\frac{\sigma(T_{pm}^2 + T_a^2)(T_{pm} + T_a)}{\frac{1}{\epsilon_p} + \frac{(2M + f - 1)}{\epsilon_c} - M} \right] \quad (4.35)$$

where $f = (1 - 0.04 h_w + 0.0005 h_w^2) (1 + 0.091 M)$

$$C = 365.9(1 - 0.00883 \beta + 0.0001298 \beta^2)$$

M = number of glass covers

While using Eq. (4.35), T_{pm} and T_a are expressed in K, h_w in $\text{W/m}^2\text{-K}$, σ in $\text{W/m}^2\text{-K}^4$, and β in degrees. The value of U_t is obtained in $\text{W/m}^2\text{-K}$. The range of conditions over which Eq. (4.35) has been developed are as follows

- $320 \leq T_{pm} \leq 420 \text{ K}$
- $260 \leq T_a \leq 310 \text{ K}$
- $0.1 \leq \epsilon_p \leq 0.95$
- $0 \leq V_w \leq 10 \text{ m/s}$
- $1 \leq M \leq 3$
- $0 \leq \beta \leq 90^\circ$

Although not explicitly stated, it appears that the values of ϵ_c and L have been taken to be constant and equal to 0.88 and 2.54 cm respectively. The standard deviation of the differences in values of U_t

obtained from Eq. (4.35) and by the procedure described earlier is 0.14 $\text{W/m}^2\text{-K}$.

In developing the correlation, Klein has assumed that the value of h_w could be obtained from Eq. (4.26). If Eq. (4.27) has to be used, a reasonable assumption will have to be made for the temperature of the topmost cover.

A number of empirical correlations having the same form as Eq. (4.35) have also been suggested. Garg and Datta* have made a detailed study of these correlations as well as Klein's correlation and have concluded that the correlation suggested by Malhotra *et al.*† agrees best with the exact iterative solution. Malhotra *et al.* have given the following correlation

$$U_t = \left[\left(\frac{C}{T_{pm}} \right) \left(\frac{T_{pm} - T_a}{M + f} \right)^{0.252} + \frac{1}{h_w} \right]^{-1} \\ + \left[\frac{\sigma(T_{pm}^2 + T_a^2)(T_{pm} + T_a)}{\frac{1}{\epsilon_p} + \frac{0.0425 M(1 - \epsilon_p)}{\epsilon_c} + \frac{2M + f - 1}{\epsilon_c} - M} \right] \quad (4.36)$$

$$\text{where } f = \left(\frac{9}{h_w} - \frac{30}{h_w^2} \right) \left(\frac{T_a}{316.9} \right) (1 + 0.091M)$$

$$C = 204.429(\cos \beta)^{0.252} / L^{0.24}$$

L = spacing (m)

4.6 COLLECTOR EFFICIENCY FACTOR

In Sec. 4.5, procedures for calculating the overall loss coefficient were described. The heat lost from the collector can thus be calculated, if the average plate temperature is known. However, this temperature is generally not known. It will, therefore, be necessary to consider the flow of heat in the absorber plate and across the fluid tubes to the fluid so that the values of T_{pm} can be related to the value of the inlet fluid temperature, which is a known quantity.

In order to simplify the problem, the approach adopted will be to

*H. P. Garg and G. Datta, "The Top Loss Calculation for Flat-plate Solar Collectors,"

conduct a number of one-dimensional analyses. First, the one-dimensional flow of heat in the absorber plate in a direction at right angles to the direction of fluid flow will be considered. This will be followed by a consideration of the heat flow from the plate to the fluid adjacent to the tube wall. Finally, the one-dimensional flow of fluid inside the tubes will be analysed.

Consider a collector having an absorber plate of length L_1 and width L_2 . Assume that there are N fluid tubes and that the pitch of the tubes is $W (= L_2/N)$. Let D_i and D_o be the inside and outside diameters of the tubes.

Consider a section of the absorber plate with two adjacent fluid tubes. The temperature in the plate (T_p) will vary in the x -direction in the manner as shown in Fig. 4.9. It will be assumed that the same distribution exists between any two tubes. Above the fluid tubes, the temperature will be constant, while in between the tubes, temperature will pass through a maximum. Taking a slice dy along the flow direction and neglecting heat conduction in the plate in that direction, we can write an energy balance for an element $dx \times dy$ of the plate

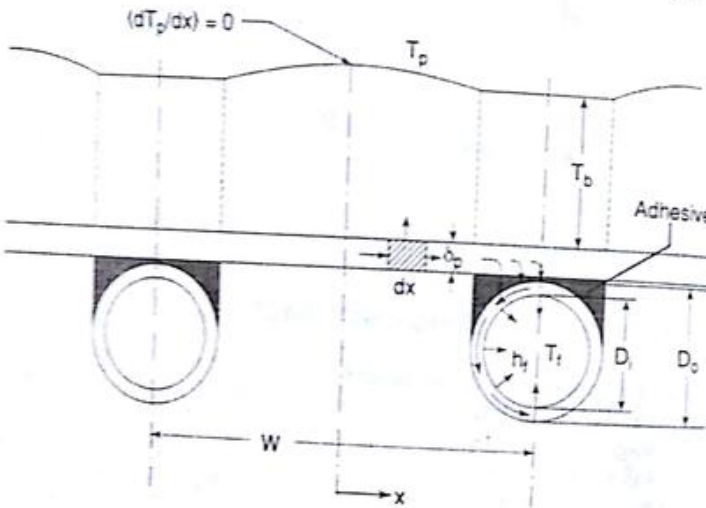


Fig. 4.9 Temperature Distribution in an Absorber Plate in a Direction at Right Angles to the Fluid Flow

(Net heat conducted into element) + (Incident energy absorbed) = Heat lost from element.

$$k_p \delta_p \frac{d^2 T_p}{dx^2} dx dy + S dx dy = U_i dx dy (T_p - T_a)$$

Simplifying,

$$\frac{d^2 T_p}{dx^2} = \frac{U_i}{k_p \delta_p} \left[T_p - T_a - \frac{S}{U_i} \right] \quad (4.37)$$

Equation (4.37) is then solved using the boundary conditions

$$x = 0, \quad \frac{dT_p}{dx} = 0$$

$$\text{and } x = \left(\frac{W - D_o}{2} \right), \quad T_p = T_{po}$$

This yields the solution

$$\frac{T_p - \left(T_a + \frac{S}{U_i} \right)}{T_{po} - \left(T_a + \frac{S}{U_i} \right)} = \frac{\cosh mx}{\cosh \left[m \left(\frac{W - D_o}{2} \right) \right]}$$

$$\text{where } m = (U_i/k_p \delta_p)^{1/2}.$$

The temperature distribution obtained is similar to that for a long rectangular fin. The rate at which energy is conducted through the plate to one fluid tube from both sides

$$= -2k_p \delta_p \left(\frac{dT_p}{dx} \right)_{x=(W-D_o)/2} dy \\ = 2 \left(\frac{k_p \delta_p}{U_i} \right)^{1/2} [S - U_i(T_{po} - T_a)] \tanh \left(\frac{m(W - D_o)}{2} \right) dy$$

The rate at which energy absorbed just above the tube flows in

$$= D_o [S - U_i(T_{po} - T_a)] dy$$

Thus the useful energy gain for all the N tube of the collector over a length dy is given by

$$dq_u = N[S - U_i(T_{po} - T_a)]$$

$$\times \left[2 \left(\frac{k_p \delta_p}{U_i} \right)^{1/2} \tanh \frac{m(W - D_o)}{2} + D_o \right] dy \quad (4.38)$$

Equation (4.38) can be written in a simpler manner by introducing the concept of plate effectiveness ϕ , which is defined as the ratio of the heat conducted through the plate to the fluid tube, to the heat which would have been conducted if the thermal conductivity of the plate material was infinite. It is easily shown that

$$\phi = \frac{\tanh [m(W - D_o)/2]}{[m(W - D_o)/2]}$$

Thus,

$$\frac{1}{N} \left(\frac{dq_u}{dy} \right) = [S - U_l(T_{po} - T_a)] [\phi(W - D_o) + D_o] \quad (4.39)$$

We next consider the flow of heat from the plate to the fluid. The three thermal resistances in the path are due to the adhesive used for attaching the tubes to the absorber plate, the tube wall and the heat transfer coefficient at the inner surface of the tube. Assuming the thermal resistance of the tube wall to be negligible,

$$\frac{1}{N} \left(\frac{dq_u}{dy} \right) = \frac{(T_{po} - T_f)}{\left(\frac{\delta_a}{k_a D_o} + \frac{1}{\pi D_i h_f} \right)} \quad (4.40)$$

where δ_a = average thickness of the adhesive, k_a = thermal conductivity of the adhesive material, T_f = local fluid temperature,and h_f = heat transfer coefficient on the inside surface of the tube.Combining Eqs (4.39) and (4.40) so as to eliminate the intermediate temperature T_{po} , we have

$$\frac{1}{N} \left(\frac{dq_u}{dy} \right) = \frac{[S - U_l(T_f - T_a)]}{U_l \left[\frac{1}{U_l(W - D_o)\phi + D_o} + \frac{\delta_a}{k_a D_o} + \frac{1}{\pi D_i h_f} \right]} \quad (4.41)$$

We now define a term called the *collector efficiency factor* (F') as follows

$$F' = \frac{1}{W U_l \left[\frac{1}{U_l(W - D_o)\phi + D_o} + \frac{\delta_a}{k_a D_o} + \frac{1}{\pi D_i h_f} \right]} \quad (4.42)$$

Substituting this definition into Eq. (4.41), we get

$$\frac{1}{N} \left(\frac{dq_u}{dy} \right) = W F' [S - U_l(T_f - T_a)] \quad (4.43)$$

where F' represents the ratio of the actual useful gain rate per tube per unit length to the gain which would occur if the collector absorber plate were at the temperature T_f .

4.7 COLLECTOR HEAT-REMOVAL FACTOR

The final one-dimensional analysis will be performed along the direction of fluid flow with the objective of determining the variation of fluid temperature. This analysis will help in linking the useful heat gain rate with the fluid inlet temperature.

Consider as a control volume, an elementary length dy of one tube (Fig. 4.10). Applying the first law of thermodynamics, Rate of change of enthalpy of the fluid flowing through the control volume

= Rate of heat transfer to fluid inside the control volume.

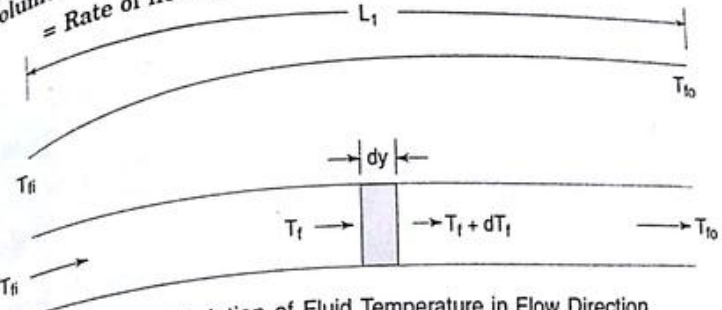


Fig. 4.10 Variation of Fluid Temperature in Flow Direction

$$\text{Thus, } \left(\frac{\dot{m}}{N} \right) C_p dT_f = \frac{1}{N} dq_u = W F' [S - U_l(T_f - T_a)] dy$$

$$\frac{dT_f}{dy} = \frac{W F' U_l}{(\dot{m}/N) C_p} \left[\left(\frac{S}{U_l} + T_a \right) - T_f \right] \quad (4.44)$$

Integrating and using the inlet condition $y = 0, T_f = T_{fi}$ the temperature distribution

$$\frac{\left(\frac{S}{U_l} + T_a \right) - T_f}{\left(\frac{S}{U_l} + T_a \right) - T_{fi}} = \exp \left\{ - \frac{L_1 F' U_l}{\dot{m} C_p} y \right\} \quad (4.45)$$

The fluid outlet temperature T_{fo} is obtained by substituting $T_f = T_{fo}$ and $y = L_1$ in Eq. (4.45). Thus,

$$\frac{\left(\frac{S}{U_l} + T_a \right) - T_{fo}}{\left(\frac{S}{U_l} + T_a \right) - T_{fi}} = \exp \left\{ - \frac{F' U_l L_1}{\dot{m} C_p} \right\} \quad (4.46)$$

Subtracting both sides of Eq. (4.46) from unity,

$$\frac{(T_{fo} - T_{fi})}{\left(\frac{S}{U_l} + T_a \right) - T_{fi}} = 1 - \exp \left\{ - \frac{F' U_l A_p}{\dot{m} C_p} \right\} \quad (4.47)$$

Thus, the useful heat gain rate for the collector

$$\begin{aligned} q_u &= \dot{m}C_p(T_{f0} - T_{fi}) \\ &= \dot{m}C_p \left[\left(\frac{S}{U_l} + T_a \right) - T_{fi} \right] \left[1 - \exp \left\{ - \frac{F'U_lA_p}{\dot{m}C_p} \right\} \right] \\ &= \frac{\dot{m}C_p}{U_l} [S - U_l(T_{fi} - T_a)] \left[1 - \exp \left\{ - \frac{F'U_lA_p}{\dot{m}C_p} \right\} \right] \\ q_u &= F_R A_p [S - U_l(T_{fi} - T_a)] \end{aligned} \quad (4.48)$$

where,

$$F_R = \frac{\dot{m}C_p}{U_l A_p} \left[1 - \exp \left\{ - \frac{F'U_l A_p}{\dot{m}C_p} \right\} \right] \quad (4.49)$$

The term F_R is called the *collector heat-removal factor*. It is an important design parameter since it is a measure of the thermal resistance encountered by the absorbed solar radiation in reaching the collector fluid. From Eq. (4.48), it can be seen that F_R represents the ratio of the actual useful heat gain rate to the gain which would occur if the collector absorber plate was at the temperature T_{fi} everywhere. As such its value ranges between 0 and 1.

Equation (4.48) is a very convenient expression for calculating the useful energy gain because the inlet fluid temperature is usually a known quantity. It is often referred to as the *Hottel-Whillier-Bliss equation*.

4.8 A NUMERICAL EXAMPLE

We will now illustrate the use of the equations derived in the preceding sections through a detailed numerical example.

Example 4.3

A flat-plate collector is made up of a GI absorber plate, GI tubes fixed on the under side and two glass covers. The following data is given:

- Length of collector = 1.6 m
- Width of collector = 1.1 m
- Length of absorber plate = 1.5 m
- Width of absorber plate = 1.0 m
- Plate to cover spacing = 2.5 cm
- Spacing between covers = 2.5 cm
- Thermal conductivity of plate material = 35 W/m·°C
- Plate thickness = 1.3 mm

Plate absorptivity/emissivity	= 0.95
Outer diameter of tube	= 18 mm
Inner diameter of tube	= 14 mm
Tube centre-to-centre distance	= 12 cm
Glass cover emissivity/absorptivity	= 0.88
$K\delta_c$	= 0.0524 per plate
Refractive index of glass relative to air	= 1.526
Location of collector	= Pune (18°32' N, 73°51' E)
Date	= May 15
Time	= 11 a.m. (IST)
Collector tilt	= Latitude angle
Surface azimuth angle	= 0°
I_b (uniformly distributed over the sky)	= 665 W/m ²
I_d (adhesive resistance)	= Negligible
Fluid to tube heat transfer coefficient	= 205 W/m ² ·°C
Water flow rate	= 70 kg/h
Water inlet temperature	= 60°C
Ambient temperature	= 25°C
Wind speed	= 3.1 m/s
Back insulation thickness	= 5 cm
Insulation thermal conductivity	= 0.04 W/m·°C
Assume that the side loss coefficient is 10 per cent of the bottom loss coefficient.	
Calculate,	
1. the angle of incidence of beam radiation on the collector,	
2. the total solar flux incident on the collector,	
3. $(\tau\alpha)_b$ and $(\tau\alpha)_d$	
4. the incident flux absorbed by the absorber plate,	
5. the collector heat-removal factor and overall loss coefficient,	
6. the water outlet temperature, and	
7. the instantaneous efficiency.	

1. Angle of Incidence of Beam Radiation

On May 15, $n = 135$. From Eq. (3.2),

$$\begin{aligned} \delta &= 23.45 \sin \left[\frac{360}{365} (284 + 135) \right] \\ &= 18.79^\circ \end{aligned}$$

From Eq. (3.12),

$$\begin{aligned} \text{LAT} &= 11 \text{ h} - 4(82.50 - 73.85) \text{ minutes} + (+2.6 \text{ minutes}) \\ &= 11 \text{ h} - 32.0 \text{ min} \\ &= 10 \text{ h} 28.0 \text{ min.} \end{aligned}$$

$$\alpha = \frac{92.0}{60} \times 15 = 23.0^\circ$$

Therefore, substituting into Eq. (3.6), we have

$$\begin{aligned} \cos \theta &= \sin 18.79^\circ \sin 0^\circ + \cos 18.79^\circ \cos 23.0^\circ \cos \alpha \\ &= 0.8714 \\ \theta &= 29.37^\circ \end{aligned}$$

2. Solar Flux Incident on Collector

From Eq. (3.30)-(3.32),

$$\begin{aligned} r_1 &= \frac{0.8714}{\sin 18.79^\circ \sin 18.53^\circ + \cos 18.79^\circ \cos 18.53^\circ \cos 23.0^\circ} \\ &= 0.9384 \\ r_2 &= \frac{1 + \cos 18.53^\circ}{2} = 0.9741 \\ r_r &= 0.2 \left(\frac{1 - \cos 18.53^\circ}{2} \right) = 0.0052 \end{aligned}$$

Therefore, from Eq. (3.33),

$$\begin{aligned} I_T &= (665 \times 0.9384) + (230 \times 0.9741) + (895 \times 0.0052) \\ &= 852.7 \text{ W/m}^2 \end{aligned}$$

3. $(\tau\alpha)_s$ and $(\tau\alpha)_d$

Angle of incidence = 29.37°

$$\begin{aligned} \text{Therefore, angle of refraction} &= \sin^{-1} (\sin 29.37^\circ / 1.526) \\ &= 18.72^\circ \end{aligned}$$

From Eqs (4.6), (4.7), (4.10), (4.11) and (4.9),

$$\rho_I = \frac{\sin^2 (29.37^\circ - 18.72^\circ)}{\sin^2 (29.37^\circ + 18.72^\circ)} = 0.0613$$

$$\rho_{II} = \frac{\tan^2 (29.37^\circ - 18.72^\circ)}{\tan^2 (29.37^\circ + 18.72^\circ)} = 0.0283$$

$$\tau_{II} = \frac{1 - 0.0613}{1 + (3 \times 0.0613)} = 0.793$$

$$\tau_{III} = \frac{1 - 0.0283}{1 + (3 \times 0.0283)} = 0.896$$

$$\tau_r = \frac{1}{2} (0.793 + 0.896) = 0.8445$$

From Eq. (4.15),

$$\tau_e = \exp [-(0.0524 \times 2 \cos 18.72^\circ)] = 0.896$$

Therefore, from Eq. (4.4),

$$\tau = 0.8445 \times 0.896 = 0.756$$

Substituting into Eq. (4.16) and using the value of $\rho_2 = 0.22$ for two covers,

$$(\tau\alpha)_s = \frac{0.756 \times 0.95}{1 - (1 - 0.95) 0.22} = 0.727$$

For diffuse radiation, the angle of incidence is taken to be 60° .
Therefore, angle of refraction

$$\begin{aligned} &= \sin^{-1} [\sin 60^\circ / 1.526] \\ &= 34.58^\circ \end{aligned}$$

Following the same procedure as for $(\tau\alpha)_s$, it can be shown that

$$\rho_I = 0.1855$$

$$\tau_{II} = 0.523$$

$$\rho_{II} = 0.0014$$

$$\tau_{III} = 0.994$$

$$\tau_r = \frac{1}{2} (0.523 + 0.994) = 0.759$$

$$\tau_e = \exp [-(0.0524 \times 2 \cos 34.58^\circ)] = 0.881$$

$$\tau = 0.759 \times 0.881 = 0.668$$

$$(\tau\alpha)_d = \frac{0.668 \times 0.95}{1 - (1 - 0.95) 0.22} = 0.642$$

4. Incident Flux Absorbed by Absorber Plate

The amount of incident flux absorbed by the absorber plate is given by Eq. (4.2).

$$\begin{aligned} S &= (665 \times 0.9384 \times 0.727) + (230 \times 0.9741 \times 0.642) \\ &\quad + (895 \times 0.0052 \times 0.642) \\ &= 600.4 \text{ W/m}^2 \end{aligned}$$

5. Collector Heat-removal Factor and Overall Loss Coefficient

An iterative procedure will be required since both F_R and U_l cannot be directly determined and the value of one is dependent on the other.

First Iteration: Assume $U_l = 4.0 \text{ W/m}^2 \cdot ^\circ\text{C}$. This is a reasonable assumption for a collector with two glass covers and a non-selective absorber surface.

$$m = \left(\frac{4.0}{35 \times 1.3 \times 10^{-3}} \right)^{1/2} = 9.38 \text{ m}^{-1}$$

$$\frac{m(W - D_o)}{2} = \frac{9.38(0.12 - 0.018)}{2} = 0.4782$$

$$\text{Effectiveness } \phi = \frac{\tanh 0.4782}{0.4782} = 0.930$$

From Eq. (4.42), the collector efficiency factor

$$F' = \frac{1}{0.12 \times 4.0 \left[\frac{1}{4.0(0.102 \times 0.930 + 0.018)} + \frac{1}{205 \times \pi \times 0.014} \right]} = 0.895$$

$$\frac{\dot{m}C_p}{A_p} = \frac{70}{1.5} \times \frac{4.18 \times 1000}{3600} = 54.18 \text{ W/m}^2 \cdot ^\circ\text{C}$$

Therefore, from Eq. (4.49), the collector heat-removal factor

$$F_R = \frac{54.18}{4.0} \left[1 - \exp \left\{ - \frac{4.0 \times 0.895}{54.18} \right\} \right] = 0.866$$

and from Eq. (4.48), the useful heat gain

$$\begin{aligned} q_u &= F_R A_p [S - U_l (T_{fi} - T_a)] \\ &= 0.866 \times 1.5 [600.4 - 4.0(60 - 25)] \\ &= 598.1 \text{ W} \end{aligned}$$

Therefore,

$$\begin{aligned} q_l &= 600.4 \times 1.5 - 598.1 \\ &= 302.5 \text{ W} \end{aligned}$$

From Eq. (4.17),

$$q_l = 4.0 \times 1.5 \times (T_{pm} - 25)$$

Thus,

$$T_{pm} = 50.42 + 25 = 75.42^\circ\text{C} = 348.6 \text{ K}$$

We will calculate the value of the top loss coefficient using the value of $T_{pm} = 348.6 \text{ K}$. Following the same procedure as in Example 4.2, we have

$$T_{sky} = 298.2 - 6 = 292.2 \text{ K}$$

$$\begin{aligned} \frac{q_t}{A_p} &= h_{p-c1} (348.6 - T_{c1}) + \frac{5.67 \times 10^{-8} (348.6^4 - T_{c1}^4)}{\left(\frac{1}{0.95} + \frac{1}{0.88} - 1 \right)} \\ &= h_{p-c1} (348.6 - T_{c1}) + 4.7687 \times 10^{-8} (147.676 \times 10^8 - T_{c1}^4) \quad (4.50) \end{aligned}$$

$$\frac{q_t}{A_p} = h_{c1-c2} (T_{c1} - T_{c2}) + \frac{5.67 \times 10^{-8} (T_{c1}^4 - T_{c2}^4)}{\left(\frac{1}{0.88} + \frac{1}{0.88} - 1 \right)}$$

$$= h_{c1-c2} (T_{c1} - T_{c2}) + 4.455 \times 10^{-8} (T_{c1}^4 - T_{c2}^4) \quad (4.51)$$

$$\begin{aligned} \frac{q_t}{A_p} &= h_w (T_{c2} - 298.2) + 5.67 \times 10^{-8} \times 0.88 (T_{c2}^4 - 292.2^4) \\ &= h_w (T_{c2} - 298.2) + 4.990 \times 10^{-8} (T_{c2}^4 - 72.899 \times 10^8) \quad (4.52) \end{aligned}$$

Assume $T_{c1} = 331 \text{ K}$ and $T_{c2} = 310 \text{ K}$.

Calculation of h_{p-c1} :

$$\text{Mean temperature} = \frac{348.6 + 331}{2} = 339.8 \text{ K} = 66.6^\circ\text{C}$$

$$k = 0.0295 \text{ W/m-K}$$

$$v = 19.66 \times 10^{-6} \text{ m}^2/\text{s}$$

$$\text{Pr} = 0.695$$

$$\begin{aligned} \text{Ra}_L \cos \beta &= 9.81 \times \frac{1}{339.8} \times \frac{(348.6 - 331) \times 0.025^3}{19.66^2 \times 10^{-12}} \times 0.695 \cos 18.53^\circ \\ &= 13536 \end{aligned}$$

$$\begin{aligned} \text{Nu}_L &= 0.229 \times (13536)^{0.252} \\ &= 2.517 \end{aligned}$$

$$\begin{aligned} h_{p-c1} &= 2.517 \times 0.0295 / 0.025 \\ &= 2.971 \text{ W/m}^2 \cdot \text{K} \end{aligned}$$

Calculation of h_{c1-c2} :

$$\text{Mean temperature} = \frac{331 + 310}{2} = 320.5 \text{ K} = 47.3^\circ\text{C}$$

$$k = 0.0281 \text{ W/m-K}$$

$$v = 17.68 \times 10^{-6} \text{ m}^2/\text{s}$$

$$\text{Pr} = 0.698$$

$$\begin{aligned} \text{Ra}_L \cos \beta &= 9.81 \times \frac{1}{320.5} \times \frac{21 \times 0.025^3}{17.68^2 \times 10^{-12}} \times 0.698 \cos 18.53^\circ \\ &= 21264 \end{aligned}$$

$$\text{Nu}_L = 0.229 \times (21264)^{0.252} = 2.821$$

$$h_{c1-c2} = \frac{2.821 \times 0.0281}{0.025} = 3.171 \text{ W/m}^2 \cdot \text{K}$$

Calculation of h_w :

$$\text{Mean temperature} = \frac{310 + 298.2}{2} = 304.1 \text{ K} = 30.9^\circ\text{C}$$

$$\rho = 1.162 \text{ kg/m}^3$$

$$C_p = 1.005 \text{ kJ/kg-K}$$

$$\nu = 16.09 \times 10^{-6} \text{ m}^2/\text{s}$$

$$\Pr = 0.701$$

$$L^* = \frac{4 \times 1.6 \times 1.1}{2(1.6 + 1.1)} = 1.304 \text{ m}$$

$$Re_L^* = \frac{3.1 \times 1.304}{16.09 \times 10^{-6}} = 0.2512 \times 10^6$$

$$j = 0.86 \times (0.2512 \times 10^6)^{-1/2} \\ = 0.001716$$

$$h_w = 0.001716 \times 1.162 \times 1.005 \times 3.1 \times 10^3 \times (0.701)^{1/2} \\ = 7.889 \text{ W/m}^2\text{-K}$$

A trial and error method involving small adjustments in the values of T_{c1} and T_{c2} will now be required such that the values of (q_i/A_p) calculated from Eqs (4.50), (4.51) and (4.52) agree with each other. This is shown in the following table:

T_{c1} (K)	T_{c2} (K)	q_i/A_p (W/m ²)		
		Eq. (4.50)	Eq. (4.51)	Eq. (4.52)
331	310	52.29 + 131.81 = 184.10	66.59 + 123.33 = 189.92	93.09 + 97.07 = 190.16
330.6	309.8	53.48 + 134.57 = 188.05	65.96 + 121.81 = 187.78	91.51 + 95.88 = 187.40

$$(q_i/A_p)_{av} = 187.74 \text{ W/m}^2$$

$$U_t = \frac{187.74}{(348.6 - 298.2)} = 3.725 \text{ W/m}^2\text{-K}$$

Now, from Eq. (4.29),

$$U_b = \frac{0.04}{0.05} = 0.8 \text{ W/m}^2\text{-K}$$

Therefore,

$$U_s = 0.08 \text{ W/m}^2\text{-K}$$

$$U_t = 3.725 + 0.8 + 0.08 \\ = 4.605 \text{ W/m}^2\text{-K}$$

Since this value of U_t is considerably different from the assumed value, a second iteration will be necessary.

Second Iteration

$$m = \left(\frac{4.605}{35 \times 1.3 \times 10^{-3}} \right)^{1/2} = 10.06 \text{ m}^{-1}$$

$$\frac{m(W - D_o)}{2} = \frac{10.06(0.12 - 0.018)}{2} = 0.5131$$

$$\phi = \frac{\tanh 0.5131}{0.5131} = 0.9207$$

$$F' = \frac{1}{0.12 \times 4.605 \left[\frac{1}{4.605[(0.102 \times 0.9207) + 0.018]} + \frac{1}{205 \times \pi \times 0.14} \right]}$$

$$= 0.8824$$

$$F_R = \frac{54.18}{4.605} \left[1 - \exp \left\{ - \frac{4.605 \times 0.8824}{54.18} \right\} \right]$$

$$= 0.8501$$

$$q_s = 0.8501 \times 1.5[600.4 - 4.605(60 - 25)]$$

$$= 560.1 \text{ W}$$

$$q_t = 600.4 \times 1.5 - 560.1$$

$$= 340.5 \text{ W}$$

$$= 4.605 \times 1.5(T_{pm} - 25)$$

$$T_{pm} = 74.29^\circ\text{C} = 347.5 \text{ K}$$

This value of T_{pm} is not very different from the value 348.6 K obtained after the first iteration. It will not therefore be necessary to perform any more iterations and the values obtained for ϕ , F , F_R , q_s and T_{pm} in the second iteration can be accepted as being correct.

6. Water Outlet Temperature

The water outlet temperature is obtained from the heat balance equation. Substituting,

$$70 \times 4.18(T_{fo} - 60) = \frac{560.1 \times 3600}{1000}$$

$$\text{Hence } T_{fo} = 66.89^\circ\text{C} = 340.1 \text{ K}$$

7. Instantaneous Efficiency

Using Eq. (4.3), the instantaneous efficiency based on the absorber plate area is given by

$$\eta_i = \frac{560.1}{852.7 \times 1.5}$$

$$= 0.438, \text{ i.e. } 43.8 \text{ per cent.}$$

Considering the fact that the water inlet temperature is only 40°C , the efficiency of the given collector is rather low. This is so because the glass covers used are of poor quality and have a low transmissivity. Also the thermal conductivity of the absorber plate material is low. A similar collector having a copper or aluminium absorber plate and fitted with better glass covers having a lower extinction coefficient would, under comparable conditions, yield a higher efficiency between 50 and 55 per cent (see problem 7). However, it should be noted that such a collector would cost more than the GI collector.

Performance Over a Day

It is of interest to study the performance of a collector over a whole day. This is done for the same GI collector by using radiation data measured over a whole day. For the sake of simplicity, the water flow rate, water inlet temperature, ambient temperature and wind speed are all assumed to be constant at the values given earlier.

The radiation data used and the results obtained are given in Table 4.1. It is seen that the values of the useful heat gain and the efficiency (Fig. 4.11) increase sharply from 0800 to 1000 h, touch a peak around noon and then drop sharply after 1500 h. The variation obtained is typical for a flat-plate collector and indicates the strong dependence of these factors on the radiation incident on the collector. It is also seen that the value of the top loss coefficient does not vary much.

Table 4.1 Performance of a Flat-plate Collector Over a Whole Day

IST (h)	0800	0900	1000	1100	1200	1300	1400	1500	1600	1700
I_b (W/m ²)	213	390	547	665	725	715	615	476	337	186
I_d (W/m ²)	149	192	210	230	230	233	239	221	185	141
I_T (W/m ²)	319.2	535.8	712.4	852.7	914.7	908.2	814.8	658.2	482.8	290.9
T_{ew} (K)	334.1	339.6	344.1	347.5	349.1	348.9	346.6	342.9	338.5	333.7
U_t (W/m ² -K)	3.55	3.62	3.66	3.72	3.72	3.72	3.70	3.65	3.60	3.55
q_u (W)	37.1	252.5	427.3	560.1	619.6	613.5	524.6	378.2	209.9	20.8
T_{fo} (K)	333.6	336.3	338.4	340.1	340.8	340.7	339.6	337.8	335.7	333.4
η_i (%)	7.7	31.4	40.0	43.8	45.0	45.0	42.9	38.3	29.0	4.8

The average efficiency over the whole period, during which useful

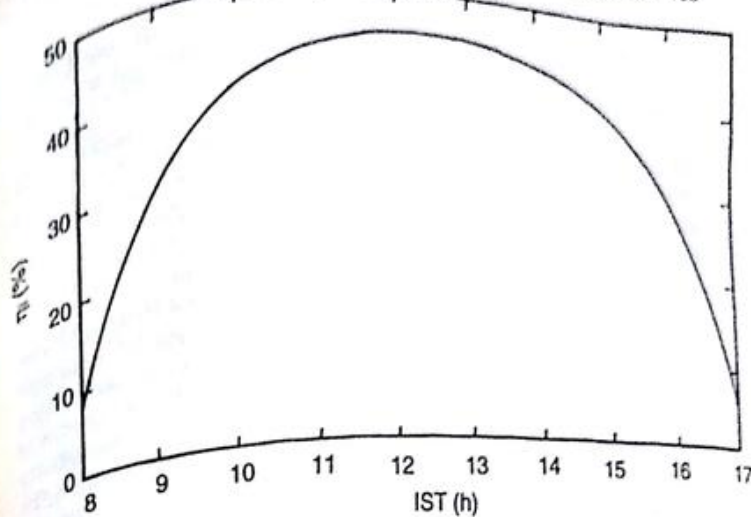


Fig. 4.11 Variation of Instantaneous Efficiency of a GI Collector over a Day (η_i , Based on Absorber Plate Area)

energy is collected, can be approximately calculated if it is assumed that the values of instantaneous efficiency and solar radiation are valid for half an hour on either side of the instant considered. Making this approximation, the efficiency averaged over 10 hours from 0730 to 1730 h works out to be 37.4 per cent.

4.9 EFFECTS OF VARIOUS PARAMETERS ON PERFORMANCE

It is evident from the preceding sections and from Example 4.3 that a large number of parameters influence the performance of a liquid flat-plate collector. These parameters could be classified as design parameters, operational parameters, meteorological parameters and environmental parameters. In this section, the effects of some of these will be considered. The parameters discussed are the selectivity of the absorber surface, the number of glass covers, the spacing between the covers, the tilt of the collector, the fluid inlet temperature, the incident solar flux, and dust settlement on the top glass cover.

4.9.1 Selective Surfaces

Absorber plate surfaces which exhibit the characteristics of a high value of absorptivity for incoming solar radiation and a low value of emissivity for out-going re-radiation are called *selective surfaces*. Such surfaces are desirable because they maximize the absorption of solar

energy and minimize the emission of the radiative loss. Obviously, the absorptivity and emissivity are equal.

The possibility of having selective absorber plate surfaces for flat-plate collectors was suggested first by Tabor* and later by Gier and Dunkle†. The basis for the suggestion can be understood if one compares the spectral distribution of extra-terrestrial solar radiation with that of black-body radiation from a source at 350 K (which corresponds approximately to the temperature of the absorber plate). These are shown in Fig. 4.12 (a) and it is immediately obvious that there is almost no overlap between the two. Unlike solar radiation, which lies almost exclusively in the wavelength region up to 4 μm , the radiation coming off from the absorber plate is of large wavelengths with a maximum at 8.3 μm . It follows therefore that if a surface that has a high absorptivity for wavelengths less than 4 μm and a low emissivity for wavelengths greater than 4 μm can be prepared, it would have the characteristics desirable for an absorber plate surface to act in a selective fashion. The characteristics desired for an ideal selective surface ($\alpha_\lambda = \varepsilon_\lambda = 1$ for $\lambda < 4 \mu\text{m}$ and $\alpha_\lambda = \varepsilon_\lambda = 0$ for $\lambda > 4 \mu\text{m}$) are shown in Fig. 4.12 (b). For comparison, the variation obtained for one of the earliest surfaces synthesised by Tabor is also shown.

The development of selective surfaces on various metal substrates has been the subject of intensive work for many years. As a result, a number of surfaces having characteristics approaching those of an ideal surface have been synthesised and a few have been commercialised. In most of these surfaces the selectivity is achieved by having a polished and cleaned metal base and depositing on it a thin surface layer which is transparent to large wavelengths, but highly absorbing for small wavelength solar radiation. The surface layer is less than 1 μm in thickness and is deposited by a variety of methods. These include electroplating, chemical vapour deposition, chemical conversion, anodic oxidation and rf-magnetron sputtering. Some of the successful developments in this field will now be described.

Surface layers of copper oxide and "nickel black" were the first selective surfaces found to be suitable from a practical standpoint. The copper oxide layer was formed by chemical conversion, by treating a cleaned and polished copper plate in a hot solution of sodium hydroxide and sodium chlorite for a specified time. Values of absorptivity (α) and emissivity (ε_p) obtained for this surface were 0.89 and 0.17 respectively,

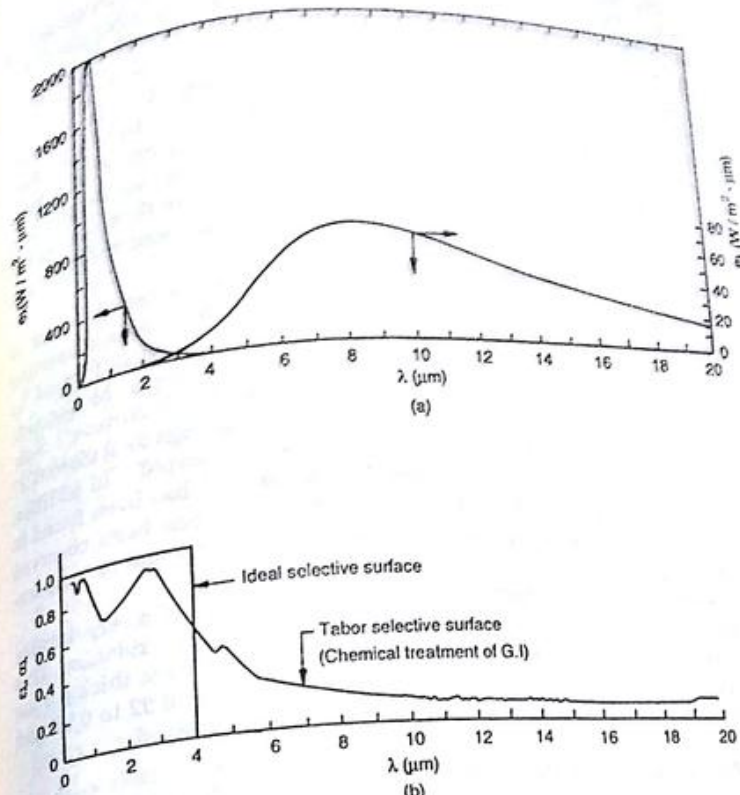


Fig. 4.12 (a) Spectral Distribution of Extra-terrestrial Solar Radiation and Blackbody Radiation from a Source at 350 K
 (b) Monochromatic Emissivity/Absorptivity Variation Desired for an Ideal Selective Surface and Variation Obtained for a Selective Surface by Tabor

α being the average value of α_λ over the solar radiation wavelength range and ε_p being the average value of ε_λ for large wavelength radiation. This surface was commercialised in Australia* and found to be durable for low temperature applications like solar water heating.

*H. Tabor, "Selective Radiation", *Bulletin Research Council of Israel*, 5A, 119 (1956).

†J.T. Gier and R.V. Dunkle, "Selective Spectral Characteristics as an Important Factor in the Efficiency of Solar Collectors", *Trans. Conf. on the Use of Solar Energy*, 2, Part I, 41 (1958).

*D.J. Close, "Flat Plate Solar Absorbers: The Production and Testing of a Selective Surface for Copper Absorber Plates", *Report E.D. 7, C.S.I.R.O.*, Melbourne, Australia (1962).

The "nickel black" surface was developed and commercialized in Israel*. The process involved the careful cleaning of a galvanized sheet and subsequent electroplating of a "nickel black" coating. Immersion of the sheet as the cathode in an aqueous electrolyte of nickel sulphate, zinc sulphate, ammonium sulphate, ammonia thiocyanate and citric acid. Values of $\alpha = 0.81$ and $\epsilon_p = 0.16$ to 0.18 were obtained for this selective surface. Subsequently Cathro *et al.* described procedures for electroplating "nickel black" on copper and mild steel. In these cases, a bright nickel plating was first put on the base metal before electroplating "nickel black". Values of $\alpha = 0.83$ and $\epsilon_p = 0.09$ to 0.15 were reported.

One of the most successful selective surfaces developed so far is "black chrome". This coating is a metal-dielectric composite consisting of a Cr_2O_3 layer over a Cr particle/ Cr_2O_3 composite. It is formed by electroplating on a nickel plated copper or steel base. McDonald reported values of $\alpha = 0.868$ and $\epsilon_p = 0.088$ for "black chrome". Subsequently with further refinements, values of α as high as 0.92 to 0.95 and values of ϵ_p as low as 0.04 to 0.06 have been reported. In addition to its excellent selective properties, "black chrome" has been found to be very durable. No degradation in performance has been observed even after prolonged exposure to a humid atmosphere and to temperatures up to 400°C .

Andersson *et al.*++ have reported the development of a very durable metal-dielectric composite coating formed by anodic oxidation. The coating consists of grains of nickel embedded in a $0.7\text{ }\mu\text{m}$ thick porous layer of Al_2O_3 . Values of absorptivity in the range of 0.92 to 0.97 and emissivity in the range of 0.1 to 0.26 have been obtained.

Effect on Collector Performance

The effect of a selective surface on the performance of a collector can be best illustrated by taking a specific situation. The GI collector of

*H. Tabor, J. Harris, H. Weinberger and B. Doron, "Further Studies on Selective Black Coatings", *Proceedings U.N. Conference on New Sources of Energy*, 4, 618 (1964).
++K.J. Cathro, E.A. Christie and A.F. Reid, "Nickel Black as a Selective Absorbing Surface", Meeting on Applications of Solar Energy Research and Development in Australia, Melbourne (1975).

++G.E. McDonald, "Spectral Reflective Properties of Black Chrome for Use as a Solar Selective Coating", *Solar Energy*, 17, 119 (1975).

++R.R. Sowell and D.M. Mattox, "Properties and Composition of Electroplated Black Chrome", Symposium on Coatings for Solar Collectors, American Electroplaters Society, Winter Park, Florida, USA (1976).

++A. Andersson, O. Hunderi and C.G. Granqvist, "Nickel Pigmented Anodic Aluminium Oxide for Selective Absorption of Solar Energy", *Journal of Applied Physics*, 51, 754 (1980).

Sec. 4.8 is considered again and its performance with and without a selective surface at 1200 h (IST) calculated. The only changes made from the earlier data are as follows:

- (1) It is assumed now that the tubes are clamped on the underside of the absorber plate instead of being brazed. This is a cheaper method of fabrication but results in a bond resistance which is assumed to be $0.15\text{ m}^{-2}\text{C/W}$ in this case.
- (2) The mean flow rate is taken as 60 kg/h .
- (3) The ambient air temperature is assumed to be 30°C .
- (4) With the selective surface, two cases are considered. In one case, it is assumed that $\alpha = 0.95$ and $\epsilon_p = 0.12$, while in the other, it is assumed that $\alpha = 0.85$ and $\epsilon_p = 0.11$.

The calculations are repeated in a manner similar to that adopted earlier and the results obtained are indicated in Table 4.2.

Table 4.2 Effect of a Selective Surface on Performance of GI Collector

	Nonselective absorber plate $\alpha = \epsilon_p = 0.95$	Selective absorber plate	
	$\alpha = 0.95$	$\alpha = 0.85$	$\epsilon_p = 0.12$
$T_{\text{pm}}\text{ (K)}$	356.1	359.3	357.0
$U_t\text{ (W/m}^2\text{-K)}$	3.87	2.56	2.51
$q_s\text{ (W)}$	593.6	682.9	616.1
$T_b\text{ (K)}$	341.7	342.95	342.0
$\eta_t\text{ (%)}$	43.3	49.8	44.9

It is seen from Table 4.2 that with a nonselective absorber plate, the top loss coefficient is $3.87\text{ W/m}^2\text{-K}$ and the efficiency is 43.3 per cent. These values are similar to those given in Table 4.1, where $U_t = 3.72\text{ W/m}^2\text{-K}$ and $\eta_t = 45.2$ per cent. The differences are due to the changes (1) to (3). On the other hand, with the first selective surface, in which the value of α is unchanged while the value of ϵ_p is 0.12, significant differences are observed. The top loss coefficient drops to $2.56\text{ W/m}^2\text{-K}$, while the efficiency increases by 6.6 per cent to 49.8 per cent. With the second selective surface, in which the value of α is much less, it is observed that while the value of U_t is the same as that for the first selective surface, the efficiency is much lower and almost the same as for the non-selective surface. This is primarily due to the fact that the value of S decreases with lower α . It is to be noted that for both the selective surfaces, the value of (α/ϵ_p) is almost the same. For the first, it is 7.9 and for the second 7.7. This shows that a high value of (α/ϵ_p) is not adequate for obtaining a good performance with selective surface. Along with the high value of (α/ϵ_p) , it is necessary that the value of α should also be high.

4.9.2 Number of Covers

The number of covers (glazings) used in a collector is usually two. We will study the effect of the number of covers on performance by again taking the example of the GI collector with one, two and three covers. It is assumed that the changes (1) to (3) indicated in Sec. 4.4 are again made.

The results obtained are given in Table 4.3 and show that for the situation studied the efficiency goes through a maximum value of 41.8 per cent for the case of two covers. This can be explained as follows.

As the number of covers increases, the values of both $(\tau\alpha)_b$ and $(\tau\alpha)_d$ decrease. Thus, the flux S absorbed in the absorber plate decreases. The addition of more covers also causes the value of U_t to decrease, hence the heat loss, to decrease. However, the amount of decrease is not the same in both cases. For this reason, the efficiency goes through a maximum. This kind of result is obtained with all collectors, the maximum efficiency being usually obtained with one or two covers. In fact, for the GI collector under study, the efficiency will be found to be a maximum with only one cover if a selective absorber surface is used. This is seen from Table 4.4.

Table 4.3 Effect of Number of Covers on Performance of GI Collector (Non-selective Surface)

	Number of covers		
	1	2	3
$(\tau\alpha)_b$	0.8316	0.7305	0.6447
$(\tau\alpha)_d$	0.7567	0.6424	0.5631
U_t (W/m ² -K)	6.39	3.87	2.72
η_i (%)	40.6	43.3	41.8

Table 4.4 Effect of Number of Covers on Performance of GI Collector (Selective Surface, $\alpha = 0.85$, $\varepsilon_p = 0.11$)

	Number of covers	
	1	2
$(\tau\alpha)_b$	0.7563	0.6999
$(\tau\alpha)_d$	0.6882	0.5891
U_t (W/m ² -K)	3.61	2.51
η_i (%)	47.0	44.9

4.9.3 Spacing

The proper spacing to be kept between the absorber plate and the first

cover, or between two covers has been the subject of considerable discussion. From the point of view of the heat loss from the top, it is evident that the spacing must be such that the values of the convective heat transfer coefficients are minimized. It is, therefore, useful to examine the behaviour of the correlating equations (4.25). This is done in Fig. 4.13 in which the variation of the heat transfer coefficient with spacing is drawn. Curves for two temperature differences are plotted with the mean air temperature and the tilt being kept fixed.

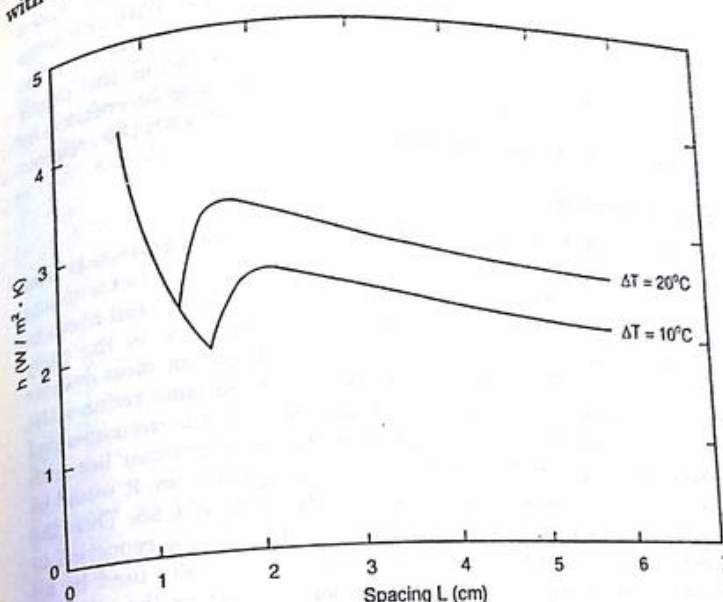


Fig. 4.13 Plot of Eq. 4.25 Showing Variation of Heat Transfer Coefficient with Spacing. $T_{mean} = 70^\circ\text{C}$, $\beta = 20^\circ$

It is seen that for a particular temperature difference, the value of h first decreases and reaches a minimum. This variation corresponds to the conduction regime in which $Nu_L = 1$, with the minimum occurring at a spacing corresponding to $Ra_L \cos \beta = 1708$. Thereafter, as the spacing increases the value of h increases first sharply and then gradually. It goes through a maximum and then gradually decreases. With large values of spacing, the value drops below the previous minimum value.

It will be noted that the spacings at which the minimum and maximum values occur vary with the temperature difference. They

also vary with the tilt. Since collectors are designed to operate in different locations with varying tilts and under varying service conditions, an optimum value of spacing is difficult to specify. It appears best to use a sufficiently large spacing away from the local minimum and maximum. Spacings from 4 to 8 cm have been suggested from the point of view by Buchberg *et al.*

Buchberg *et al.* have also studied the effect of spacing on the performance of a collector. They have done calculations for a single and double cover collector with a non-selective absorber plate and a single cover collector with a selective absorber plate. With the same operating conditions, two spacings have been tried out and the efficiency calculated. It has been shown that by using the larger spacing, around 5 cm, collector area requirements can be reduced by 2 to 8 per cent, the higher reduction being obtained with the collector having the selective absorber plate.*

Effect of Shading

The main problem associated with the use of larger spacings is that shading of the absorber plate by the side walls of the collector casing increases. Some shading always occurs in every collector and needs to be corrected for. The shading is particularly important in the early morning and late evening hours. It is estimated that for most designs using spacings of 2 to 3 cm between the covers, shading reduces the radiation absorbed by about 3 per cent. Accordingly, it is recommended that the absorbed flux S be calculated in the usual manner but with a multiplying factor of 0.97. With larger spacings of 5 cm, it would be necessary to use a smaller multiplying factor around 0.95. Thus the gain obtained by using a larger spacing is offset by the reduction in S . For this reason, spacings of 2 or 3 cm are generally used by all manufacturers. It may be noted that in some collectors the inside of the side walls is lined with a reflecting surface in order to alleviate the effects of shading.

4.9.4 Collector Tilt

Flat-plate collectors are normally fixed in one position and do not track the sun. The question of the amount of tilt one should give to them is therefore of considerable importance. The basis for arriving at an optimum tilt will now be discussed.

One of the earliest studies on the subject is due to Morse and

*H. Buchberg, I. Catton and D.K. Edwards, "Natural Convection in Enclosed Spaces—A Review of Application to Solar Energy Collection", *Journal of Heat Transfer*, Trans. ASME, 98, 182 (1976).

Czarnecki* who simplified the problem by assuming that extraterrestrial insolation was falling on the collector. They calculated the annual insolation per unit area by integrating the expression for the flux on a tilted surface first over the day length and then summing up over the days of the year. Taking $\gamma = 0$, so that the daily insolation is maximized, the following expression is obtained

$$\text{Annual Insolation} = \sum_{n=1}^{365} I_{sc} \int_{-\omega_s}^{+\omega_s} \left(1 + 0.033 \cos \frac{360n}{365} \right)$$

$$\times (\sin \delta \sin \phi - \beta + \cos \delta \cos \omega \cos (\phi - \beta)) d\omega$$

They have plotted their results in the form of relative insolation (the ratio of annual insolation for given values of ϕ and β to the annual insolation for $\phi = 0$ and $\beta = 0$) against the latitude ϕ for tilts of 0, 0.9ϕ , 1.2ϕ and 1.5ϕ . The results are shown in Fig. 4.14 and indicate

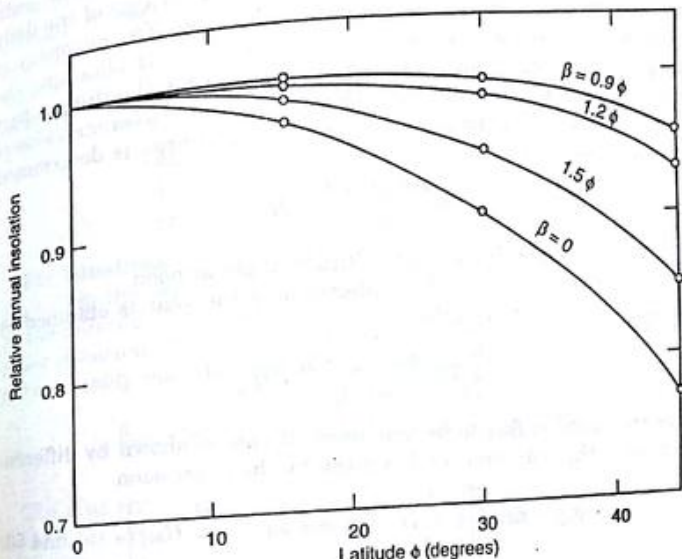


Fig. 4.14 Variation of Relative Annual Insolation with Latitude for Collectors Tilted at Various Values of β and with $\gamma = 0^\circ$

*R.N. Morse and J.T. Czarnecki, "Flat-plate Solar Absorbers: The Effect on Incident Radiation of Inclination and Orientation", Report E.E.6, Mechanical Engineering Division, C.S.I.R.O., Melbourne (1958).

that the optimum tilt which will result in maximizing the insolation is given by $\beta = 0.9\phi$. It is also seen that for latitudes within 30°, small deviations of a degree or two from the optimum tilt will cause much change in the relative insolation.

The effect of having surface azimuth angles other than zero for collectors which do not slope precisely towards the south in the northern hemisphere (or the north in the southern hemisphere) has also been considered by Morse and Czarnecki. In this case also, it has been found from their results that surface azimuth angles up to $\pm 5^\circ$ result in very small reductions (less than 1 per cent) in the relative insolation.

The above analysis for optimum tilt can be criticised on the ground that it considers only beam radiation falling on the collector and assumes it to have the extra-terrestrial value. Other analyses have considered the measured radiation data for specific locations which have therefore been performed. One such simple analysis is due to Kern and Harris.* They have considered a collector oriented with a zero azimuth angle and having a tilt β , and used the monthly averages of the daily beam and diffuse radiation measured at a location. The geometry of the situation existing at solar noon has been used for obtaining the appropriate tilt factor for beam radiation, while for the diffuse part the tilt factor is taken to be unity. Thus, the monthly average value of the energy falling on the collector plane per unit area is determined approximately† to be

$$\bar{H}_b \frac{\sin(\bar{\alpha}_n + \beta)}{\sin \bar{\alpha}_n} + \bar{H}_d$$

where $\bar{\alpha}_n$ is the monthly average altitude angle at noon.

The total flux falling on the collector over the year is obtained by summing over all the months

$$\sum_{i=1}^{12} \bar{H}_{bi} \frac{\sin(\bar{\alpha}_{ni} + \beta)}{\sin \bar{\alpha}_{ni}} + \bar{H}_{di}$$

For this annual flux to be maximum, it can be shown by differentiation that the optimum tilt β is given by the expression

$$\beta_{opt} = \tan^{-1} \left[\left\{ \sum_{i=1}^{12} \bar{H}_{bi} \tan |\phi - \delta_i| \right\} \Big/ \left\{ \sum_{i=1}^{12} \bar{H}_{di} \right\} \right] \quad (4.53)$$

Calculations by Kern and Harris for four locations in South Africa

show that the value of the optimum tilt is approximately equal to the latitude of the location and that the energy collected is not very sensitive to small deviations from the best angle. Thus the conclusion reached is similar to that of Morse and Czarnecki.

It is to be noted however that the optimum tilt would be different if the nature of the energy demand is different. For example, for an application like space heating, the demand may be high in the winter months of December, January and February. On the other hand, if solar energy were to be used for running an absorption refrigeration plant, the duty would be highest in months like April, May and June having high ambient temperatures. In such cases, it would obviously be desirable to use a tilt greater than the latitude for a winter application and the reverse for a summer application. The usual practice is to recommend values of $(\phi + 10^\circ)$ or $(\phi + 15^\circ)$ for the former and $(\phi - 10^\circ)$ or $(\phi - 15^\circ)$ for the latter.

Equation (4.53) has been derived for the situation $\gamma = 0^\circ$ and $\gamma_i = 0^\circ$ existing at solar noon for all months of the year. We shall call this situation (1). Situation (1) would generally occur at a location having a latitude greater than 23.45° . Apart from situation (1), it is possible to have the following situations for some or all the months of the year.

Situation	γ (deg)	γ_i (deg)
(2)	0	180
(3)	180	0
(4)	180	180

For situations (2) and (3), we would have to substitute $(\bar{\alpha}_n - \beta)$ for $(\bar{\alpha}_n + \beta)$ in the expression for the monthly average value of flux falling on the collector plane while for situation (4), the expression is the same as for situation (1). Thus the expression for the annual flux would have to be suitably modified and the optimum tilt is now given by

$$\beta_{opt} = \tan^{-1} \left[\left\{ \sum_{i=1}^{12} \pm \bar{H}_{bi} \tan |\phi - \delta_i| \right\} \Big/ \left\{ \sum_{i=1}^{12} \bar{H}_{di} \right\} \right]$$

The plus sign before \bar{H}_{bi} is valid for the months in which situations (1) and (4) exist, while the negative sign is valid for the months in which situations (2) and (3) exist.

Example 4.4

A flat-plate collector array is to be installed in New Delhi (28.58°N).

Calculate the optimum tilt for the following three situations: (i) Insolation falling on the array over the whole year is to be maximized. (ii) Insolation for the months of April, May and June is to be maximized. (iii) Insolation for the months of December, January and February is to be maximized. The following radiation data are given:

*J. Kern and I. Harris, "On the Optimum Tilt of a Solar Collector", *Solar Energy*, 17, 97 (1975).

†A more accurate procedure would be to consider monthly averages of the hourly variation of beam and diffuse radiation and to use corresponding tilt factors varying over the day.

Month	J	F	M	A	M	J	J	A	S	O	N	D
\bar{H}_s (kWh/m ² -day)	3.987	5.001	6.138	6.935	7.287	6.544	5.334	5.053	5.602	5.355	4.523	3.845
H_d (kWh/m ² -day)	1.240	1.474	1.861	2.473	2.922	3.540	3.135	2.727	2.152	1.465	1.141	1.117

At New Delhi, $\gamma_s = 0^\circ$ at solar noon throughout the year. We will use Eq. (4.53) under the assumption* that situation (1) exists, i.e. the collector array is facing due south with $\gamma = 0^\circ$. For part (i), the summation in Eq. (4.53) will be done over all the 12 months, while for parts (ii) and (iii), the summation will be done only for the months specified. The calculations are shown in Table 4.5, with the declination angles being calculated for the middle days of the month. It is seen that the values obtained for the optimum tilt are in approximate agreement with the recommendations given earlier.

Table 4.5 Calculations for Optimum Tilt for a Collector Array in New Delhi

	\bar{H}_b kWh/m ²	n	δ deg	$(\phi - \delta)$ deg	$\bar{H}_b \tan(\phi - \delta)$ kWh/m ²
J	2.747	16	-21.10	49.68	3.237
F	3.527	45	-13.62	42.20	3.198
M	4.277	75	-2.42	31.00	2.570
A	4.462	105	9.41	19.17	1.517
M	4.365	136	19.03	9.55	0.734
J	3.004	166	23.31	5.27	0.277
J	2.199	197	21.35	7.23	0.279
A	2.326	228	13.45	15.13	0.629
S	3.450	258	2.22	26.36	1.710
O	3.890	289	-8.97	37.55	2.990
N	3.382	319	-19.15	47.73	3.721
D	2.726	350	-23.37	51.95	3.483
Σ	40.355				24.345

$$(1) \beta_{opt} = \tan^{-1} \left[\frac{24.345}{40.355} \right] = 31.1^\circ$$

$$(2) \beta_{opt} = \tan^{-1} \left[\frac{1.517 + 0.734 + 0.277}{4.462 + 4.365 + 3.004} \right] = 12.1^\circ$$

$$(3) \beta_{opt} = \tan^{-1} \left[\frac{3.483 + 3.237 + 3.198}{2.726 + 2.747 + 3.527} \right] = 47.8^\circ$$

*If this assumption is incorrect, one would obtain a negative value of β_{opt} . It would then be necessary to reverse the assumption, take $\gamma = 180^\circ$ and recalculate the value of β_{opt} .

4.9.5 Fluid Inlet Temperature

The fluid inlet temperature is an operational parameter which strongly influences the performance of a flat-plate collector. The effect is best illustrated by again doing calculations for the case of the GI collector of Sec. 4.9.2. Results are obtained with fluid inlet temperature varying from 40 to 90°C, while the values of the other parameters are held constant (Table 4.6).

Table 4.6 Effect of Fluid Inlet Temperature on Performance of GI Collector at 1200 h (IST)

T_{fi} (°C)	40	50	60	70	80	90
T_{pm} (K)	340.9	348.5	356.1	363.6	371.0	378.4
U_f (W/m ² ·K)	3.69	3.77	3.87	3.95	4.05	4.15
q_u (W)	712.8	654.8	593.6	531.3	465.7	398.1
T_{fo} (K)	323.4	332.6	341.7	350.8	359.9	368.9
η_f (%)	52.0	47.7	43.3	38.7	33.9	29.0

It is seen from Table 4.6 that the efficiency of the collector decreases sharply and at an increasing rate with increasing values of T_{fi} (see also Fig. 4.15), the value falling from 52.0 to 29.0 per cent as T_{fi} increases from 40 to 90°C. This decrease is because of the higher temperature level at which the collector as a whole operates when the fluid inlet temperature increases. Because of this, the top loss coefficient as well as the temperature difference with the surroundings increases, the heat lost increases and the useful heat gain decreases.

4.9.6 Incident Solar Flux

The influence of incident flux on the collector efficiency is plotted in Fig. 4.16 from the results given earlier in Table 4.1. It is seen that the efficiency increases with the flux, the increase being more pronounced at lower values of flux. As stated in Sec. 4.9.5, the fluid inlet temperature and the ambient temperature essentially determine the losses from a collector. Hence, if these quantities are constant and the incident flux increases, the useful heat gain and the efficiency must increase. It should be noted that the incident flux is composed of beam, diffuse and reflected radiation and that the variation obtained in Fig. 4.16 is influenced by the relative proportion of these components.

4.9.7 Dust on the Top Cover

The preceding calculations of the flux transmitted through the covers of the collector have been done under the assumption that the top cover is clean and has no dust accumulated on it. This assumption is acceptable only if the cover is continuously cleaned. However, in any

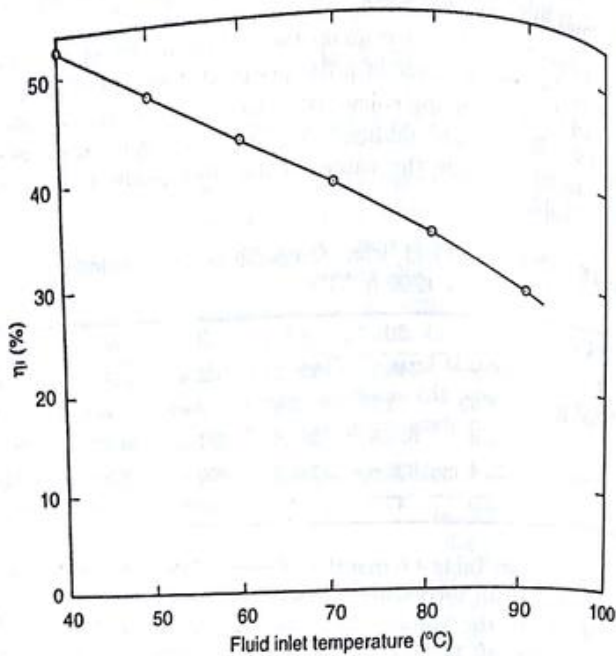


Fig. 4.15 Variation of Efficiency of the GI Collector with Fluid Inlet Temperature (η , Based on Absorber Plate Area)

practical situation, this is not possible. Cleaning is generally done once every few days. For this reason, it is recommended that the incident flux be multiplied by a correction factor which accounts for the reduction in intensity because of the accumulation of dust.

There is, however, considerable difficulty in assigning a value to the correction factor in a specific situation because of its dependence on a number of parameters. The value depends obviously on the location of the collector and the time of the year. It also depends upon the material of the cover (glass or plastic), the tilt of the collector and the frequency of cleaning.

The results of two studies are as follows.

For collectors inclined at 30° in Boston, USA, Hottel and Woertz* found a reduction of less than 1 per cent in the transmitted radiation and accordingly recommended a correction factor of 0.99. However this

*H.C. Hottel and B.B. Woertz, "Performance of Flat-plate Solar-heat Collectors", *Trans. ASME*, 64, 51 (1942).

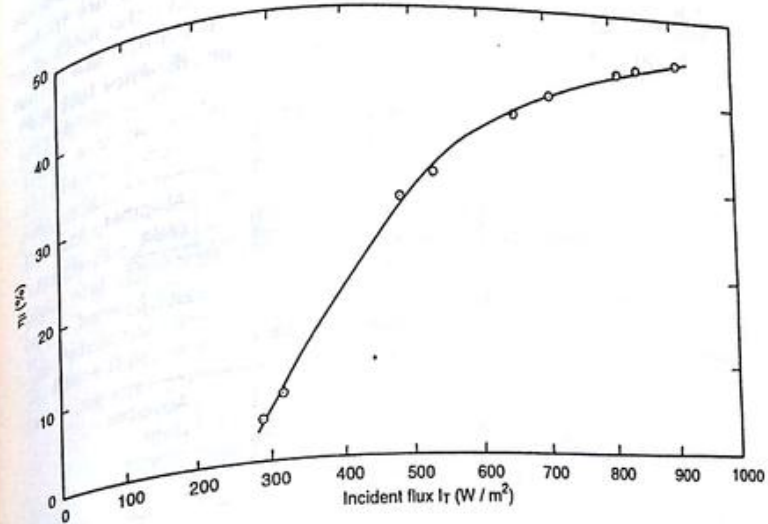


Fig. 4.16 Variation of Efficiency of the GI Collector with Incident Flux. (η , Based on Absorber Plate Area)

recommendation seems to be on the higher side. Garg* conducted studies at Roorkee on glass covers inclined at various angles. The experiments were performed during May and June, which are relatively dusty months. For a collector inclined at 45° , Garg obtained a correction factor of 0.92 for a cleaning frequency of 20 days.

The above two studies represent somewhat extreme situations. In general, a value for the correction factor between 0.92 and 0.99 seems to be indicated.

4.10 ANALYSIS OF COLLECTORS SIMILAR TO THE CONVENTIONAL COLLECTOR

So far we have considered only the conventional liquid flat-plate collector having the geometry of a flat absorber plate with tubes bonded below. We now consider two other types, which are fairly similar to the

*H.P. Garg, "Effect of Dirt on Transparent Covers in Flat-plate Solar Energy Collectors", *Solar Energy*, 15, 299 (1974).

one analysed thus far. In one of these, the tubes are bonded on the side of the absorber plate, while in the other, the tubes are in line with the absorber plate (Fig. 4.17). It can be shown for both these types that the method of analysis is identical to the case considered. The only difference is that different expressions are obtained for the collector efficiency factor.

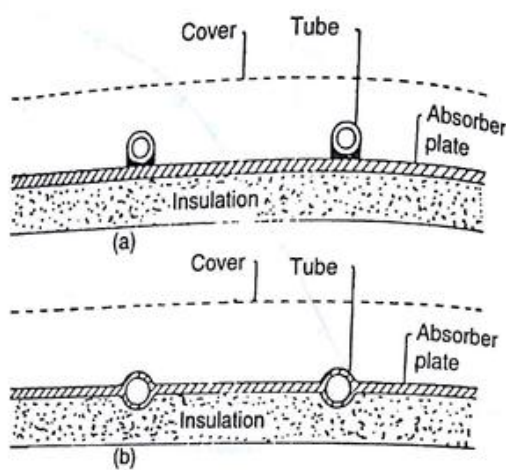


Fig. 4.17 Plate and Tube Flat-plate Collectors (a) Tubes Bonded above Absorber Plate (b) Tubes In-line with Absorber Plate

In the case of tubes bonded above,

$$F' = \frac{1}{WU_l \left[\frac{1}{\left\{ \frac{1}{U_l(W-D_o)\phi} + \frac{\delta_a}{k_a D_o} \right\}^{-1} + U_l D_o} + \frac{1}{\pi D_i h_f} \right]} \quad (4.54)$$

In the case of tubes in line with the absorber plate,

$$F' = \frac{1}{WU_l \left[\frac{1}{U_l((W-D_o)\phi + D_o)} + \frac{1}{\pi D_i h_f} \right]} \quad (4.55)$$

In the second case, there is no term involving the bond (adhesive) resistance because the tubes are usually fabricated integral with the absorber plate.

4.11 TRANSIENT ANALYSIS

The analysis done so far has assumed that a quasi-steady state exists.

Although this is a valid assumption for most situations, there are also some situations which require a transient analysis. Surprisingly very few of these appear to have been studied. We will now consider one type of transient problem. On any day, a collector takes a few hours in the morning to reach its operating temperature, after which it may operate under quasi-steady conditions. Thus, a transient analysis is needed for these hours (from say 7 to 10 a.m.) to consider the heating of the collector from its overnight low temperature to its operating temperature. Following Duffie and Beckman*, we will do an approximate lumped-parameter analysis for a single-cover collector for this situation. We assume that the absorber plate and tubes, the bottom and side insulation, and the water in the tubes have a heat capacity $(mC)_p$ and are at the same temperature T_{pm} , while the cover has a heat capacity $(mC)_c$ and is at a temperature T_c . Since there is no useful heat gain during this period, we obtain the following energy balance equations for the absorber plate and the cover

$$\frac{(mC)_p}{A_p} \frac{dT_{pm}}{dt} = S - \left[h_{p-c}(T_{pm} - T_c) + \frac{\sigma(T_{pm}^4 - T_c^4)}{\left(\frac{1}{\epsilon_p} + \frac{1}{\epsilon_c} - 1 \right)} \right] - (U_b + U_s)(T_{pm} - T_a) \quad (4.56)$$

$$\frac{(mC)_c}{A_p} \frac{dT_c}{dt} = \left[h_{p-c}(T_{pm} - T_c) + \frac{\sigma(T_{pm}^4 - T_c^4)}{\left(\frac{1}{\epsilon_p} + \frac{1}{\epsilon_c} - 1 \right)} \right] - [h_w(T_c - T_a) + \sigma \epsilon_c(T_c^4 - T_{sky}^4)] \quad (4.57)$$

We combine the convective and radiative losses from the top by defining overall coefficients U_{t1} and U_{t2} as follows

$$U_{t1}(T_{pm} - T_c) = h_{p-c}(T_{pm} - T_c) + \frac{\sigma(T_{pm}^4 - T_c^4)}{\left(\frac{1}{\epsilon_p} + \frac{1}{\epsilon_c} - 1 \right)}$$

and $U_{t2}(T_c - T_a) = h_w(T_c - T_a) + \sigma \epsilon_c(T_c^4 - T_{sky}^4)$

Thus, Eqs (4.56) and (4.57) become

$$\frac{(mC)_p}{A_p} \frac{dT_{pm}}{dt} = S - U_{t1}(T_{pm} - T_c) - (U_b + U_s)(T_{pm} - T_a) \quad (4.58)$$

*J.A. Duffie and W.A. Beckman, *Solar Energy Thermal Processes*, John Wiley, New York, 1974.

$$\frac{(mC)_e}{A_p} \frac{dT_c}{dt} = U_{t1}(T_{pm} - T_c) - U_{t2}(T_c - T_a) \quad (4.59)$$

Now in the steady state

$$U_{t2}(T_c - T_a) = U_t(T_{pm} - T_a) \quad (4.60)$$

We assume that this relation holds during the transient state also and that T_a is a constant. Differentiating Eq. (4.60), we have

$$U_{t2} \frac{dT_c}{dt} = U_t \frac{dT_{pm}}{dt} \quad (4.61)$$

Substituting for U_{t2} and $\frac{dT_c}{dt}$ in Eq. (4.59) and then adding Eqs (4.58) and (4.59), we have

$$\frac{1}{A_p} \left[(mC)_p + (mC)_e \frac{U_t}{U_{t2}} \right] \frac{dT_{pm}}{dt} = S - U_t(T_{pm} - T_a) \quad (4.62)$$

The quantity within the square brackets represents an effective heat capacity of the collector and will be denoted by the symbol $(mC)_e$. The differential equation (4.62) can be integrated under the assumption that the values of S and T_a are constants. This is valid if the time interval of the integration is kept reasonably small. Using the initial condition

$$t = 0, T_{pm} = T_{pi}$$

we get

$$\frac{S - U_t(T_{pm} - T_a)}{S - U_t(T_{pi} - T_a)} = \exp \left[- \frac{A_p U_t t}{(mC)_e} \right] \quad (4.63)$$

Equation (4.63) can be used either to find the time taken by the collector to reach the mean plate temperature corresponding to its prescribed fluid inlet temperature or to determine the mean plate temperature after a certain amount of time has elapsed.

Example 4.5

A water-heating flat-plate collector operates at a mean plate temperature of 70°C. Determine the time by which it will reach this temperature if there is no useful heat gain till that time. The following data is given:

Length of absorber plate	= 1.6 m
Width of absorber plate	= 1 m
Number of covers	= 1
Overall loss coefficient	= 7.2 W/m ² ·K
Top loss coefficient	= 6.4 W/m ² ·K
U_{t2}	= 22.8 W/m ² ·K

- (mC) for plate and tubes
- (mC) for insulation
- Volume of water in collector
- (mC) for glass cover
- Mean plate temperature at 6 a.m.

$$\begin{aligned} &= 4.5 \text{ kJ/K} \\ &= 2.0 \text{ kJ/K} \\ &= 2.1 \text{ litres} \\ &= 16 \text{ kJ/K} \\ &= 14^\circ\text{C} \end{aligned}$$

Time a.m.	Flux incident on collector I_t (W/m ²)	Average transmissivity absorptivity product $(\tau\alpha)_{av}$	Ambient temperature T_a (°C)
6-7	30	0.25	14.0
7-8	175	0.50	15.0
8-9	380	0.70	16.0
9-10	555	0.86	18.0
10-11	700	0.89	20.5

Starting with the initial condition at 6 a.m., we apply Eq. (4.63) for intervals of one hour or less.

$$\begin{aligned} (mC)_e &= 4.5 + 2.0 + (2.1 \times 4.18) + \left(16 \times \frac{6.4}{22.8} \right) \\ &= 19.79 \text{ kJ/K} \end{aligned}$$

From 6 to 7 a.m., the absorbed flux

$$S = 30 \times 0.25 = 7.5 \text{ W/m}^2$$

Applying Eq. (4.63),

$$\frac{7.5 - 7.2(T_{pm} - 14)}{7.5 - 7.2(14 - 14)} = \exp \left[- \frac{1.6 \times 1 \times 7.2 \times 1}{19.79} \times \frac{3600}{1000} \right] = 0.123$$

Therefore

$$T_{pm} \text{ at 7 a.m.} = 14.91^\circ\text{C}$$

Similarly, from 7 to 8 a.m., $S = 87.5 \text{ W/m}^2$ and T_{pm} at 8 a.m. = 25.65°C.

From 8 to 9 a.m., $S = 266 \text{ W/m}^2$ and T_{pm} at 9 a.m. = 49.59°C. Since the temperature at 10 a.m. will cross the operating value, we shall find out the time after 9 a.m. which will be required to reach 70°C. Assuming that the value of $S = 477.3 \text{ W/m}^2$ from 9 to 10 a.m. holds for part of the hour also, we get from Eq. (4.63),

$$\frac{477.3 - 7.2(70 - 18)}{477.3 - 7.2(49.59 - 18)} = \exp \left[- \frac{1.6 \times 1 \times 7.2 \times t}{19.79} \times \frac{3600}{1000} \right]$$

Solving, we get

$$t = 0.42 \text{ h} = 25 \text{ min.}$$

Thus the collector will attain a mean plate temperature of 70°C at 9.25 a.m.

4.12 TESTING PROCEDURES

Finally we will describe certain standard procedures for the testing and rating of collectors. Standardized testing and rating procedures provide an equitable basis for comparing the efficiency of different types of collectors and an essential basis for design and selection and use. The procedure described here has been widely used and was proposed by the National Bureau of Standards (NBS) and the American Society of Heating, Refrigerating, and Air-Conditioning Engineers (ASHRAE).⁴ Essential details are also given in a paper by Hill and Strand.⁵ Recently, this procedure has also been adopted as an ASHRAE Standard 93 (Part 5).⁶

A schematic diagram showing the essential features of the set-up is shown in Fig. 4.18. It is a closed loop consisting of a

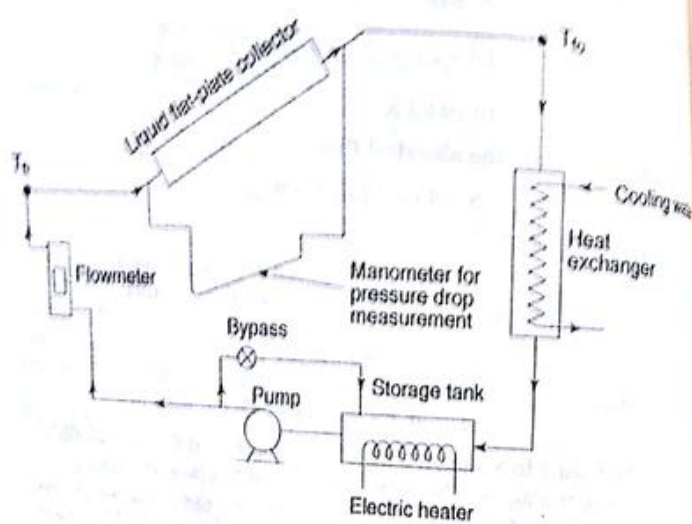


Fig. 4.18 Schematic Diagram of Set-up for Testing Liquid Flat-plate Coagulation

*ASHRAE Standard 93-77, "Method of Testing to Determine Thermal Performance of Solar Collectors" (1977).

J.E. Hill and E.R. Street, "A Method of Testing for Rating Solar Collectors Based on Thermal Performance", *Solar Energy*, 18, 193-199, 1972.

12933 (Part 5): 1992, Bureau of Indian Standards (1992).

collector under test, a liquid pump, a heat exchanger, and a storage tank with an electric immersion heater. A bypass is provided around the pump so that the mass flow rate can be adjusted to the saturation value. The purpose of the heat exchanger is to remove heat. Thus the combination of the heat exchanger and the storage tank (with the electric immersion heater) provide a means for adjusting and controlling the inlet fluid temperature to the collector to a desired value.

The standard specifies that the collector shall be tested under clear sky conditions in order to determine its efficiency characteristics. On any given day, data is recorded under steady state conditions for fixed values of m and T_f . For each set of fixed values, it is recommended that an equal number of tests be conducted symmetrically before and after solar noon. Thus, for example, if data of four tests are recorded, these could be at 1100, 1130, 1230 and 1300 h (LAT). In this way, any bias because of transient effects is eliminated. If such data is recorded for four inlet temperatures on different days, then a total of 16 data sets are obtained. This is the minimum number recommended.

The principal measurements made in each data set are the fluid flow rate (m), the fluid inlet and outlet temperatures of the collector (T_{in} and T_{out}), the solar radiation incident on the collector plane (I_T), the ambient temperature (T_a), the pressure drop across the collector (Δp), and the wind speed (V_w). The efficiency is calculated from the equation

$$\eta_i = \frac{q_a}{A_c I_T} = \frac{\dot{m} C_p (T_{fo} - T_{fi})}{A_c I_T} \quad (4.64)$$

As stated earlier, readings are recorded under steady state conditions. A collector is considered to be operating under steady state conditions if the deviation of the experimental parameters is less than the following specified limits over a 15 minute period:

- | | |
|--|-------------------------|
| • Global radiation incident on collector plane | $\pm 50 \text{ W/m}^2$ |
| • Ambient temperature | $\pm 1^\circ\text{C}$ |
| • Fluid flow rate | $\pm 1\%$ |
| • Fluid inlet temperature | $\pm 0.1^\circ\text{C}$ |
| • Temperature rise across collector | $\pm 0.1^\circ\text{C}$ |

In addition, it is specified that the value of I_T should be greater than 600 W/m^2 , the wind speed should be between 3 and 6 m/s, and the fluid flow rate should be set at approximately 0.02 kg/s per square metre of collector gross area. It is to be noted that although the procedure suggested is for outdoor testing, it is also applicable for indoor testing with a solar simulator.

The efficiency values calculated from Eq. (4.64) are plotted against the parameter $(T_{fi} - T_a)/J_T$. The reason for doing this is apparent if one considers the Hottel-Whillier-Bliss equation. Dividing both sides of Eq. (4.48) by $A_J J_T$, we have

$$\eta_i = F_R \left(\frac{A_p}{A_c} \right) \left[\frac{S}{I_T} - U_l \frac{(T_{fi} - T_a)}{I_T} \right] \quad (4.67)$$

We put

$$S = I_T(\tau\alpha)_{av}$$

where $(\tau\alpha)_{av}$ is an average transmissivity-absorptivity product for both beam and diffuse radiation. Hence

$$\eta_i = F_R \frac{A_p}{A_c} \left[(\tau\alpha)_{av} - U_l \frac{(T_{fi} - T_a)}{I_T} \right] \quad (4.67)$$

Since the values of F_R , $(\tau\alpha)_{av}$ and U_l are essentially constant, it is seen from Eq. (4.67) that if η_i is plotted against $(T_{fi} - T_a)/I_T$ a straight line with a negative slope would be obtained. The intercept on the y-axis would give the value of $[F_R(\tau\alpha)_{av} A_p/A_c]$, while the slope of the line would give the value of $[F_R U_l A_p/A_c]$.

In Eq. (4.64), the value of η_i is based on the collector gross area. It could be based on the absorber plate area also. In that case, the term (A_p/A_c) would drop out of Eqs (4.65) and (4.67). The intercept on the y-axis would then be $F_R(\tau\alpha)_{av}$ and the slope of the line would be $F_R U_l$.

Experimental values of η_i plotted against the parameter $(T_{fi} - T_a)/I_T$ generally yield straight lines. However, the scatter of the data is always large. A typical set of results obtained by testing a commercially available, conventional collector in the Heat Transfer Laboratory at I.I.T. Bombay is shown in Fig. 4.19. A straight line fitted to the data by the method of least squares has the following equation*

$$\eta_i = 0.572 - 4.796(T_{fi} - T_a)/I_T \quad (4.68)$$

For the given collector, $A_p/A_c = 0.848$.

Thus $F_R(\tau\alpha)_{av} = (0.572/0.848) = 0.675$

and $F_R U_l = 4.796/0.848 = 5.656 \text{ W/m}^2 \cdot \text{K}$

It is to be noted that for liquid flat-plate collectors, changes in mass flow rate do not appreciably affect the performance because of the relatively high value of the liquid side heat transfer coefficient h_f . For this reason, although the efficiency curve of a collector is determined for a particular value of mass flow rate, it can also be used for predicting the behaviour of the collector for other flow rates which differ a little from the value used during testing.

It may also be noted that the practice followed in Europe is to plot

*The efficiency values obtained are a little lower than what one might expect from a good quality collector of this type.

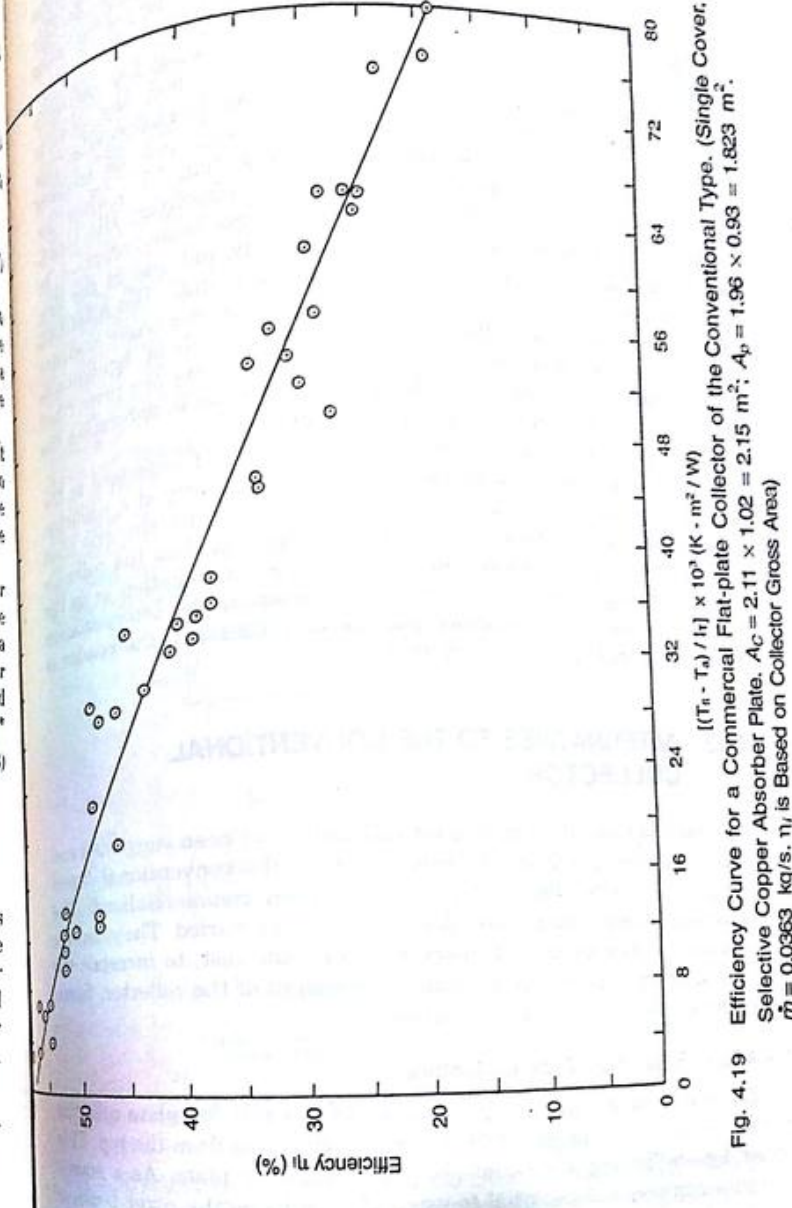


Fig. 4.19

Efficiency Curve for a Commercial Flat-plate Collector of the Conventional Type. (Single Cover, Selective Copper Absorber Plate. $A_c = 2.11 \times 1.02 = 2.15 \text{ m}^2$; $A_p = 1.96 \times 0.93 = 1.823 \text{ m}^2$. $\dot{m} = 0.0363 \text{ kg/s}$. η_i is Based on Collector Gross Area)

the efficiency values against the parameter $(\bar{T}_f - T_a)/I_T$, where \bar{T}_f is the arithmetic mean of the liquid inlet and outlet temperatures. In this case also a straight line is obtained, the intercept on the y-axis being $[F'U_lA_p/A_c]$ and the slope being $(F'U_lA_p/A_c)$.

The standard procedure described for determining the efficiency requires that the tests be conducted on a clear day, close to solar noon, so that the value of I_T would be greater than 600 W/m^2 . As a result the beam radiation component is dominant and the angle of incidence of the beam radiation is small (less than 15°). Thus the $(\tau\alpha)_{av}$ term in the parameter $[F_R(\tau\alpha)_{av}A_p/A_c]$ is effectively the transmissivity-absorptivity product for normal incidence beam radiation. In order to characterise collector performance early and late in the day when the angle of incidence of beam radiation is high, the ASHRAE Standard 93-77 defines a term called the *incidence angle modifier*, K_{ta} which is the ratio of the $(\tau\alpha)$ product at any angle of incidence to the $(\tau\alpha)$ product at normal incidence. Additional tests are prescribed to be conducted at angles of incidence up to 60° so as to determine the dependence of K_{ta} on the angle of incidence.

One more parameter of interest in the testing of collectors is the *time constant*, which is a measure of the heat capacity of a collector. The time constant is defined as the time required for the exit fluid temperature T_{fo} to change by a prescribed amount when the collector is subjected to a step change in the incident solar radiation or in the inlet fluid temperature. For more details regarding the determination of the incidence angle modifier and the time constant, the reader is referred to ASHRAE Standard 93-77.

4.13 ALTERNATIVES TO THE CONVENTIONAL COLLECTOR

A number of novel designs of solar collectors have been suggested and developed over the years as alternatives to the conventional liquid flat-plate collector. Some of these have been commercialised. The objectives in developing these designs have been varied. They include a desire to improve the efficiency, to reduce the cost, to increase the operating temperature, or to reduce the weight of the collector. Some of these designs will now be described.

4.13.1 Evacuated Tube Collectors

One way of improving the performance of a liquid flat-plate collector is to reduce or suppress the heat lost by convection from the top. This is done by having a vacuum above the absorber plate. As a consequence, it becomes essential to use a glass tube as the cover because

only a tubular surface is able to withstand the stresses introduced by the pressure difference.

A number of evacuated tube collector (ETC) designs have been developed. One design consists of a number of long cylindrical flat-plate collector modules side-by-side. Each module (Fig. 4.20a) has a metal absorber plate with two fluid tubes housed in an evacuated, cylindrical glass tube. The absorber plate has a selective surface coating on it. Glass-to-metal seals are provided between the fluid tubes and the end cover of the glass tube. From the point of view of thermal stresses, it is necessary to have these at one end. For this reason, the two tubes are joined at the other end inside the glass cover and form a 'U', with one tube acting as the inlet tube and the other as the outlet tube.

A second design is shown in Fig. 4.20b. Here each module consists of three concentric tubes with the space between the outer two tubes, which are made from glass, being evacuated. The outer surface of the middle tube acts as the absorbing surface and has a selective surface coating on it. The liquid flows in through the innermost metal tube and flows out through the annulus between this tube and the middle tube.

In a third design (Fig. 4.20c), the U tube of Fig. 4.20a is replaced by a heat pipe. The length of the heat pipe inside the evacuated glass tube constitutes the evaporator section in which heat is absorbed and the fluid inside the heat pipe evaporates. The evaporated fluid rises to the condenser section where it condenses. The heat of condensation

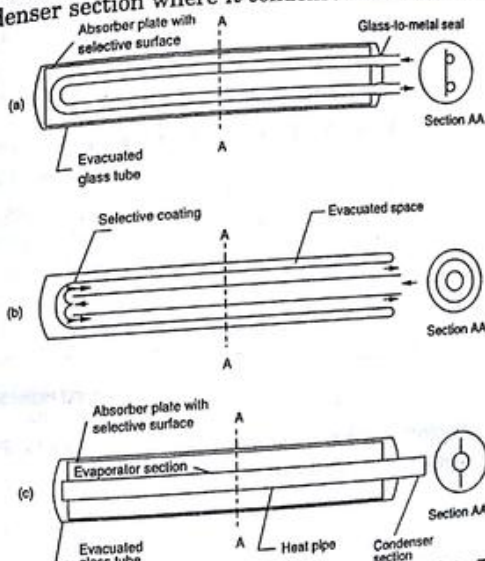


Fig. 4.20 Various Designs of ETC Modules: (a) Flat-plate Type (b) Concentric Tube Type (c) Flat-plate Type with Heat Pipe

is conducted to the fluid flowing in the collector header pipe through an aluminium block clamped on the heat pipe and the header pipe. Two types of layouts are used for the modules in evacuated collectors. In one type, the modules are stacked side-by-side, with a gap between them, while in another, a spacing of a few centimetres is kept between the modules and a back reflector is used. The back reflector may be a plane white surface acting as a diffuse reflector, a curved surface acting as a specular reflector* (Fig. 4.21). Thus the radiation falling on the absorber surface in each module consists of beam and diffuse radiation falling directly as well as the radiation reflected from the back reflector.

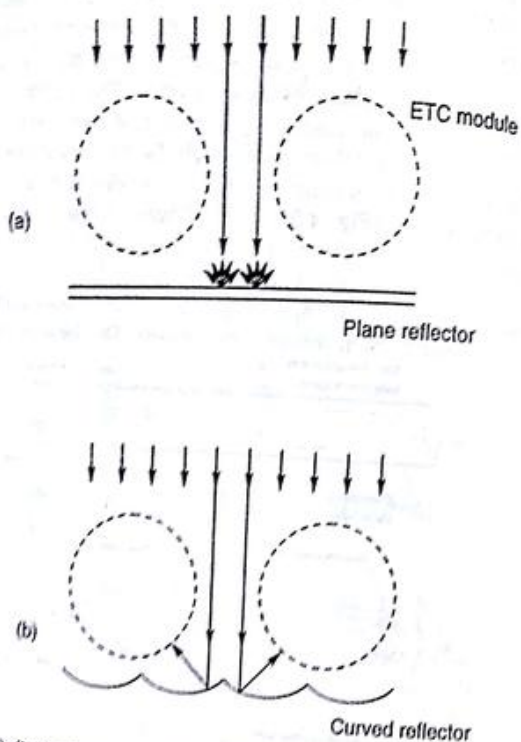


Fig. 4.21 Reflectors used in Evacuated Tube Collectors (a) Plane Diffuse Reflector (b) Curved Specular Reflector

⁴In some commercial ETCs, the curved surface is a truncated CPC reflector (see Sec. 6.4).

In commercially available versions of ETCs, the collector gross area is usually about 2 m^2 . The diameter of the evacuated glass tube of a module is 6 or 7 cm and it is 1.5 to 2 m long. The number of modules used in a collector depends upon whether the modules are stacked side-by-side or stacked apart, and ranges from 10 to 20. Because of the suppression of convection and the provision of a selective surface, the overall loss coefficient of an ETC is low. Consequently its efficiency is significantly higher than that of a conventional collector at high inlet fluid temperatures. A typical performance plot obtained on a commercially available ETC using heat-pipe modules and curved surface back reflectors is given in Fig. 4.22. A straight line fitted to the data yields the following equation for the efficiency based on the gross collector area

$$\eta_i = 0.527 - 1.736(T_{fi} - T_a)/I_T \quad (4.69)$$

A comparison of Eqs (4.69) and (4.68) shows that the efficiency of the ETC tested is nearly twice the efficiency of the conventional collector when the value of $(T_{fi} - T_a)/I_T = 0.08 \text{ K-m}^2/\text{W}$. It may be noted that an ETC of the same type having modules stacked side-by-side with no spacing would yield a higher efficiency. Its performance characteristic is likely to be a straight line with essentially the same slope as in Eq. (4.69) but with a higher intercept on the ordinate axis.

Evacuated tube collectors are very expensive compared to conventional flat-plate collectors and cost more than Rs 10 000 per m^2 . Thus it is possible to consider using them only at high fluid temperatures, in the range of 100 to 130°C.

4.13.2 The Transparent Insulation Honeycomb Collector

The low efficiency of conventional flat-plate collectors at high temperatures (around 100°C) is mainly due to the high heat losses through the collector cover. These heat losses can be reduced by interposing a transparent insulation in the form of a thin-walled honeycomb structure between the absorber plate and the cover. Fig. 4.23 is a sketch of such a collector. The honeycomb structure is made from glass or plastic materials like polymethyl-methacrylate, polycarbonate or polyethylene. The two main types of structures are arrays of capillary tubes and square (or rectangular) cross section cells. Typically the hydraulic diameter of the openings are 3 or 4 mm, the thickness of the walls is about 100 µm with glass and 20 µm with plastics, and the thickness of the structure is about 10 cm. An air gap of 1 or 2 cm separates the honeycomb from the absorber plate. The presence of the honeycomb effectively suppresses both the convection and the re-radiation losses from the absorber plate to the surroundings. Thus the value of the top

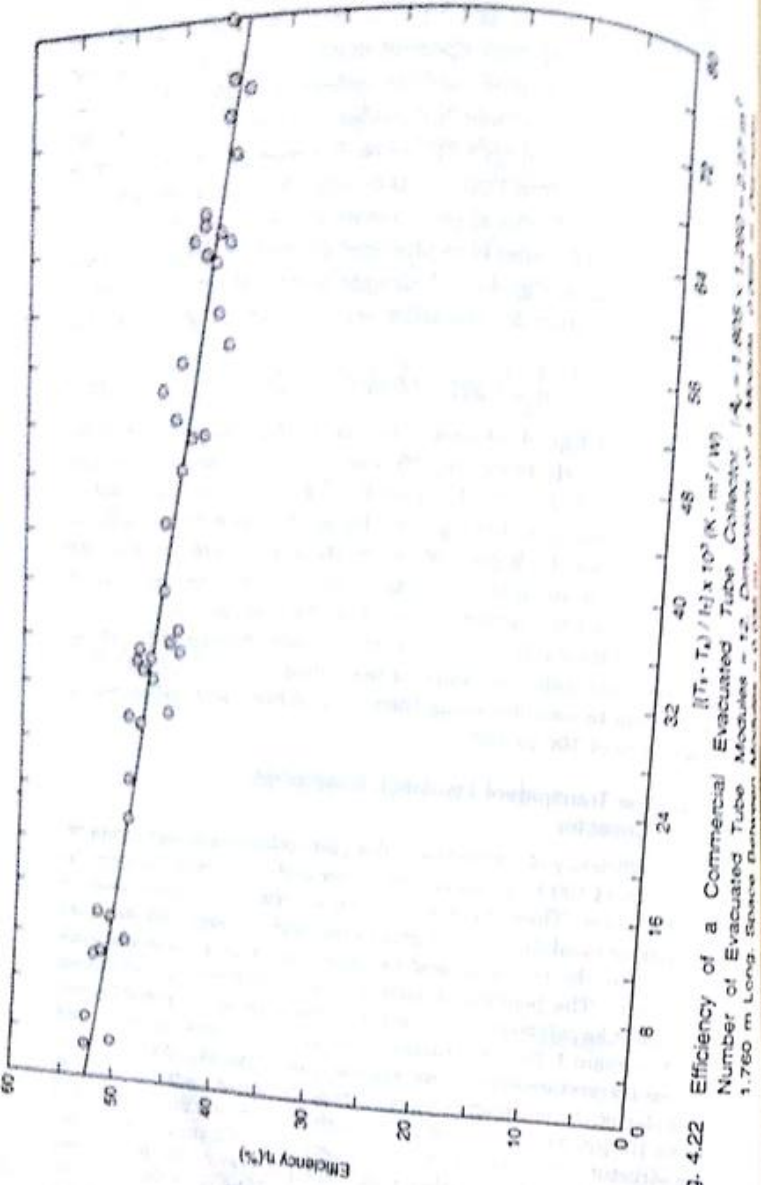


Fig. 4.22

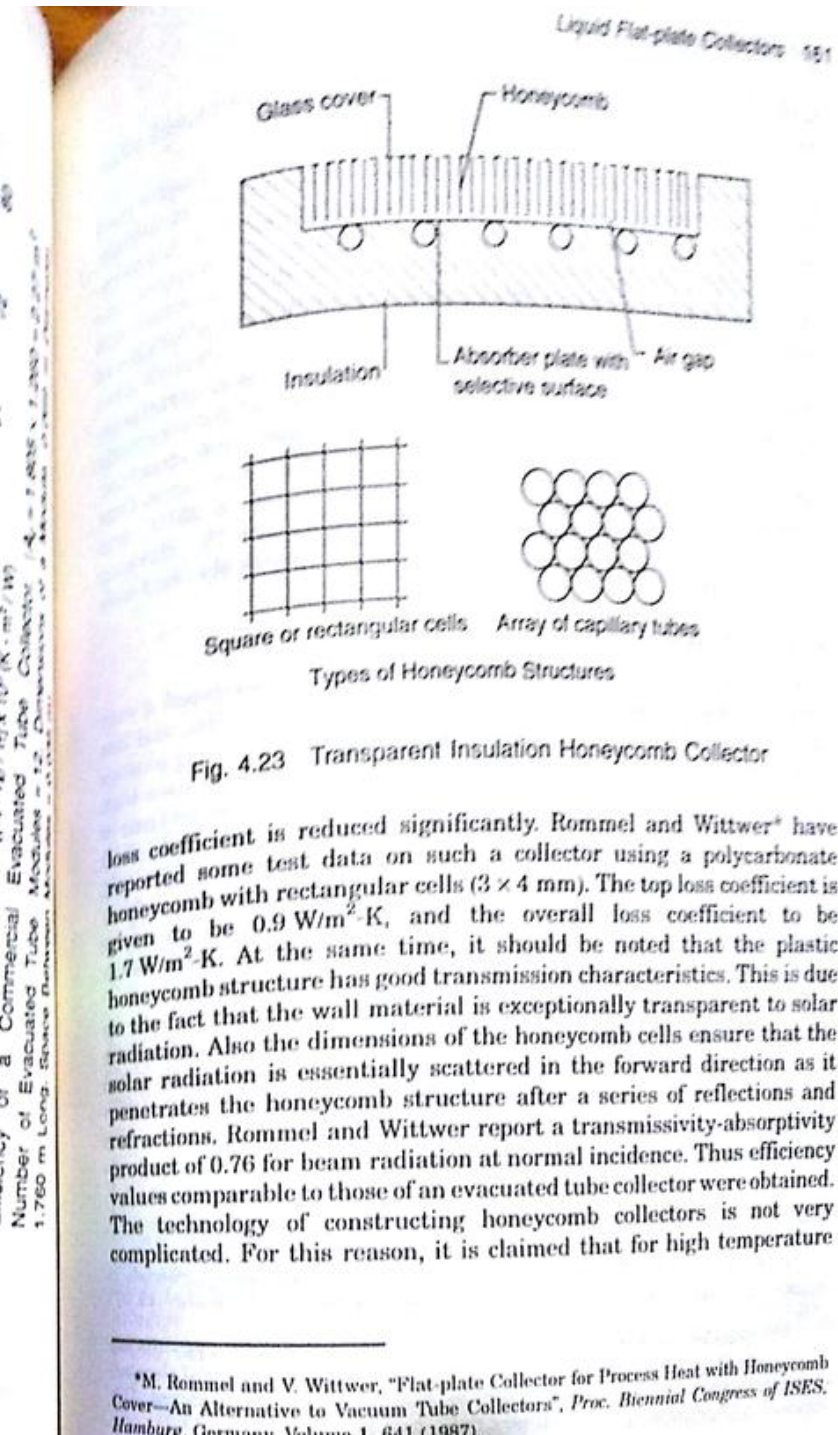


Fig. 4.23 Transparent Insulation Honeycomb Collector

loss coefficient is reduced significantly. Rommel and Wittwer⁸ have reported some test data on such a collector using a polycarbonate honeycomb with rectangular cells (3 × 4 mm). The top loss coefficient is given to be 0.9 W/m²·K, and the overall loss coefficient to be 1.7 W/m²·K. At the same time, it should be noted that the plastic honeycomb structure has good transmission characteristics. This is due to the fact that the wall material is exceptionally transparent to solar radiation. Also the dimensions of the honeycomb cells ensure that the solar radiation is essentially scattered in the forward direction as it penetrates the honeycomb structure after a series of reflections and refractions. Rommel and Wittwer report a transmissivity-absorptivity product of 0.76 for beam radiation at normal incidence. Thus efficiency values comparable to those of an evacuated tube collector were obtained. The technology of constructing honeycomb collectors is not very complicated. For this reason, it is claimed that for high temperature

⁸M. Rommel and V. Wittwer, "Flat-plate Collector for Process Heat with Honeycomb Cover—An Alternative to Vacuum Tube Collectors", *Proc. Biennial Congress of ISES, Hamburg, Germany, Volume 1*, 641 (1987).

applications, honeycomb collectors may be a more economical alternative than evacuated tube collectors.

Although the polycarbonate honeycomb collector has yielded a good performance at high temperatures, it has not yet been commercialised. This is because of its inability to withstand high stagnation temperatures. Polycarbonate honeycombs start melting at temperatures around 120°C. The presence of an air gap between the honeycomb and the absorber plate permits slightly higher operating temperatures of 140°C. In order to operate at still higher temperatures, attempts have been made to manufacture glass capillary honeycomb structures. These have been successful and Rommel and Wagner* have recently reported data on a collector fitted with such a honeycomb structure. The collector used a thermic fluid and the value of T_{fi} was varied from 105 to 180°C. A very high stagnation temperature of 261°C was recorded for an incident flux $I_T = 999 \text{ W/m}^2$ and $T_a = 24.3^\circ\text{C}$. However the efficiency values were a little lower than the values obtained with the polycarbonate honeycomb collector.

4.13.3 The BNL Collector

The Brookhaven National Laboratory† in USA has developed a very light flat-plate solar collector that is simple in construction and has the potential of low cost because of the use of new engineering plastics like polymer coatings, films and rigid foams. The design uses high performance polymer films for the cover and weather seal portions of the collector. These films are adhesively attached to a bent aluminium sheet frame that mates with a rigid polymer foam core (Fig. 4.24). In the monocoque construction used in the collector, the cover and back weather seal films are thermally shrunk to form tension members against the rigid insulating polymer foam core. This procedure makes the structure rigid and permits an extremely light structure.

Most of the components perform multiple functions in order to minimize material requirements. The transparent cover film functions as a structural tension member as well as an optical window and thermal convection suppressor. The back film performs as a tension member and weather seal, and the polymer foam core performs the function of insulation as well as being a dimensionally stable compres-

*M. Rommel and A. Wagner, "Application of Transparent Insulation Materials in Improved Flat-plate Collectors and Integrated Collector Storages", *Solar Energy*, 49, 371 (1992).

†W.G. Wilhelm and B.D. Ripel, "Low Cost Thin Material Solar Technology—The Key to a Viable Energy Alternative", and V. Mubayi, "Brookhaven National Laboratory Designed Collector - Performance in India", in *Progress in Solar Engineering*, D.Y. Goswami (Editor), Hemisphere Publishing Corp., New York, pp. 209-220 (1987).

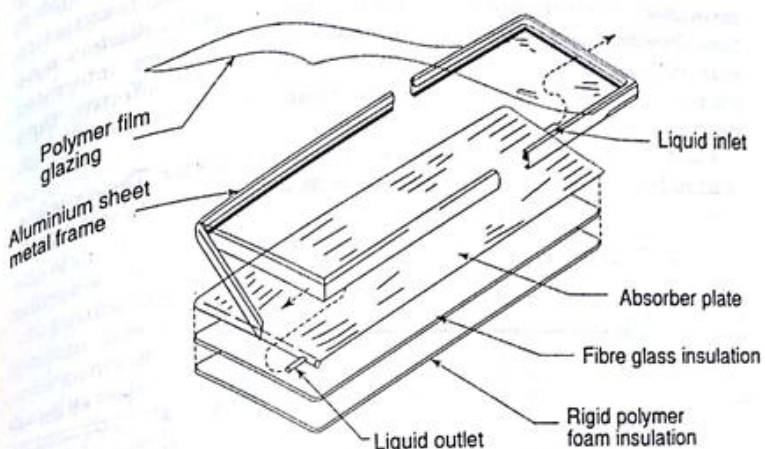


Fig. 4.24 BNL Solar Flat-plate Collector

sion member. These construction techniques with careful selection of engineering polymers have resulted in a light product which has a very high strength-to-weight ratio.

The absorber is a conventional copper sheet with attached tubes and has a selective surface to minimize re-radiation losses. The polymer film used in the cover has an optical band width much wider than glass. This wider band width results in a higher transmissivity and permits more solar energy to reach the absorber. Consequently a high thermal performance is achieved. Test data have been correlated by the following equation

$$\eta_i = 0.75 - 4.54(T_{fi} - T_a)/I_T \quad (4.70)$$

4.13.4 The Concrete Collector

A large amount of metal (copper, aluminium, galvanized iron, etc.) is used in conventional flat-plate collector systems. But studies on the energy inputs required for the production of different materials indicate that metals need a large amount of fossil fuel energy for their production. Furthermore, individual collector modules are connected to form a large array to meet the required demand. Thus, the solar system forms a separate entity, which has its own individual cost and adds dead loads on a building structure. In the long run, it would seem

desirable that solar collectors be made an integral part of building elements, like the roof and wall panels. Thus, the separate solar system investment would be partially merged into the building construction investment. With these facts in mind, concrete solar collectors have been developed and tested at IIT Bombay.* Such collectors integrated with building structures are likely to be more cost effective than conventional collectors for providing domestic hot water even though their collection efficiency would be lower.

Fig. 4.25 shows a cross section of the concrete collector. The absorber (1.31 m long and 0.68 m wide) is made from a thin concrete slab about

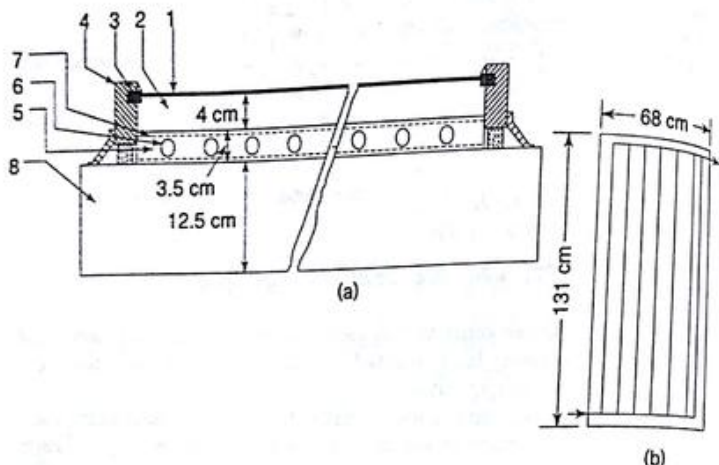


Fig. 4.25 (a) Cross section of Concrete Collector (1. Glass Cover, 2. Air Gap, 3. Rubber Gasket, 4. Wooden Frame, 5. Concrete Slab, 6. PVC Tube, 7. Wire Mesh, 8. Cellular Concrete Insulation)
(b) Schematic of PVC tube Network

3.5 cm thick with a network of 1.7 cm (inner diameter) PVC tubes embedded inside. A layer of galvanized iron wire mesh on either side of the PVC tubes provides reinforcement to the concrete. The top of the slab is painted black with an ordinary black-board paint and glazed. A commercially available slab of cellular concrete (12.5 cm

*J.K. Nayak, S.P. Sukhatme, R.G. Limaye and S.V. Bopshetty, "Performance Studies on Solar Concrete Collectors", *Solar Energy*, 42, 45 (1989).

thick) is used to support the absorber plate. This slab is light-weight and has a low thermal conductivity. Thus, it provides adequate insulation on the back side of the collector. The PVC network is arranged in such a manner that it provides a parallel flow through the individual tubes. The metal mesh reinforcement helps to increase the ability of the concrete to withstand handling stresses. A concrete collector is thermally massive; hence, the concept of instantaneous efficiency does not carry any significant meaning with respect to its thermal performance. On the other hand, the performance is best judged on the basis of the daily efficiency (η), which is defined as the ratio of the useful energy obtained during the day to the total radiation incident on the collector area during the day (H_T).

Extensive tests have been carried out to find out the effect of tube spacings, flow rates and fluid inlet temperatures on the thermal performance of the collector. Of the collectors tested, it has been found that the collector with a pitch of 6 cm, operating at a flow rate of 1.2 lpm gives the best thermal performance.

Typical results of a whole day's testing at a fixed fluid inlet temperature are shown in Fig. 4.26. The figure shows the variation of the useful energy gain and solar flux incident on the collector plane. It is observed that the useful energy of the collector follows the same pattern of variation as that of the solar radiation. However, unlike a conventional collector, the useful energy from the concrete collector is available only after sometime has elapsed in the morning. This is because the concrete collector has a large thermal mass and requires more time to heat up to the operating conditions. For the same reason, the maximum of the useful energy occurs after the maximum of solar flux, the phase lag being about 40 to 45 minutes. Furthermore, the collector continues to deliver useful energy for sometime even after sunset.

Experimental values of the daily efficiency of the collector are plotted against the parameter $(T_{fi} - \bar{T}_a)/H_T$, where T_{fi} is the fluid inlet temperature and \bar{T}_a is the average ambient temperature for the day. It is seen that the daily efficiency varies linearly with $(T_{fi} - \bar{T}_a)/H_T$ and decreases as $(T_{fi} - \bar{T}_a)/H_T$ increases. This behaviour is similar to the dependence of the instantaneous efficiency on the parameter $(T_{fi} - T_a)/I_T$ in the case of a conventional collector. The daily efficiency of a concrete collector can be expressed by an equation of the form

$$\eta = A - B[(T_{fi} - \bar{T}_a)/H_T] \quad (4.71)$$

where A and B are constants. For the collector having a tube pitch of 6 cm and a flow rate of 1.2 lpm, $A = 0.527$ (dimensionless) and $B = 0.239 \text{ MJ/m}^2\text{-day}^{-\circ}\text{C}$.

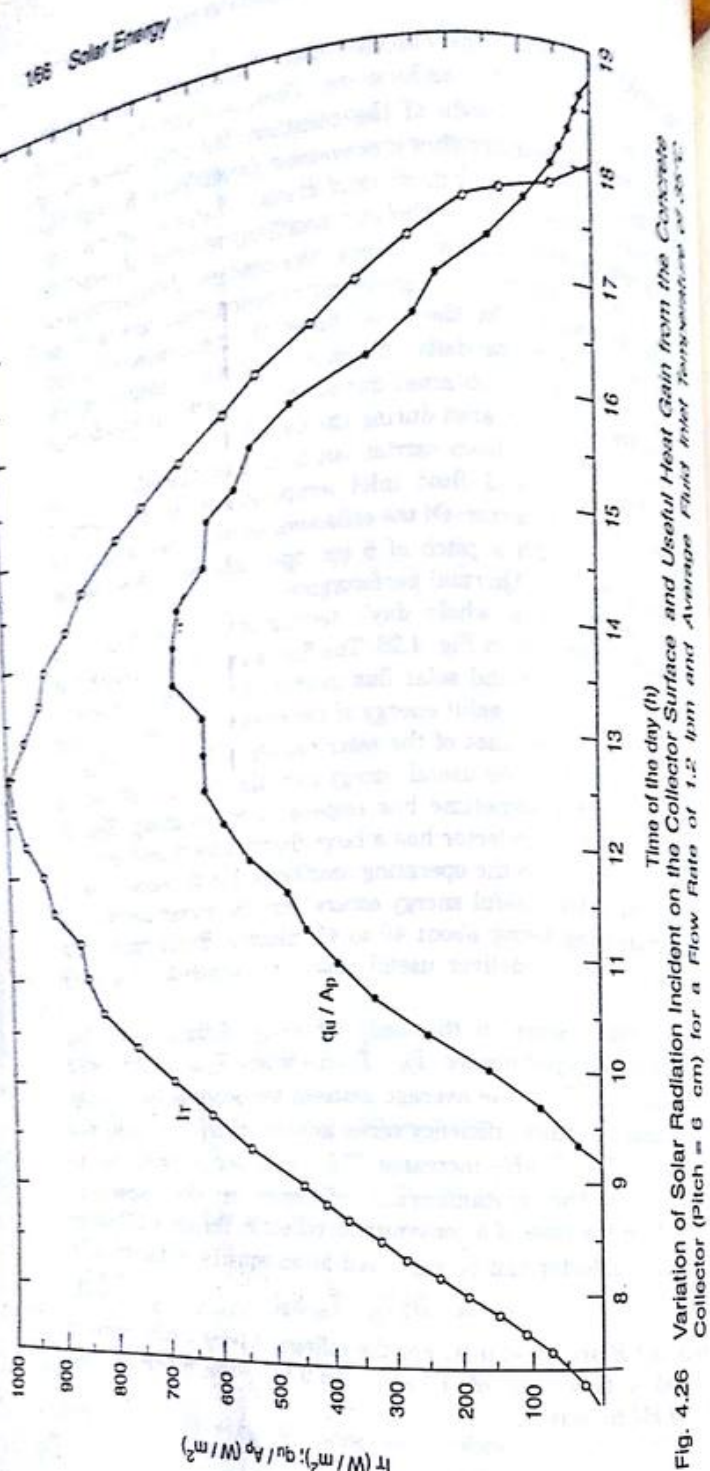
PROBLEMS

1. Prove Eq. (4.6).
 2. Consider absorption and reflection simultaneously and derive the following expression for the transmissivity of a single glass cover
- $$\tau = [(1 - \rho)^2 e^{-KL_c \cos \theta_p}] / [1 - \rho^2 e^{-2KL_c \cos \theta_p}]$$
3. Calculate the transmittance-absorptance product $(\tau\alpha)_b$ for a flat-plate collector with two glass covers each 4 mm thick. The incidence angle is 30° and the value of the extinction coefficient is 0.10 cm^{-1} . Take the value of α for the absorber plate to be 0.86 and the refractive index to be 1.526.
 4. Use Eqs (4.35) and (4.36) to calculate the top loss coefficient for the data of Example 4.2. Take $h_w = 7.04 \text{ W/m}^2\text{-K}$. Compare the answers with the value obtained by the exact procedure adopted in Example 4.2.
 5. Verify the value of $U = 2.56 \text{ W/m}^2\text{-K}$ given in Table 4.2 for the GI collector with the selective absorber plate having $\alpha = 0.95$ and $\varepsilon_p = 0.12$. Take $T_{pm} = 359.3 \text{ K}$ and adopt the iterative procedure.

6. Calculate and comment on the variation of the top loss coefficient of a flat-plate collector as the absorber plate emissivity varies from 0 to 1, given $T_{pm} = 80^\circ\text{C}$, $T_s = 20^\circ\text{C}$, $M = 1$, $\beta = 25^\circ$, $L = 3 \text{ cm}$, $h_w = 10 \text{ W/m}^2\text{-K}$, $\varepsilon_c = 0.88$. Use Eq. (4.36).

7. A liquid flat-plate collector for heating water is made of a non-selective aluminium absorber plate with integral in-line tubes as shown in Fig. 4.17 (b). The following data is given:

Length of absorber plate	= 1.4 m
Width of absorber plate	= 0.755 m
Thickness of absorber plate	= 2 mm
Thermal conductivity of aluminium	= 200 W/m·K
Plate absorptivity/emissivity	= 0.95
Number of glass covers	= 2
Spacing between absorber plate and first glass cover	= 12 mm
Spacing between first and second glass cover	= 12 mm
Tube centre-to-centre distance	= 3.4 cm
Tube outer diameter	= 1.1 cm
Tube inner diameter	= 0.9 cm
Glass cover emissivity/absorptivity	= 0.88
$K\delta_c$	= 0.037 per plate
Index of refraction	= 1.526
Location of collector	= Bombay (19.11°N)
Date	= February 12, 1980
Time	= 1400 h (LAT)
Collector tilt	= latitude angle
Surface azimuth angle	= 0°
I_b	= 645 W/m ²



I_T

Water flow rate	= 142 W/m^2 (assumed uniformly distributed)
Water side heat transfer coefficient	= 33 $\text{W/m}^2\text{-K}$
Water inlet temperature	= 70°C
Ambient temperature	= 36°C
Wind speed	= 1.25 m/s
Back insulation thickness	= 9 cm
Side insulation thickness	= 5 cm
Insulation thermal conductivity	= 0.05 W/m-K

Calculate the instantaneous efficiency based on the absorber plate area and the exit temperature of the water.

8. (a) Calculate the variation in efficiency of a liquid flat-plate collector with the inlet temperature. Given:

Geometry of collector	= Absorber plate with tubes bonded below
Width of plate	= 2 m
Length of plate	= 2 m
Plate thickness	= 1.2 mm
Plate material	= Aluminium ($k = 210 \text{ W/m-K}$)
Tube material	= Aluminium
Tube outer diameter	= 15.9 mm
Tube inner diameter	= 12.7 mm
Tube centre-to-centre distance	= 20 cm
Bond resistance	= Negligible
Water inlet temperature	= 20, 50, 80°C
Ambient temperature	= 20°C
Number of glass covers	= 2
$(\tau\alpha)_{av}$	= 0.75
I_T	= 1000 W/m^2
Overall loss coefficient	= 4 $\text{W/m}^2\text{-K}$
Fluid to tube heat transfer coefficient	= 300 $\text{W/m}^2\text{-K}$
Water flow rate	= 90 kg/h

- (b) Calculate the efficiency again if the following changes are made in the data:

Number of glass covers = 1

$(\tau\alpha)_{av}$ = 0.89

U_f = 7.5 $\text{W/m}^2\text{-K}$

Comment on the variations obtained in cases (a) and (b) and compare them with each other. Base the efficiency on the absorber plate area.

- (c) Calculate the collector stagnation temperatures for cases (a) and (b).

9. Derive Eq. (4.53).

10. The following radiation measurements are available for Thiruvananthapuram (8.48°N, 76.95°E):

Month	J	F	M	A	M	J	J	A	S	O	N	D
\bar{H}_s (kW/m^2 day)	5.932	6.356	6.682	6.166	6.490	6.250	5.027	5.559	6.942	5.232	4.954	5.131
\bar{H}_d (kW/m^2 day)	1.770	1.914	2.196	2.617	2.827	2.974	3.133	3.135	2.765	2.557	2.264	2.030

Calculate the optimum tilt of a flat-plate collector for the three situations studied in Example 4.4.

11. Calculate the optimum tilt angle for a flat-plate collector array located at Bombay (19.12°N) if (i) insulation falling over the whole year is to be maximized, (ii) insulation falling for all months excepting July and August is to be maximized. Use the data given in Table A3.3 and A3.4. Comment on the results obtained.

12. Develop a more accurate formulation than the procedure indicated in Sec. 4.9.4 for the optimum tilt problem by considering monthly averages of the hourly variation of beam and diffuse radiation.

13. Extend the transient analysis of Sec. 4.11 to the situation of a flat-plate collector having two glass covers and show that the final result given by Eq. (4.63) still holds true with $(mC)_e$ given by

$$(mC)_e = (mC)_p + (mC)_{c1} U_t \left(\frac{1}{U_{t2}} + \frac{1}{U_{t3}} \right) + (mC)_{c2} \frac{U_t}{U_{t3}}$$

In the above expression, the subscripts $c1$ and $c2$ refer to the inner and outer glass covers respectively, U_{t2} is the overall convective-radiative coefficient based on the temperature difference $(T_{c1} - T_{c2})$, and U_{t3} is the overall coefficient based on the temperature difference $(T_{c2} - T_a)$.

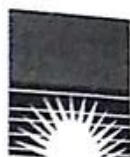
14. A water heating flat-plate collector is fitted with two glass covers and a non-selective absorber plate of dimensions $1 \times 2 \text{ m}$. The collector is tested by the standard procedure described in Sec. 4.12 and the following data is obtained:

T_{f1} (°C)	T_{f2} (°C)	T_a (°C)	I_T (W/m ²)
84.95	93.98	23.0	885
79.97	89.83	22.4	879
75.63	85.51	22.1	862
69.54	79.24	21.6	841
68.19	77.36	21.3	827
50.05	61.19	20.4	819
43.37	54.06	20.4	792
38.17	49.79	19.3	770
33.92	45.44	19.0	761

Given: $(\tau\alpha)_{av} = 0.74$; $\dot{m} = 1.10 \text{ kg/min}$; $C_p = 4.18 \text{ kJ/kg}^{-1}\text{°C}$; $A_c/A_p = 1.2$.

- (a) Calculate the values of η_0 and plot these against the parameter $(T_{\infty} - T_0)$. Draw a best fit straight line and determine the values of U_1 and F_R .
- (b) How does the value of F_R change if the value of m is increased to 1.5 kg/min? Assume that the value of F' does not change significantly because of the increase in m .
15. Compare graphically the efficiency characteristics of the single cover conventional flat-plate collector, Eq. (4.68), with those of the following alternatives described in Sec. 4.13.
- An evacuated tube collector with heat pipe modules and a curved surface heat reflector, Eq. (4.69).
 - A transparent insulation honeycomb collector for which $(\eta_0)_{\text{avg}} = 0.75$, $U_1 = 1.7 \text{ W m}^{-2} \text{ K}$, $F_R = 0.85$ and $(A_c/A_p) = 1.20$.
 - The plastic BNL collector, Eq. (4.70).

Comment on the nature of the graphs obtained.



Five

Solar Air Heaters

This chapter deals with the description and analysis of various types of solar air heaters. The principal applications in which solar air heaters are used are drying for agricultural and industrial purposes, and space heating. Indeed, they are the logical choice for these applications, compared to liquid flat-plate collectors, because they eliminate the need to transfer heat from one fluid to another.

5.1 INTRODUCTION

A conventional solar air heater generally consists of an absorber plate with a parallel plate below forming a passage of high aspect ratio through which the air to be heated flows. As in the case of the liquid flat-plate collector, a transparent cover system is provided above the absorber plate, while a sheet metal container filled with insulation is provided on the bottom and sides. The arrangement is sketched in Fig. 5.1 (a). Two other arrangements, which are not so common, are also shown in Fig. 5.1. In the arrangement shown in Fig. 5.1 (b), the air to be heated flows between the cover and the absorber plate itself instead of through a separate passage, while in Fig. 5.1 (c), the air flows between the cover and the absorber plate, as well as through the passage below the absorber plate.

Like a liquid flat-plate collector, a solar air heater is simple in design and does not

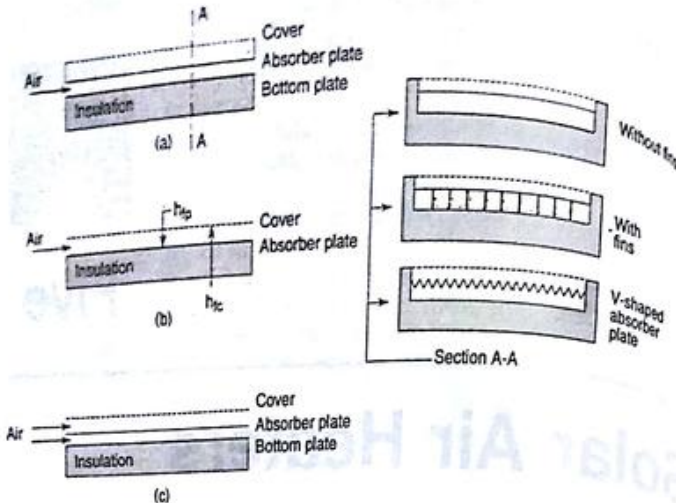


Fig. 5.1 Various Types of Solar Air Heaters

freeze, the solar air heater has the advantage of not requiring any special attention at temperatures below 0°C . Corrosion and leakage problems are also less severe. However, the value of the heat transfer coefficient between the absorber plate and the air is low and this results in a lower efficiency. For this reason, the surfaces are sometimes roughened or longitudinal fins are provided in the air-flow passage. Another variation is to use a V-shaped or corrugated absorber plate [see Sec. A-A, Fig. 5.1 (a)].

A further disadvantage associated with the use of a solar air heater is that large volumes of fluid have to be handled. As a result, the electrical power required to blow the air through a system can be significant if the pressure drop is not kept within prescribed limits.

The face areas of solar air heaters range from 1 to 2 m^2 . Materials of construction and sizes are similar to those used with liquid flat-plate collectors (see Sec. 4.1). Thus, the absorber plate is a metal sheet about 1 mm in thickness, usually made of GI or steel. Glass of thickness 4 to 5 mm is the most commonly used cover material. However, plastics of thickness 5 to 8 cm are being used in increasing numbers. Mineral wool or glass wool of thickness 5 to 8 cm is used for the bottom and side insulation. The whole assembly is contained in a sheet metal box and inclined at a suitable angle.

Compared to liquid flat-plate collectors, the pace of commercialisation for the production of solar air heaters has been slow all over the world. This is true in India as well, where they have been used primarily in systems for forced convection drying of various kinds of agricultural products. Only about 100 such systems have been installed

so far. The reason for the slow pace is the fact that drying of agricultural products is a seasonal activity, requiring energy for only a few months. As a result, the drying systems remain idle for a large part of the year and the economics in terms of the payback period is poor. It seems essential to pursue other applications like drying for industrial purposes and space heating in the northern parts of the country if the market for solar air heaters is to increase.

5.2 PERFORMANCE ANALYSIS OF A CONVENTIONAL AIR HEATER

We now consider the performance analysis of the conventional air heater shown in Fig. 5.1 (a). The heater has an absorber plate of length L_1 and width L_2 . The air flows in a parallel plate passage below the absorber plate. Details are shown in Fig. 5.2.

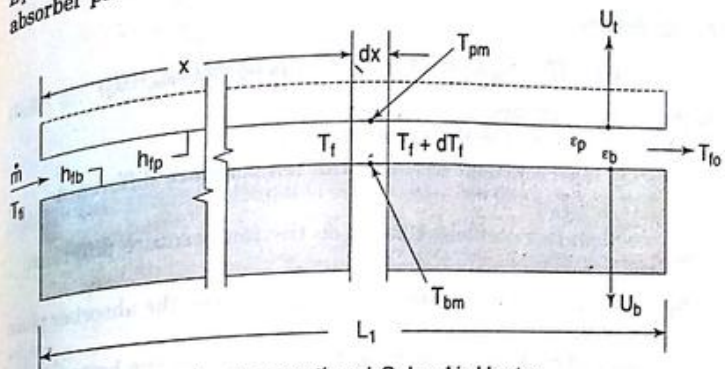


Fig. 5.2 Analysis of a Conventional Solar Air Heater

The analysis is due to Whillier* and proceeds along lines identical to those adopted for the liquid flat-plate collector (Chapter 4) for the calculation of $(\tau\alpha)_b$, $(\tau\alpha)_d$, U_t and U_b . Considering a slice of width L_2 and thickness dx at a distance x from the inlet, we write down energy balances for the absorber plate, the plate below it, and the air flowing in between. We assume that (i) the bulk mean temperature of the air changes from T_f to $(T_f + dT_f)$ as it flows through the distance dx , (ii) the air mass flow rate is \dot{m} , (iii) the mean temperatures of the absorber plate and the plate below are T_{pm} and T_{bm} respectively and their

*A. Whillier, "Black-painted Solar Air Heaters of Conventional Design", *Solar Energy*, 8, 31 (1963).

variation may be neglected, and (iv) side losses can be neglected, the following equations are obtained:

For Absorber Plate

$$SL_2 dx = U_t L_2 dx (T_{pm} - T_a) + h_{fp} L_2 dx (T_{pm} - T_f) + \frac{\sigma L_2 dx}{\left(\frac{1}{\epsilon_p} + \frac{1}{\epsilon_b} - 1\right)} (T_{pm}^4 - T_{bm}^4)$$

For Bottom Plate

$$\frac{\sigma L_2 dx}{\left(\frac{1}{\epsilon_p} + \frac{1}{\epsilon_b} - 1\right)} (T_{pm}^4 - T_{bm}^4) = h_{fb} L_2 dx (T_{bm} - T_f) + U_b L_2 dx (T_{bm} - T_a)$$

For Air Stream

$$\dot{m} C_p dT_f = h_{fp} L_2 dx (T_{pm} - T_f) + h_{fb} L_2 dx (T_{bm} - T_f)$$

In the above equations,

S = flux absorbed in the absorber plate,

U_t = top loss coefficient based on the temperature difference $(T_{pm} - T_a)$,

U_b = bottom loss coefficient based on the temperature difference $(T_{bm} - T_a)$,

h_{fp} = convective heat transfer coefficient between the absorber plate and the air stream,

h_{fb} = convective heat transfer coefficient between the bottom plate and the air stream,

ϵ_p = emissivity of the absorber plate surface, and

ϵ_b = emissivity of the bottom plate surface.

While writing the energy balance Equations (5.1)–(5.3), we distinguish between h_{fp} , the convective heat transfer coefficient for the absorber plate and the air, and h_{fb} , the convective heat transfer coefficient for the bottom plate and the air. However this distinction is usually not made in the correlations available for calculating the convective heat transfer coefficients. Thus while using these correlations, we will have to assume $h_{fp} = h_{fb}$.

We introduce an equivalent radiative heat transfer coefficient h_r defined in this case by

$$h_r (T_{pm} - T_{bm}) = \frac{\sigma}{\left(\frac{1}{\epsilon_p} + \frac{1}{\epsilon_b} - 1\right)} (T_{pm}^4 - T_{bm}^4) \quad (5.4)$$

For small values of the temperature difference $(T_{pm} - T_{bm})$, it is readily shown that the expression $(T_{pm}^4 - T_{bm}^4)$ can be approximated by the expression $4T_{av}^3 (T_{pm} - T_{bm})$ where $T_{av} = (T_{pm} + T_{bm})/2$. Then

$$h_r = \frac{4\sigma T_{av}^3}{\left(\frac{1}{\epsilon_p} + \frac{1}{\epsilon_b} - 1\right)} \quad (5.4a)$$

Further, it is assumed for purposes of simplification that the bottom loss coefficient U_b is much smaller in magnitude than the top loss coefficient U_t . Consequently the bottom loss term can be deleted from Eq. (5.2) and clubbed with the top loss term in Eq. (5.1). Equations (5.1)–(5.3) thus reduce to

$$S = U_t (T_{pm} - T_a) + h_{fp} (T_{pm} - T_f) + h_r (T_{pm} - T_{bm}) \quad (5.5)$$

$$h_r (T_{pm} - T_{bm}) = h_{fb} (T_{bm} - T_f) \quad (5.6)$$

$$\frac{\dot{m} C_p}{L_2} \frac{dT_f}{dx} = h_{fp} (T_{pm} - T_f) + h_{fb} (T_{bm} - T_f) \quad (5.7)$$

From Eq. (5.6), we get

$$T_{bm} = \frac{h_r T_{pm} + h_{fb} T_f}{h_r + h_{fb}} \quad (5.8)$$

Substituting this expression into Eq. (5.5), we have

$$T_{pm} = \frac{S + U_t T_a + h_r T_f}{U_t + h_r} \quad (5.9)$$

$$h_r = \left[h_{fp} + \frac{h_r h_{fb}}{h_r + h_{fb}} \right] \quad (5.10)$$

is an effective heat transfer coefficient between the absorber plate and airstream.

$$\text{Hence, } (T_{pm} - T_a) = \frac{S + h_r (T_f - T_a)}{U_t + h_r}$$

From Eqs (5.5), (5.6) and (5.7), we have

$$\frac{\dot{m} C_p}{L_2} \frac{dT_f}{dx} = S - U_t (T_{pm} - T_a) \quad (5.11)$$

Substituting the expression for $(T_{pm} - T_a)$ into Eq. (5.11), we get the differential equation

$$\frac{\dot{m} C_p}{L_2} \frac{dT_f}{dx} = \frac{1}{\left(1 + \frac{U_t}{h_r}\right)} \left\{ S - U_t (T_f - T_a) \right\} \quad (5.12)$$

In an analogous manner to the liquid flat-plate collector, we now define a collector efficiency factor F' given by

$$F' = \left(1 + \frac{U_l}{h_e}\right)^{-1}$$

Eq. (5.12) thus becomes

$$\frac{\dot{m}C_p}{L_2} \frac{dT_f}{dx} = F'(S - U_l(T_f - T_a)) \quad (5.14)$$

Eq. (5.14) is identical to Eq. (4.44) derived earlier. The solution now proceeds along identical lines and we obtain the fluid temperature distribution

$$\frac{\left(\frac{S}{U_l} + T_a\right) - T_f}{\left(\frac{S}{U_l} + T_a\right) - T_{fi}} = \exp\left[-\frac{L_2 F' U_l x}{\dot{m}C_p}\right] \quad (5.15)$$

Similarly, the useful heat gain rate for the collector is given by

$$q_u = F_R A_p [S - U_l(T_{fi} - T_a)] \quad (5.16)$$

where F_R = collector heat-removal factor

$$= \frac{\dot{m}C_p}{U_l A_p} \left[1 - \exp\left\{-\frac{F' U_l A_p}{\dot{m}C_p}\right\}\right] \quad (5.17)$$

and A_p = area of the absorber plate = $L_1 L_2$.

It is worth noting that if the simplifying assumption of deleting U_l from Eq. (5.2) and clubbing it with Eq. (5.1) had not been made, we would obtain the following differential equation instead of Eq. (5.14)

$$\frac{\dot{m}C_p}{L_2} \frac{dT_f}{dx} = F'[S - U_l''(T_f - T_a)] \quad (5.18)$$

where U_l'' is an equivalent overall loss coefficient. F' and U_l'' are defined as follows:

$$F' = \left(1 + \frac{U_l'}{h_e}\right)^{-1} \quad (5.19)$$

$$U_l'' = U_l' + \frac{1}{F'} \frac{U_b h_{fb}}{(h_r + h_{fb} + U_b)} \quad (5.20)$$

where

$$U_l' = U_t + \frac{h_r U_b}{(h_r + h_{fb} + U_b)} \quad (5.21)$$

and

$$h_e = h_{fp} + \frac{h_r h_{fb}}{(h_r + h_{fb} + U_b)} \quad (5.22)$$

The useful heat gain rate for the collector is then given by

$$q_u = F_R A_p [S - U_l''(T_{fi} - T_a)] \quad (5.23)$$

where F_R = collector heat-removal factor

$$= \frac{\dot{m}C_p}{U_l'' A_p} \left[1 - \exp\left\{-\frac{F' U_l'' A_p}{\dot{m}C_p}\right\}\right] \quad (5.24)$$

Heat Transfer and Pressure Drop in a Parallel Plate Duct

In order to calculate the performance based on Eq. (5.16) or Eq. (5.23), we need to know the values of the convective heat transfer coefficient with one of the long sides heated and the other insulated. It can be considered to be fully developed if the length-to-equivalent diameter ratio exceeds a value of about 30. The following two correlations are then appropriate if the surfaces are smooth,

$$Nu = 0.0158 Re^{0.8} \quad (5.25)$$

$$Nu = \frac{0.01344 Re^{0.75}}{1 - 1.586 Re^{-0.125}} \quad (5.26)$$

Equation (5.25) is based on the data of Kays,* while Eq. (5.26) has been suggested by Malik and Buelow.† In the above equations, the characteristic dimension is the equivalent diameter d_e given by

$$d_e = \frac{4 \times \text{Cross-sectional area of duct}}{\text{Wetted perimeter}}$$

Properties are evaluated at the arithmetic mean of the fluid inlet and outlet temperature, and the values of h_{fp} and h_{fb} are taken to be equal. Nusselt numbers calculated from Eqs (5.25) and (5.26) agree within 10 per cent for Reynolds numbers ranging from 10 000 to 20 000. These values are normally obtained in solar air heater applications.

The dimensionless pressure drop in the duct can be calculated from the well-known Blasius equation which is valid for smooth surfaces.

$$f = 0.079 Re^{-0.25} \quad (5.27)$$

where f is the friction factor and the characteristic dimension is again the equivalent diameter d_e .

*W.M. Kays, *Convective Heat and Mass Transfer*, McGraw-Hill, New York (1966).

†M.A.S. Malik and F.H. Buelow, "Hydrodynamic and Heat Transfer Characteristics of a Heated Air Duct", *Heliotherapy and Development*, 2, 3 (1975).

Example 5.1

Calculate the performance of a conventional solar air heater with the following data:

- Length of absorber plate = 2 m
- Width of absorber plate = 1 m
- Spacing between absorber plate and bottom plate = 1.5 cm
- Air flow rate = 200 kg/h
- Air inlet temperature = 50°C
- Ambient temperature = 20°C
- Solar flux incident on collector face = 950 W/m²
- $(\tau\alpha)_{av}$ = 0.85
- Top loss coefficient = 6.2 W/m²·K
- Bottom loss coefficient = 0.8 W/m²·K
- $\epsilon_p = \epsilon_b$ = 0.95

Neglect heat loss from the sides.

We will first calculate the value of the convective heat transfer coefficients h_{fp} and h_{fb} . Assuming that the mean fluid temperature T_{fm} is 55°C, the properties of air are

$$\rho = 1.077 \text{ kg/m}^3$$

$$C_p = 1.005 \text{ kJ/kg-K}$$

$$\mu = 19.85 \times 10^{-6} \text{ N-s/m}^2$$

$$k = 0.0287 \text{ W/m-K}$$

$$\text{Equivalent diameter} = \frac{4 \times 1 \times 0.015}{2(1 + 0.015)} = 0.0296 \text{ m}$$

Therefore,

$$\frac{L_1}{d_e} = \frac{2}{0.0296} = 68$$

$$\text{Average air velocity} = \frac{200}{3600 \times 1.077 \times 1 \times 0.015} = 3.439 \text{ m/s}$$

$$Re = \frac{\rho V d_e}{\mu} = \frac{1.077 \times 3.439 \times 0.0296}{19.85 \times 10^{-6}} = 5515$$

Hence, the flow is turbulent and fully developed. Assuming the surfaces to be smooth and using Eq. (5.25), we have

$$Nu = 0.0158 \times 5515^{0.8} = 15.56$$

$$\text{Therefore, } h_{fp} = h_{fb} = 15.56 \times \frac{0.0287}{0.0296} = 15.08 \text{ W/m}^2\text{-K}$$

From Eq. (5.4), the radiative heat transfer coefficient is given by

$$h_r = \frac{\sigma}{\left(\frac{1}{\epsilon_p} + \frac{1}{\epsilon_b} - 1 \right)} (T_{pm} + T_{bm})(T_{pm}^2 + T_{bm}^2)$$

For purposes of calculating h_r , we assume that the mean temperature of the absorber plate and the bottom plate can be taken to be equal to the mean fluid temperature T_{fm} . This is a good assumption since the absolute value of temperature has to be used in calculating h_r , and the values of $(T_{pm} - T_{fm})$ and $(T_{bm} - T_{fm})$ are likely to be small, of the order of 10 K. Thus

$$h_r = \frac{5.67 \times 10^{-8} \times 4 \times (273.2 + 55)^3}{\left(\frac{1}{0.95} + \frac{1}{0.95} - 1 \right)} \frac{1 + T_{av}^3}{\left(\frac{1}{\epsilon_p} + \frac{1}{\epsilon_b} - 1 \right)} = 7.24 \text{ W/m}^2\text{-K}$$

From Eq. (5.10),

$$h_e = 15.08 + \frac{7.24 \times 15.08}{7.24 + 15.08} \quad h_e = \left[h_{fp} + \frac{h_r h_{fb}}{h_r + h_{fb}} \right] = 19.97 \text{ W/m}^2\text{-K}$$

From Eq. (5.13),

$$\text{Collector efficiency factor } F' = \left(1 + \frac{6.2 + 0.8}{19.97} \right)^{-1} = 0.740 \quad F' = \left(\frac{\mu V \epsilon}{h_r} \right)$$

$$\frac{\dot{m} C_p}{UA_p} = \frac{200}{3600} \times \frac{1.005 \times 1000}{7 \times 1 \times 2} = 3.988$$

Hence from Eq. (5.17),

$$\text{Collector heat-removal factor } F_R = 3.988 (1 - e^{-0.740/3.988}) = 0.675$$

$$\text{Useful heat gain rate } q_u = 0.675 \times 1 \times 2 [950 \times 0.85 - 7(50 - 20)] = 806.6 \text{ W}$$

$$\text{Instantaneous efficiency } \eta_i = \frac{806.6}{950 \times 1 \times 2} = 0.425$$

The air outlet temperature is obtained from the energy balance equation

$$\frac{200}{3600} \times 1.005 \times (T_{fo} - 50) = \frac{806.6}{1000}$$

$$\text{Hence } T_{fo} - 50 = 14.45^\circ\text{C and } T_{fo} = 64.45^\circ\text{C}$$

The pressure drop across the collector is calculated from Eq. (5.23). We have

$$f = 0.079 \times 5515^{-0.25} = 0.009167$$

$$\text{Hence pressure drop} = \frac{4f\rho L_1 V^2}{2d_e}$$

$$= \frac{4 \times 0.009167 \times 1.077 \times 2 \times 3.439^2}{2 \times 0.0296}$$

$$= 15.78 \text{ N/m}^2$$

$$= 1.61 \text{ mm of water}$$

Finally, it may be noted that if we use the more correct performance Eqs (5.18) to (5.24), we would obtain the following slightly different results,

$$F' = 0.754$$

$$F_R = 0.686$$

$$q_u = 813.9 \text{ W}$$

$$\eta_i = 0.428$$

and

5.3 OTHER TYPES OF AIR HEATERS

5.3.1 Variations on the Conventional Type

We now describe solar air heaters which are variations on the conventional type. Some of them are shown in Fig. 5.1.

Flow Between the Cover and Absorber Plate

Consider first the air heater of Fig. 5.1 (b) in which the air flows in a parallel plate passage between the cover and the absorber plate. The method of analysis of this type is similar to that adopted for the conventional type. Making the same assumptions as in Sec. 5.2, and writing energy balances for the absorber plate, the cover plate and the air flowing in between, we get

For Absorber Plate

$$S = h_{fp}(T_{pm} - T_f) + h_r(T_{pm} - T_c) + U_b(T_{pm} - T_a) \quad (5.28)$$

For Cover

$$h_r(T_{pm} - T_c) = U_t(T_c - T_a) + h_{fc}(T_c - T_f) \quad (5.29)$$

For Air Stream

$$\frac{\dot{m}C_p}{L_2} \frac{dT_f}{dx} = h_{fp}(T_{pm} - T_f) + h_{fc}(T_c - T_f) \quad (5.30)$$

where

$$h_r = \frac{\sigma}{\left(\frac{1}{\epsilon_p} + \frac{1}{\epsilon_c} - 1\right)} \frac{(T_{pm}^4 - T_c^4)}{(T_{pm} - T_c)} \quad (5.31)$$

In the above equations, values of the convective heat transfer coefficients h_{fc} and h_{fp} would be calculated from either Eqs (5.25) or (5.26). It is also to be noted that the top loss coefficient U_t is based on the temperature difference $(T_c - T_a)$, while the bottom loss coefficient U_b is based on the temperature difference $(T_{pm} - T_a)$. Solving Eqs (5.28)–(5.30), one again obtains Eqs (5.23) and (5.24) for the useful heat gain rate and the collector heat removal factor. However, the equivalent overall loss coefficient and the collector efficiency factor are now given by the following expressions:

$$U_t' = \frac{(U_t + U_b)(h_{fc}h_{fp} + h_{fc}h_r + h_{fp}h_r) + U_t U_b (h_{fc} + h_{fp})}{h_{fc}h_r + h_{fp}U_t + h_{fp}h_r + h_{fc}h_{fp}} \quad (5.32)$$

$$F' = \frac{h_{fc}h_r + h_{fp}U_t + h_{fp}h_r + h_{fc}h_{fp}}{(U_t + h_r + h_{fc})(U_b + h_r + h_{fp}) - h_r^2} \quad (5.33)$$

Solar air heaters of this type are simpler in construction than the conventional design. However, they yield lower efficiencies because of higher losses from the top.

Conventional Air Heater with Continuous Longitudinal Fins

The addition of continuous longitudinal fins to the bottom side of the absorber plate improves the heat transfer. This is desirable because it increases the efficiency. We now analyse such a heater in which fins of height L_f and thickness δ_f are spaced at a distance W centre-to-centre apart (Fig. 5.3). The distance between the absorber plate and the bottom plate is L . Consequently the clearance between the fins and the bottom plate is $(L - L_f)$. Considering a slice of width W and thickness dx at a distance x from the inlet, we again write down energy balances for the absorber plate, the bottom plate, and the air flowing in between. The assumptions made earlier in Sec. 5.2 are again made. We get

$$S W dx = U_t W dx (T_{pm} - T_a) + h_{fp} W dx (T_{pm} - T_f) + 2L_f dx \phi_f h_{ff}(T_{pm} - T_f) + h_r W dx (T_{pm} - T_{bm}) \quad (5.34)$$

$$h_r W dx (T_{pm} - T_{bm}) = h_{fb} W dx (T_{bm} - T_f) + U_b W dx (T_{bm} - T_a) \quad (5.35)$$

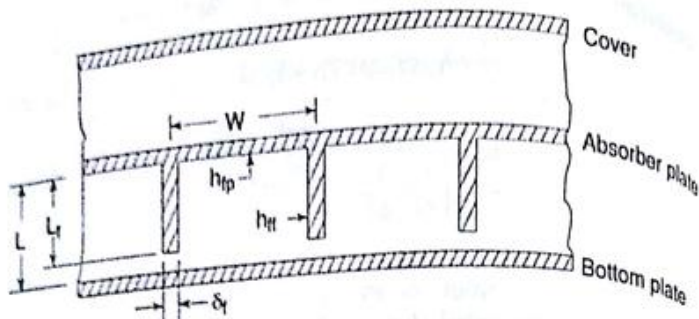


Fig. 5.3 Conventional Air Heater with Fins

$$\frac{W}{L_2} \dot{m} C_p dT_f = h_{fp} W dx (T_{pm} - T_f) + 2L_f dx \phi_f h_{ff} (T_{pm} - T_f) + h_{fb} W dx (T_{bm} - T_f) \quad (5.36)$$

It will be seen that additional terms are introduced in Eqs (5.34) and (5.36) to take account of heat transfer from the fin surfaces.

In these equations,

ϕ_f = fin effectiveness,*

h_{ff} = convective heat transfer coefficient between the fin surface and the air stream,

h_r = equivalent radiative heat transfer coefficient†

As in Sec. 5.2, we delete the bottom loss term from Eq. (5.35) and club it with the top loss term in Eq. (5.34). Eqs (5.34) to (5.36) then simplify to

$$S = U_i (T_{pm} - T_a) + h_{fp} \left(1 + \frac{2L_f \phi_f h_{ff}}{W h_{fp}} \right) (T_{pm} - T_f) + h_r (T_{pm} - T_{bm}) \quad (5.37)$$

$$h_r (T_{pm} - T_{bm}) = h_{fb} (T_{bm} - T_f) \quad (5.38)$$

$$\frac{\dot{m} C_p}{L_2} \frac{dT_f}{dx} = h_{fp} \left(1 + \frac{2L_f \phi_f h_{ff}}{W h_{fp}} \right) (T_{pm} - T_f) + h_{fb} (T_{bm} - T_f) \quad (5.39)$$

Equations (5.37) to (5.39) become the same as Eqs (5.5) to (5.7) if $h_{fp} \left(1 + \frac{2L_f \phi_f h_{ff}}{W h_{fp}} \right)$ is replaced by h_{fp} . Thus, the solutions given in

Eqs (5.16) and (5.17) for the useful heat gain rate and the collector heat removal factor are still valid. The expression for the collector efficiency factor F' is also given by Eq. (5.13) with the effective heat transfer coefficient h_r now being given by

$$h_r = h_{fp} \left(1 + \frac{2L_f \phi_f h_{ff}}{W h_{fp}} \right) + \frac{h_r h_{fb}}{h_r + h_{fb}} \quad (5.40)$$

Whillier has also given an expression for the collector efficiency factor of a finned air heater by neglecting the radiative heat transfer but by considering an absorber plate effectiveness ϕ_p . The two expressions for F' can be shown to be identical if h_r is made equal to zero in one and ϕ_p is made equal to unity in the other.

In order to calculate the performance of a finned solar air heater, correlations are needed for determining the values of the convective heat transfer coefficient and the pressure drop. Thombre and Sukhatme* have conducted extensive experiments for this situation and their data show that the well-known Dittus-Boelter equation is applicable if the clearance-to-spacing ratio $(L - L_f)/(W - \delta_f)$ is less than one or the spacing-to-fin height ratio $(W - \delta_f)/L_f$ is greater than one. These constraints are usually satisfied in practice. The Nusselt Number is then given by

$$Nu = 0.023 Re^{0.8} Pr^{0.4} \quad (5.41)$$

where the characteristic dimension used in the definitions of Nu and Re is the equivalent diameter d_e given by

$$d_e = \frac{4 \times \text{Cross-sectional area of a fin channel}}{\text{Wetted perimeter of a fin channel}} = \frac{4 (WL - \delta_f L_f)}{2 (W + L_f)} \quad (5.42)$$

Properties are evaluated at the arithmetic mean of the air inlet and outlet temperature, and the values of h_{fp} , h_{ff} and h_{fb} are taken to be equal.

The following correlation is developed for calculating the pressure drop

$$f = M Re^{-m} \quad (5.43)$$

where,

$$M = 0.040 [2.058 - \{(L - L_f)/L_f\}^{0.313}] \text{ for } Re < 15000 \\ = 0.033 [1.394 - \{(L - L_f)/L_f\}^{0.408}] \text{ for } Re > 15000$$

*The fin effectiveness is given by $\phi_f = (\tanh m L_f)/m L_f$ where $m = (2h_{ff}/k_f \delta_f)^{1/2}$.

†The procedure for calculating h_r is not described there.

*S.B. Thombre and S.P. Sukhatme, "Turbulent Flow Heat Transfer and Friction Factor Characteristics of Shrouded Fin Arrays with Uninterrupted Fins", *Experimental Thermal and Fluid Sciences*, 10, 288 (1995).

$$m = 0.075[3.40 - \{(L - L_f)/L_f\}^{0.711}] \text{ for } Re < 15000$$

$$= 0.138[1.435 - \{(L - L_f)/L_f\}^{0.773}] \text{ for } Re > 15000$$

f is the friction factor and the characteristic dimension in Re is again the equivalent diameter d_e .

Example 5.2

Consider again the solar air heater of Example 5.1 with continuous longitudinal fins fixed to the bottom side of the absorber plate. Assuming the following additional data:

Centre-to-centre distance between fins	= 2.5 cm
Fin height	= 1.3 cm
Fin thickness	= 0.3 cm

Take the value of the radiative heat transfer coefficient to be the same. Calculate

- (1) air outlet temperature,
- (2) instantaneous efficiency, and
- (3) pressure drop.

We will first use Eq. (5.41) to calculate the values of the convective heat transfer coefficients. Assuming a mean fluid temperature of 60°C for the purpose of evaluating the properties of air, we have

$$\rho = 1.060 \text{ kg/m}^3$$

$$C_p = 1.005 \text{ kJ/kg-K}$$

$$k = 0.0290 \text{ W/m-K}$$

$$\nu = 18.97 \times 10^{-6} \text{ m}^2/\text{s}$$

$$\text{Pr} = 0.696$$

$$\text{Equivalent diameter } d_e = \frac{4(2.5 \times 1.5 - 0.3 \times 1.3)}{2(2.5 + 1.3)}$$

$$= \frac{4 \times 3.36}{7.6}$$

$$= 1.768 \text{ cm}$$

$$\text{Average air velocity} = \frac{200}{3600 \times 1.060 \times 40 \times 3.36 \times 10^{-4}} = 3.900 \text{ m/s}$$

$$Re = \frac{Vd_e}{\nu} = \frac{3.900 \times 1.768 \times 10^{-2}}{18.97 \times 10^{-6}} = 3635$$

Substituting into Eq. (5.41),

$$\begin{aligned} Nu &= 0.023 \times 3635^{0.8} \times 0.696^{0.4} \\ &= 14.035 \end{aligned}$$

$$\begin{aligned} h_{fp} &= h_{ff} = h_{fb} = 14.035 \times \frac{0.0290}{1.768 \times 10^{-2}} \\ &= 23.02 \text{ W/m}^2\text{-K} \end{aligned}$$

Thus

Next we calculate the fin effectiveness assuming that the fins are made of steel ($k = 50 \text{ W/m-K}$).

$$mL_f = \left(\frac{2 \times 23.02}{50 \times 0.3 \times 10^{-2}} \right)^{1/2} \times 1.3 \times 10^{-2} = 0.2277$$

$$\text{Therefore } \phi_f = \frac{\tanh mL_f}{mL_f} = \frac{0.2238}{0.2277} = 0.9830$$

$$\begin{aligned} \text{From Eq. (5.40), the effective heat transfer coefficient } h_e \\ &= 23.02 \left(1 + \frac{2 \times 1.3 \times 10^{-2} \times 0.9830}{2.5 \times 10^{-2}} \right) + \left(\frac{7.24 \times 23.02}{7.24 + 23.02} \right) \\ &= 52.05 \text{ W/m}^2\text{-K} \end{aligned}$$

From this point in the calculation, the equations for a conventional solar air heater are applicable. From Eqs (5.13) and (5.17),

$$F' = \left(1 + \frac{7.0}{52.05} \right)^{-1} = 0.8815$$

$$\frac{\dot{m}C_p}{U_t A_p} = \frac{200}{3600} \times \frac{1.005 \times 1000}{7.0 \times 1 \times 2} = 3.988$$

$$F_R = 3.988(1 - e^{-0.8815/3.988}) = 0.7909$$

$$\begin{aligned} q_u &= 0.7909 \times 1 \times 2 [950 \times 0.85 - 7.0(50 - 20)] \\ &= 945.1 \text{ W} \end{aligned}$$

The air outlet temperature is obtained from the equation

$$\frac{200}{3600} \times 1.005 \times (T_{fo} - 50) = \frac{945.1}{1000}$$

Hence $(T_{fo} - 50) = 16.93^\circ\text{C}$ and $T_{fo} = 66.93^\circ\text{C}$

$$\text{Instantaneous efficiency } \eta_i = \frac{945.1}{950 \times 1 \times 2} = 0.498$$

The pressure drop across the air heater is calculated from Eq. (5.43). We have

$$M = 0.040 \left[2.058 - \left(\frac{0.2}{1.3} \right)^{0.313} \right] = 0.06006$$

$$m = 0.075 \left[3.40 - \left(\frac{0.2}{1.3} \right)^{0.711} \right] = 0.2352$$

$$\text{Therefore } f = 0.06006 \times 3635^{0.2352} = 0.008734$$

$$\text{Pressure drop} = \frac{4 \times 0.008734 \times 1.060 \times 2 \times 3.900^2}{2 \times 0.01768}$$

$$= 31.85 \text{ N/m}^2$$

Comparing these results with those of Example 5.1, we see that the efficiency of the air heater has increased significantly from 42.5 per cent to 49.8 per cent, a gain of 7.3 per cent in absolute terms. However, the pressure drop has also increased by a factor of 2 from 15.78 N/m^2 to 31.85 N/m^2 .

Some experimental studies* on finned solar air heaters are available. These also indicate a substantial improvement in efficiency. However, as seen in Example 5.2, the addition of fins introduces an extra pressure drop. Thus, there is an optimum spacing below which it does not pay to increase the number of fins because of the increased pressure drop.

Two-pass Solar Air Heater

Satcunanathan and Deonarine† have suggested the use of a two-pass solar air heater in order to reduce the losses from the top. They constructed a unit in which the air was first passed between the covers of a two-glass cover heater and then under the absorber plate (Fig. 5.4 (a)). When operated as an open system with inlet air at ambient temperature, it was found that the outer glass cover temperature was lowered by 2 to 5°C and that it operated nearer the ambient temperature. As a result, the losses were reduced and the efficiency of the collector was measured to be 10 to 15 per cent higher than of a conventional heater.

Subsequently Wijeyasundara *et al.*‡ have studied the two-pass concept in greater detail both analytically and experimentally. Two two-pass flow arrangements were considered. One arrangement was the same as the one studied by Satcunanathan and Deonarine (Fig. 5.4 (a)), while in the other, the inlet air flowed first above the absorber plate and then under it (Fig. 5.4 (b)). For open systems, with inlet air at ambient temperature, both the two-pass arrangements gave an efficiency of about 10-15 per cent more than the conventional single pass arrangement.

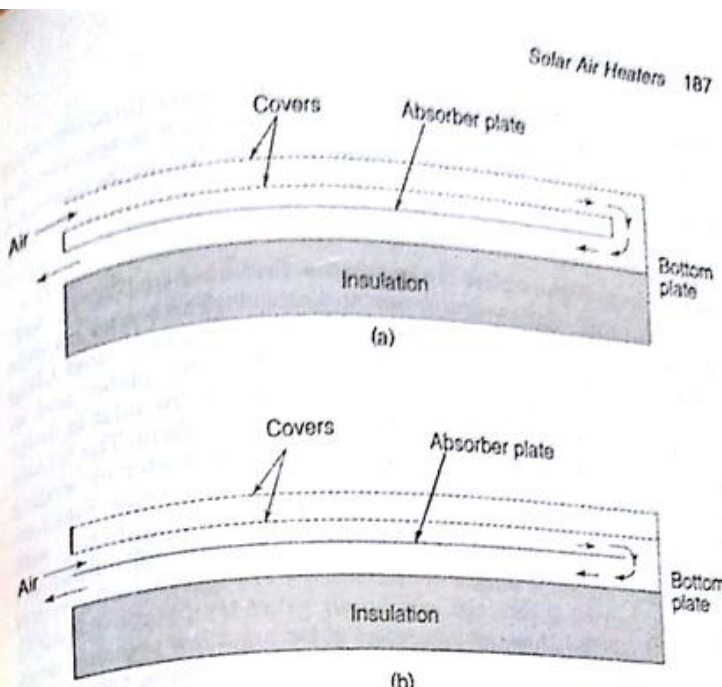


Fig. 5.4 Two-pass Solar Air Heater

ment over a wide range of operating conditions. However, for closed air recirculating systems, the two-pass arrangements yielded a better performance only up to a certain value of the difference between the air inlet temperature to the collector and the ambient temperature. With the arrangement shown in Fig. 5.4 (a), the two-pass design was found to be better than the single pass design up to an inlet air temperature difference of 20°C , while with the arrangement shown in Fig. 5.4 (b), the two-pass design was better up to an inlet air temperature difference of 50°C .

5.3.2 Some Novel Designs

A number of novel designs have also been suggested from time to time by many investigators. Some of these will now be briefly described. They are (i) the overlapped glass plate air heater, (ii) the matrix air heater, (iii) the honeycomb porous-bed air heater, (iv) the all-plastic air heater, and (v) the jet plate air heater. In the first four designs, the air flows through the absorbing surface. For this reason, they are referred to as collectors with porous absorbers. Such collectors generally yield higher efficiencies than conventional designs. In addition, because of larger flow areas, they have smaller pressure drops. In spite of these advantages, they have not been used extensively. A possible deterrent could be the fact that the air flows directly under the cover.

*T.M. Kuzay, M.A.S. Malik and K.W. Boer, "Solar Collectors of Solar One", *Proc. Workshop Solar Collectors Heating Cooling Buildings*, 99 (1974).

†S. Satcunanathan and S. Deonarine, "A Two-pass Solar Air Heater", *Solar Energy*, 15, 41 (1973).

‡N.E. Wijeyasundara, L.L. Ah and I.E. Tjioe, "Thermal Performance Study of Two-pass Solar Air Heaters", *Solar Energy*, 28, 363 (1982).

As a result, a breakage in a glass cover or a cut in a plastic cover would cause a breakdown in the air heating system. The fifth design, viz. the jet plate air heater, also yields a higher efficiency but at the cost of a higher pressure drop.

Overlapped Glass Plate Air Heater

The overlapped glass plate air heater was first used in 1957 by Lof in a residential solar heating system in Colorado. The heater consists of a series of overlapping parallel glass plates, the lower most being blackened (Fig. 5.5). Air flows parallel to the glass plates and is directed by a honeycomb cell passage at the inlet in order to direct the air and to ensure that its velocity is uniform. The bottom of the unit is insulated. Selcuk† has analysed the heater by writing energy balance equations for each glass plate and air stream. Solutions have been obtained by numerical techniques and compared with experimental data. From these it is seen that good efficiencies are obtained for moderate temperature rises. For example, an efficiency of about 60 per cent is obtained with an air outlet temperature of 40°C. The air heater also has the advantage of having a low pressure drop. On the other hand, the area of glass required is excessive, being about four times the collector face area.

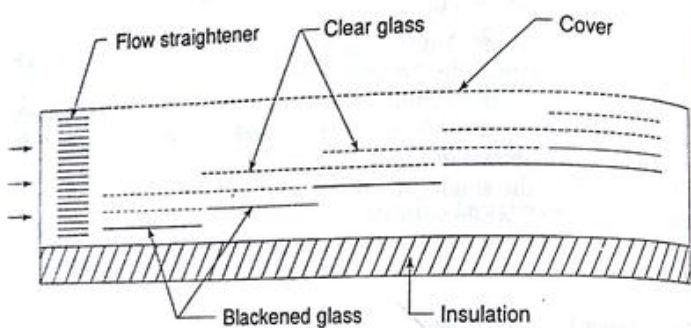


Fig. 5.5 Overlapped Glass Plate Solar Air Heater

Matrix Air Heater

In the matrix air heater, the fluid flows through a porous matrix on which solar radiation is directly incident. The radiation thus

penetrates the matrix and is gradually absorbed. This is quite unlike a conventional non-porous absorber surface in which radiation is only absorbed at the surface. The inlet air is introduced at the top and is heated as it flows down through the matrix (Fig. 5.6). This flow direction is preferred to the other possible arrangement in which the air flows up through the matrix in the reverse manner. The reason for this is that in the first arrangement both the glass cover and the top surface of the matrix are in contact with the incoming air and are thus at the lowest possible temperatures. As a result, top losses are reduced.

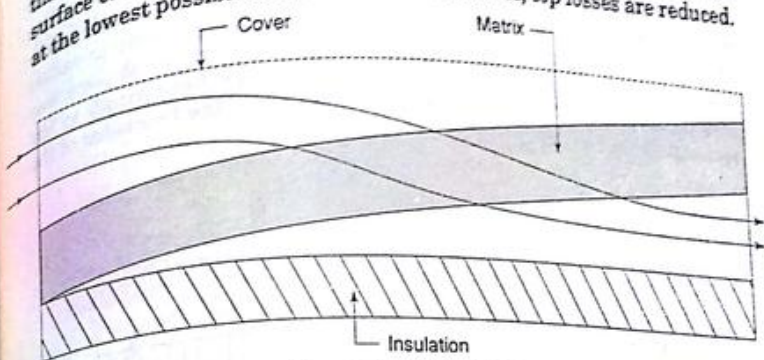


Fig. 5.6 Matrix Air Heater

The matrices used have been made by stacking wire screen meshes or slit-and-expanded metallic foils. Hamid and Beckman* have studied the absorption characteristics and temperature profiles in matrices made by stacking copper wire screens. Heat transfer and pressure drop characteristics of such matrices are available in Kays and London.‡ Characteristics of a number of slit-and-expanded aluminium foil matrices have been obtained by Chiou, El-Wakil and Duffie.‡ Based on their studies, they find a matrix depth of about 4 cm to be adequate. With an inlet air temperature of 21°C, it is estimated that an efficiency of 75 per cent would be obtained with the matrix air heater as opposed to a value of 58 per cent obtained with a conventional solar air heater. The pressure drop in the matrix is also very small. It is estimated to be only (1/200)-times that in the passage of a conventional heater.

*G.O.G. Lof, M.M. El-Wakil and J.A. Duffie, "The Performance of Colorado Solar House", U.N. Conference on New Sources of Energy, Rome (1961).

†M.K. Selcuk, "Thermal and Economic Analysis of the Overlapped Glass Plate Solar Air Heater", *Solar Energy*, 13, 165 (1971).

‡Y.H. Hamid and W.A. Beckman, "Performance of Air-cooled Radiatively Heated Screen Matrices", *J. Eng. for Power, Trans. ASME*, 93, 221 (1971).

‡W.M. Kays and A.L. London, *Compact Heat Exchangers*, McGraw-Hill, New York (1964).

‡J.P. Chiou, M.M. El-Wakil and J.A. Duffie, "A Slit-and-Expanded Aluminium-foil Matrix Solar Collector", *Solar Energy*, 9, 73 (1965).

However, it is to be noted that the above estimates require a uniform flow through the matrix. This is rather difficult to achieve.

Honeycomb Porous-bed Air Heater

The honeycomb porous-bed air heater was suggested by Lalude and Buchberg.* It is a variation on the matrix air heater, a honeycomb being placed over the matrix (Fig. 5.7). Because of the presence of the honeycomb, the top losses are reduced. Measurements made with a test module having a rectangular honeycomb yielded very high collection efficiencies, between 78 and 67 per cent, corresponding to values of $(\bar{T}_f - T_a)/T_f$ equal to 18 and 53 $^{\circ}\text{C}\cdot\text{m}^2/\text{kW}$. The honeycomb used was selectively reflecting, the ratio of the depth of the honeycomb to the smaller side of the rectangle was 7.1, while that of the two sides of the rectangle was 3.4.

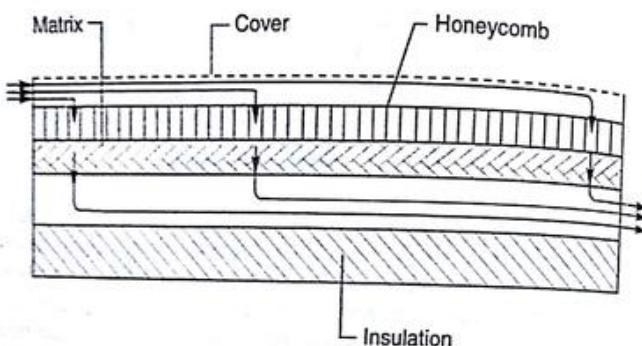


Fig. 5.7 Honeycomb Porous-bed Air Heater

All-plastic Air Heater

All-plastic solar air heaters capable of handling large volumes of air have been developed by Bansal *et al.*† The heaters are fabricated from flexible plastic sheets and attain their shape because of the pressure of the air blown through them. The absorber is a porous black textile of polyester. It is attached at the edges to two transparent sheets of

polyvinyl chloride and is covered by them from both sides (Fig. 5.8). Ring holes are provided at the edges for fixing the stretched heaters on a stand. Three collectors were fabricated and tested, two having an area of about 10 m^2 and the third having an area of about 20 m^2 . All the collectors were about 1 m wide. Different back insulations were tried, best results being obtained with 6 cm thick polyethylene. With this insulation, one of the 10 m^2 heaters gave an efficiency of 67.9% with a flow rate of $770 \text{ m}^3/\text{h}$ of ambient air and incident radiation of 759 W/m^2 .

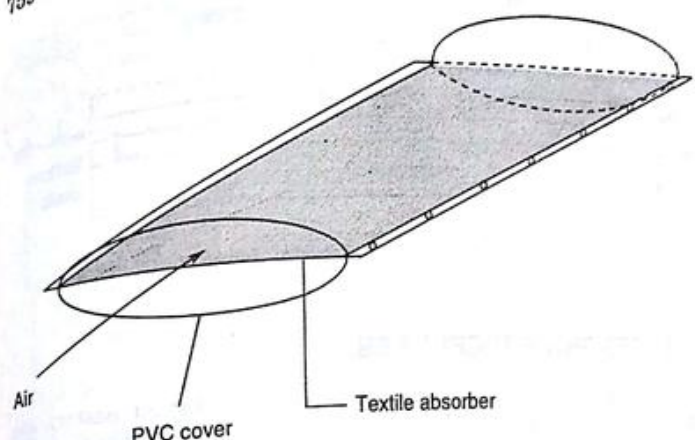


Fig. 5.8 All-plastic Air Heater

Jet Plate Solar Air Heater

The jet plate solar air heater was suggested by Choudhury and Garg.* Compared to the conventional air heater, in this case an additional plate called a jet plate is introduced between the absorber and the bottom plate (Fig. 5.9). The jet plate has a number of equally spaced holes drilled in it. The air entering the heater flows in between the absorber plate and the jet plate (m_2) as well as between the jet plate and the bottom plate (m_1). The flow m_1 impinges out of the holes in the jet plate and hits the bottom of the absorber plate before mixing with the flow m_2 . Thus the flow rate ($m_1 + m_2$) exits from the heater from the space between the absorber plate and the jet plate. The impinging air jets increase the value of the convective heat transfer coefficient from the bottom of the absorber plate. This results in a

*O. Lalude and H. Buchberg, "Design and Application of Honeycomb Porous-bed Solar-air Heaters", *Solar Energy*, 13, 223 (1971).

†N.K. Bansal, R. Uhlemann and A. Boettcher, "Plastic Solar Air Heaters of a Novel Design - Testing and Performance", Report No. 26, Kernforschungs anlage Jülich, Germany (1982).

*C. Choudhury and H.P. Garg, "Evaluation of a Jet Plate Solar Air Heater", *Solar Energy*, 46, 199 (1991).

significant improvement in the useful heat gain and the efficiency. For the specific case of a spacing of 10 cm between the absorber plate and the bottom plate and a flow length of 2 m, the increase in efficiency was calculated to be 26.5 per cent for a mass flow rate per unit area of 50 kg/h-m^2 . However, the authors have not calculated the additional pressure drop associated with the introduction of the jet plate. This is also likely to be significant.

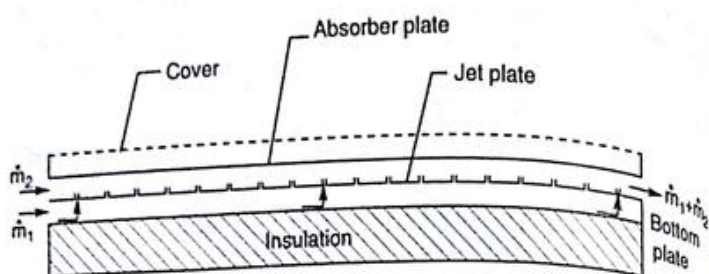


Fig. 5.9 Jet Plate Solar Air Heater

5.4 TESTING PROCEDURES

The standard procedures suggested for testing solar air heaters are similar in most respects to those described in Sec. 4.12 for testing liquid flat-plate collectors. A schematic diagram showing the essential features of the test set-up is shown in Fig. 5.10. It is a closed loop consisting of the solar air heater to be tested, a blower and an apparatus for reconditioning the air which ensures that the air enters the air heater at the desired temperature T_f . Provision is made for measuring the same quantities specified earlier. Some precautions are, however, necessary. Since the fluid is air, it has to be ensured that it is well mixed at the exit from the air heater before its temperature is measured. The mixing is achieved with the help of vanes. As an additional precaution, the temperature both at the inlet and exit of the air heater is measured at a number of locations across the duct cross section.

Measurements are made under the conditions specified earlier and the results are also presented in the same manner. A typical set of results given by Gupta and Garg* is shown in Fig. 5.11. It will be noted that the European practice of plotting the parameter $(\bar{T}_f - T_a)/I_T$ on the

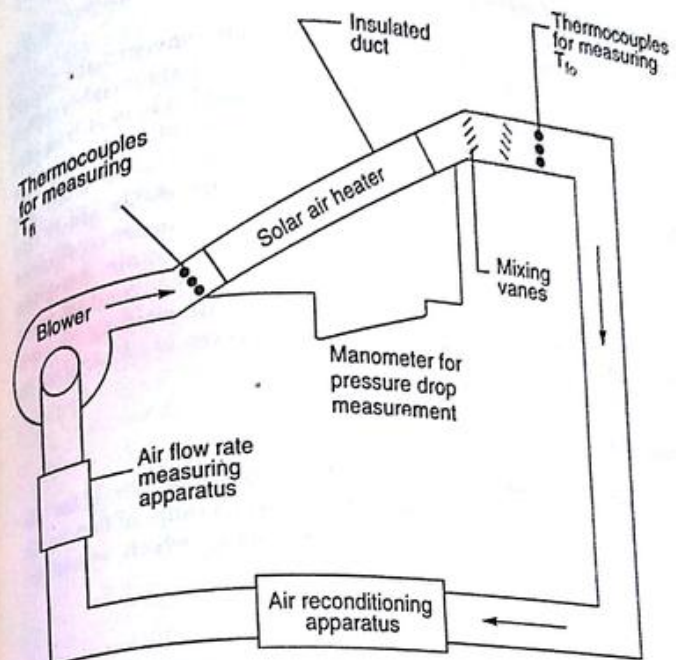


Fig. 5.10 Schematic Diagram of Set-up for Testing Solar Air Heaters

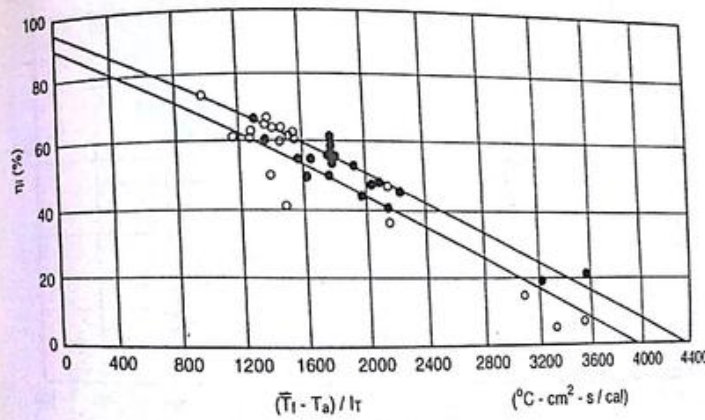


Fig. 5.11 Typical Performance Curves for Two Solar Air Heaters Using Data from Gupta and Garg. Used With

*C.L. Gupta and H.P. Garg, "Performance Studies of Solar Air Heaters", *Solar Energy*, 11, 25 (1967).

x-axis has been followed. It will also be seen that the scatter of the data is again large. It has been mentioned in Sec. 4.12 that for conventional liquid flat-plate collectors, changes in the value of \dot{m} do not appreciably affect the performance because of high values of the liquid side heat transfer coefficient h_f . A single test curve is, therefore, generally adequate for predicting the behaviour of such collectors. In the case of solar air heaters, however, changes in the values of \dot{m} appreciably affect the performance because the value of the air side heat transfer coefficient (h_{fp}) is relatively low. For this reason, in order to obtain complete information on a solar air heater, it becomes necessary to conduct tests over a range of mass flow rates with each flow rate yielding its own efficiency curve. The use of the performance curves is illustrated in Example 5.3.

Example 5.3

The efficiency curves shown in Fig. 5.12 are obtained for a solar air heater ($L_1 = 1.2 \text{ m}$, $L_2 = 0.9 \text{ m}$) which is tested over a range of flow rates varying from 25 to 200 kg/h. Find the efficiency which would be

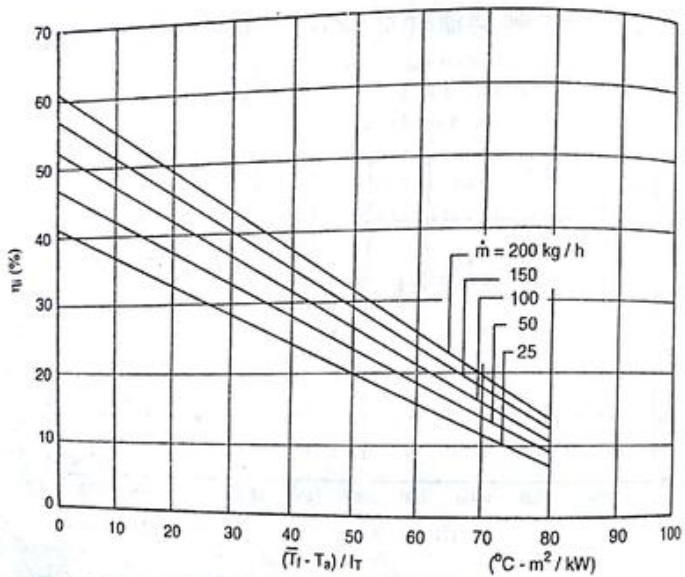


Fig. 5.12 Data for Example 5.2 (η_i is Based on Absorber Plate Area)

obtained and the corresponding mass flow rate if the air heater is used under the following conditions:

Air inlet temperature

= 55°C

Air outlet temperature

= 75°C

Ambient temperature

= 27°C

Solar flux incident on collector face

= 950 W/m²

For the given conditions, the *x*-axis parameter

$$(\bar{T}_f - T_a)/I_T = \left(\frac{55 + 75}{2} - 27 \right) / 0.950$$

$$= 40^\circ\text{C} \cdot \text{m}^2/\text{kW}$$

A trial-and-error procedure will be necessary in order to find the required values of η_i and \dot{m} .

(i) Assume $\dot{m} = 25 \text{ kg/h}$.

From Fig. 5.12, the value of $\eta_i = 24.2$ per cent.

Therefore, useful heat gain rate $q_u = 0.242 \times 950 \times 1.2 \times 0.9$

$$= 248.3 \text{ W}$$

$$\dot{m} = \frac{q_u}{C_p(T_{fo} - T_{fi})} = \frac{248.3 \times 3600}{1.007 \times (75 - 55) \times 1000} = 44.4 \text{ kg/h}$$

(ii) Since the value of \dot{m} calculated from the useful heat gain rate does not match the assumed value, we assume $\dot{m} = 50 \text{ kg/h}$. This yields

$$\eta_i = 28.0 \text{ per cent}$$

$$q_u = 287.3 \text{ W}$$

$$\dot{m} = 51.4 \text{ kg/h}$$

and

(iii) Assume $\dot{m} = 51.4 \text{ kg/h}$.

This yields

$$\eta_i = 28.09 \text{ per cent}$$

$$q_u = 288.3 \text{ W}$$

$$\dot{m} = 51.5 \text{ kg/h}$$

and

We accept these values as the solution to the problem.

PROBLEMS

1. The following data is given for a conventional solar air heater with one glass cover:

Length of absorber plate = 1.90 m

Width of absorber plate = 0.80 m

Spacing between absorber plate and bottom plate = 2 cm

Absorber plate/bottom plate emissivity (for long wavelength radiation (for the surfaces facing each other)	= 0.93
Absorber plate absorptivity for solar radiation	= 0.93
Glass cover thickness	= 3 mm
Refractive index of glass	= 1.526
Extinction coefficient	= 10.5 m^{-1}
Air flow rate	= 440 kg/h
Air inlet temperature	= 48°C
Location of collector	= Madras (13.00° N)
Date	= March 3
Time	= 1230 h (LAT)
Collector tilt	= latitude angle
Surface azimuth angle	= 0°
I_s	= 0.968 kW/m ²
I_d	= 0.195 kW/m ²
Ambient temperature	= 31.5°C
Top loss coefficient	= 4.5 W/m ² ·K
Bottom loss coefficient	= 0.55 W/m ² ·K

- (i) Calculate the instantaneous efficiency, the exit air temperature and the pressure drop. (Assume that the heat transfer surfaces are smooth.)
- (ii) Is it advantageous to have a low or a high value of emissivity (for large wavelength radiation) for the surfaces of the absorber plate?
2. How do the results obtained in Problem 1 change if the heat transfer surfaces in the air duct are roughened? Assume that because of the roughening, the convective heat transfer coefficient increases by 40 per cent, while the friction factor is doubled.
3. How do the results obtained in Problem 1 change if longitudinal steel fins ($k = 50 \text{ W/m}\cdot\text{K}$) are fixed to the bottom side of the absorber plate? Take $W = 2 \text{ cm}$, $L_f = 1.8 \text{ cm}$, and $\delta_f = 1 \text{ mm}$. Assume for the sake of simplicity that the value of the radiative heat transfer coefficient does not change because of the presence of the fins.
4. Calculate the performance of a solar air heater of the type shown in Fig. 5.1(b). Use the data given in Example 5.1 in the text with the following changes/additions:
- Spacing between absorber plate and cover = 1.5 cm
 - Top loss coefficient = 12.7 W/m²·K
 - $\epsilon_c = 0.88$.
- Data regarding the spacing between the absorber plate and bottom plate, and the emissivity of the bottom plate may be deleted as it is not applicable in this case.
5. Derive the governing energy balance equations for the solar air heater shown in Fig. 5.1(c) in which the air flows between the cover and the absorber plate as well as between the absorber plate and the bottom plate.



Concentrating Collectors

In Chapters 4 and 5, we have considered flat-plate collectors for heating liquids and gases to temperatures up to and around 100°C. We now take up the description and analysis of some types of concentrating collectors. These are needed when higher temperatures are required. Typical thermal applications requiring the use of concentrators are medium or high temperature energy conversion cycles and numerous systems for supplying industrial process heat at intermediate temperatures from 100 to 400°C or at high temperatures above 400°C.

Brief descriptions of a few concentrating collectors have been given in Sec. 2.1. We begin this chapter by mentioning briefly the characteristics associated with concentrating collectors (Sec. 6.1). After this, various terms are defined and typical collector geometries described. Flat-plate collectors with reflectors are considered in Sec. 6.2, and the cylindrical parabolic collector in Sec. 6.3. The tracking modes adopted with it are listed and compared, and a performance analysis of the collector is given. The compound parabolic collector is analysed in Sec. 6.4. The chapter concludes with descriptions of the paraboloidal dish collector in Sec. 6.5 and the central receiver collector in Sec. 6.6.

6.1 INTRODUCTION

6.1.1 General Characteristics

Concentration of solar radiation is achieved by using a reflecting arrangement of mirrors or a refracting arrangement of lenses. The optical system directs the solar radiation onto an absorber of smaller area which is usually surrounded by a transparent cover. Because of the optical system, certain losses (in addition to those which occur while the radiation is transmitted through the cover) are introduced. These include reflection or absorption losses in the mirrors or lenses, and losses due to geometrical imperfections in the optical system. The combined effect of all such losses is indicated through the introduction of a term called the *optical efficiency*. The introduction of more optical losses is compensated for by the fact that the flux incident on the absorber surface is concentrated on a smaller area. As a result, the thermal loss terms do not dominate to the same extent as in a flat-plate collector and the collection efficiency is usually higher.

It has been noted earlier that some of the attractive features of a flat-plate collector are simplicity of design and ease of maintenance. The same cannot be said of a concentrating collector. Because of the presence of an optical system, a concentrating collector usually has to follow or "track" the sun so that the beam radiation is directed onto the absorber surface. The method of tracking adopted and the precision with which it has to be done varies considerably. In collectors giving a low degree of concentration, it is often adequate to make one or two adjustments of the collector orientation every day. These can be made manually. On the other hand, with collectors giving a high degree of concentration, it is necessary to make continuous adjustments of the collector orientation. The need for some form of tracking introduces a certain amount of complexity in the design. Maintenance requirements are also increased. All these factors add to the cost. An added disadvantage is the fact that much of the diffuse radiation is lost because it does not get focussed.

In the last few years, significant advances have been made in the development of concentrating collectors and a number of types have been commercialised abroad. Almost all of them are line-focussing cylindrical parabolic collectors, and yield temperatures up to 400°C.

6.1.2 Definitions

In order to be consistent in the use of terms, we will use the phrase "concentrating collector" to denote the whole system. The term "concentrator" will be used only for the optical subsystem which directs the solar radiation onto the absorber, while the term "receiver" will

normally be used to denote the subsystem consisting of the absorber, its cover and other accessories.

We will now define three terms: aperture, concentration ratio and acceptance angle. The *aperture* (W) is the plane opening of the concentrator through which the solar radiation passes. For a cylindrical or linear concentrator, it is characterized by the width, while for a surface of revolution, it is characterized by the diameter of the opening.

The *concentration ratio** (C) is the ratio of the effective area of the aperture to the surface area of the absorber. Values of the concentration ratio vary from unity (which is the limiting case for a flat-plate collector) to a few thousand for a parabolic dish.

The *acceptance angle* ($2\theta_a$) is the angle over which beam radiation may deviate from the normal to the aperture plane and yet reach the absorber. Collectors with large acceptance angles require only occasional adjustments, while collectors with small acceptance angles have to be adjusted continuously.

6.1.3 Methods of Classification

Concentrating collectors are of various types and can be classified in many ways. They may be of the reflecting type utilizing mirrors or of the refracting type utilizing Fresnel lenses. The reflecting surfaces used may be parabolic, spherical or flat. They may be continuous or segmented. Classification is also possible from the point of view of the formation of the image, the concentrator being either imaging or nonimaging. Further, the imaging concentrator may focus on a line or at a point.

The concentration ratio is also used as a measure for classifying concentrating collectors. Since this ratio approximately determines the operating temperature, this method of classification is equivalent to classifying the collector by its operating temperature range.

A final possibility is to describe concentrating collectors by the type of tracking adopted. Depending upon the acceptance angle, the tracking may be intermittent (one adjustment daily or every few days) or continuous. Further, the tracking may be required about one axis or two axes.

6.1.4 Types of Concentrating Collectors

A number of concentrating collector geometries are shown in Fig. 6.1.

*The quantity defined here is more precisely referred to as the area or geometric

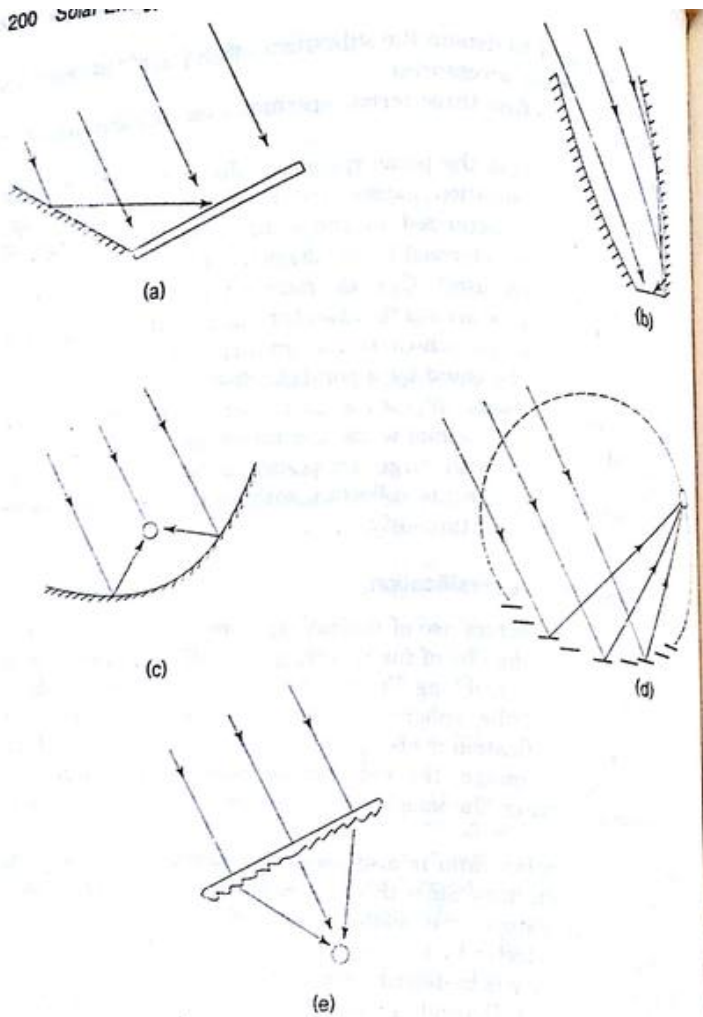


Fig. 6.1 Types of Concentrating Collectors: (a) Flat-plate Collector with Plane Reflectors, (b) Compound Parabolic Collector, (c) Cylindrical Parabolic Collector, (d) Collector with Fixed Circular Concentrator and Moving Receiver, (e) Fresnel Lens Concentrating Collector

The first type shown in Fig. 6.1 (a) is a flat-plate collector with adjustable mirrors at the edges to reflect radiation onto the absorber plate. It is simple in design, has a concentration ratio a little above unity and is useful for giving temperatures about 20 or 30°C higher

than those obtained with a flat-plate collector alone. It is discussed further in Sec. 6.2.

A compound parabolic concentrating collector (CPC) is shown in Fig. 6.1 (b). The concentrator consists of curved segments which are parts of two parabolas. Like the first type, this collector is also nonimaging. The concentration ratio is moderate and generally ranges from 3 to 10. The main advantage of the compound parabolic collector is that it has a high acceptance angle and consequently requires only occasional tracking. In addition its concentration ratio is equal to the maximum value possible for a given acceptance angle. The CPC is considered in Sec. 6.4.

The next type of collector [Fig. 6.1 (c)] is a *cylindrical parabolic collector* in which the image is formed on the focal axis of the parabola. Many commercial versions of this type are now available. For this reason, it is described and analysed in detail in Sec. 6.3.

Unlike the cylindrical parabolic collector in which the concentrator has to rotate in order to track the sun, the type shown in Fig. 6.1 (d) has a fixed concentrator and a moving receiver. The concentrator is an array of long, narrow, flat mirror strips fixed along a cylindrical surface. The mirror strips produce a narrow line image which follows a circular path as the sun moves. This path is on the same circle on which the mirror strips are fixed. Thus, the receiver has to be moved along the circular path in order to track the sun.

Concentration is also achieved by using lenses. The most commonly used device is the *Fresnel lens* shown in Fig. 6.1 (e). The one shown in the figure is a thin sheet, flat on one side and with fine longitudinal grooves on the other. The angles of these grooves are such that radiation is brought to a line focus. The lens is usually made of extruded acrylic plastic sheets. Line focussing collectors like the ones shown in Figs 6.1 (c), (d), (e) usually have concentration ratios between 10 and 80 and yield temperatures between 150 and 400°C.

In order to achieve higher concentration ratios and temperatures, it becomes necessary to have point focussing rather than line focussing. The point focussing *paraboloid dish collector* has been mentioned earlier in Chapter 2 (Fig. 2.4). Such collectors can have concentration ratios ranging from 100 to a few thousand and have yielded temperatures up to 2000°C. However, from the point of view of the mechanical design, there are limitations to the size of the concentrator and hence, the amount of energy which can be collected by one dish. Commercial versions have been built with dish diameters up to 17 m. In order to collect larger amounts of energy at one point, the *central receiver concept* (see Fig. 2.16) has been adopted. In this case, beam radiation is reflected from a number of independently controlled mirrors called heliostats to a central receiver located at the top of a tower.

6.2 FLAT-PLATE COLLECTORS WITH PLANE REFLECTORS

A flat-plate collector with plane reflectors is a simple nonimaging concentrating collector and represents an effective means of getting slightly higher temperatures than are obtainable with a flat-plate collector alone. With a single collector, it is possible to use four reflectors, all around. On the other hand, with an array of flat-plate collectors, it is possible to have only two arrays of reflectors, one of which faces north and the other south (Fig. 6.2). The reflectors used may reflect the radiation in a specular or diffuse manner. The concentration ratios obtained are low and normally range from one to four. Operating temperatures up to 130 to 140°C can be attained. An advantage associated with this type of concentrating collector is that the diffuse component of the incoming solar radiation is not entirely wasted.

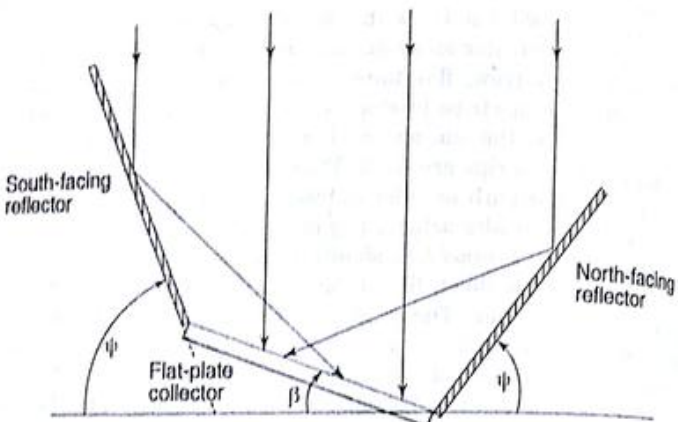


Fig. 6.2 Flat-plate Collector with Reflectors

With an array of flat-plate collectors, the usual practice is to use an array of north-facing reflectors only, since these are more convenient to handle and adjust than south-facing reflectors. The inclination of the reflectors is usually adjusted once every few days. For the case of a north-facing specular reflector array whose dimensions are equal to those of the flat-plate collector array, it can be shown (Chapter 3, Problem 6) that the inclination ψ of the reflectors should be

$$\psi = (\pi - \beta - 2\phi + 2\delta)/3 \quad (6.1)$$

where β = slope of the collectors. Eq. (6.1) is derived under the assumption that the reflector mirrors are adjusted in such a way that

Concentrating Collectors 203

the sun's rays striking the top edge of the mirrors at 1200 h (LAT) are reflected to the top edge of the collectors. If we assume the location to be Bombay and take the collector slope to be equal to the latitude, the value of ψ is found to vary from 25° to 57° as the declination varies from its minimum value of -23.45° to its maximum value of +23.45°. At times other than noon, only a certain fraction of the radiation falling on the reflectors will be reflected usefully onto the collectors with the remaining falling on the sides of the collector. McDaniels et al.,* and Grassie and Sheridan have given results for determining this fraction for the two cases of specular and diffuse reflection. It has also been shown that specular reflectors are more effective in augmenting the radiation than diffuse reflectors.

6.3 CYLINDRICAL PARABOLIC COLLECTOR

6.3.1 Description

The cylindrical parabolic collector is also referred to as a parabolic trough or a linear parabolic collector (refer Photo No. 5). As stated earlier, the basic elements making up a conventional collector are, (i) the absorber tube located at the focal axis through which the liquid to be heated flows, (ii) the concentric transparent cover, and (iii) the parabolic concentrator.

The aperture areas of commercially available collectors range from 1 to 6 m² with the length being larger than the aperture width. Concentration ratios range from 10 to 80, and rim angles (see Fig. 6.4) from 70 to 120°.

The absorber tube is usually made of mild steel or copper and has a diameter of 2.5 to 5 cm. It is coated with a heat resistant black paint and is generally surrounded by a concentric glass cover with an annular gap of 1 or 2 cm. In the case of high-performance collectors, the absorber tube is coated with a selective surface like black chrome and the space between the tube and the glass cover is evacuated. In some collectors, the concentric cover is replaced by a glass or plastic sheet covering the whole aperture area of the collector. Such an arrangement helps in protecting the reflecting surface from the weather.

The liquid heated in the collector depends upon the temperature required. Usually organic heat transfer liquids (referred to as thermic

*D.K. McDaniels, D.H. Lowndes, H. Mathew, J. Reynolds and R. Gray, "Enhanced Solar Energy Collection using Reflector-solar Thermal Collector Combinations", *Solar Energy*, 17, 277 (1975).

†S.L. Grassie and N.L. Sheridan, "The Use of Planar Reflectors for Increasing the Energy Yield of a Linear Parabolic Collector", *Solar Energy*, 19, 663 (1977).

fluids) are used. Because of their low thermal conductivities, these liquids yield low heat transfer coefficients. Augmentative devices in the form of twisted tapes or central plugs (which create annular passages) are therefore used to increase the value of the heat transfer coefficient.

The reflecting surface is generally curved back silvered glass. Thin electropolished anodized aluminium sheets and silver coated acrylic films have also been used.

The reflector is fixed on a light-weight structure usually made of aluminium sections. The proper design of this supporting structure and of the system for its movement is important, since it influences the shape and orientation of the reflecting surface. Some of the factors to be considered in designing the structure are that it should not distort significantly due to its own weight and that it should be able to withstand wind loads.

Compared to flat-plate collectors, there are very few manufacturers of concentrating collectors all over the world. The volume of production is also low. In India, many experimental collectors have been built and tested. However, commercial manufacture has not yet begun.

6.3.2 Orientation and Tracking Modes

A cylindrical parabolic collector is oriented with its focal axis pointed either in the east-west or the north-south direction. In the east-west orientation, the focal axis is horizontal, while in the north-south orientation, the focal axis may be horizontal or inclined. The various tracking modes, which can be adopted, are as follows:

Mode I

The focal axis is east-west and horizontal. The collector is rotated about a horizontal E-W axis and adjusted once every day so that the solar beam is normal to the collector aperture plane at solar noon on that day.

In this mode, the aperture plane is an imaginary surface with either $\gamma = 0^\circ$ or $\gamma = 180^\circ$. The case of $\gamma = 0^\circ$ occurs when $(\phi - \delta) > 0$, while the case of $\gamma = 180^\circ$ occurs when $(\phi - \delta) < 0$. In order to find the slope β of the aperture plane, we substitute the condition at solar noon, viz. $\omega = 0^\circ$, $\theta = 0^\circ$ in Eq. (3.3). This yields,

$$\beta = (\phi - \delta) \quad \text{for } \gamma = 0^\circ \quad (6.2a)$$

and

$$\beta = (\delta - \phi) \quad \text{for } \gamma = 180^\circ \quad (6.2b)$$

The angle of incidence of the beam radiation on the aperture plane throughout the day is obtained by putting Eqs (6.2a) and (6.2b) in Eq. (3.3). For both cases, $\gamma = 0^\circ$ and $\gamma = 180^\circ$, we obtain the same relation

$$\cos \theta = \sin^2 \delta + \cos^2 \delta \cos \omega \quad (6.3)$$

Mode II

The focal axis is east-west and horizontal. The collector is rotated about a horizontal E-W axis and adjusted continuously so that the solar beam makes the minimum angle of incidence with the aperture plane at all times.

In this mode also, the aperture plane is an imaginary surface with either $\gamma = 0^\circ$ or $\gamma = 180^\circ$. Eq. (3.3) is applicable with $\gamma = 0^\circ$ or 180° . In order to find the condition to be satisfied for θ to be a minimum, we differentiate the right hand side of the resulting equation with respect to β and equate it to zero. Thus, we get

$$\tan(\phi - \beta) = [\tan \delta / \cos \omega] \quad \text{for } \gamma = 0^\circ \quad (6.4a)$$

$$\tan(\phi + \beta) = [\tan \delta / \cos \omega] \quad \text{for } \gamma = 180^\circ \quad (6.4b)$$

and

Equations (6.4a) and (6.4b) can be used for finding the slope of the aperture plane. Eq. (6.4a) corresponding to $\gamma = 0^\circ$ is used if the magnitude of the solar azimuth angle γ_s is less than 90° , while Eq. (6.4b) corresponding to $\gamma = 180^\circ$ is used if the magnitude of the solar azimuth angle is greater than 90° .

The expression for the corresponding minimum angle of incidence is obtained by substituting Eqs (6.4a) and (6.4b) in the appropriate version of Eq. (3.3). For both cases, we obtain

$$\cos \theta = (1 - \cos^2 \delta \sin^2 \omega)^{1/2} \quad (6.5)$$

Mode III

The focal axis is north-south and horizontal. The collector is rotated about a horizontal N-S axis and adjusted continuously so that the solar beam makes the minimum angle of incidence with the aperture plane at all times.

In this mode, the surface azimuth angle $\gamma = +90^\circ$ before noon and -90° after noon. Thus, before noon, Eq. (3.3) becomes

$$\cos \theta = (\sin \phi \sin \delta + \cos \phi \cos \delta \cos \omega) \cos \beta + \cos \delta \sin \omega \sin \beta \quad (6.6)$$

In order to find the condition to be satisfied for θ to be a minimum, we differentiate the right hand side of Eq. (6.6) with respect to β and equate it to zero. Thus, we get

$$\beta = \tan^{-1} \left[\frac{\cos \delta \sin \omega}{\sin \phi \sin \delta + \cos \phi \cos \delta \cos \omega} \right] \quad (6.7)$$

Equation (6.7) is used for finding the slope of the aperture plane at any time before noon. The expression for the corresponding minimum angle of incidence is obtained by substituting Eq. (6.7) in Eq. (6.6), giving

$$\cos \theta = [(\sin \phi \sin \delta + \cos \phi \cos \delta \cos \omega)^2 + \cos^2 \delta \sin^2 \omega]^{1/2} \quad (6.8)$$

After noon, i.e., with $\gamma = -90^\circ$, we would obtain

$$\beta = \tan^{-1} \left[\frac{-\cos \delta \sin \omega}{\sin \phi \sin \delta + \cos \phi \cos \delta \cos \omega} \right]$$

The expression for $\cos \theta$ remains the same.

Mode IV

The focal axis is north-south and inclined at a fixed angle equal to the latitude. Thus, it is parallel to the earth's axis. This orientation is sometimes referred to as a polar mount. The collector is rotated about an axis parallel to the earth's axis at an angular velocity equal and opposite to the earth's rate of rotation (115° per hour). It is adjusted such that at solar noon the aperture plane is an inclined surface facing due south. Thus, putting $\beta = \phi$ and $\omega = 0$ in Eq. (3.6), we get

$$\theta = \delta$$

This is also seen from Fig. 6.3 in which the circle represents the longitude through the location of the collector. At all other times, since the collector is rotated at speed equal to the earth's rate of rotation and about an axis parallel to the earth's axis, it follows that Eq. (6.10) is still valid.

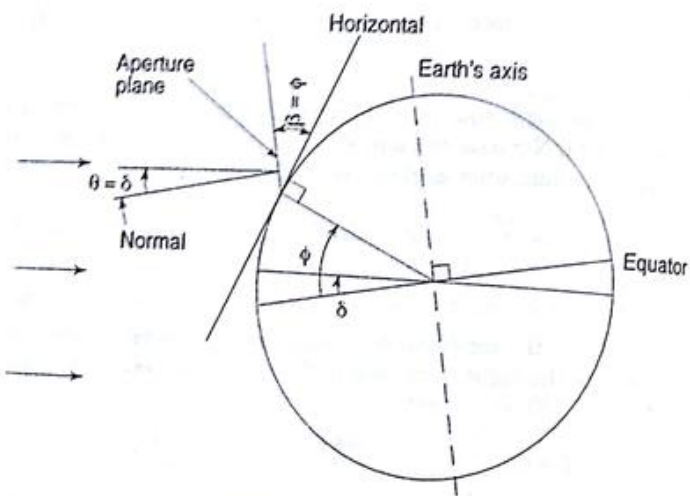


Fig. 6.3 Tracking Mode IV for a Cylindrical Parabolic Collector. Angle of Incidence θ is equal to the Declination δ

Mode V

The focal axis is north-south and inclined. The collector is rotated continuously (but not at a constant angular velocity) about an axis

parallel to the focal axis, as well as about a horizontal axis perpendicular to this axis, and adjusted so that the solar beam is normally incident on the aperture plane at all times. In this situation, obviously $\cos \theta = 1$. It is easy to show that at solar noon,

$$\beta = |\phi - \delta|$$

It is of interest to compare the amounts of beam radiation which would be incident on a collector's aperture plane over a day if one adopted the various tracking modes. This comparison is made through a numerical example.

Example 6.1

A cylindrical parabolic collector is used in New Delhi (28.58° N, 77.20° E). Compare the beam radiation which would fall on one square metre of the aperture plane of this collector from 0600 to 1800 h (LAT) on June 10 for the five tracking modes just described. The following values of I_b are available.

Time (h)	I_b (W/m ²)	Time (h)	I_b (W/m ²)
0630	110	1230	523
0730	240	1330	495
0830	333	1430	445
0930	424	1530	322
1030	495	1630	220
1130	550	1730	118

On June 10, $n = 161$ and $\delta = 23.012^\circ$.

We show a sample calculation for one time, viz. 1030 h. From Eq. (3.5),

$$\cos \theta_z = \sin 28.58^\circ \sin 23.012^\circ + \cos 28.58^\circ \cos 23.012^\circ \cos 22.5^\circ$$

$$= 0.9338$$

For tracking mode I, from Eq. (6.3),

$$\begin{aligned} \cos \theta &= \sin^2 23.012^\circ + \cos^2 23.012^\circ \cos 22.5^\circ \\ &= 0.9355 \end{aligned}$$

Therefore, tilt factor, r_b for the aperture plane

$$= \frac{\cos \theta}{\cos \theta_z} = \frac{0.9355}{0.9338} = 1.002$$

Beam flux incident normally on aperture plane

$$\begin{aligned} &= I_b r_b \\ &= 495 \times 1.002 \\ &= 495.9 \text{ W/m}^2 \end{aligned}$$

Similarly for the other tracking modes we obtain the following results:

	Tracking mode			
	II	III	IV	V
$\cos \theta$	0.9359	0.9980	0.9204	1
r_b	1.0023	1.0688	0.9857	1.0709
$I_b r_b (\text{W/m}^2)$	496.1	529.0	487.9	530.1

The values of $I_b r_b$ obtained over the day are given in Table 6.1. The total incident energy from 0600 to 1800 h is also obtained by adding the values of $I_b r_b$. The assumption made is that the instantaneous value is also the average value for a one hour period. It is seen that the maximum total is obtained with mode V. This is as expected since mode V involves two-axis tracking and gives normal incidence. The other modes involve continuous one-axis tracking or one daily adjustment and yield lesser totals. The results obtained are obviously dependent on the latitude of the location, the day of the year and the input radiation data.

Table 6.1 Comparison of Tracking Modes

LAT (h)	$I_b r_b (\text{W/m}^2)$				
	Mode I	Mode II	Mode III	Mode IV	Mode V
0630	99.1	153.8	360.4	346.1	376.1
0730	230.7	254.5	476.1	445.1	483.6
0830	327.9	335.0	489.0	451.3	490.4
0930	422.3	424.0	511.9	471.2	511.9
1030	495.9	496.1	529.0	487.9	530.1
1130	552.4	552.4	554.0	512.2	556.4
1230	525.3	525.3	526.9	487.0	529.1
1330	495.9	496.1	529.0	487.9	530.1
1430	443.2	445.0	537.2	494.5	537.2
1530	317.0	323.9	472.8	436.4	474.2
1630	211.4	233.2	436.5	408.0	443.3
1730	106.3	165.0	386.6	371.3	403.4
Total (kWh/m^2)	4.227	4.404	5.809	5.399	5.866

In practice, modes II, III and IV are the most common. Mode V is not preferred because of the complexity of providing motion about two axes, while mode I is not used because it does not yield an image on

the focal axis. From a design standpoint, modes II and III are the simpler of the three modes II, III and IV. Since the focal axis is horizontal, it is easy to connect collectors in series (the outlet of one collector being the inlet of the next) and to provide common shaft arrangements for tracking. Land space is also used more effectively in these modes.

6.3.3 Performance Analysis

We now consider the performance analysis of a cylindrical parabolic concentrating collector whose concentrator has an aperture W , length L and rim angle ϕ_r (Fig. 6.4). The absorber tube has an inner diameter

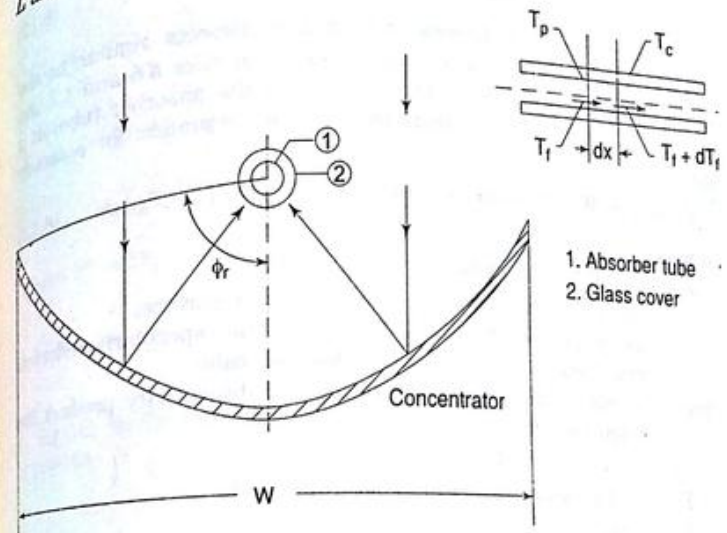


Fig. 6.4 Cylindrical Parabolic Collector in Cross Section

D_i and an outer diameter D_o , and it has a concentric glass cover of inner diameter D_{ci} and outer diameter D_{co} around it. The fluid being heated in the collector has a mass flow rate \dot{m} , a specific heat C_p , an inlet temperature T_{fi} and an outlet temperature T_{fo} .

The collector is operated in any one of the modes described in Sec. 6.3.2 and the beam radiation normally incident on its aperture is I_{b0} , whose value can be calculated from the equations derived in Sec. 6.3.2. In some of the tracking modes, the sun's rays are incident at an angle and will, therefore, come to a focus a little beyond the length of the concentrator. We assume that the absorber tube is long enough to intercept this image. In practice this would mean that the

absorber tube might be a little longer (say about 10 per cent) than the concentrator and that the flux falling on the tube would not be uniform along the length. For the purposes of analysis, however, we will not take into account this extra tube length, and we will assume that the radiation flux is the same all along the length. We will also make the assumption that the temperature drop across the absorber tube and the glass cover are negligible.

The concentration ratio of the collector is given by*

$$C = \frac{\text{Effective aperture area}}{\text{Absorber tube area}} = \frac{(W - D_o)L}{\pi D_o L}$$

$$= \frac{(W - D_o)}{\pi D_o} \quad (6.12)$$

The analysis which follows is in many respects similar to the analysis of a liquid flat-plate collector given in Secs 4.6 and 4.7. An energy balance on an elementary slice dx of the absorber tube, at a distance x from the inlet, yields the following equation for a steady state:

$$dq_u = [I_b r_b (W - D_o) \rho \gamma (\tau \alpha)_b + I_b r_b D_o (\tau \alpha)_b - U \pi D_o (T_p - T_a)] dx \quad (6.13)$$

in which

dq_u = useful heat gain rate for a length dx ,

ρ = specular reflectivity of the concentrator surface,

γ = intercept factor, the fraction of the specularly-reflected radiation intercepted by the absorber tube,

$(\tau \alpha)_b$ = average value of the transmissivity-absorptivity product of beam radiation,

U_l = overall loss coefficient,

T_p = local temperature of absorber tube, and

T_a = ambient temperature.

The first term on the right hand side in Eq. (6.13) represents the incident beam radiation absorbed in the absorber tube after reflection, while the second term represents the absorbed incident beam radiation which falls directly on the absorber tube. The second term is small in comparison with the first, but cannot be ignored when the concentration ratio is small. The third term represents the loss by convection and reradiation.†

*There are small but significant differences in the application of the definition of concentration ratio. Some authors take $(W - D_{co})L$ as the effective aperture area in the numerator, while others use the whole aperture area, viz., WL .

†Heat losses due to conduction at the ends through the supports for the receiver are generally significant and are also sometimes accounted for in the value of U_l .

In a manner similar to that adopted for a flat-plate collector, we define an absorbed flux S as follows,

$$S = I_b r_b \rho \gamma (\tau \alpha)_b + I_b r_b (\tau \alpha)_b \left(\frac{D_o}{W - D_o} \right) \quad (6.14)$$

Equation (6.13) thus becomes,

$$dq_u = \left[S - \frac{U_l}{C} (T_p - T_a) \right] (W - D_o) dx \quad (6.15)$$

The useful heat gain rate dq_u can also be written as

$$dq_u = h_f \pi D_o (T_p - T_f) dx$$

$$= \dot{m} C_p dT_f \quad (6.16)$$

where h_f = heat transfer coefficient on the inside surface of the tube, and T_f = local fluid temperature.

We combine Eqs (6.15) and (6.16) in such a manner as to eliminate the absorber tube temperature T_p , and obtain

$$dq_u = F' \left[S - \frac{U_l}{C} (T_f - T_a) \right] (W - D_o) dx \quad (6.18)$$

where F' is the collector efficiency factor defined by

$$F' = \frac{1}{U_l \left[\frac{1}{U_l} + \frac{D_o}{D_l h_f} \right]} \quad (6.19)$$

Again, combining Eqs (6.17) and (6.18), we obtain the differential equation

$$\frac{dT_f}{dx} = \frac{F' \pi D_o U_l}{\dot{m} C_p} \left[\frac{CS}{U_l} - (T_f - T_a) \right] \quad (6.20)$$

Integrating and using the inlet condition at $x = 0$, $T_f = T_{fi}$ we have the temperature distribution

$$\frac{\left(\frac{CS}{U_l} + T_a \right) - T_f}{\left(\frac{CS}{U_l} + T_a \right) - T_{fi}} = \exp \left\{ - \frac{F' \pi D_o U_l x}{\dot{m} C_p} \right\} \quad (6.21)$$

The fluid outlet temperature is obtained by putting $T_f = T_{fo}$ and $x = L$ in Eq. (6.21). Making this substitution and subtracting both sides of the resulting equation from unity, we have

$$\frac{(T_{fo} - T_{fi})}{\frac{CS}{U_l} + T_a - T_{fi}} = 1 - \exp \left\{ - \frac{F' \pi D_o U_l L}{\dot{m} C_p} \right\} \quad (6.22)$$

Thus, the useful heat gain rate

$$\begin{aligned} q_u &= \dot{m}C_p(T_{fo} - T_{fi}) \\ &= \dot{m}C_p \left[\frac{CS}{U_l} + T_a - T_{fi} \right] \left[1 - \exp \left\{ - \frac{F' \pi D_o U_l L}{\dot{m} C_p} \right\} \right] \\ &= F_R (W - D_o) L \left[S - \frac{U_l}{C} (T_{fi} - T_a) \right] \end{aligned} \quad (6.23)$$

where F_R is the heat removal factor defined by

$$F_R = \frac{\dot{m}C_p}{\pi D_o L U_l} \left[1 - \exp \left\{ - \frac{F' \pi D_o U_l L}{\dot{m} C_p} \right\} \right] \quad (6.24)$$

Equation (6.23) is the equivalent of the Hottel-Whillier-Bliss Eq. (4.48) for a flat-plate collector.

The instantaneous collection efficiency η_i is given by

$$\eta_i = \frac{q_u}{(I_b r_b + I_d r_d) WL} \quad (6.25)$$

if ground-reflected radiation is neglected. The instantaneous efficiency can also be calculated on the basis of beam radiation alone, in which case

$$\eta_{ib} = \frac{q_u}{I_b r_b WL} \quad (6.26)$$

6.3.4 Overall Loss Coefficient and Heat Transfer Correlations

In this section, we will give the procedure for calculating the overall loss coefficient U_l and the correlations required for calculating the individual heat transfer coefficients. The calculation of the overall loss coefficient based on convection and reradiation losses alone proceeds in a manner similar to that adopted in Sec. 4.5.1 for the top loss coefficient. We consider the absorber tube and the glass cover around it to constitute a system of long, concentric tubes. Making the same assumptions, we have

$$\frac{q_l}{L} = h_{p-c}(T_{pm} - T_c) \pi D_o + \frac{\sigma \pi D_o (T_{pm}^4 - T_c^4)}{\left\{ \frac{1}{\epsilon_p} + \frac{D_o}{D_{ci}} \left(\frac{1}{\epsilon_c} - 1 \right) \right\}} \quad (6.27)$$

$$= h_w (T_c - T_a) \pi D_{co} + \sigma \pi D_{co} \epsilon_c (T_c^4 - T_{sky}^4) \quad (6.28)$$

where q_l/L = heat loss rate per unit length,

h_{p-c} = convective heat transfer coefficient between the absorber tube and the glass cover,

T_{pm} = average temperature of the absorber tube, and

T_c = temperature attained by the cover

All other symbols have been defined earlier. Equations (6.27) and (6.28) are a set of two nonlinear equations which have to be solved for the unknowns (q_l/L) and T_c after substituting the values of h_{p-c} and h_w .

Heat Transfer Coefficient between the Absorber Tube and the Cover

The natural convection heat transfer coefficient h_{p-c} for the enclosed annular space between a horizontal absorber tube and a concentric cover is calculated by using a correlation due to Raithby and Hollands.*

$$\frac{k_{eff}}{k} = 0.317 (Ra^*)^{1/4} \quad (6.29)$$

where k_{eff} = effective thermal conductivity defined as the thermal conductivity that the motionless air in the gap must have to transmit the same amount of heat as the moving air, and

Ra^* = modified Rayleigh number related to the usual Rayleigh number by the following equation

$$(Ra^*)^{1/4} = \frac{\ln (D_{ci}/D_o)}{b^{3/4} \left(\frac{1}{D_o^{3/5}} + \frac{1}{D_{ci}^{3/5}} \right)^{5/4}} Ra^{1/4} \quad (6.30)$$

The characteristic dimension used for the calculation of the Rayleigh number is the radial gap $b = (D_{ci} - D_o)/2$. Properties are evaluated at the mean temperature $(T_{pm} + T_c)/2$. It is to be noted that the effective thermal conductivity k_{eff} cannot be less than the thermal conductivity k . Hence (k_{eff}/k) is put equal to unity if the use of Eq. (6.29) yields a value less than unity.

The relationship between the heat transfer coefficient h_{p-c} and the effective thermal conductivity can be found by equating expressions for the heat exchange rate per unit length. We have

$$\frac{2\pi k_{eff}}{\ln (D_{ci}/D_o)} (T_{pm} - T_c) = h_{p-c} \pi D_o (T_{pm} - T_c)$$

$$\text{Thus, } h_{p-c} = \frac{2k_{eff}}{D_o \ln (D_{ci}/D_o)} \quad (6.31)$$

The limitations on using Eq. (6.29) are that Ra^* should be less than 10^7 , and b should be less than $0.3D_o$.

*G.D. Raithby and K.G.T. Hollands, "A General Method of Obtaining Approximate Solutions to Laminar and Turbulent Heat-Transfer Problems", *Advances in Heat Transfer*, Vol. 10, 1974, p. 1.

Heat Transfer Coefficient on the Outside Surface of the Cover

The convective heat transfer coefficient h_w on the outside surface of the cover (sometimes called the wind heat transfer coefficient) can be calculated by using the well-known correlation based on the data of Hilpert,* who conducted experiments on air flowing at right angles across cylinders of various diameters at low levels of free stream turbulence. Hilpert's data can be correlated by the equation

$$Nu = C_1 Re^n$$

where C_1 and n are constants having the following values: (6.32)

$$\text{For } 40 < Re < 4000, C_1 = 0.615, n = 0.466$$

$$\text{For } 4000 < Re < 40000, C_1 = 0.174, n = 0.618$$

$$\text{For } 40000 < Re < 400000, C_1 = 0.0239, n = 0.805$$

D_{ch} is the characteristic dimension to be used in Eq. (6.32). Properties are to be evaluated at the mean temperature $(T_c + T_a)/2$.

As noted earlier, Eq. (6.32) has been obtained at low levels of turbulence intensity. In practice, the turbulence intensity in the wind flowing over the cover may not be insignificant. As a result, there is an uncertainty in the value of h_w and the value predicted by Eq. (6.32) may be lower than the actual value by 10 or 15 per cent. Fortunately, this uncertainty affects the value of the overall loss coefficient by only 1 or 2 per cent.

Heat Transfer Coefficient on the Inside Surface of the Absorber Tube

The convective heat transfer coefficient h_f on the inside surface of the absorber tube can be calculated under the assumption that the flow is fully developed. This assumption is justified because the length-to-diameter ratio (L/D_i) is large, usually greater than 20. For a Reynolds number less than 2000, the flow is laminar and the heat transfer coefficient may be calculated from the equation

$$Nu = 3.66 \quad (6.33)$$

On the other hand, for a Reynolds number greater than 2000, the flow is turbulent and the heat transfer coefficient may be calculated from the well-known Dittus-Boelter equation

$$Nu = 0.023 Re^{0.8} Pr^{0.4} \quad (6.34)$$

The characteristic dimension used for calculating Nu and Re in Eqs (6.33) and (6.34) is D_i . Properties are evaluated at the mean

*R. Hilpert, "Wärmeabgabe von geheizten Drahten und Rohren". *Forsch. Gebiete Innenbautechnik*, 1938, 1, 101.

temperature $(T_{fi} + T_{fo})/2$. It should be noted that Eqs (6.33) and (6.34) are also valid for calculating the value of h_f for a liquid flat-plate collector.

In most situations, the mass flow rate m is small and the flow is laminar. Equation (6.33) is therefore used. As a consequence, the value of h_f is sometimes so small as to adversely affect the value of F_R . This is particularly true when the liquid used is a heat transfer oil. These oils have high boiling points, but are characterized by low thermal conductivities and high Prandtl numbers. In such cases, it is desirable to use some kind of augmentative technique to increase the heat transfer coefficient. One of the simplest techniques is to use a twisted tape of width D_i inserted all along the inside of the absorber tube. Hong and Bergles* have suggested the following correlation for this case:

$$Nu = 5.172 [1 + 0.005484 (\Pr (Re/X)^{1.78})^{0.7}]^{0.5} \quad (6.35)$$

where X = tape twist ratio = H/D_i
and H = length over which the tape is twisted through 180° .

The characteristic dimension used for calculating Nu and Re is D_i . Calculations with Eq. (6.35) show that the use of a twisted tape results in very significant increases in the heat transfer coefficient when the Prandtl number is high. At the same time, the pressure drop does not increase in the same proportion. The pressure drop may be calculated from the following correlations based on the work of Date and Singham†:

$$f Re = 38.4 (Re/X)^{0.05} \quad \text{for } 6.7 \leq (Re/X) \leq 100 \\ = C_2 (Re/X)^{0.3} \quad \text{for } (Re/X) > 100 \quad (6.36)$$

where f = friction factor,

$$C_2 = 8.8201 X - 2.1193 X^2 + 0.2108 X^3 - 0.0069 X^4$$

Example 6.2

Calculate the overall loss coefficient U_l for the receiver of a cylindrical parabolic concentrating collector system. The receiver consists of a selectively-coated absorber tube with one glass cover around it. The following data is given:

*S.W. Hong and A.E. Bergles, "Augmentation of Laminar Flow Heat Transfer in Tubes by Means of Twisted Tape Inserts", *Journal of Heat Transfer, Trans. ASME*, 98, 251 (1976).

†A.W. Date and J.R. Singham, "Numerical Prediction of Friction and Heat Transfer Characteristics of Fully Developed Laminar Flow in Tubes Containing Twisted Tapes".

Absorber tube, inner diameter 7.5 cm, outer diameter 8.1 cm	
Glass cover, inner diameter 14.4 cm, outer diameter 15.0 cm	
Emissivity of absorber tube surface	= 0.15
Emissivity of glass	= 0.88
Mean temperature of absorber tube	= 170°C
Ambient temperature	= 25°C
Wind velocity	= 4 m/s

Substituting the given data into Eqs (6.27) and (6.28), we get

$$\frac{q_l}{L} = h_{p-c}(443.2 - T_c)\pi \times 0.081 + \frac{5.67 \times 10^{-8} \times \pi \times 0.081(443.2^4 - T_c^4)}{\left\{ \frac{1}{0.15} + \frac{0.081}{0.144} \left(\frac{1}{0.88} - 1 \right) \right\}} \\ = 0.2545h_{p-c}(443.2 - T_c) + 0.2140 \times 10^{-8}(385.8 \times 10^8 - T_c^4) \quad (6.37)$$

$$\frac{q_l}{L} = h_w(T_c - 298.2)\pi \times 0.15 + 5.67 \times 10^{-8} \times \pi \times 0.15 \times 0.88(T_c^4 - 292.2^4) \\ = 0.4712h_w(T_c - 298.2) + 2.3513 \times 10^{-8}(T_c^4 - 72.90 \times 10^8) \quad (6.38)$$

Equations (6.37) and (6.38) have to be solved for the unknowns (q_l/L) and T_c . For this, the values h_{p-c} and h_w are needed. Since these values depend upon T_c , a trial-and-error method is necessary. Assume $T_c = 310$ K.

Calculation of h_{p-c}

Mean temperature of air between tube and cover

$$= \frac{443.2 + 310}{2} = 376.6 \text{ K} = 103.4^\circ\text{C}$$

At this temperature,

$$k = 0.0323 \text{ W/m-K}$$

$$v = 23.52 \times 10^{-6} \text{ m}^2/\text{s}$$

$$Pr = 0.688$$

$$Ra = 9.81 \times \frac{1}{376.6} \times \frac{(443.2 - 310) \times 0.0315^3}{23.52^2 \times 10^{-12}} \times 0.688 = 134877$$

From Eq. (6.29),

$$\frac{h_{eff}}{h} = 0.317 \times \frac{\ln(0.144/0.081)}{0.0315^{3/4} \left(\frac{1}{0.081^{3/5}} + \frac{1}{0.144^{3/5}} \right)^{5/4}} \times (134877)^{1/4} \\ = 3.6349$$

and from Eq. (6.31),

$$h_{p-c} = \frac{2 \times 3.6349 \times 0.0323}{0.081 \ln(0.144/0.081)} \\ = 5.036 \text{ W/m}^2\text{-K}$$

Calculation of h_w

Mean temperature of air between the cover and ambient

$$= \frac{310 + 298.2}{2} = 304.1 \text{ K} = 30.9^\circ\text{C}$$

At this temperature,

$$k = 0.0268 \text{ W/m-K}$$

$$v = 16.09 \times 10^{-6} \text{ m}^2/\text{s}$$

Assuming that the wind velocity is at right angles to the axis of the collector and using Eq. (6.32), we have,

$$Re = \frac{4 \times 0.15}{16.09 \times 10^{-6}} = 37300$$

$$Nu = 0.174(37300)^{0.618} = 116.4$$

$$h_w = 116.4 \times \frac{0.0268}{0.15} = 20.79 \text{ W/m}^2\text{-K}$$

Substituting the values of h_{p-c} and h_w in Eqs (6.37) and (6.38), we obtain the values of T_c and (q_l/L) by trial-and-error.

T_c (K)	(q_l/L) from	
	Equation (6.37)	Equation (6.38)
310	233.5	161.3
315	225.9	224.7
315.1	225.6	226.0

The values of (q_l/L) in the last line are reasonably close to each other. The average value of 225.8 W/m will therefore be accepted. Since the values of h_{p-c} and h_w will not change much if the initial guess of $T_c = 310$ K is changed to 315.1 K, it will not be necessary to repeat the calculation.

$$\text{Hence} \quad U_l = \frac{225.8}{\pi \times 0.081 \times (170 - 25)} \\ = 6.12 \text{ W/m}^2\text{-K.}$$

Empirical Equation for the Overall Loss Coefficient

Based on calculations for a large number of cases covering a broad range of conditions encountered with cylindrical parabolic collectors, Mullick

and Nanda* have developed a semi-empirical equation for directly calculating the overall loss coefficient. This equation eliminates the need for an iterative calculation.

$$\frac{1}{U_l} = \frac{1}{C_3(T_{pm} - T_c)^{0.25}} + \left[\sigma(T_{pm}^2 + T_c^2)(T_{pm} + T_c) \left/ \left(\frac{1}{r_p} + \frac{D_o}{D_{ci}} \left(\frac{1}{r_c} - 1 \right) \right) \right. \right] \\ + \left(\frac{D_o}{D_{ci}} \right) \left(\frac{1}{h_w + \sigma r_c (T_c^2 + T_a^2)(T_c + T_a)} \right) \quad (6.39)$$

The constant C_3 has been obtained from the correlation of Raithby and Hollands and is given by the expression

$$C_3 = \frac{17.74}{(T_{pm} + T_c)^{0.4} D_o (D_o^{-0.76} + D_{ci}^{-0.75})} \quad (6.40)$$

The cover temperature T_c is given by

$$\left(\frac{T_c - T_a}{T_{pm} - T_a} \right) = 0.04075 \left(\frac{D_o}{D_{ci}} \right)^{0.4} h_w^{-0.67} \left[2 - 3r_p + \frac{(6 + 9r_p)T_{pm}}{100} \right] \quad (6.41)$$

if $333 < T_{pm} < 513$ K, and by

$$\left(\frac{T_c - T_a}{T_{pm} - T_a} \right) = 0.163 \left(\frac{D_o}{D_{ci}} \right)^{0.4} h_w^{-0.67} \left[2 - 3r_p + \frac{(1 + 3r_p)T_{pm}}{100} \right] \quad (6.42)$$

if $513 < T_{pm} < 623$ K.

While using Eqs (6.39)-(6.42), T_{pm} , T_c and T_a are expressed in K, D_o , D_{ci} and D_{co} in m, σ in $\text{W/m}^2\text{-K}^4$, and h_w in $\text{W/m}^2\text{-K}$. The value of U_l is obtained in $\text{W/m}^2\text{-K}$. Eq. (6.39) has been developed for the following range:

$$0.1 \leq r_p \leq 0.95$$

$$0.0125 \leq D_o \leq 0.15 \text{ m}$$

$$15 \leq h_w \leq 60 \text{ W/m}^2\text{-K}$$

$$273 \leq T_a \leq 313 \text{ K}$$

Eqs (6.41) and (6.42) estimate the glass cover temperature to within $\pm 10^\circ\text{C}$. This estimate is good enough to obtain U_l from Eq. (6.39) to an accuracy of ± 1 per cent for $333 < T_{pm} < 513$ K, and to an accuracy of ± 2 per cent for $513 < T_{pm} < 623$ K.

6.3.5 A Numerical Example

We will now illustrate the procedure for calculating the performance of a cylindrical parabolic collector through a detailed numerical example.

Example 6.3

A cylindrical parabolic collector located in Bombay, operating in tracking mode II, is used for heating a thermic fluid. The concentrator has an aperture of 1.25 m and a length of 3.657 m, while the absorber tube (3.81 cm inner and 4.135 cm outer diameter) has a concentric glass cover (5.60 cm inner and 6.30 cm outer diameter) around it. A twisted tape with a tape twist ratio of 4 is used inside the absorber tube. Values of other design parameters of the collector are as follows:

Specular reflectivity of concentrator surface	= 0.85
Glass cover transmissivity for solar radiation	= 0.85
Glass cover emissivity/absorptivity	= 0.88
Absorber tube emissivity/absorptivity	= 0.95
Intercept factor	= 0.95

Values of the operational and meteorological parameters are as follows:

• Date	= April 15
• Time	= 1230 h (LAT)
• I_b	= 705 W/m^2
• I_g	= 949 W/m^2
• Ambient temperature	= 31.9°C
• Wind speed	= 5.3 m/s
• Mass flow rate of thermic fluid	= 0.0986 kg/s
• Inlet temperature	= 150°C

Calculate,

1. the slope of the aperture plane and the angle of incidence on the aperture plane,
2. the absorbed flux S ,
3. the convective heat transfer coefficient on the inside surface of the absorber tube,
4. the collector heat-removal factor and overall loss coefficient,
5. the exit temperature of the thermic fluid,
6. the instantaneous efficiency,
7. the pressure drop.

*B.C. Mullick and S.K. Nanda, "An Improved Technique for Computing the Heat Loss Factor of a Tubular Absorber", *Solar Energy*, 42, 1 (1989).

1. Slope of the Aperture Plane and Angle of Incidence

In tracking mode II, the slope of the aperture plane and angle of incidence are given by Eqs (6.4) and (6.5).
On April 15, $n = 105$.

$$\delta = 23.45 \sin \left[\frac{360}{365} (284 + 105) \right] = 9.415^\circ$$

Therefore, substituting $\delta = 9.415^\circ$, $\omega = -7.5^\circ$ and $\phi = 19.12^\circ$ in Eq (6.4), we have

$$\beta = 9.625^\circ$$

$$\text{and } \cos \theta = [1 - \cos^2 9.415^\circ \sin^2 (-7.5^\circ)]^{1/2} = 0.9917$$

$$\theta = 7.398^\circ$$

2. Absorbed Flux S

From Eq. (3.30),

$$S = \frac{0.9917}{\sin 19.12^\circ \sin 9.415^\circ + \cos 19.12^\circ \cos 9.415^\circ \cos (-7.5^\circ)} = 1.0143.$$

Therefore, substituting in Eq. (6.14) and taking $(\tau\alpha)_b = \tau\alpha$, we have

$$S = 705 \times 1.0143 \left[0.85 \times 0.95 \times 0.85 \times 0.95 + \frac{0.85 \times 0.95 \times 0.04135}{(1.25 - 0.04135)} \right] = 486.03 \text{ W/m}^2$$

3. Convective Heat Transfer Coefficient h_f

We will use Eq. (6.35) for calculating h_f . The properties of the fluid are given in Fig. 6.5. Keeping in mind that the rise of temperature of the fluid will only be a few degrees in this case, properties will be taken at a mean fluid temperature of 152°C .

Thus, $\rho = 750.3 \text{ kg/m}^3$, $C_p = 2.449 \text{ kJ/kg-K}$,

$$v = 2.42 \times 10^{-6} \text{ m}^2/\text{s}$$

$$\text{Average velocity } V = \frac{\dot{m}}{\frac{\pi}{4} D_i^2 \rho} = \frac{0.0986}{\frac{\pi}{4} \times 0.0381^2 \times 750.3} = 0.1153 \text{ m/s}$$

$$\text{Reynolds number } Re = \frac{VD_i}{v} = \frac{0.1153 \times 0.0381}{2.42 \times 10^{-6}} = 1815$$

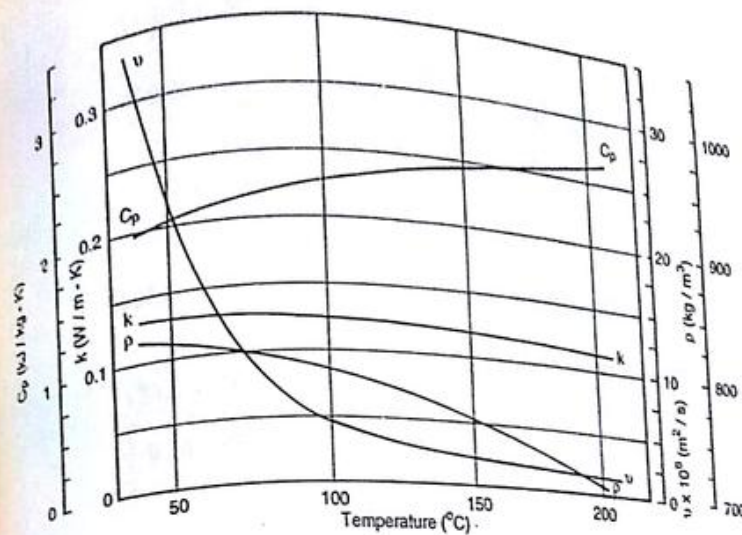


Fig. 6.5 Example 6.3—Properties of Thermic Fluid

$$\text{Prandtl number } Pr = \frac{C_p v \rho}{k} = \frac{2.449 \times 2.42 \times 10^{-6} \times 750.3 \times 1000}{0.119} = 37.37$$

$$\text{Nusselt number } Nu = 5.172 \left[1 + 0.005484 \left\{ 37.37 \left(\frac{1815}{4} \right)^{1/8} \right\}^{0.7} \right]^{0.5} = 61.70$$

$$\text{Therefore } h_f = 61.70 \times \frac{0.119}{0.0381} = 192.7 \text{ W/m}^2\text{-K}$$

4. Collector Heat-removal Factor and Overall Loss Coefficient

As in the case of the flat-plate collector, an iterative procedure will be required since the values of F_R and U_l cannot be directly determined and the value of one depends on the other.

Assume $U_l = 13.28 \text{ W/m}^2\text{-K}^*$. From Eq. (6.19), the collector efficiency factor

*In this case, the correct value of U_l has been determined by doing the iterative procedure on a computer. We therefore illustrate the procedure with the correct values of $U_l = 13.28 \text{ W/m}^2\text{-K}$ and $T_c = 60.23^\circ\text{C}$.

$$F' = \frac{1}{13.28 \left[\frac{1}{13.28} + \frac{0.04135}{0.0381 \times 192.7} \right]} = 0.9304$$

$$\frac{\dot{m}C_p}{\pi D_o U_l L} = \frac{0.0986 \times 2.449 \times 10^3}{\pi \times 0.04135 \times 13.28 \times 3.657} = 38.275$$

Therefore, from Eq. (6.24), heat-removal factor

$$F_R = 38.275 [1 - \exp(-0.9304/38.275)] \\ = 0.9192$$

$$\text{Concentration ratio } C = \frac{(1.25 - 0.04135)}{\pi \times 0.04135} = 9.304$$

Thus from Eq. (6.23),

$$\text{useful heat gain rate } q_u = 0.9192(1.25 - 0.04135) \times 3.657 \\ \times \left[486.03 - \frac{13.28}{9.304} (150 - 31.9) \right] \\ = 1289.8 \text{ W}$$

Therefore, rate of heat loss

$$= (W - D_o)LS - q_u \\ = (1.25 - 0.04135) \times 3.657 \times 486.03 - 1289.8 \\ = 858.46 \text{ W} \\ = \pi D_o L U_l (T_{pm} - T_a)$$

$$\text{Hence } (T_{pm} - T_a) = \frac{858.46}{\pi \times 0.04135 \times 3.657 \times 13.28} = 136.07^\circ\text{C} \\ T_{pm} = 167.97^\circ\text{C} = 441.13 \text{ K}$$

We will now calculate the value of U_l corresponding to this value of T_{pm} and show that it is equal to the assumed value. The procedure of Example 6.2 will be followed.

$$\text{Assume } T_e = 60.23^\circ\text{C} = 333.39 \text{ K}$$

From Eqs (6.29) and (6.31), we get

$$h_{p-e} = 5.113 \text{ W/m}^2\text{-K}$$

From Eq. (6.32),

$$h_w = 34.119 \text{ W/m}^2\text{-K}$$

Substituting these values of T_e , h_{p-e} and h_w in Eqs (6.27) and (6.28), we have

$$\frac{q_l}{L} = 5.113(441.13 - 333.39)\pi \times 0.04135 \\ + \frac{5.67 \times 10^{-8} \times \pi \times 0.04135 (441.13^4 - 333.39^4)}{\left\{ \frac{1}{0.95} + \frac{0.04135}{0.0560} \left(\frac{1}{0.88} - 1 \right) \right\}} \\ = 234.5 \text{ W/m}$$

and

$$\frac{q_l}{L} = 34.119(333.39 - 305.06)\pi \times 0.063 \\ + \frac{5.67 \times 10^{-8} \times 0.063 \times 0.88 (333.39^4 - 299.06^4)}{234.5 \text{ W/m}}$$

The two values of (q_l/L) match with each other. The corresponding value of U_l is given by

$$U_l = \frac{234.5}{\pi \times 0.04135 \times (441.13 - 305.06)} \\ = 13.27 \text{ W/m}^2\text{-K}$$

which also matches the original guess.

5. Exit Temperature

Equating the heat gained by the fluid to the useful heat gain rate, we get

$$0.0986 \times 2.449 \times (T_{fo} - 150) = \frac{1289.8}{1000}$$

$$T_{fo} = 155.34^\circ\text{C}$$

Hence

6. Instantaneous Efficiency

Using Eq. (6.25),

$$\eta_i = \frac{1289.8}{(705 \times 1.0143 + 244 \times 0.9930)1.25 \times 3.657} = 0.295$$

Using Eq. 6.26

$$\eta_{ib} = \frac{1289.8}{705 \times 1.0143 \times 1.25 \times 3.657} = 0.395$$

7. Pressure Drop

We use Eq. (6.36) to get

$$\frac{Re}{X} = \frac{1815}{4} = 453.75$$

Hence

$$C_2 = 13.0964$$

$$\begin{aligned} f \text{Re} &= 13.0964 \times (453.75)^0.3 = 82.069 \\ f &= 0.0452 \\ \Delta p &= \frac{4f \rho L V^2}{2D_i} \\ &= \frac{4 \times 0.0452 \times 750.3 \times 3.657 \times 0.1153^2}{2 \times 0.0381} \\ &= 86.6 \text{ N/m}^2 \\ &= 0.88 \text{ cm of water} \end{aligned}$$

This is a reasonable value.

The values of η_i and η_{ib} obtained in this example are low and the difference between them is significant. The low values are partly due to the fact that the inlet fluid temperature is rather high for the given concentration ratio, while the difference between the two values is due to the high diffuse component in the global radiation.

In order to obtain a break-up of the losses occurring in the collector, we distinguish between optical losses and thermal losses. Optical losses are those which occur in the path of the incident solar radiation before it is absorbed at the surface of the absorber tube, while thermal losses are due to convection and reradiation from the absorber tube and conduction through the ends. On this basis, we define an *optical efficiency* η_o as the fraction of the solar radiation incident on the aperture of the collector which is absorbed at the surface of the absorber tube. Thus,

$$\begin{aligned} \eta_o &= \frac{I_b r_b \rho (\tau \alpha)_b (W - D_o) L + I_b r_b (\tau \alpha)_b D_o L}{I_b r_b W L} \\ &= \rho (\tau \alpha)_b \frac{(W - D_o)}{W} + (\tau \alpha)_b \frac{D_o}{W} \\ &= \frac{S}{I_b r_b} \frac{(W - D_o)}{W} \end{aligned} \quad (6.3)$$

Substituting the numerical values of this example, we get

$$\begin{aligned} \eta_o &= \frac{486.03}{705 \times 1.0143} \times \frac{(1.25 - 0.04135)}{1.25} \\ &= 0.657 \end{aligned}$$

6.3.5 Parametric Study of Collector Performance*

As in the case of the flat-plate collector, Sec. 4.9, we now study the

*K.M. Kelkar, "Performance Analysis of a Cylindrical Parabolic Collector", B.Tech thesis, Mechanical Engineering Department, IIT Bombay, 2000.

effect of some important parameters on the performance of a cylindrical parabolic collector. This has been done by writing a general computer programme which executes the procedure of Example 6.3.

Performance Over a Day with Different Tracking Modes

Using input data for solar radiation, ambient temperature and wind speed, the performance of the collector of Example 6.3 is first studied over two whole days, April 15 and December 15. The calculations are done for all the tracking modes described earlier in Sec. 6.3.2.* The input data and the results are presented in Tables 6.2 and 6.3. Average values of efficiency over a day are given in the last column. Plots showing the variation of the angle of incidence and the

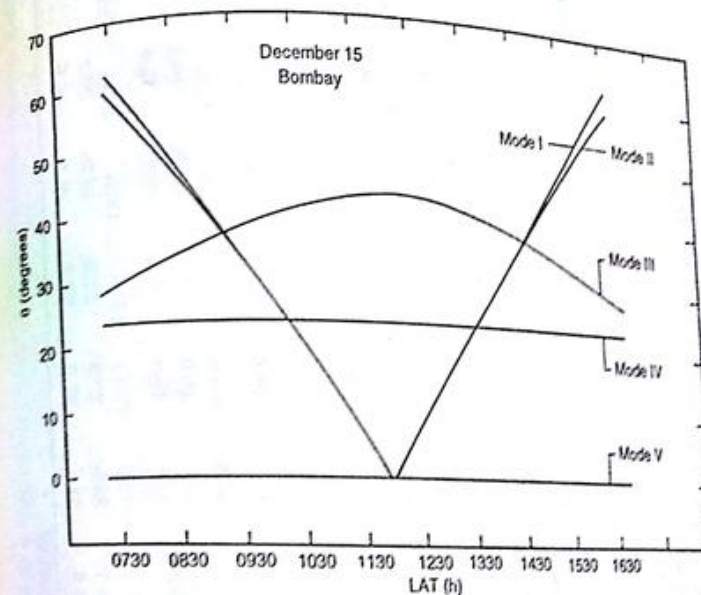


Fig. 6.6 Variation of Angle of Incidence in Different Tracking Modes—Data of Example 6.3

*It is assumed that the heat transfer correlations (6.29) to (6.31) for calculating the value of h_{p-e} are valid for all the five tracking modes. Strictly speaking, this is not correct, but is necessary in view of the fact that correlations for an inclined annulus are not available.

Table 6.2 Performance of Location: Bomba

Lat (h)	Latitudes for Collector Over a Whole Day in Various Tracking Modes									
	0730	0830	0930	1030	1130	1230	1330	1430	1530	1630
I_b (W/m ²)	145	292	465	593	684	705	665	562	385	Average value
I_d (W/m ²)	145	201	235	252	244	225	200	175	205	
T_a (°C)	27.8	29.6	31.0	31.8	32.0	31.9	31.8	31.5	31.0	30.2
V_a (m/s)	1.7	2.3	3.1	4.1	4.9	5.3	5.4	5.4	5.3	4.9
Mode I: q_u (W)	—	195.9	661.4	1000	1239	1289	1177	888.8	398.4	—
η_i (%)	—	8.7	20.6	25.7	28.7	29.5	28.7	25.4	15.6	—
η_{lb} (%)	—	14.7	30.9	36.5	39.1	39.5	38.2	34.3	22.7	—
Mode II: q_u (W)	—	200.0	662.5	1001	1240	1289	1183	890.1	403.8	—
η_i (%)	—	8.9	20.6	25.7	28.7	29.5	28.7	25.4	15.8	—
η_{lb} (%)	—	15.0	30.9	36.5	39.1	39.5	38.2	34.4	22.9	—
Mode III: q_u (W)	378.5	680.8	971.5	1111	1229	1280	1300	1260	1030	710.3
η_i (%)	18.1	23.5	26.7	27.5	28.6	29.3	30.4	31.1	29.5	26.2
η_{lb} (%)	23.4	31.7	36.5	37.9	39.0	39.4	39.5	39.1	36.4	31.1
Mode IV: q_u (W)	366.0	664.8	958.4	1106	1229	1280	1294	1245	1010	692.8
η_i (%)	16.3	22.0	26.0	27.3	28.8	29.5	30.2	30.5	28.8	24.5
η_{lb} (%)	23.0	31.4	36.2	37.8	39.0	39.4	39.5	38.9	36.1	30.7
Mode V: q_u (W)	379.0	682.0	979.7	1129	1255	1304	1321	1270	1032	710.9
η_i (%)	18.1	23.5	26.8	27.8	28.9	29.7	30.6	31.2	29.6	26.2
η_{lb} (%)	23.5	31.7	36.6	38.1	39.3	39.6	39.7	39.2	36.4	31.1

Table 6.3 Performance of a Cylindrical Parabolic Collector Over a Whole Day in Various Tracking Modes
Location: Bombay Date: December 15

LAT (h)	0730	0830	0930	1030	1130	1230	1330	1430	1530	1630	Average value
I_b (W/m ²)	81	250	404	518	580	519	405	255	94	61	
I_d (W/m ²)	61	92	113	129	137	139	133	119	98	28.8	27.4
T_a (°C)	23.6	25.3	27.4	29.0	30.0	30.4	30.3	29.8		3.4	3.1
V_a (m/s)	2.3	2.8	2.9	2.9	3.0	3.1	3.4	3.6			
Mode I: q_u (W)	—	514.5	998.8	1341	1522	1521	1337	997.0	539.1	—	29.8
η_i (%)	—	22.4	31.4	35.1	36.6	36.5	34.8	31.0	22.9	—	35.0
η_b (%)	—	26.8	36.6	40.7	42.2	42.2	40.5	36.4	27.5	—	
Mode II: q_u (W)	—	539.8	1005	1342	1522	1521	1338	1004	564.9	44.5	30.1
η_i (%)	—	23.4	31.6	35.2	36.6	36.5	34.9	31.3	23.9	3.4	35.1
η_b (%)	—	27.5	36.7	40.7	42.2	42.2	40.5	36.5	28.2	4.0	
Mode III: q_u (W)	328.6	786.2	928.8	971.2	981.5	980.8	967.9	927.3	815.4	475.4	28.6
η_i (%)	18.5	29.1	30.3	30.0	29.7	29.6	29.7	30.0	29.4	25.4	33.7
η_b (%)	20.6	33.0	35.5	36.3	36.5	36.5	36.1	35.4	33.6	25.7	
Mode IV: q_u (W)	378.7	935.3	1178	1304	1362	1301	1177	967.2	533.6	31.7	37.0
η_i (%)	19.4	30.7	33.3	34.2	34.5	34.4	33.9	32.9	31.0	27.4	37.0
η_b (%)	22.5	35.5	38.8	40.3	40.9	40.9	40.1	38.7	36.0	30.0	
Mode V: q_u (W)	467.6	1074	1339	1474	1637	1657	1471	1396	1049	626.4	34.6
η_i (%)	23.3	33.9	36.0	36.6	36.8	36.7	36.3	35.6	34.1	25.7	39.0
η_b (%)	25.5	37.4	40.5	41.8	42.3	42.3	40.3	37.9	40.3	30.0	

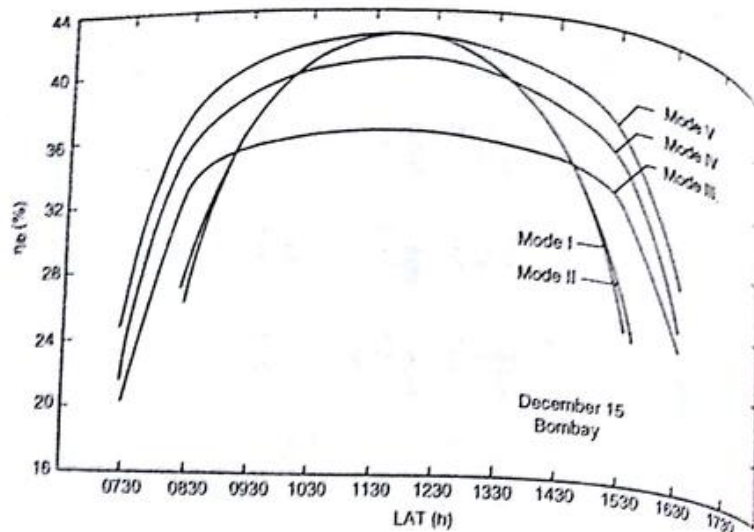


Fig. 6.7 Variation of Efficiency of a Cylindrical Parabolic Collector in Different Tracking Modes—Data of Example 6.3

instantaneous efficiency with time on one day, viz. December 15, are given in Figs 6.6 and 6.7. It will be noted from Fig. 6.7 that the general pattern of efficiency variation over a day is the same for all modes. The value of efficiency first increases, reaches a peak value around noon and then decreases. This is due to the fact that the efficiency is strongly influenced by the incident beam radiation and therefore follows its variation.

On any day and at any time, the performance of the collector under mode V has to be the best. Hence an assessment of the collector's performance under the other modes can be made by comparison with the best possible performance.

Modes I and II

In mode II, the collector is rotated about a horizontal E-W axis. Thus, the tracking takes care of the swing in the altitude of the sun, but not the swing in the azimuthal direction. Hence, the angle of incidence at times away from solar noon is high as seen in Fig. 6.6. In addition, since the insolation is also less at these times of the day, the collection efficiency is poor. However, at noon, the sun's rays are incident normally and the performance is the same as that obtained with mode V.

Mode I is similar to mode II. Thus, calculations show that the performance closely matches that obtained with mode II at all times of the year. However, since only one adjustment is made every day, the incidence angles are a little greater than those in mode II and the performance is, therefore, slightly inferior. It is to be noted however that the value of the intercept factor has been assumed to be constant in the calculations. This may not be valid for mode I because the image is not formed on the focal axis.

Mode III

In this mode, the collector is rotated about a horizontal N-S axis. Thus, the tracking takes care of the azimuthal swing of the sun, but not the swing in the altitude. On both the days considered, the angle of incidence is small in the early and late hours of the day and goes through a maximum at noon. However, the change in the angle of incidence over a day is not as large as in modes I and II. For this reason, the performance under this mode at times away from solar noon is significantly better than the performance at these times in modes I and II. On the other hand, at solar noon, the performance under this mode is not equal to that obtained with mode V, since the angle of incidence is not zero. Thus, as seen in Fig. 6.7, the efficiency variation curve for mode III intersects the efficiency variation curves obtained with modes I and II and tends to be flat for four or five hours every day. This results in a fairly uniform useful heat gain.

The performance of the collector is now quite sensitive to the latitude as well as the day of operation. Thus in the example considered, since the latitude of Bombay is 19.12°N and since on April 15 the declination is only $+9.4^{\circ}$, the angle of incidence through the whole day is small. It varies from a minimum of 1.8° at 0730 h to a maximum of 9.7° at noon. The performance of the collector in mode III at all times of the day on April 15 is therefore very near to that obtained with mode V. On the other hand, on Dec. 15 the declination is -23.3° , and the performance deviates significantly from that obtained in mode V.

Mode IV

In this mode, the collector is rotated about a N-S axis parallel to the earth's axis of rotation and the angle of incidence is always equal to the declination angle. As a result, the performance of the collector is independent of the latitude. Since the declination varies only between the limits of -23.45° and $+23.45^{\circ}$, the performance in this mode is always close to that obtained in mode V. On the two equinox days of March 21 and September 21, when the declination is zero, the performance is the same as in mode V.

Effect of Inlet Temperature

As the fluid inlet temperature increases, the temperature of the absorber tube surface also increases. As a result, losses due to reradiation and convection to the surroundings increase, resulting in a decrease in efficiency. This is apparent from Eq. (6.23) which gives the useful heat gain rate for the collector. In order to illustrate this effect, calculations are done for the case of the parabolic collector of Example 6.3 operating under the same conditions with only inlet temperature varying from 120°C to 180°C. The results are plotted in Fig. 6.8. It is seen that the value of η_{ib} decreases significantly with

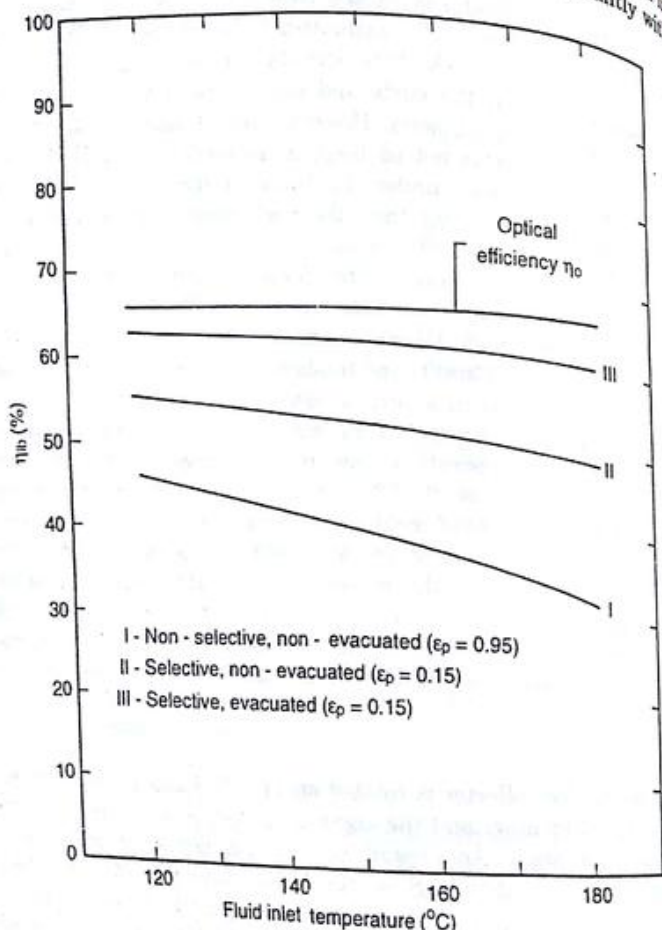


Fig. 6.8 Variation of Efficiency with Fluid Inlet Temperature for Three Receiver Designs—Data of Example 6.3

T_{fi} , the decrease being slightly non-linear. The non-linearity is due to the fact that the value of the overall loss coefficient increases slightly as T_{fi} increases. The value of the optical efficiency (which does not change with inlet temperature) is also shown in Fig. 6.8. The difference between the values of η_o and η_{ib} is a measure of the losses due to re-radiation and convection.

Effect of Mass Flow Rate

An increase in the mass flow rate of the thermic fluid increases the value of the inside heat transfer coefficient h_f . Due to this, the collector efficiency factor and the collector heat-removal factor increase and the mass flow rate is varied from 0.0329 kg/s to 0.1315 kg/s. It is seen that the slope of the efficiency curve goes on decreasing with increasing values of \dot{m} and that the value of η_{ib} tends to some asymptotic value. At the same time, the pressure drop increases, thereby increasing the demand for pumping power. Fortunately this increase is not so rapid because of the high Prandtl number of the fluid and the presence of a twisted tape. Thus, an optimum value of \dot{m} would be one for which the asymptotic value of η_{ib} has almost been attained without an unduly high pressure drop. In the present case, this optimum value would seem to lie around 0.12 kg/s.

Effect of Selectivity of Absorber Tube Surface and Evacuation of Annulus

From Fig. 6.8, it is evident that losses due to reradiation and convection are very high. Any means to reduce or suppress these losses would obviously help in significantly improving the collection efficiency. Losses due to reradiation are reduced by the use of a selective surface, while losses due to convection are reduced by having a vacuum in the annular space between the absorber tube and the glass cover. The effect of introducing these measures is also shown in Fig. 6.8 in which the variation of η_{ib} with T_{fi} is shown for (i) a selective surface with $\epsilon_p = 0.15$ and a non-evacuated annulus, and (ii) a selective surface with $\epsilon_p = 0.15$ and an evacuated annulus. It will be seen that there is a dramatic improvement in efficiency and that the rate of decrease of η_{ib} with T_{fi} is also reduced. The increase in η_{ib} is of course due to the decrease in the value of U_l . For example, at $T_{fi} = 120^\circ\text{C}$, the value of U_l decreases from $12.28 \text{ W/m}^2\text{-K}$ to $6.34 \text{ W/m}^2\text{-K}$ and $1.65 \text{ W/m}^2\text{-K}$ respectively for the above two cases.

Effect of Concentration Ratio

The effect of increasing the concentration ratio by decreasing the size of the absorber tube is shown in Fig. 6.10. It is seen that the efficiency

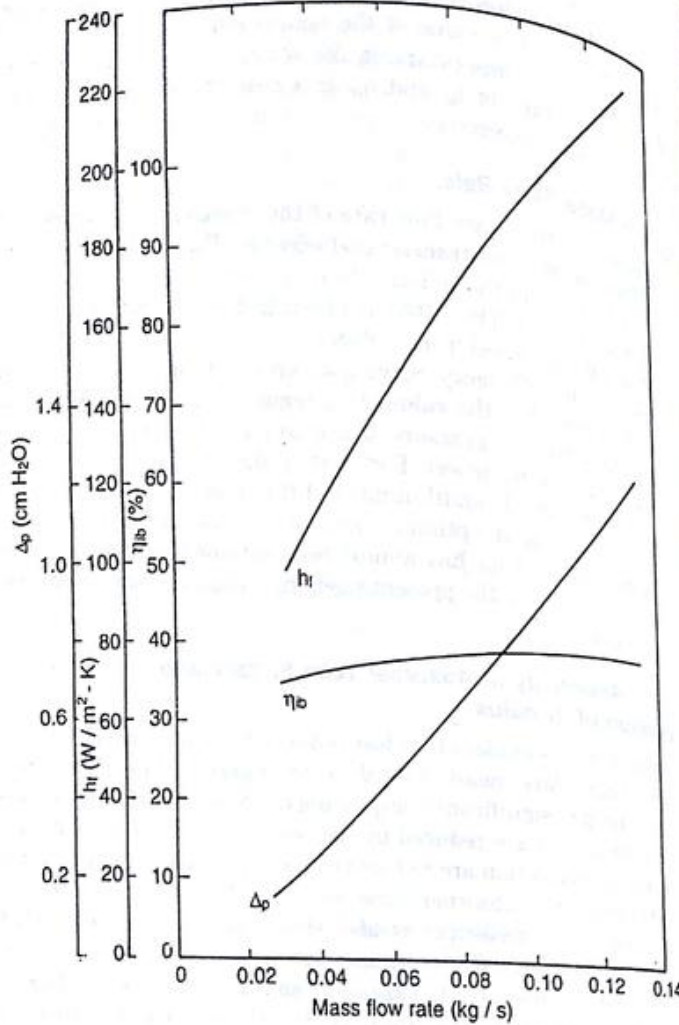


Fig. 6.9 Variation of Performance with Mass Flow Rate—Data of Example 6.3

increases. This result is evident from Eq. (6.23). When the concentration ratio increases without a decrease in the intercept factor, the value of the optical efficiency changes very slightly. However, the losses from the absorber tube which are inversely proportional to C , decrease and hence the collection efficiency increases.

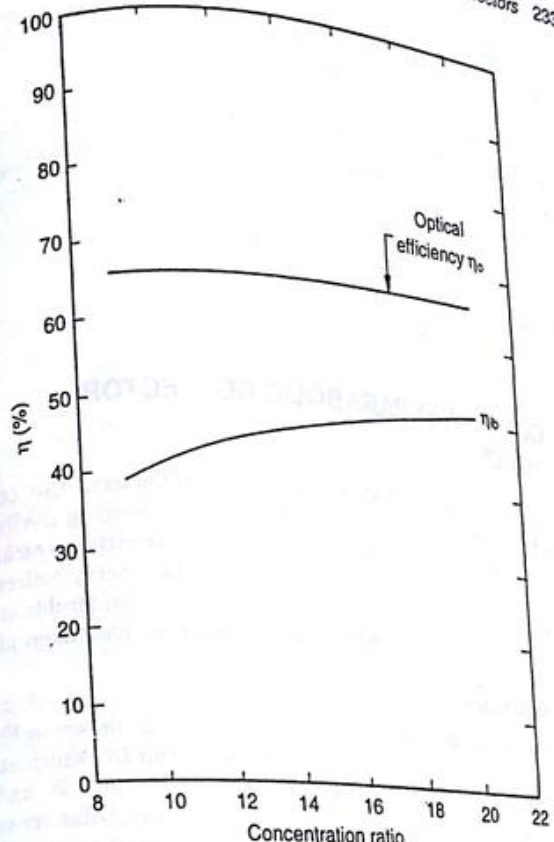


Fig. 6.10 Variation of Efficiency with Concentration Ratio—Data of Example 6.3

6.3.7 The Luz Collector

Before concluding this section on the cylindrical parabolic collector, it will be of interest to note the dimensions and characteristics of the collector modules used in the 80 MW solar thermal electric power plant set up by Luz in California. This would enable the reader to gain an appreciation of the state-of-the-art achieved thus far. The data is as follows:

- Aperture 5.76 m
- Length 95.2 m
- Reflecting surface 224 curved mirror glass panels

• Reflectivity	0.94
• Glass cover transmissivity	0.965
• Vacuum in annular space	10^{-4} torr
• Absorber tube O.D.	0.070 m
• Tube surface absorptivity	0.97
• Tube surface emissivity	0.15
• Optical efficiency	0.772
• Peak collection efficiency (based on beam radiation)	0.68
• Annual collection efficiency (based on beam radiation)	0.53

6.4 COMPOUND PARABOLIC COLLECTOR (CPC)

Like the flat-plate collector with plane reflectors, the parabolic concentrating collector is also a non-imaging device. It has a large acceptance angle and requires only intermittent tracking. The usefulness of the geometry of the CPC for solar energy collection was noted by Winston* and it has been the subject of considerable attention. However, no significant commercial development has taken place.

6.4.1 Geometry

The geometry of an ideal two-dimensional CPC is shown in Fig. 6.11. The concentrator consists of two segments AB and DC which are parts of two parabolas 1 and 2. AD is the aperture of width W , and BC is the absorber surface of width b . The axes of two parabolas are oriented to each other at an angle in such a manner that the point C is the focus of parabola 1 and point B is the focus of parabola 2. Tangents drawn to the parabolas at points A and D are parallel to the axis of the CPC.

The acceptance angle of the CPC is the angle AED ($2\theta_a$), made by the lines obtained by joining each focus to the opposite aperture edge. The concentration ratio is given by $C = (W/b)$. It can be shown that $(W/b) = (1/\sin \theta_a)$ and that this concentration ratio is the maximum possible for the acceptance angle $2\theta_a$.

Using the x - y coordinate system shown in Fig 6.11, with origin O at the vertex of parabola 2, it is easy to show that the equation for parabola 2 is

*R. Winston, "Principles of Solar Concentrators of a Novel Design", *Solar Energy*, 16, 89 (1974).

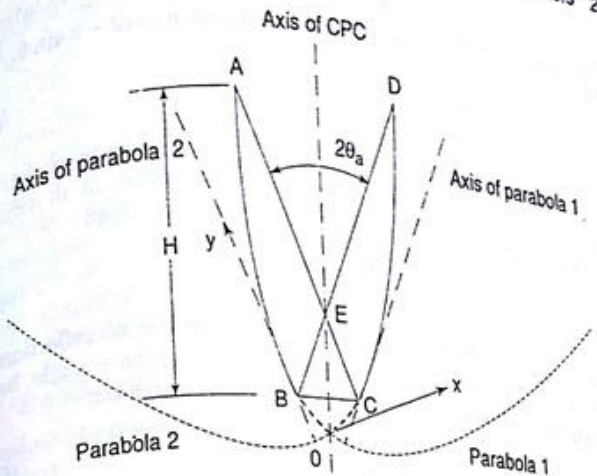


Fig. 6.11 Geometry of a Compound Parabolic Concentrating Collector

$$y = \frac{x^2}{2b(1 + \sin \theta_a)} \quad (6.44)$$

where the focal length $OB = \frac{b}{2}(1 + \sin \theta_a)$. The coordinates of the end points of the segment CD are as follows,

$$\text{Point } C: \quad x = b \cos \theta_a$$

$$y = \frac{b}{2}(1 - \sin \theta_a)$$

$$\text{Point } D: \quad x = (b + W) \cos \theta_a$$

$$y = \frac{b}{2}(1 - \sin \theta_a) \left(1 + \frac{1}{\sin \theta_a} \right)^2$$

The height-to-aperture ratio of the concentrator is given by

$$\frac{H}{W} = \frac{1}{2} \left(1 + \frac{1}{\sin \theta_a} \right) \cos \theta_a = \frac{1}{2} (1 + C) \left(1 - \frac{1}{C^2} \right)^{1/2} \quad (6.45)$$

The surface area of the concentrator is obtained by integrating along the parabolic arc. Rabl* has shown that the ratio of the surface area of the concentrator to the area of the aperture is given by the expression

*A. Rabl, "Optical and Thermal Properties of Compound Parabolic Concentrators", *Solar Energy*, 18, 497 (1976).

$$\frac{A_{\text{con}}}{WL} = \sin \theta_a (1 + \sin \theta_a) \left[\frac{\cos \theta_a}{\sin^2 \theta_a} + \ln \left\{ \frac{(1 + \sin \theta_a)(1 + \cos \theta_a)}{\sin \theta_a [\cos \theta_a + (2 + 2 \sin \theta_a)^{1/2}]} \right\} - \frac{\sqrt{2} \cos \theta_a}{(1 + \sin \theta_a)^{3/2}} \right] \quad (6.46)$$

For values of concentration ratio greater than 3, it can be shown that the following simple expression (which predicts values to an accuracy better than 5 per cent) may be used in place of Eq. (6.46).

$$\frac{A_{\text{con}}}{WL} = 1 + C \quad (6.47)$$

Rabl has also shown that the average number of reflections m undergone by all radiation falling within the acceptance angle, before reaching the absorber surface, is given by the expression

$$m = \frac{1}{2 \sin \theta_a} \left(\frac{A_{\text{con}}}{WL} \right) - \frac{(1 - \sin \theta_a)(1 + 2 \sin \theta_a)}{2 \sin^2 \theta_a} \quad (6.48)$$

where the value of (A_{con}/WL) is to be calculated from Eq. (6.46). Thus, the effective reflectivity of the concentrator surface is given by

$$\rho_e = \rho^m \quad (6.49)$$

where ρ_e = effective reflectivity,

and ρ = reflectivity value for a single reflection.

Example 6.4

A compound parabolic collector, 1 m long, has an acceptance angle of 20° . The absorber surface of the collector is flat and has a width of 10 cm. Calculate the concentration ratio, the aperture, the height and the surface area of the concentrator.

$$\text{Concentration ratio } C = \frac{1}{\sin 10^\circ} = 5.76$$

Therefore, Aperture $W = 5.76 \times 10 = 57.6$ cm

From Eqs (6.45) and (6.47),

$$\begin{aligned} \frac{H}{W} &= \frac{1}{2} \left(1 + \frac{1}{\sin 10^\circ} \right) \cos 10^\circ \\ &= 3.328 \end{aligned}$$

and

$$\frac{A_{\text{con}}}{WL} = 1 + 5.76 = 6.76$$

Therefore,

$$\begin{aligned} \text{Height } H &= 3.328 \times 57.6 \\ &= 191.7 \text{ cm} \end{aligned}$$

Surface area of concentrator,

$$\begin{aligned} A_{\text{con}} &= 6.76 \times 0.576 \times 1 \\ &= 3.90 \text{ m}^2 \end{aligned}$$

The results of Example 6.4 show that compared to a cylindrical parabolic collector, a CPC is very deep and requires a large concentrator area for a given aperture. Fortunately, however, it has been shown that a large portion of the top of a CPC can be removed with negligible loss in performance. Thus, in practice, a CPC is generally truncated (reduced in height) by about 50 per cent in order to reduce its cost. A detailed study on the effects of truncation has also been carried out by Rabl.*

6.4.2 Tracking Requirements

A two-dimensional CPC is usually oriented with its length parallel to the horizontal east-west direction and aperture plane sloping towards the south. As stated earlier, only intermittent tracking is required, the frequency of adjustment depending upon the concentration ratio. Thus, for example, for a concentration ratio of 10, the acceptance angle is 11.5° and a tracking adjustment may be needed once every few days in order to ensure collection for 7 or 8 hours every day. On the other hand, for a lower concentration ratio of 5, the acceptance angle is 23.1° and a tracking adjustment may be needed only once in a month or two months.

In order to calculate the tracking requirement, we will use the solar geometry equations of Chapter 3. The apparent plane of motion of the sun does not coincide with the east-west plane passing through the axis of the CPC. Hence the sun "rises" and "falls" with respect to the CPC, an extreme position being attained at solar noon. It is thus necessary to calculate the solar "swing" for the time period of the day for which collection is to be done. Referring to Fig. 6.12, assume that OG is a vertical stick whose shadow in the horizontal plane is GE . $EFGH$ is a rectangle in the horizontal plane, with EF and GH being east-west lines. Thus angle OEG is the solar altitude angle α_a . The projection of this angle in a vertical north-south plane, i.e. angle OGF , may be called the *solar elevation angle*. We will denote it by the symbol α_v . The change in the angle α_v over the specified time period is the *solar swing*.

From Fig. 6.12,

$$\tan \alpha_v = \frac{OG}{FG} = \left(\frac{OG}{OE} \right) \left(\frac{EH}{OE} \right) = \frac{\sin \alpha_a}{\cos OEH}$$

*A Rabl, *ibid.*

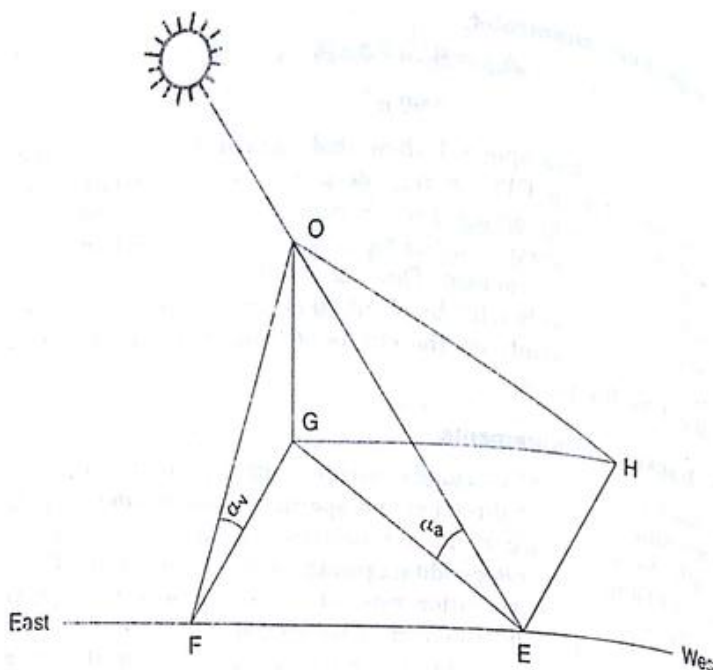


Fig. 6.12 Calculation of Solar Swing

Substituting expressions for $\sin \alpha_a$ and $\cos \alpha_a$ from Eqs (3.5) and (3.7) respectively, we have

$$\tan \alpha_v = \frac{\sin \phi \sin \delta + \cos \phi \cos \delta \cos \omega}{\sin \phi \cos \delta \cos \omega - \cos \phi \sin \delta} \quad (6.50)$$

At noon, when $\omega = 0$, we have,

$$\tan \alpha_v = \frac{\cos(\phi - \delta)}{\sin(\phi - \delta)} = \cot(\phi - \delta)$$

Therefore, $(\alpha_v)_{\omega=0} = \frac{\pi}{2} - (\phi - \delta) \quad (6.51)$

The solar swing angle over a time period corresponding to an hour angle ω_t to $-\omega_t$ is the change in α_v from the time corresponding to the angle $\pm \omega_t$ to solar noon. Thus the magnitude of the solar swing angle

$$= \left| \left[\frac{\pi}{2} - (\phi - \delta) \right] - \tan^{-1} \left[\frac{\sin \phi \sin \delta + \cos \phi \cos \delta \cos \omega_t}{\sin \phi \cos \delta \cos \omega_t - \cos \phi \sin \delta} \right] \right| \quad (6.52)$$

Equation (6.52) has been expressed in a neater form by Rabl.* He defines a solar elevation angle α'_v measured with reference to the

equatorial plane rather than the horizontal plane. α'_v is related to α_v by the equation

$$\alpha'_v = \alpha_v - \left(\frac{\pi}{2} - \phi \right) \quad (6.53)$$

Thus,

$$\tan \alpha'_v = - \frac{\cos \phi - \tan \alpha_v \sin \phi}{\tan \alpha_v \cos \phi + \sin \phi}$$

Substituting the expression for $\tan \alpha_v$ from Eq. (6.50), we get

$$\tan \alpha'_v = \tan \delta / \cos \omega$$

$$\alpha'_v = \tan^{-1}(\tan \delta / \cos \omega)$$

or, the magnitude of the solar swing angle

$$= |(\alpha'_v)_{\omega=0} - (\alpha'_v)_{\omega=\omega_t}|$$

$$= |\delta - \tan^{-1}(\tan \delta / \cos \omega_t)| \quad (6.55)$$

Equations (6.52) and (6.55) give the same values for the solar swing angle. However, Eq. (6.55) has the advantage of being simpler and of showing explicitly that the solar swing angle is independent of the latitude.

Example 6.5

A compound parabolic collector is located in Bombay (19.12°N) and is to be used for 8 h of collection on December 21 without making a tracking adjustment during the day. Calculate the minimum acceptance angle required for the collector, its concentration ratio and its orientation.

First we calculate the solar swing angle on December 21 from 0800 h to 1200 h (LAT). Substituting $\delta = -23.45^\circ$, $\omega_t = 60^\circ$ in Eq. (6.55),

$$\begin{aligned} \text{Solar swing angle} &= | -23.45^\circ - \tan^{-1}[\tan(-23.45^\circ) / \cos 60^\circ] | \\ &= | -23.45^\circ - (-40.94^\circ) | \\ &= 17.5^\circ \end{aligned}$$

The minimum acceptance angle required for the collector is obviously equal to the solar swing angle. Thus, $2\theta_a = 17.5^\circ$ and concentration ratio $C = (1 / \sin 8.75^\circ) = 6.57$.

The slope of the collector aperture plane would have to be adjusted such that the sun's rays enter parallel to the axis of the upper parabolic segment at 0800 h. This will ensure that the sun's rays at noon enter parallel to the axis of the lower parabolic segment. Now from Eq. (6.51),

$$\begin{aligned} (\alpha_v)_{\omega=0} &= \frac{\pi}{2} - (19.12^\circ + 23.45^\circ) \\ &= 47.43^\circ \end{aligned}$$

*A. Rabl, "Comparison of Solar Concentrators", *Solar Energy*, 18, 93 (1976).

Therefore, angle made by the axis of the lower parabolic segment with the horizontal = 47.43° .
 Angle made by axis of CPC with the horizontal
 $= 47.43^\circ - \theta_a$
 $= 38.68^\circ$

It should be noted that the solar swing angle is maximum on the solstice days, viz. June 21 and December 21, and equal to zero on the equinox days, viz. March 21 and September 21. Thus a collector having an acceptance angle of 17.5° would give 8 or more hours of collection on all the days of the year without requiring a diurnal tracking adjustment.

Equation (6.55) can also be used for calculating the collection time per day for a CPC with a given acceptance angle or for calculating the number of adjustments required in a year for a CPC with a given acceptance angle and a required minimum collection time per day. This calculation has been done by Rabl.* The procedure adopted was as follows: On June 21, the collector is assumed to be oriented with its axis pointing at an angle θ_a above the solar noon altitude angle. It is left in this position until the day when the collection time falls below the minimum specified value. On this day, it is adjusted with its axis again pointing at an angle θ_a above the solar noon altitude angle. The procedure is repeated over a time span of one year in order to obtain the number of adjustments per year.

6.4.3 Performance Analysis

Consider a compound parabolic collector having an aperture W , length L and acceptance angle $2\theta_a$ (Fig. 6.13). The absorber surface has a width b . The heat collected at the absorber surface is transferred to a fluid flowing through N tubes, having an outer diameter D_o and an inner diameter D_i , attached to the bottom side. The fluid enters at a temperature T_{fi} , leaves at a temperature T_{fo} and has a mass flow rate \dot{m} . The aperture, which is covered with a transparent sheet, is assumed to be sloping south at such an angle that the beam radiation incident on it is within the acceptance angle of the collector. It is also assumed that the length of the absorber surface is a little more than the length L so that it intercepts all the reflected radiation.

We first derive an expression for the flux S absorbed at the absorber surface. Because of its large acceptance angle, a CPC accepts both beam and diffuse radiation. The beam radiation flux falling on the aperture plane is $I_b r_b$, while the diffuse radiation flux within the

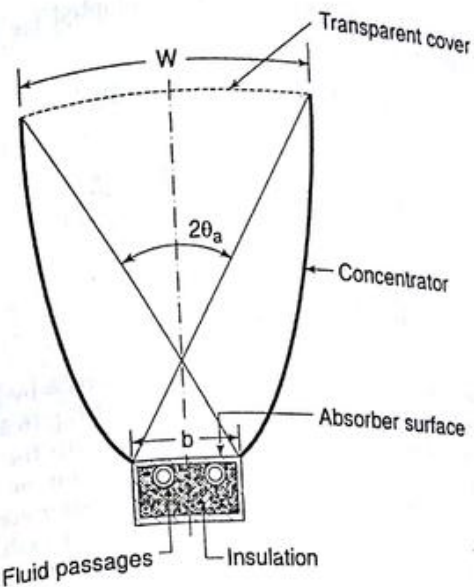


Fig. 6.13 Compound Parabolic Collector with Flat Absorber Surface

acceptance angle* is given by (I_d/C) . Thus, the total effective flux entering the aperture plane is $[I_b r_b + (I_d/C)]$ and

$$S = \left[I_b r_b + \frac{I_d}{C} \right] \tau \rho_e \alpha \quad (6.56)$$

where τ = transmissivity of the cover,

ρ_e = effective reflectivity of the concentrator surface for all radiation,

α = absorptivity of the absorber surface.

The values of τ , ρ_e and α are assumed to be the same for beam and diffuse radiation. It is to be noted that the flux S is based on the area of the aperture.

In order to obtain an expression for the useful heat gain rate, we take an energy balance on an elementary slice dx of the absorber surface at a distance x from the inlet. This yields the equation

$$dq_u = \left[S - \frac{U_l}{C} (T_p - T_a) \right] W dx \quad (6.57)$$

Proceeding along lines similar to those adopted for the cylindrical parabolic collector, we obtain

$$q_u = F_R WL \left[S - \frac{U_l}{C} (T_{fi} - T_a) \right]$$

where,

$$F_R = \frac{\dot{m} C_p}{b U_l L} \left[1 - \exp \left\{ - \frac{F' b U_l L}{\dot{m} C_p} \right\} \right] \quad (6.58)$$

and

$$\frac{1}{F'} = U_l \left[\frac{1}{U_l} + \frac{b}{N \pi D_t h_f} \right] \quad (6.59)$$

The instantaneous collection efficiency is then given by Eq. (6.25). The main difficulty associated with the use of Eq. (6.58) is that the overall loss coefficient U_l cannot be calculated with the same degree of accuracy as in the case of a flat-plate collector or a cylindrical parabolic collector. Adequate convective heat transfer correlations are not available for the purpose and the radiative heat exchange calculation is also more complicated. Based on some approximate correlations, Rabl* has estimated the value of U_l for different values of the absorber plate temperature, plate emissivity and the concentration ratio. These values are given in Table 6.4. It is seen that they vary from 4 to 19.4 $\text{W/m}^2\text{-K}$. Values of U_l for situations differing from those given in Table 6.4 may be obtained by interpolation.

Table 6.4 Overall Loss Coefficient in a Compound Parabolic Concentrator (Units: $\text{W/m}^2\text{-K}$)

T_{pm} ($^{\circ}\text{C}$)	$C = 1.6$		4.0		8.0	
	$\epsilon_p = 0.1$	0.9	0.1	0.9	0.1	0.9
110	4.0	8.2	5.6	10.5	6.9	11.8
210	5.0	11.8	7.8	16.0	10.4	19.4

Apart from the flat one-sided absorber surface shown in Fig. 6.13, CPCs can also be designed for other absorber surfaces. Two shapes, (a) tubular, and (b) tubular with longitudinal fins, are shown in Fig. 6.14. Unlike the flat absorber surface, these shapes have the advantage of not having a back side through which heat can be lost.

*A. Rabl, *ibid.*

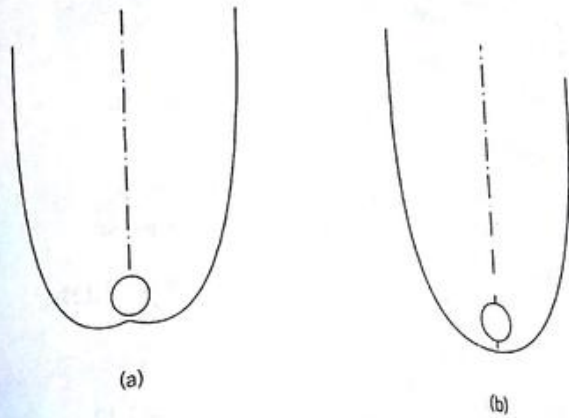


Fig. 6.14 Other Absorber Shapes used in CPCs:
(a) Tubular, (b) Tubular with Longitudinal Fins

Example 6.6

A CPC is mounted on a horizontal east-west axis and oriented with its aperture plane sloping at an angle of 40° . The concentration ratio of the collector is 6.5, the width of its absorber plate is 6 cm and its length is 2 m. The collector is used for heating a fluid ($C_p = 2.35 \text{ kJ/kg-K}$) which enters at a temperature of 130°C . Calculate the exit temperature of the fluid and the instantaneous collection efficiency for the following situation:

- Location of collector = New Delhi (28.58°N)
- Date = Nov. 5
- Time = 1100 h (LAT)
- I_g = 0.735 kW/m^2
- I_d = 0.162 kW/m^2
- Number of tubes = 2
- Tube outer diameter = 18 mm
- Tube inner diameter = 14 mm
- Transmissivity of glass cover = 0.89
- Reflectivity of concentrator = 0.87
- Absorptivity of absorber surface = 0.94
- Overall loss coefficient = $10.5 \text{ W/m}^2\text{-K}$
- Heat transfer coefficient on inside of absorber tube = $230 \text{ W/m}^2\text{-K}$

- Mass flow rate of fluid
- Ambient temperature

$$= 1.25 \text{ kg/min}$$

$$= 21^\circ\text{C}$$

Geometry of Collector

$$\text{Half acceptance angle } \theta_a = \sin^{-1} \left(\frac{1}{6.5} \right) = 8.85^\circ$$

Therefore acceptance angle = 17.70°

Aperture width $W = 0.06 \times 6.5 = 0.39 \text{ m}$

Substituting the value of θ_a in Eq. (6.46), we get

$$\frac{A_{\text{con}}}{WL} = 0.1538 \times 1.1538 (41.7459 + 1.7832 - 1.1275)$$

$$= 7.524$$

Therefore, from Eq. (6.48),

$$\text{average number of reflections } m = 1.12$$

Flux S

The flux S is calculated from Eq. (6.56). Before doing so, we must check that the beam radiation is within the acceptance angle of the collector.

On November 5, $n = 309$ and $\delta = -16.55^\circ$. Therefore, from Eq. (6.56), the solar elevation angle is given by,

$$\tan \alpha_v = \frac{\sin 28.58^\circ \sin (-16.55^\circ) + \cos 28.58^\circ \cos (-16.55^\circ) \cos 15^\circ}{\sin 28.58^\circ \cos (-16.55^\circ) \cos 15^\circ - \cos 28.58^\circ \sin (-16.55^\circ)}$$

$$= 0.9766$$

$$\alpha_v = 44.32^\circ$$

Since the slope of the aperture plane is 40° , the axis of the CPC makes an angle of 50° with the horizontal. Thus, beam radiation having a solar elevation angle between the limits of $(50^\circ \pm 8.85^\circ)$, i.e. between 58.85° and 41.15° , would be accepted by the collector. In the present problem, the beam radiation is within these limits.

Now, from Eq. (3.30),
tilt factor r_b

$$= \frac{\sin (-16.55^\circ) \sin (28.58^\circ - 40^\circ) + \cos (-16.55^\circ) \cos 15^\circ \cos (28.58^\circ - 40^\circ)}{\sin 28.58^\circ \sin (-16.55^\circ) + \cos 28.58^\circ \cos (-16.55^\circ) \cos 15^\circ}$$

$$= 1.4243$$

$$\text{Therefore, } S = \left(573 \times 1.4243 + \frac{162}{6.5} \right) 0.89 \times 0.87^{1.12} \times 0.94$$

$$= 602.3 \text{ W/m}^2$$

Useful Heat Gain Rate

From Eqs (6.58), (6.59) and (6.60),

$$\frac{1}{F'} = 10.5 \left[\frac{1}{10.5} + \frac{0.06}{2 \times \pi \times 0.014 \times 230} \right]$$

$$= 1.0311$$

$$F' = 0.9698$$

$$\frac{\dot{m}C_p}{bU_L} = \frac{1.25}{60} \times \frac{2350}{0.06 \times 10.5 \times 2} = 38.856$$

$$F_R = 38.856 [1 - \exp(-0.9698/38.856)]$$

$$= 0.9578$$

$$\text{Useful heat gain rate } q_u = 0.9578 \times 0.39 \times 2 \times \left[602.3 - \frac{10.5}{6.5} (130 - 21) \right]$$

$$= 318.4 \text{ W}$$

Exit Fluid Temperature and Collection Efficiency

The exit fluid temperature is calculated from the equation

$$\frac{1.25}{60} \times 2350 \times (T_{f0} - 130) = 318.43$$

$$T_{f0} = 136.50^\circ\text{C}$$

From Eq. (6.25),

$$\eta_i = \frac{318.4}{\left[573 \times 1.4243 + \frac{162(1 + \cos 40^\circ)}{2} \right] 0.39 \times 2}$$

$$= 0.4256$$

6.4.4 Test Results

Rabl *et al.** have reported results obtained on two collector modules developed on the basis of extensive research. The first module was a panel ($0.91 \text{ m} \times 1.83 \text{ m}$) with 7 CPC troughs placed side by side, each trough having an area of $0.13 \times 1.83 \text{ m}^2$, and a depth of 0.305 m . The absorber was a steel tube of 0.79 cm outer diameter with a selective black chrome coating. The collector had a concentration ratio of 5.2.

*A. Rabl, J. O'Gallagher and R. Winston, "Design and Test of Non-evacuated Solar

The above dimensions do not correspond to those of an ideal CPC. The absorber tube is slightly oversized to take care of optical misalignments. The reflecting surface was an aluminised mylar sheet on a urethane foam backing. A 3 mm thick acrylic cover was used for protecting the reflecting surface. The collector required 24 tilt adjustments per year in order to ensure a minimum of 7 hours of collection per day.

Data was obtained with water as the test fluid both in the 'open loop' configuration (in which T_f is close to T_a) and in the 'closed loop' configuration under a variety of weather conditions. The data was found to fit the following equation,

$$\eta_i = 0.680 - 1.85(\bar{T}_f - T_a)/I_T$$

The second module was a panel (0.76 m \times 1.70 m) with two troughs having a depth of 0.46 m. The absorber was a copper tube of 1.59 cm outer diameter, having two longitudinal fins of height 2.54 cm fixed to it. The absorber surface had a selective black chrome coating, while the reflector was a thin polished aluminium sheet. A 3 mm thick glass cover was used to protect the reflector surface. The collector had a concentration ratio of 3. Unlike the first module, this module required only two tilt adjustments in a year, at intervals of six months, in order to ensure a minimum of 7 hours of collection per day. The following performance equation was deduced from the experimental data obtained with water

$$\eta_i = 0.59 - 2.72(\bar{T}_f - T_a)/I_T \quad (6.62)$$

It is of interest to compare the data obtained with the second CPC module with performance data on flat-plate collectors presented in Chapter 4. Comparing Eq. (6.62) with Eq. (4.68) for a single cover conventional collector and with Eq. (4.69) for an evacuated tube collector with a back reflector, we see that the performance of the CPC is better than the conventional FPC and comparable to that of the ETC.

When research and development work on compound parabolic collectors began in 1974, the emphasis was on attaining high temperatures with concentration ratios of 5 to 10. The test results just described and other optimization studies show that this emphasis was probably misplaced. In fact, CPCs seem to be better suited and cost effective for solar applications requiring temperatures in the range of 70 to 100°C. These CPCs would have low concentration ratios (not exceeding 3) and would require very few tilt adjustments.

6.4.5 A Novel Design

It has been mentioned in Chapter 4 that some commercial ETC designs use CPC reflectors. Following the same principle, O'Gallagher

et al.¹ have proposed a novel integrated design of an ETC in which the outer glass envelope of the evacuated tube itself has the shape of a CPC. A crosssection profile of this design is shown in Fig. 6.15. The authors claim that such a design results in a higher optical efficiency and does not get degraded.

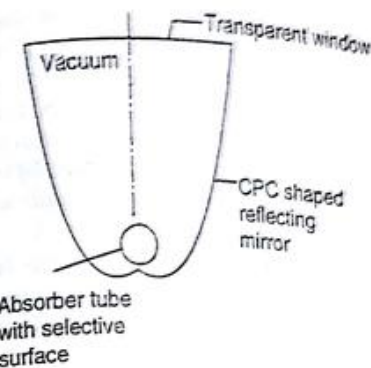


Fig. 6.15 An Evacuated Tube Collector with a CPC Shaped Reflector as the Outer Envelope

6.5 PARABOLOID DISH COLLECTOR

Some commercial designs of paraboloid dish collector systems have been developed in the last ten years for electric power production. Two of these will be described in this section.

A 7.5 m diameter stretched metal membrane concentrator has been developed by a German firm. The membrane is a stainless steel sheet (0.23 mm thick) fixed on both sides of a circular ring. The two membranes are deformed plastically to a parabolic shape by applying a water load and a partial vacuum, the vacuum being maintained during operation of the concentrator. The front membrane is covered with thin glass mirrors having a reflectivity of 0.90 and an area of 42 m². The concentrator is suspended at two points in a polar mounting and tracks the sun by rotating daily about a vertical axis and seasonally about a horizontal axis. The focal length is 5 m. A cavity-

¹J.J. O'Gallagher, K. Snail, R. Winston, C. Peek and J.D. Garrison, "A New Evacuated CPC Collector Tube", *Solar Energy*, 29, 575 (1982).

type receiver having a diameter of 0.2 m is kept at the focus. About 27 kW of energy is absorbed in the receiver if the incident beam radiation is 800 W/m^2 . A Stirling engine located at the focus converts this thermal input to 8 kW with an energy conversion efficiency of 0.3. More recently, the same firm has built two 17 m diameter dishes of the same design generating 50 kW each. These are in operation in Saudi Arabia. Dish/Stirling engine systems have also been built by other manufacturers.

It is generally felt that paraboloid dish systems are best suited for applications which utilize solar energy directly at the focus of each collector. However in the USA, a 5 MW power plant utilizing the steam generated by seven hundred dishes has been erected. Each dish consists of a reflecting array of twenty four 1.5 m diameter mirrors having an area of 42 m^2 . The mirrors are made of reflective polymeric film fixed on circular aluminium frames and subjected to a continuous applied vacuum. The receiver is an insulated cylindrical cavity about 0.9 m long and of diameter 0.6 m, and contains a molten salt. Pipes carrying water/steam pass through the salt bath. Thus the solar energy is first absorbed by the molten salt and then transferred to the water/steam, the salt bath acting as a storage which takes care of small variations in solar radiation.

Out of the total number of seven hundred dishes, six hundred are used to obtain saturated steam at 275°C , while the remaining one hundred dishes are used to superheat the steam to 400°C . The steam is used to run two turbine-generator sets—one a main set of 3.68 MW and the other, a peaking set of 1.24 MW.

6.6 CENTRAL RECEIVER COLLECTOR

The principle of working of a central receiver power plant had been described in Sec. 2.2.3. The idea of building such a plant was first suggested by Baum, Aparasi and Garf.* Based on their calculations, they indicated the possibility of erecting an installation in the sunny regions of the USSR, to produce 11 to 13 t of steam per hour at 30 atm and 400°C . The optical system was calculated to consist of 1293 mirrors of dimensions $3 \times 5 \text{ m}$. These heliostats were proposed to be mounted on carriages which moved on rails in arcs around the tower.

A number of small pilot plants were built by Francia† in Italy in

the period 1965 to 1967. In one of these, he collected 50 kW of energy. After a break of a few years, the design of central receiver collector systems again attracted attention in the eighties and a number of plants ranging in capacity from 0.5 to 10 MWe were built. These have been listed in Table 2.1 along with some technical specifications.

The two major components making up a central receiver collector are the heliostats and the receiver. These will now be described.

Heliostats

The heliostats form an array of circular arcs around the central tower. They intercept, reflect and concentrate the solar radiation onto the receiver. The array is served by a tracking control system which continuously focusses beam radiation towards the receiver during collection. In addition, when solar radiation is not being collected, the control system orients the heliostats in a safe direction so that the receiver is not damaged.

As stated earlier, the 10 MWe plant at Barstow was the largest of the pilot plants built. It was operated for six years, from 1982 to 1988. The plant had a field of 1818 heliostats positioned all round a central tower of height 80 m. Each heliostat was an assembly of 12 slightly concave glass mirrors mounted on a support structure and geared drive that could be controlled for azimuth as well as elevation. The total reflective area of each heliostat was 39.3 m^2 . A rear view sketch is shown in Fig. 6.16. The 12 mirror panels in each heliostat were $1 \times 3 \text{ m}$ in size and were made from 3 mm low iron float glass. When clean, the heliostats had an average reflectivity of 0.903. However, dirt accumulated due to exposure to the environment reduced the average reflectivity to 0.82. A goal of 0.92 has been set for future heliostat arrays. In order to achieve this goal along with reduced cost and weight, a number of new concepts are being experimented. For example, larger size glass-mirror heliostats having areas of 150 m^2 and reflectivity values up to 0.94 have been built. Also a new type of cost effective heliostat using a stretched membrane has been developed. In this heliostat, the reflector is a silvered polymer film laminated to a thin metal foil which is stretched over a large-diameter metal ring. The reflectivity of this surface has been measured to be 0.92. Because of its simplicity and reduced weight, a stretched-membrane heliostat would be about 30 per cent less costly than a glass-mirror design.

Receiver

The receiver is the most complex part of the collection system. The main factor influencing its design is its ability to accept the large and variable heat flux which results from the concentration of the solar radiation by the heliostats. This flux has to be transferred to the

*V.A. Baum, R.R. Aparasi and B.A. Garf, "High Power Solar Installations", *Solar Energy*, 1, 6 (1957).

†G. Francia, "Pilot Plants of Solar Steam Generating Stations", *Solar Energy*, 12, 51 (1968).

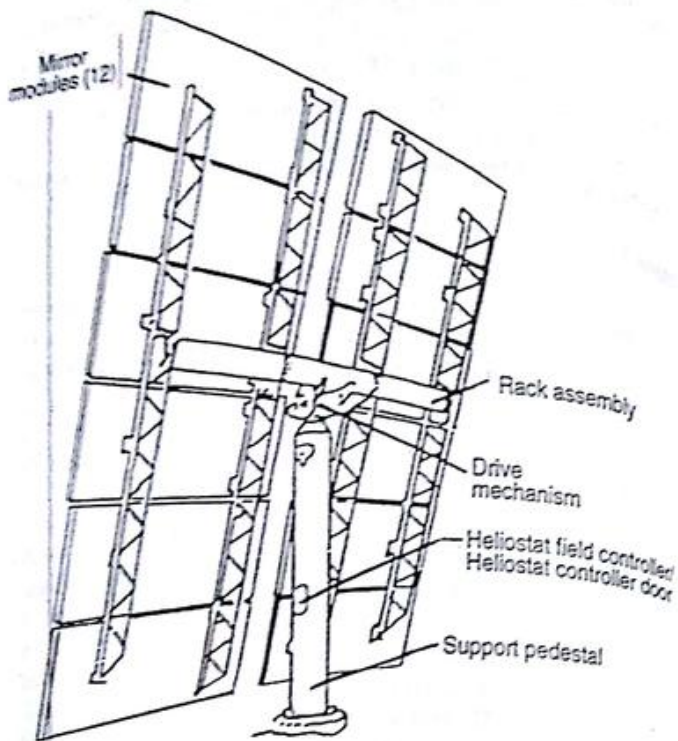


Fig. 6.16 A Heliostat

receiver fluid. The value of the heat flux can range from 100 to 1000 kW/m^2 and this results in high temperatures, high thermal gradients and high stresses in the receiver. The value depends on the concentration ratio and varies with the season and the day. It also varies over the surface of the receiver. For these reasons, attention has to be given to the absorber shape, the heat transfer fluid, the arrangement of tubes to carry the fluid and the materials used for construction.

There are two types of receiver designs: the external type and the cavity type (Fig. 6.17). The external receiver is usually cylindrical in shape. The solar flux is directed onto the outer surface of the cylinder consisting of a number of panels and is absorbed by the receiver fluid flowing through closely spaced tubes fixed on the inner side. On the other hand, in a cavity receiver, the solar flux enters through one or more small apertures in an insulated enclosure. The cavity contains a suitable tube configuration through which the receiver fluid flows. The geometry of the cavity is such that it maximises the absorption of the entering radiation, minimizes heat losses by convection and radiation

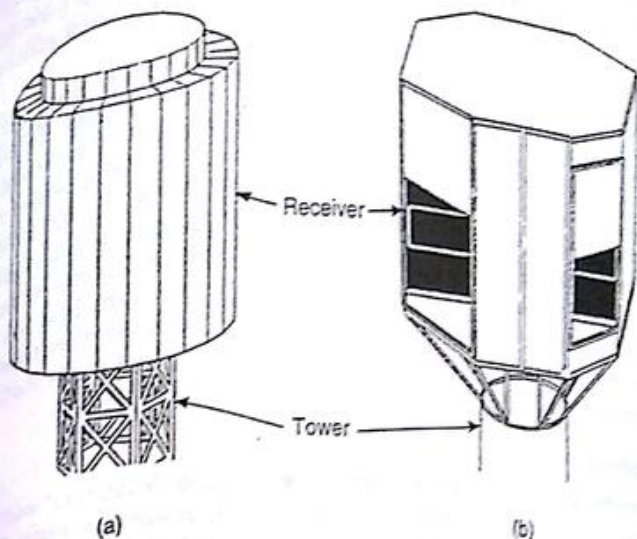


Fig. 6.17 Receivers: (a) External Type, (b) Cavity Type with Four Apertures

to the ambient and at the same time accommodates the heat exchanger that transfers the radiant energy to the receiver fluid. Both types of receivers have their advantages and disadvantages. The external type has a very wide acceptance angle, while the cavity type has a small acceptance angle. On the other hand, the cavity type traps the solar flux more effectively and consequently has a higher efficiency than the external type.

The 10 MWe plant at Barstow had an external type of receiver in which water was heated directly and converted to superheated steam. The receiver was a cylinder, 7 m in diameter and 13.5 m in height, made up of 24 vertical panels painted black. Tubes made from Incoloy 800 (0.6 cm I.D., 1.25 cm O.D.) were fixed on the inside. The receiver was located on a tower 80 m high and produced steam at 102 bar and 510°C. The receiver had an annual efficiency of 0.69, which was rather low. In order to achieve higher efficiencies, it is planned that the next design will use a molten salt as the heat transfer fluid instead of

water/steam. With a molten salt, the receiver can operate with higher incident solar fluxes. Consequently the size of the receiver would be reduced resulting in smaller thermal losses. In addition, the molten salt would be essentially at atmospheric pressure, thereby permitting the use of thinner walled tubes in the receiver. An annual efficiency goal of 0.90 has been set for this design.

Finally it may be mentioned that an experimental cavity type receiver with a capacity of 2.5 MWth and using air as the working fluid has also been tested recently. Air has obvious advantages when used as the working fluid. In the experimental receiver, the air is heated to a temperature of 700°C at an average solar flux density of 300 kW/m². The heat transfer process takes place in the absorber, which is made up of thin wire mesh mats stacked one over the other. The concentrated solar flux causes the wires to heat up and these in turn heat the air flowing through them. Since the wire mesh is thin, the absorption of solar radiation takes place over a certain depth and not at the surface. Consequently thermal losses due to re-radiation are reduced.

Analysis

Consider a central receiver collector consisting of N mirrors* each of area A_m and span w covering a ground area A_g around the tower. The mirrors have to be laid out in such a manner that incident or reflected radiation associated with one heliostat is not blocked by a neighbouring heliostat. As a result, they have to be spaced apart and cover only a fraction of the ground area. If the fraction of the ground area covered is ψ , then

$$NA_m = \psi A_g \quad (6.63)$$

In most central receiver collector designs, the value of ψ is around 0.4.

Let the receiver's absorber surface (on which the radiation is focussed) have an area A_p and be located on top of a tower of height H . Taking an energy balance on the absorber, we obtain the following expression for the useful heat gain rate,

$$q_u = I_b \left[\sum_{j=1}^N r_{bj} \right] \rho \tau \alpha A_m - U_p A_p (T_{pm} - T_a) \quad (6.64)$$

Defining an average tilt factor

$$(r_b)_{av} = \frac{1}{N} \sum_{j=1}^N r_{bj} \quad (6.65)$$

*The mirrors could be circular in which case $A_m = \pi w^2/4$, or square in which case $A_m = w^2$

and using Eq. (6.63), we have

$$q_u = I_b (r_b)_{av} \psi A_g \rho \tau \alpha - U_p A_p (T_{pm} - T_a) \\ = \psi A_g \left[I_b (r_b)_{av} \rho \tau \alpha - \frac{U_p}{C} (T_{pm} - T_a) \right] \\ C = (NA_m/A_p) = (\psi A_g/A_p) \quad (6.66)$$

where

In order to obtain expressions for the size of the absorber and the concentration ratio, we assume that the mirror field is circular with the tower at the centre. The rim angle, i.e. the angle made by the line joining the absorber and the outermost mirror with the vertical is taken to be ϕ_r (Fig. 6.18). Thus the distance between the outermost

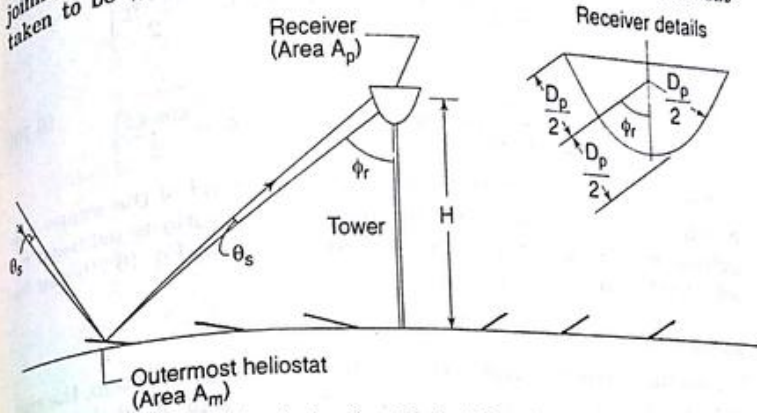


Fig. 6.18 Analysis of a Central Receiver Collector

mirror and the absorber is $(H/\cos \phi_r)$. If the mirrors are flat, it follows that the size of the image at the absorber is given by

$$L_i = \frac{H}{\cos \phi_r} (\theta_s + \theta_e) + w \quad (6.67)$$

where θ_s is the angle subtended by the sun at the earth and θ_e is the total angular error associated with the reflection due to factors like mirror surface imperfections and mirror orientation. If the mirrors are suitably dished, then the spread of the image due to the mirror span could be eliminated, and the size L_i is obtained by putting $w = 0$ in Eq. (6.67).

Vant-Hull and Hildebrandt* have suggested that an appropriate shape for the absorber could be a spherical segment with a conical section as shown in Fig. 6.18. The area of such a shape is given by

*L.L. Vant-Hull and A.F. Hildebrandt, "Solar Thermal Power System based on Optical Transmission", *Solar Energy*, 18, 31 (1976).

$$A_p = \frac{\pi}{2} D_p^2 \left(1 + \sin \phi_r - \frac{\cos \phi_r}{2} \right)$$

where D_p is the diameter of the sphere as well as the apparent height of the absorber when viewed from the outermost mirror. Equating D_p with the image size given in Eq. (6.67), we have

$$A_p = \frac{\pi}{2} \left\{ \frac{H}{\cos \phi_r} (\theta_s + \theta_e) + w \right\}^2 \left(1 + \sin \phi_r - \frac{\cos \phi_r}{2} \right)$$

Thus, the concentration ratio for this shape is given by

$$C = \frac{NA_m}{\frac{\pi}{2} \left\{ \frac{H}{\cos \phi_r} (\theta_s + \theta_e) + w \right\}^2 \left(1 + \sin \phi_r - \frac{\cos \phi_r}{2} \right) \psi \pi H^2 \tan^2 \phi_r}$$

$$= \frac{\pi}{2} \left\{ \frac{H}{\cos \phi_r} (\theta_s + \theta_e) + w \right\}^2 \left(1 + \sin \phi_r - \frac{\cos \phi_r}{2} \right) \quad (6.70)$$

For suitably dished mirrors, in which the spread of the image due to mirror span is eliminated, the concentration ratio is obtained by putting $w = 0$ in Eq. (6.70). Expressions similar to Eq. (6.70) can be obtained for other absorber shapes.

Example 6.7

In a central receiver collector, the height of the tower is 150 m, the rim angle is 50° and the diameter of the mirrors is 4.5 m. Find the size of the image formed by the outermost mirror at the receiver, the area of the absorber (if it is as shown in Fig. 6.18) and the corresponding concentration ratio. Assume that mirrors are (i) flat, and, (ii) dished. Take $\psi = 0.38$ and $\theta_e = 0.002$ radians.

(i) From Eqs (6.67) and (6.68),

$$L_i = \frac{150}{\cos 50^\circ} \left(\frac{32\pi}{60 \times 180} + 0.002 \right) + 4.5$$

$$= 7.14 \text{ m}$$

$$A_p = \frac{\pi}{2} \times 7.14^2 \left(1 + \sin 50^\circ - \frac{\cos 50^\circ}{2} \right)$$

$$= 115.67 \text{ m}^2$$

Thus,

$$C = \frac{0.38 \times \pi \times 150^2 \times \tan^2 50^\circ}{115.67}$$

$$= 330$$

(ii) If the mirrors are dished,

$$L_i = \frac{150}{\cos 50^\circ} \left(\frac{32\pi}{60 \times 180} + 0.002 \right)$$

$$= 2.64 \text{ m}$$

$$A_p = \frac{\pi}{2} \times 2.64^2 \left(1 + \sin 50^\circ - \frac{\cos 50^\circ}{2} \right)$$

$$= 15.82 \text{ m}^2$$

$$C = \frac{0.38 \times \pi \times 150^2 \times \tan^2 50^\circ}{15.82}$$

$$= 2412$$

Thus,

PROBLEMS

1. Obtain the expression

$$\psi = (\pi + \beta + 2\phi - 2\delta)/3$$

for the correct inclination of a south-facing specular reflector fixed on the top edge of a flat-plate collector (as shown in Fig. 6.2) and having the same dimensions as the flat-plate collector.

2. Compare the values of the tilt factor for beam radiation incident on a flat-plate collector with the tilt factors obtained for north and south-facing reflectors fixed to it. Given the following data:

- Location of collector-reflector array : Madras (13.00°N)
- Slope of collector : 13° facing south
- Date : Jun. 21 and Dec. 21
- Time : 1200 h (LAT)

Assume that the reflectors are inclined at angles given by Eq. (6.1) and by Problem 1.

3. A cylindrical parabolic collector is operated in Calcutta (22.65° N, 88.45° E) in tracking mode II. Calculate the variation in the slope of the aperture plane from 0800 to 1600 h (LAT) on June 21.

4. A cylindrical parabolic collector is located in Pune (18.53° N) and operates in tracking mode II on May 1. Calculate the values of the slope of the aperture plane from 0600 to 1200 h (LAT) at hourly intervals and the corresponding angle of incidence. Calculate also the time at sunrise.

5. Calculate the overall loss coefficient for an evacuated glass tube cylindrical parabolic focussing collector with the following data:

- Absorber tube: Outer diameter = 6.5 cm
Inner diameter = 6.0 cm
- Glass cover: Outer diameter = 15.8 cm
Inner diameter = 15.0 cm
- Aperture : 1.90 m
- Length of concentrator : 3.50 m

- Emissivity of absorber tube surface = 0.22
 - Emissivity/absorptivity of glass = 0.88
 - Average temperature of absorber tube = 200°C
 - Ambient temperature = 20°C
 - Wind velocity = 1.5 m/s
6. Use Eqs (6.39–6.42) to calculate the glass cover temperature and the overall loss coefficient for the data of Example 6.3. Take $h_w = 34.119 \text{ W/m}^2\text{K}$. Compare the answers with the values obtained by the iterative procedure.
7. In order to check the sensitivity of the overall loss coefficient to the value of h_w , repeat the calculation of Problem 6 with a value of h_w which is 10 per cent higher. What is the per cent change in the value of U_f ?
8. A cylindrical parabolic focussing collector is used for heating a thermal fluid ($C_p = 2.2 \text{ kJ/kg}\text{K}$) which enters with a temperature of 160°C. The concentrator has an aperture of 1.8 m and a length of 3 m. The absorber tube has an inner diameter of 2.6 cm and outer diameter of 3.2 cm and has a concentric glass cover around it. Given that:
- Specular reflectivity of concentrator surface = 0.82
 - Intercept factor = 0.91
 - $(\alpha_s)_s$ = 0.8
 - Beam radiation incident normally on aperture plane = 556 W/m^2
 - Diffuse radiation incident on aperture plane = 152 W/m^2
 - Overall loss coefficient = 9.5 $\text{W/m}^2\text{K}$
 - Convective heat transfer coefficient on inside of absorber tube = 325 $\text{W/m}^2\text{K}$
 - Ambient temperature = 27°C
 - Mass flow rate of fluid = 360 kg/h
- Calculate the useful heat gain rate, the exit temperature of the fluid and η_{th} instantaneous efficiency.
9. Calculate the performance of the cylindrical parabolic collector of Example 6.3 for the situation when (i) the absorber tube surface is selective ($\epsilon_p = 0.15$), (ii) q_s annulus is evacuated, and (iii) the fluid inlet temperature is 180°C. All other data remain the same.
10. Study the effect of having two glass covers instead of one on the performance of the cylindrical parabolic collector of Example 6.3. Assume that the outer glass cover has an outer diameter of 8.0 cm and an inner diameter of 7.2 cm, while the dimensions of the inner glass cover are unchanged. All other data remain the same. Calculate the value of η_{th} for inlet temperatures of 120, 150 and 180°C and plot the variation. It should be noted that the curve obtained with two glass covers will intersect the curve with one glass cover (Fig. 6.8, curve I).
11. Study the effect of varying the annular gap between the absorber tube and the glass cover on the performance of the cylindrical parabolic collector of Example 6.3. Keep all data the same and calculate the efficiency for two situations (i) $D_{co} = 5.5 \text{ cm}$, $D_{ci} = 4.8 \text{ cm}$, and (ii) $D_{co} = 7.1 \text{ cm}$, $D_{ci} = 6.4 \text{ cm}$. Compare the results with those obtained in Example 6.3. Is there an optimum annular gap?
12. Derive an expression for the useful heat gain rate of a parabolic dish collector having a cylindrical absorber at its focus. The diameter and length of the absorber on the outside are D_o and L_o , and on the inside, D_i and L_i . Assume that the heat transfer fluid changes its phase as it passes through the absorber and consequently remains at a constant temperature T_{fi} .

13. An untruncated CPC has a half-acceptance angle of 36° and an absorber width of 10 cm. Calculate the concentration ratio, the aperture, the height, and the surface area of the concentrator per metre length.
14. A CPC has an acceptance angle of 7.5°. Find the maximum collection period possible on April 15 without making a tracking adjustment.
15. Solve Example 6.7 by assuming that the absorber has the shape of a hemispherical bowl.
16. A central receiver collector system consists of 1800 heliostats, each $6.5 \times 6 \text{ m}$ in size. The height of the central tower is 80 m and the rim angle is 51°. Find the size of the image formed by the outermost arc of heliostats at the receiver. The receiver is a vertical cylinder whose height is two times the diameter. Calculate the size of the receiver and the concentration ratio. Assume that the angular error associated with the heliostats does not exceed 0.0055 radians and that the heliostats are suitably dished.

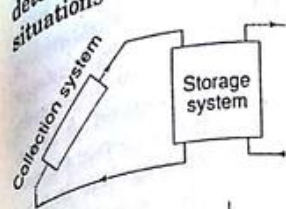
Thermal Energy Storage

This chapter deals with the description and analysis of various thermal energy storage systems. The chapter commences with an introductory section in which various situations requiring the use of a storage system are described and the basic methods of storing thermal energy are discussed. This is followed by a detailed description of sensible heat storage systems. Various materials, their properties and the range of temperatures over which they can be used for storage are mentioned. Analyses of a few situations are given and testing procedures described. Finally, latent heat storage systems and thermochemical storage systems are briefly described.

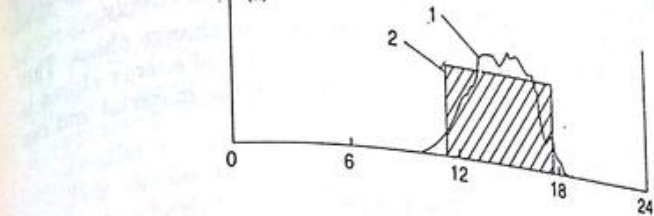
7.1 INTRODUCTION

The intermittent, variable and unpredictable nature of solar radiation generally leads to a mismatch between the rate and time of collection of solar energy and the load needs of a thermal application. As a result it is often necessary to use a storage system in between. The storage system stores energy when the collected amount is in excess of the requirement of the application and discharges energy when the collected amount is inadequate. The size of a storage system is largely

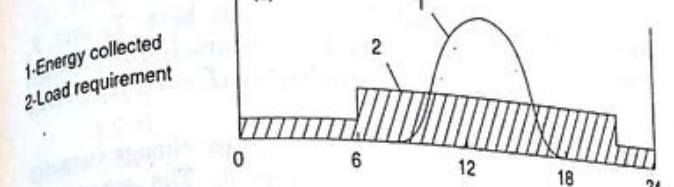
determined by the specific purpose for which it is used. Three situations are shown in Fig. 7.1.



(a)



(b)



(c)

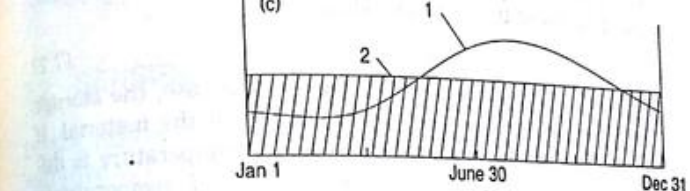


Fig. 7.1 Different Situations for Using a Thermal Energy Storage
(a) Buffer Storage, (b) Diurnal Storage, (c) Annual Storage

In Fig. 7.1 (a), the time interval during the day over which the energy is required is essentially the same as the time of collection. However, a storage system is needed because there is some mismatch between the amount of energy required and the amount collected at any instant. The storage system in such a situation has to store energy only for short intervals of time and is relatively small in size. It is called a 'buffer storage'. In Fig. 7.1 (b), the load demand shown extends over all 24 hours, whereas the collection takes place only during the sunshine hours. As a result, a system larger than a buffer storage

having the capacity to store energy for a day or two is required. Such a system is called a 'diurnal storage'. Figs 7.1 (a) and (b) are both 'short-term' storage systems. In contrast, Fig. 7.1 (c) illustrates a situation in which the storage system stores energy during the summer when the collection is in excess of the demand, and delivers the excess energy in winter when the collection is less than the demand. A large 'long-term' storage system is required for such a situation, since excess energy has to be stored over a period of months. Such a system is also called an 'annual storage'.

There are three basic methods for storing thermal energy.

- (1) Heating a liquid or a solid which does not change phase. This is called *sensible heat storage*. The amount of energy stored is dependent on the temperature change of the material and can be expressed in the form

$$E = m \int_{T_1}^{T_2} C_p dT \quad (7.1)$$

where m is the mass and C_p , the specific heat. T_1 and T_2 represent the lower and upper temperature levels between which the storage operates. The difference $(T_2 - T_1)$ is referred to as the temperature swing.

- (2) Heating a material which undergoes a phase change (usually melting). This is called *latent heat storage*. The amount of energy stored in this case depends upon the mass and the latent heat of fusion of the material. Thus,

$$E = m\lambda \quad (7.2)$$

where λ is the latent heat of fusion. In this case, the storage operates isothermally at the melting point of the material. If isothermal operation at the phase change temperature is difficult, the system operates over a range of temperatures T_1 to T_2 which includes the melting point. Then sensible heat contributions have to be considered and the amount of energy stored is given by

$$E = m \left[\left\{ \int_{T_1}^{T^*} C_{ps} dT \right\} + \lambda + \left\{ \int_{T^*}^{T_2} C_{pl} dT \right\} \right] \quad (7.3)$$

where C_{ps} and C_{pl} represent the specific heats of the solid and liquid phases and T^* is the melting point.

- (3) Using heat to produce a certain chemical reaction and then storing the products. The heat is released when the reverse reaction is made to occur. In this case also, the storage operates

essentially isothermally during the chemical reactions. However, the temperatures at which the forward and reverse reactions occur are usually different. Of the above methods, sensible and latent heat storage systems are in use, while thermochemical storage systems are being proposed for use in medium and high temperature applications. The specific application for which a thermal storage system is to be used determines the method to be adopted. Some of the considerations are as follows.

- (1) The temperature range over which the storage has to operate.
- (2) The capacity of the storage has a significant effect on the operation of the rest of the system, especially the collectors. A smaller storage unit operates at a higher mean temperature. This results in a reduced collector output as compared to a system having a larger storage unit.
- (3) Heat losses from the storage have to be kept to a minimum.
- (4) Heat losses are of particular importance for 'long-term' storage.
- (5) Cost of the storage unit. This includes the initial cost of the storage medium, the containers and insulation, and the operating cost.

Other considerations include the suitability of materials used for the container, the means adopted for transferring the heat to and from the storage, and the power requirements for these purposes.

7.2 SENSIBLE HEAT STORAGE

In the case of sensible heat storage systems, energy is stored or extracted by heating or cooling a liquid or a solid which does not change its phase during the process. A variety of substances have been used in such systems. These include liquids like water, heat transfer oils and certain inorganic molten salts, and solids like rocks, pebbles and refractories. In the case of solids, the material is invariably in the porous form and heat is stored or extracted by the flow of a gas or a liquid through the pores or voids.

The choice of the substance used largely depends on the temperature level of the application, water being used for temperatures below 100°C and refractory bricks being used for temperatures around 1000°C. Sensible heat storage systems are simpler in design than latent heat or thermochemical storage systems. However, they suffer from the disadvantage of being bigger in size. For this reason, an important criterion in selecting a material for sensible heat storage is

its (ρC_p) value. A second disadvantage associated with sensible heat storage systems is that they cannot store or deliver energy at a temperature higher than the temperature. We shall first take up for consideration the various materials used.

7.2.1 Liquids

Water is the most commonly used medium in a sensible heat storage system. Most solar water-heating and space-heating systems have large water storage tanks located either inside or outside the building, or underground. The sizes of the tanks used vary from a few hundred litres to a few thousand cubic metres. An approximate thumb rule followed for fixing the size is to use about 75 to 100 litres of water per square metre of collector area.

Water storage tanks are made from a variety of materials like concrete and fibreglass. The tanks are suitably insulated with glass wool, mineral wool or polyurethane. The thickness of insulation used is large and ranges from 10 to 20 cm. Because of this, the cost of the insulation represents a significant part of the total cost and means to reduce this cost have to be explored. Shelton* has shown that in an underground tank, the insulating value of the earth surrounding the tank may be adequate and this could provide the bulk of the insulation thickness required. However, it may take as much as one year for the earth around a large storage tank to reach a steady state by heating and drying, and a considerable amount of energy may be required for this purpose.

If the water is at atmospheric pressure, the temperature is limited to 100°C. It is possible to store water at temperatures a little above 100°C by using pressurized tanks. This has been done in a few instances.

In order to reduce the cost of water storage systems, an alternative way, which has been examined for very large systems, is to make use of naturally occurring underground aquifers which already contain water. In such systems, the need for building a storage tank is eliminated. For storing energy, hot water is pumped into the aquifer through an injection well. At the same time, cold ground water is displaced through another well. For withdrawing energy, the reverse procedure is followed. Since the investment required is a series of openings for injecting and withdrawing water, the storage costs for such systems are low (Fig. 7.2).

Heat transfer oils are used in sensible heat storage systems for

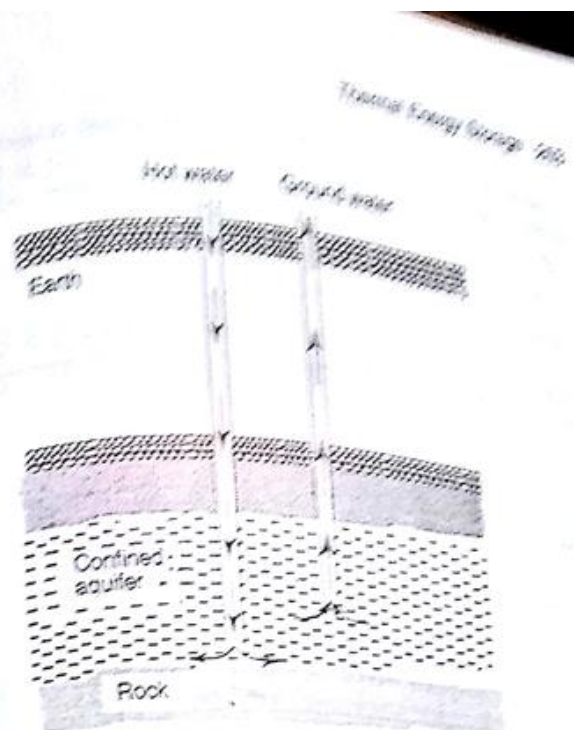


Fig. 7.2 Schematic Diagram of the Underground Aquifer Storage Concept

intermediate temperatures ranging from 100 to 300°C. Some of the US brands which are used for this purpose are Caloria HT43 and Therminol T66. One of the Indian brands which would be suitable is Servotherm. The main problem associated with the use of heat transfer oils is that they tend to degrade with time. The degradation is particularly serious if they are used above their recommended temperature limit. The use of oils also presents safety problems since there is a possibility of ignition above their flash point. For this reason, it is recommended that they be used in systems with an inert gas cover. A further limitation to the use of heat transfer oils is their cost, which ranges from Rs 15 to Rs 300 per litre. For this reason, they can be considered for use only in small storage systems.

A few molten inorganic salts have been considered for high temperatures (300°C and above). One is an eutectic mixture of 40 per cent NaNO_2 , 7 per cent NaNO_3 and 53 per cent KNO_3 (by weight) and is available under the trade name of Hitec. Hitec has a low melting point of 145°C and can be used up to a temperature of 425°C. Above this temperature, decomposition and oxidation begin to take place.

*J. Shelton, "Underground Storage of Heat in Solar Heating Systems", *Solar Energy*, 17, 138 (1975).

Apart from molten salts, liquid metals have been considered for use at high temperatures. Liquid sodium was used both as the receiver and storage fluid of the 0.5 MW solar thermal electric power station working on the central receiver concept in Spain. Properties of some of the above mentioned liquids are given in Table 7.1.

Table 7.1 Properties of Some Sensible Heat Storage Liquids

	Water*	Senvotherm*			
		Light	Medium	Heavy	Medium
Highest temperature for use (°C)	100	~ 150	~ 250	425	700
Density ρ (kg/m ³)	958.4	997	889	1769	347
Specific heat C_p (kJ/kg K)	4.22	2.24	2.22	1.51	1.27
ρC_p (kJ/m ³ K)	4044	1942	1954	2653	1673
Thermal conductivity (W/m K)	0.633	0.126	0.123	0.54	68.3

*Properties at 100°C

Properties at 400°C

Properties at 450°C

7.2.2 Solids

Energy can be stored in rocks or pebbles packed in insulated vessels. This type of storage is used very often for temperatures up to 100°C in conjunction with solar air heaters. It is simple in design and relatively inexpensive. Typically, the characteristic size of the pieces of rock used varies from 1 to 5 cm. An approximate thumb rule followed for sizing is to use 300 to 500 kg of rock per square metre of collector area for space-heating applications.

Undisturbed earth or processed earth has also been used in space-heating applications, but for long term storage. In such storage systems, the heat transfer with the air takes place through a network of plastic heat exchange tubes buried in the earth.

Refractory materials like magnesium oxide (magnesia), aluminium oxide (alumina) and silicon oxide are suitable for high-temperature sensible heat storage. Bricks made of magnesia have been used in many countries for many years for storing heat. They are available in the form of devices with electric heater elements embedded in the bricks. The heat is stored at night (when the electricity rates are low) by

switching on the electric heaters and is supplied during the day for space-heating purposes by allowing air to pass through the device. Properties of some solids used for sensible heat storage are given in Table 7.2. It will be seen that the (ρC_p) and k values for the refractory materials are higher than those for rocks or pebbles, making them more suitable from the point of view of compactness of the storage vessel. However, they are also many times more costly.

Table 7.2 Typical Properties of Some Sensible Heat Storage Solids

	Rocks	Pebbles	Magnesium oxide	Aluminium oxide	Silicon oxide
Density ρ (kg/m ³)	2245	1250	3575	4100	2300
Specific heat C_p (kJ/kg K)	(0.71-0.92)	0.81	0.90	1.06	1.12
ρC_p (kJ/m ³ K)	1818	1215	3790	4100	2276
Thermal conductivity (W/m K)	0.13	0.85	10.5	6.3	2.3

Finally it should be noted that combinations of liquid and solid sensible heat storage media are also used. In such cases, the solid is porous or granular with the liquid filling the hollow spaces. Generally the liquid is also the heat transfer fluid.

7.2.3 Analysis of a Liquid Storage Tank

Well-mixed Situation

Consider the insulated liquid-storage tank shown in Fig. 7.3 receiving energy (when available) from an array of collectors and discharging energy (when needed) to a load for use in an application. We assume that the liquid in the tank is always well-mixed and consequently is at a uniform temperature T_l , which varies only with time. An energy balance on the tank yields the following equation

$$[(\rho V C_p)_l + (\rho V C_p)_t] \frac{dT_l}{dt} = q_u - q_{load} - (UA)_l (T_l - T_a) \quad (7.4)$$

where $(\rho V C_p)_l$ represents the heat capacity of the liquid in the tank, $(\rho V C_p)_t$ the heat capacity of the tank material, q_u the rate of useful heat gain received from the collectors, q_{load} the rate at which energy is being discharged to the load, $(UA)_l$ the product of the overall heat-transfer coefficient and surface area of the tank, and T_a the ambient temperature around the tank. The heat capacity term $(\rho V C_p)_l$ is likely to be of

importance for small-sized tanks only. For large tanks, its value may be negligible in comparison to $(\rho V C_p)_t$. Denoting the sum of the two heat capacities by the symbol $(\rho V C_p)_e$ and integrating differential equation (7.4)* under the assumption that q_u , q_{load} and T_a are constants, we get, subject to the initial condition $t = 0$, $T_t = T_{t_0}$,

$$\frac{q_u - q_{load} - (UA)_t(T_t - T_a)}{q_u - q_{load} - (UA)_t(T_{t_0} - T_a)} = \exp \left[- \frac{(UA)_t t}{(\rho V C_p)_e} \right]$$

The assumption that q_u , q_{load} and T_a are constants is valid if q_u

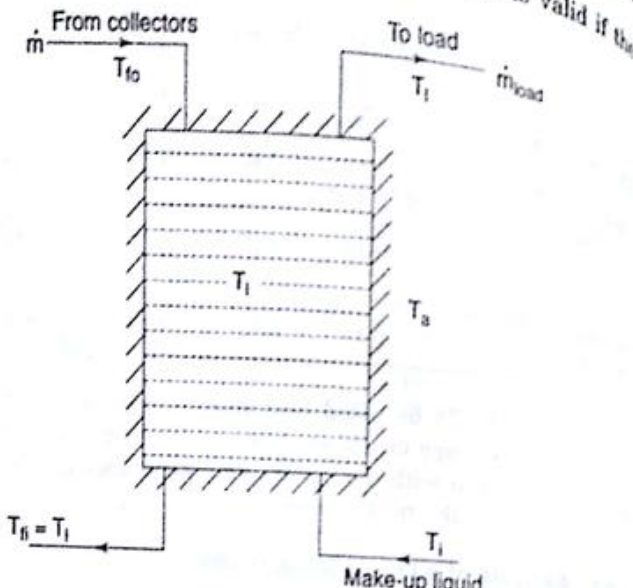


Fig. 7.3 Analysis of a Well-mixed Sensible Heat Liquid Storage Tank

time interval of the integration is kept reasonably small (say 1 hour or less). Equation (7.5) can be used to determine the variation of the temperature T_t with time if the variation of q_u and q_{load} is given.

Alternatively, the values of q_u and q_{load} may be calculated from the inlet and outlet temperatures and flow rates as

$$q_u = \dot{m} C_p (T_{t_0} - T_{t_1}) = \dot{m} C_p (T_{t_0} - T_t) \quad (7.6)$$

and

$$q_{load} = \dot{m}_{load} C_p (T_t - T_i) \quad (7.7)$$

Equation (7.4) then becomes

$$(\rho V C_p)_e \frac{dT_t}{dt} = \dot{m} C_p (T_{t_0} - T_t) - \dot{m}_{load} C_p (T_t - T_i) - (UA)_t (T_t - T_a) \quad (7.8)$$

*Equation (7.4) could also be solved by a finite-difference technique similar to the one used in Example 7.2.

It is important to note again that either q_u or q_{load} may be zero at any particular time. For example, when $T_{t_0} < T_t$, the flow through the collectors would be stopped and we would have $\dot{m} = 0$ and $q_u = 0$. Similarly if no energy is required on the load side, $\dot{m}_{load} = 0$ and $q_{load} = 0$.

Example 7.1

An cylindrical hot water storage tank, 1.7 m in diameter and 2.1 m high, is made from a steel plate ($\rho = 7800 \text{ kg/m}^3$, $C_p = 0.46 \text{ kJ/kg K}$) 6 mm thick. Apart from the mass of steel required for making the surface, an additional 200 kg of steel is required in the form of angles, etc. for strengthening the tank, which is insulated all round with glass wool insulation 20 cm thick ($k = 0.040 \text{ W/m K}$). The initial temperature of the water in the tank is 50.0°C at 0700 h in the morning on a particular day and the variation of q_u and T_a up to 2000 h is as shown.

Time	7-8	8-9	9-10	10-11	11-12	12-13	13-14
$q_u (\text{kJ/h})$	18 660	37 493	54 890	60 070	69 890	70 120	62 205
$T_a (\text{C})$	17.8	21.9	25.1	27.4	29.1	30.2	30.9
	14-15	15-16	16-17	17-18	18-19	19-20	
$q_u (\text{kJ/h})$	55 490	41 070	19 195	0	0	0	
$T_a (\text{C})$	31.2	31.3	30.8	28.9	26.0	24.0	

The load requirement is such that energy is continuously withdrawn from the tank at a constant rate of 27000 kJ/h for 18 hours a day starting at 0500 h. Assuming that the water in the tank is always well-mixed, calculate the variation of its temperature.

We shall first determine the values of $(\rho V C_p)_e$ and $(UA)_t$.

$$\text{Internal volume of the tank} = \frac{\pi}{4} \times 1.7^2 \times 2.1 = 4.767 \text{ m}^3$$

$$(\rho V C_p)_e = 971.8 \times 4.767 \times 4.195 \\ = 13432 \text{ kJ/K}$$

$$\text{Mass of steel used} = \left\{ (\pi \times 1.7 \times 2.1 + 2 \times \frac{\pi}{4} \times 1.7^2) \times 0.006 \times 7800 \right\} + 200 \\ = 937.0 \text{ kg}$$

$$\text{Therefore, } (\rho V C_p)_e = 937.0 \times 0.46 \\ = 431 \text{ kJ/K}$$

$$\text{Hence, } (\rho V C_p)_e = 19432 + 431 \\ = 19863 \text{ kJ/K}$$

In calculating the value of $(UA)_t$, we shall assume that the flow of heat through the cylindrical surface and through the flat top and bottom is one-dimensional. We shall also assume that the thermal resistance offered by the insulation dominates and that the other thermal resistances to the flow of heat at the inner and outer surfaces can be neglected by comparison. The overall heat-transfer coefficient U_1 (based on the inner diameter of the tank) for the flow of heat through the cylindrical surface is given by

$$\frac{1}{U_1} = \frac{r_1}{k_i} \ln \frac{r_2}{r_1}$$

where r_1 is the radius of the tank, r_2 is the radius with the insulation added on, and k_i is the thermal conductivity of the insulation. Substituting, we have,

$$\frac{1}{U_1} = \frac{0.85}{0.04} \ln \frac{1.05}{0.85} = 4.49$$

Therefore,

$$U_1 = 0.223 \text{ W/m}^2\text{-K}$$

Similarly the overall heat transfer coefficient U_2 for the flow of heat through the flat surfaces is given by

$$U_2 = \frac{0.04}{0.2} = 0.2 \text{ W/m}^2\text{-K}$$

Hence,

$$(UA)_t = (0.223 \times \pi \times 1.7 \times 2.1) + (0.2 \times 2 \times \frac{\pi}{4} \times 1.7^2) = 3.409 \text{ W/K}$$

We now apply Eq. (7.5) over a one hour interval of time. Substituting the given values, we have from 0700 to 0800 h,

$$\frac{18660 - 27000 - 3.409 \times 3.6(T_l - 17.8)}{18660 - 27000 - 3.409 \times 3.6(50.00 - 17.8)} = \exp \left[-\frac{3.409 \times 1 \times 3600}{19863 \times 1000} \right]$$

Hence

$$(T_l)_{0800 \text{ h}} = 49.56^\circ\text{C}$$

Continuing in the same way, we obtain the following variation for T_l up to 2000 h.

Time (h)	8	9	10	11	12	13	14
T_l (°C)	49.56	50.07	51.46	53.11	55.25	57.41	59.16
	15	16	17	18	19	20	
	60.58	61.27	60.86	59.48	58.10	56.72	

The results are plotted in Fig. 7.4. It is seen that from 0700 to 0800 h, the energy withdrawn exceeds the useful heat gain and that the water temperature decreases. Thereafter, the useful heat gain (whose variation

is typical of a clear sunny day) exceeds the energy withdrawn up to 1600 h. As a result, the tank water temperature starts increasing steadily and touches a peak around 1600 h. After this the useful heat gain decreases to zero and since energy is still being withdrawn, the tank water temperature decreases. From the load demand, it is clear that if the calculations were continued over a 24 hour period, the tank water temperature would be around 50°C at 0700 h on the next day. This indicates that there is an approximate matching between the useful heat gain and the energy withdrawn over a day and that the purpose of the storage tank in the present case is only to take care of the short term mismatch between supply and demand of energy over a day.

It should also be noted from Fig. 7.4 that the tank temperature

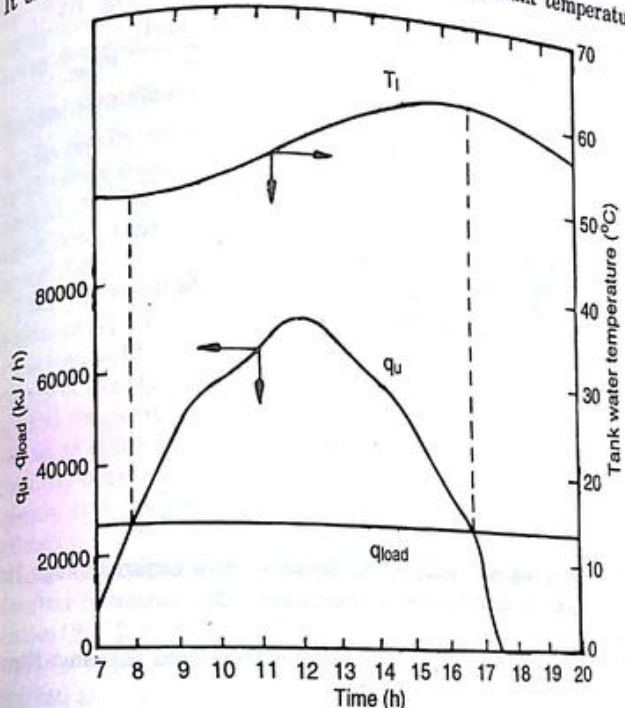


Fig. 7.4 Example 7.1—Variation of Temperature in a Well-mixed Water Storage Tank

fluctuates by about 12°C. The magnitude of this fluctuation essentially depends upon the volume of water in the tank. If the volume of the water were to be doubled, the fluctuation would be approximately halved.

The preceding analysis has been performed under the assumption that the liquid flowing through the collectors and to the load and that stored in the tank is the same, and that one stream mixes with the other. This may not always be the case. For example, in certain cases, it may be necessary from the point of view of corrosion to pass specially treated water mixed with chemical inhibitors through the collector circuit. It may also be necessary to add antifreeze compounds to the water passing through the collectors if temperatures below 0°C are likely to be encountered. In such cases, the fluid streams have to be separated and heat has to be transferred from the collector circuit liquid to the storage tank liquid through a heat exchanger. The heat exchanger may be a separate unit external to the storage tank or may be in the form of a coil immersed in the storage tank. We will now analyse the second situation shown schematically in Fig. 7.5.

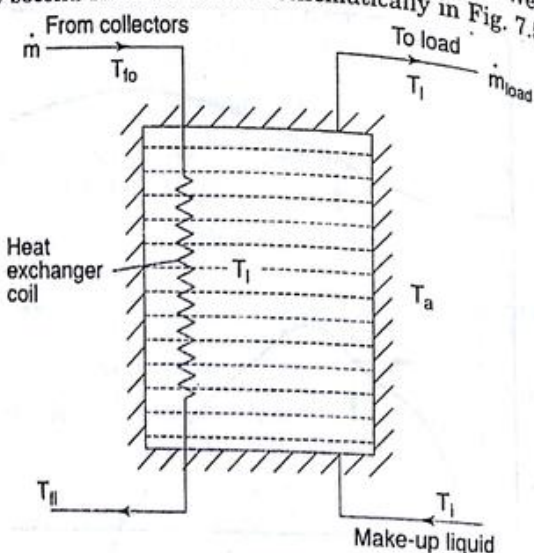


Fig. 7.5 Analysis of a Well-mixed Sensible Heat Liquid Storage Tank with an Immersed Heat Exchanger Coil

For an immersed coil, it is easy to show from heat exchange theory that

$$\frac{T_{fo} - T_{fi}}{T_{fo} - T_l} = 1 - \exp [-(UA)_e / mC_p] \quad (7.9)$$

where $(UA)_e$ is the product of the overall heat transfer coefficient and the area for the heat exchanger coil. Thus, the expression for the rate of useful heat gain becomes

$$\begin{aligned} q_u &= \dot{m}C_p(T_{fo} - T_{fi}) \\ &= \dot{m}C_p(T_{fo} - T_l)[1 - \exp [-(UA)_e / mC_p]] \end{aligned} \quad (7.10)$$

Substituting Eq. (7.10) for q_u and Eq. (7.7) for q_{load} into the energy balance Eq. (7.4), we get

$$(\rho V C_p)_e \frac{dT_l}{dt} = \dot{m}C_p(T_{fo} - T_l)[1 - \exp [-(UA)_e / mC_p]] - \dot{m}_{load}C_p(T_l - T_a) - (UA)_l(T_l - T_a) \quad (7.11)$$

In the above equation, the specific heats of the two liquid streams have been assumed to be the same. In case they are different, they would need to be distinguished in an appropriate manner.

It is important to realize that the use of a heat exchanger for a given application not only increases the complexity of the set-up but also raises the temperature level of operation of the collector array by a few degrees. Since collector efficiency decreases with increase in temperature, more collector area is required for meeting the given energy demand.

Thermal Stratification

In a thermally stratified situation, the temperature of the contained liquid varies from the bottom to the top, being less at the bottom and more at the top. This situation is in contrast to that obtained in a well-mixed tank in which the liquid temperature is uniform throughout.

Thermal stratification is obviously desirable if the temperature difference $(T_l - T_a)$, refer Fig. 7.3, is significant. If the line taking liquid to the load at the required temperature T_l is located appropriately near the top of the storage tank, then only the liquid near this exit port has to be at the temperature T_l . The rest of the liquid in the storage tank can be at a lower temperature at all times. As a result, heat losses from the tank are reduced. A second advantage is that the collectors operate at a lower temperature level and deliver a higher collection efficiency.

In some applications, thermal stratification is obtained naturally as a matter of course. An example is a natural circulation water heating system (Fig. 2.6). In such a system, the flow rates are low and a certain degree of thermal stratification is always obtained. Thermal stratification can also be obtained in a forced circulation water heating system if the fluid inlet and outlet configurations are suitably located and shaped. Ring distributors are used so that the velocities entering and leaving the tank are low and are in such a direction as to reduce mixing. In some cases, a floating inlet, made of a wide, thin-walled flexible plastic hose connected to the inlet port, is used. This type of inlet delivers hot liquid from the collectors at a level at which the inlet liquid temperature is equal to that in the storage tank.

The analysis of a thermally stratified tank is complicated by the fact

that the temperature profile has to be solved for as a function of time. In addition, in most practical situations, the problem is not one-dimensional in nature and involves consideration of the heat conduction through the walls of the storage tank.

A simplified analysis is possible by assuming that the storage tank consists of a number of well-mixed sections at different temperatures. Consider the situation in which the storage tank is assumed to consist of two well-mixed sections (Fig. 7.6) at temperatures T_{l1} and T_{l2} . Writing energy balances on each of the sections, we obtain

$$(\rho V C_p)_{e1} \frac{dT_{l1}}{dt} = \dot{m} C_p (T_{fo} - T_{l1}) - \dot{m}_{load} C_p (T_{l1} - T_{l2}) - (UA)_{l1} (T_{l1} - T_a) \quad (7.12)$$

$$(\rho V C_p)_{e2} \frac{dT_{l2}}{dt} = \dot{m} C_p (T_{l1} - T_{l2}) - \dot{m}_{load} C_p (T_{l2} - T_a) \quad (7.13)$$

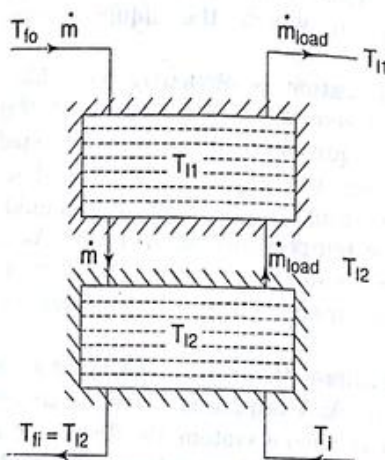


Fig. 7.6 Analysis of a Thermally Stratified Sensible Heat Liquid Storage Tank

Differential Eqs (7.12) and (7.13) have to be solved simultaneously for the unknowns T_{l1} and T_{l2} . One way of solving them is to express them in finite difference form and to choose a suitable time interval. Values of T_{l1} and T_{l2} are then obtained from one time interval to the next.

Equations (7.12) and (7.13) have been written under the assumption

that the flow from the collectors can enter the storage tank only at the top of section 1. This occurs when $T_{fo} > T_{l1}$. When $T_{fo} < T_{l1}$ no flow occurs.

In case the tank is also provided with an inlet between the two sections, three possibilities exist.

1. Flow \dot{m} enters at the top of section 1 when $T_{fo} > T_{l1}$.
2. Flow \dot{m} enters between sections 1 and 2 when $T_{l1} > T_{fo} > T_{l2}$.
3. There is no flow, and consequently no energy to be stored, when $T_{fo} < T_{l2}$.

Equations (7.12) and (7.13) can be easily modified to account for this situation.

Example 7.2

The temperatures in a hot water stratified tank are to be determined by assuming that the tank consists of two equal well-mixed sections with inlets at the top and in-between the two sections. The following data is given:

Hour	\dot{m} (kg/h)	T_{fo} (°C)	\dot{m}_{load} (kg/h)	T_a (°C)
1200-1300	2000	80	250	22
1300-1400	2000	80	240	23
1400-1500	2000	76	220	22

It is also given that,

- (1) mass of water in the tank = 5000 kg
- (2) $(UA)_{l1} = (UA)_{l2} = 30 \text{ kJ/h}\cdot\text{°C}$
- (3) make up water enters at 20°C at the same rate as the rate of withdrawal to the load,
- (4) at 1200 h, $T_{l1} = 70^\circ\text{C}$, $T_{l2} = 65^\circ\text{C}$

Calculate the values of T_{l1} and T_{l2} at 1500 h

Neglecting the value of the heat capacity term $(\rho V C_p)$, Eqs (7.12) and (7.13) can be written in a finite difference form as follows:

$$(\rho V C_p)_{l1} \left(\frac{T_{l1,f} - T_{l1,i}}{\Delta t} \right) = \dot{m} C_p \left(T_{fo} - \frac{T_{l1,f} + T_{l1,i}}{2} \right) - \dot{m}_{load} C_p \left(\frac{T_{l1,f} + T_{l1,i}}{2} - \frac{T_{l2,f} + T_{l2,i}}{2} \right) - (UA)_{l1} \left(\frac{T_{l1,f} + T_{l1,i}}{2} - T_a \right) \quad (7.14)$$

$$(\rho V C_p)_{12} \left(\frac{T_{l2,f} - T_{l2,i}}{\Delta t} \right) = \dot{m} C_p \left(\frac{T_{l1,f} + T_{l1,i}}{2} - \frac{T_{l2,f} + T_{l2,i}}{2} \right) \\ - \dot{m}_{load} C_p \left(\frac{T_{l2,f} + T_{l2,i}}{2} - T_i \right) \\ - (UA)_{12} \left(\frac{T_{l2,f} + T_{l2,i}}{2} - T_a \right) \quad (7.15)$$

In these equations, $T_{l1,f}$ and $T_{l1,i}$ represent the final and initial values of T_{l1} over the time interval Δt . A similar meaning is attached to the symbols $T_{l2,f}$ and $T_{l2,i}$. The symbols T_{f_0} , T_a and T_i now represent average values over the time interval Δt . (7.15)

We take $\Delta t = 1$ h and note the presence of the inlet in between the two sections while substituting the given data from one hour to the next.

Time interval 1200-1300 h: $T_{l1,i} = 70^\circ\text{C}$; $T_{l2,i} = 65^\circ\text{C}$.

Substituting into Eq. (7.14), we get

$$2500 \times 4.19 \times (T_{l1,f} - 70) = 2000 \times 4.19 \left(80 - \frac{T_{l1,f} + 70}{2} \right) \\ - 250 \times 4.19 \left(\frac{T_{l1,f} + 70}{2} - \frac{T_{l2,f} + 65}{2} \right) \\ - 30 \left(\frac{T_{l1,f} + 70}{2} - 22 \right)$$

or $3628.6T_{l1,f} - 125T_{l2,f} = 264282 \quad (7.16)$

Similarly, substituting into Eq. (7.15), we get

$$-1000T_{l1,f} + 3628.6T_{l2,f} = 164300 \quad (7.17)$$

Solving Eqs (7.16) and (7.17),

$$T_{l1,f} = 75.10^\circ\text{C}; \quad T_{l2,f} = 65.98^\circ\text{C}$$

Time interval 1300-1400 h: Now $T_{l1,i} = 75.10^\circ\text{C}$; $T_{l2,i} = 65.98^\circ\text{C}$

Substituting into Eqs (7.14) and (7.15), we get

$$3623.6T_{l1,f} - 120T_{l2,f} = 271457$$

and

$$-1000T_{l1,f} + 3623.6T_{l2,f} = 170882$$

Solving

$$T_{l1,f} = 77.18^\circ\text{C}; \quad T_{l2,f} = 68.46^\circ\text{C}$$

Time interval 1400-1500 h: Now $T_{l1,i} = 77.18^\circ\text{C}$; $T_{l2,i} = 68.46^\circ\text{C}$.

Since $T_{l1,i} > T_{f_0} > T_{l2,i}$, the flow from the collectors will bypass section 1 and enter in between sections 1 and 2. Thus, the first term

of the right hand side of Eq. (7.14) will be zero and in the first term of the right hand side of the Eq. (7.15), we would put T_{f_0} instead of $\frac{T_{l1,f} + T_{l1,i}}{2}$. Substituting, we get

$$2613.6T_{l1,f} - 110T_{l2,f} = 191875$$

$$3613.6T_{l2,f} = 251469$$

$$T_{l1,f} = 76.34^\circ\text{C}; \quad T_{l2,f} = 69.59^\circ\text{C}$$

and Solving,

7.2.4 Analysis of a Packed-bed Storage

We now take up for analysis a packed-bed storage unit as shown in Fig. 7.7. The unit is packed with rocks, pebbles or bricks through which air is circulated. Hot air from solar air heaters is usually passed down through the bed when sensible heat is to be stored in the particulate solid, while cold air from the load is circulated upwards when heat is to be extracted from the solid. Unlike a liquid storage tank, the two processes cannot be executed simultaneously.

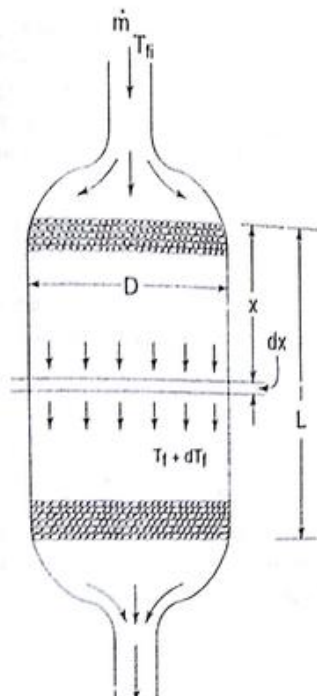


Fig. 7.7 Analysis of a Packed-bed Storage Unit

The transient heat transfer analysis which follows is due to Schumann.* Consider a packed-bed unit of length L and diameter d packed with solid having an equivalent spherical diameter d and a void fraction ϵ . The mass flow rate of the air is \dot{m} and it enters with a constant temperature T_{fi} . For the purposes of analysis, it is assumed that,

- (1) The bed material has infinite thermal conductivity in the radial direction and zero conductivity in the axial flow direction,
- (2) The heat transfer coefficient does not vary with time and place inside the bed, and
- (3) The bed is semi-infinite in the direction of the flow.

Considering separate energy balances on the bed material and air in a slice dx of the bed across which the temperature of the solid changes from T_s to $(T_s + dT_s)$ and the temperature of the air changes from T_f to $(T_f + dT_f)$, we have

$$(1 - \epsilon) \rho_s C_{ps} \frac{\partial T_s}{\partial t} = h_v (T_f - T_s) \quad (7.18)$$

$$\text{Hence, } \epsilon \rho_f C_{pf} \frac{\partial T_f}{\partial t} + \frac{4\dot{m} C_{pf}}{\pi D^2} \frac{\partial T_f}{\partial x} = h_v (T_s - T_f) \quad (7.19)$$

where h_v is the volumetric heat-transfer coefficient (in $\text{W/m}^3\text{-K}$) defined per unit volume of the bed, ρ_s and ρ_f are the densities of the solid and fluid, and C_{ps} and C_{pf} are the respective specific heats. In deriving the above equations, heat losses to the surroundings have been assumed to be negligible. Defining a dimensionless time τ and a dimensionless distance X as follows,

$$\tau = \frac{h_v t}{\rho_s C_{ps} (1 - \epsilon)} \text{ and } X = \frac{\pi D^2 h_v x}{4\dot{m} C_{pf}}$$

and neglecting the term $\epsilon \rho_f C_{pf} (\partial T_f / \partial t)$ in comparison to the other two terms in Eq. (7.19), Eqs (7.18) and (7.19) reduce to

$$\frac{\partial T_s}{\partial \tau} = (T_f - T_s) \quad (7.20)$$

$$\frac{\partial T_f}{\partial X} = (T_s - T_f) \quad (7.21)$$

Equations (7.20) and (7.21) can be solved if the solid is assumed to be initially at a uniform temperature T_i . We obtain the dimensionless temperature distributions

$$\frac{T_s - T_i}{T_{fi} - T_i} = 1 - e^{-(X + \tau)} \sum_{n=0}^{\infty} X^n M_n (X\tau) \quad (7.22)$$

$$\frac{T_f - T_i}{T_{fi} - T_i} = 1 - e^{-(X + \tau)} \sum_{n=1}^{\infty} X^n M_n (X\tau) \quad (7.23)$$

and

where

Values of $(T_s - T_i)/(T_{fi} - T_i)$ and $(T_f - T_i)/(T_{fi} - T_i)$ have been computed from Eqs (7.22) and (7.23) for $0 \leq X \leq 20$ and $0 \leq \tau \leq 30$ and are given in Tables 7.3 and 7.4 so that they can be used easily.

The value of h_v which is required for evaluating the parameters X and τ can be obtained from the following dimensional correlation given by Lof and Hawley,*

$$h_v = 650 (G/d)^{0.7} \text{ W/m}^3\text{-K} \quad (7.24)$$

where G is the mass velocity ($= 4\dot{m}/\pi D^2$) in kg/s-m^2 and d is the average diameter of the bed material in metres.

It should be noted that Eqs (7.22) and (7.23) are valid regardless of whether $T_i < T_{fi}$ or $T_i > T_{fi}$. In the first case, the bed heats up and energy is stored, while in the second case, the reverse occurs.

The pressure drop across a packed-bed storage is also of importance since large volumes of fluid are being handled. The following correlation suggested by Dunkle and Ellul† can be used,

$$\Delta p = \frac{LG^2}{\rho_f d} \left(21 + 1750 \frac{\mu_f}{Gd} \right) \quad (7.25)$$

Example 7.3

A packed-bed storage unit, 1 m in height and 0.70 m in diameter, is filled with rock pieces ($\rho_s = 2800 \text{ kg/m}^3$, $C_{ps} = 0.90 \text{ kJ/kg-K}$) having an average diameter of 2 cm. The void fraction is 0.35. Initially the bed is at a uniform temperature of 25°C everywhere. Air heated to a temperature of 70°C in solar air heaters starts flowing in with a flow rate of 1.1 kg/s. Find the temperature distributions in the bed after (i) 5 minutes, and (ii) 10 minutes. Calculate also the energy stored in the bed material as a fraction of the maximum amount which can be stored and the pressure drop across the bed.

*G.O.G. Lof and R.W. Hawley, "Unsteady-state Heat Transfer between Air and Loose Solids", *Industrial and Engineering Chemistry* 76, 40, 1061 (1984).

Table 7.3 Values of $(T_s - T_f)(T_h - T_f)$ in a Packed-bed Storage

τ	$X \rightarrow 0$	1	2	3	4	5	6	7	8	9	10	12	14	16	18	20
0	0.000	0.000	0.000	0.000	0.000	0.000	0.000	0.000	0.000	0.000	0.000	0.000	0.000	0.000	0.000	
1	0.632	0.346	0.183	0.094	0.047	0.023	0.011	0.006	0.003	0.001	0.001	0.001	0.000	0.000	0.000	
2	0.865	0.606	0.397	0.247	0.148	0.086	0.049	0.027	0.015	0.008	0.004	0.001	0.000	0.000	0.000	
3	0.950	0.775	0.585	0.417	0.283	0.185	0.117	0.072	0.044	0.026	0.015	0.005	0.001	0.000	0.000	
4	0.982	0.877	0.730	0.573	0.428	0.307	0.212	0.143	0.093	0.059	0.037	0.014	0.005	0.002	0.001	
5	0.993	0.934	0.831	0.702	0.565	0.436	0.325	0.234	0.164	0.112	0.074	0.031	0.012	0.005	0.001	
6	0.998	0.966	0.898	0.800	0.682	0.559	0.442	0.338	0.251	0.181	0.128	0.060	0.025	0.011	0.004	
7	0.999	0.983	0.940	0.870	0.776	0.667	0.554	0.446	0.349	0.265	0.197	0.101	0.048	0.022	0.009	
8	0.991	0.966	0.918	0.847	0.757	0.655	0.551	0.450	0.358	0.277	0.156	0.081	0.039	0.018	0.008	
9		0.981	0.949	0.898	0.827	0.741	0.646	0.548	0.453	0.365	0.222	0.124	0.065	0.032	0.015	
10		0.990	0.969	0.934	0.880	0.811	0.728	0.638	0.545	0.455	0.297	0.178	0.100	0.052	0.026	
12		0.989	0.974	0.946	0.905	0.851	0.784	0.707	0.625	0.545	0.312	0.197	0.116	0.065		
14		0.990	0.978	0.956	0.925	0.882	0.827	0.763	0.616	0.562	0.324	0.213	0.131			
16		0.991	0.981	0.981	0.965	0.940	0.905	0.861	0.746	0.608	0.465	0.334	0.226			
18		0.992	0.984	0.971	0.951	0.924	0.843	0.732	0.601	0.467	0.342					
20		0.993	0.987	0.977	0.961	0.909	0.828	0.720	0.595	0.465						
22		0.994	0.989	0.981	0.950	0.886	0.815	0.715	0.575	0.455						
24		0.994	0.989	0.981	0.950	0.886	0.815	0.715	0.575	0.455						
26		0.994	0.989	0.981	0.950	0.886	0.815	0.715	0.575	0.455						
28		0.994	0.989	0.981	0.950	0.886	0.815	0.715	0.575	0.455						
30		0.994	0.989	0.981	0.950	0.886	0.815	0.715	0.575	0.455						

Table 7.4 Values of $(T_s - T_f)(T_h - T_f)$ in a Packed-bed Storage

τ	$X \rightarrow 0$	1	2	3	4	5	6	7	8	9	10	12	14	16	18	20
0	1.000	0.368	0.135	0.050	0.018	0.007	0.003	0.001	0.009	0.004	0.002					
1	1.000	0.654	0.394	0.225	0.123	0.066	0.034	0.017	0.019	0.011	0.003	0.001				
2	1.000	0.817	0.604	0.415	0.270	0.169	0.102	0.060	0.034	0.019	0.011	0.003	0.001			
3	1.000	0.906	0.753	0.583	0.427	0.298	0.200	0.130	0.082	0.051	0.031	0.011	0.003			
4	1.000	0.953	0.852	0.717	0.572	0.435	0.318	0.224	0.154	0.102	0.067	0.026	0.010	0.003	0.001	
5	1.000	0.977	0.914	0.815	0.693	0.564	0.441	0.333	0.243	0.173	0.120	0.054	0.022	0.009	0.003	
6	1.000	0.989	0.951	0.883	0.788	0.676	0.558	0.446	0.345	0.259	0.189	0.095	0.044	0.019	0.008	
7	1.000	0.995	0.973	0.928	0.858	0.766	0.662	0.554	0.449	0.354	0.272	0.149	0.075	0.035	0.016	
8	1.000	0.997	0.974	0.941	0.888	0.819	0.735	0.643	0.547	0.455	0.375	0.237	0.139	0.076		
9	1.000	0.996	0.986	0.963	0.926	0.872	0.803	0.723	0.635	0.545	0.454	0.385	0.254	0.157	0.091	
10	1.000	0.995	0.988	0.974	0.837	0.749	0.651	0.550	0.452	0.362	0.216	0.119	0.060	0.039	0.024	
12	1.000	0.996	0.989	0.979	0.907	0.837	0.743	0.643	0.547	0.455	0.393	0.277	0.174	0.090	0.050	
14	1.000	0.996	0.991	0.982	0.982	0.982	0.982	0.982	0.982	0.982	0.982	0.982	0.982	0.982	0.982	
16	1.000	0.996	0.996	0.996	0.996	0.996	0.996	0.996	0.996	0.996	0.996	0.996	0.996	0.996	0.996	
18	1.000	0.996	0.996	0.996	0.996	0.996	0.996	0.996	0.996	0.996	0.996	0.996	0.996	0.996	0.996	
20	1.000	0.996	0.996	0.996	0.996	0.996	0.996	0.996	0.996	0.996	0.996	0.996	0.996	0.996	0.996	
22	1.000	0.996	0.996	0.996	0.996	0.996	0.996	0.996	0.996	0.996	0.996	0.996	0.996	0.996	0.996	
24	1.000	0.996	0.996	0.996	0.996	0.996	0.996	0.996	0.996	0.996	0.996	0.996	0.996	0.996	0.996	
26	1.000	0.996	0.996	0.996	0.996	0.996	0.996	0.996	0.996	0.996	0.996	0.996	0.996	0.996	0.996	
28	1.000	0.996	0.996	0.996	0.996	0.996	0.996	0.996	0.996	0.996	0.996	0.996	0.996	0.996	0.996	
30	1.000	0.996	0.996	0.996	0.996	0.996	0.996	0.996	0.996	0.996	0.996	0.996	0.996	0.996	0.996	

We first calculate the value of the volumetric heat-transfer coefficient.

$$\text{Mass velocity } G = \frac{1.1}{\left(\frac{\pi}{4} \times 0.7^2\right)} = 2.858 \text{ kg/s m}^2$$

Therefore, from Eq. (7.24)

$$h_v = 650 \left(\frac{2.858}{0.02} \right)^{0.7} = 20964 \text{ W/m}^3 \cdot \text{K}$$

(i) At $t = 5 \text{ min}$,

$$\tau = \frac{20964 \times 5 \times 60}{2800 \times 0.9 \times (1 - 0.35)} \times \frac{1}{1000} = 3.84$$

We will determine the values of T_s and T_f at $x = 0, 0.25, 0.5, 0.75$ and 1 m .

At $x = 0.25 \text{ m}$,

$$X = \frac{20964 \times \pi \times 0.7^2 \times 0.25}{4 \times 1.1 \times 1.009 \times 1000} = 1.82$$

Thus, for the values of x chosen, we have

$$X = 0, 1.82, 3.63, 5.45 \text{ and } 7.27$$

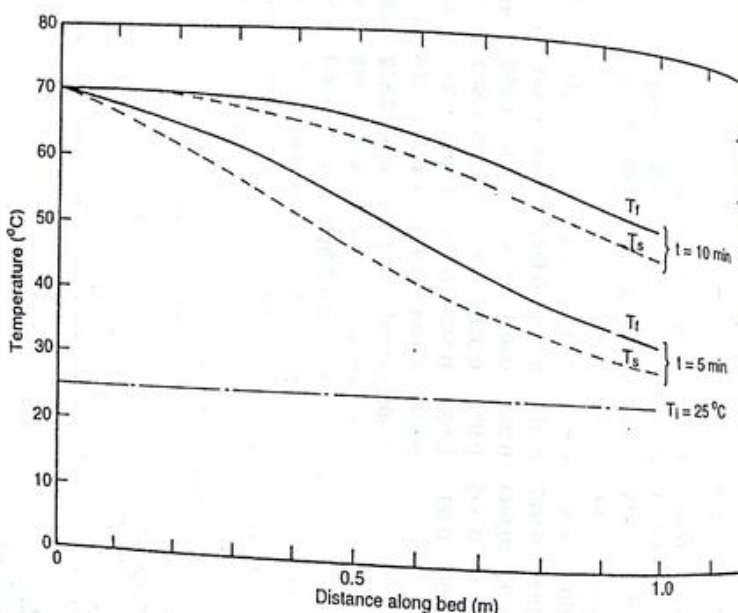


Fig. 7.8 Example 7.3—Temperature Distributions in a Packed-bed Storage

Corresponding to these values of X and for $\tau = 3.84$, the values of $(T_f - T_i)/(T_{fi} - T_i)$ and $(T_f - T_i)/(T_{fi} - T_i)$ can be read by interpolation from Tables 7.3 and 7.4 and the values of T_s and T_f can be calculated.

(ii) At $t = 10 \text{ minutes}$, $\tau = 7.68$. The calculation proceeds in the same manner as in part (i). The results are again plotted in Fig. 7.8. The trends exhibited by the temperature distributions are as expected. It is seen that temperature decreases in the direction of the flow and that there is a point of inflection in each temperature distribution.

The energy stored in the bed material at any instant of time

$$= \int_0^L (1 - \varepsilon) \frac{\pi}{4} D^2 \rho_s C_{ps} (T_s - T_i) dx$$

The maximum amount of energy which can be stored

$$= (1 - \varepsilon) \frac{\pi}{4} D^2 L \rho_s C_{ps} (T_{fi} - T_i)$$

Thus, the fraction of the maximum stored

$$F = \left\{ \int_0^L (T_s - T_i) dx \right\} / L (T_{fi} - T_i) \quad (7.26)$$

From Fig. 7.8, we obtain by numerical integration

$$F = 0.51 \text{ for } t = 5 \text{ minutes}$$

$$\text{and } F = 0.82 \text{ for } t = 10 \text{ minutes}$$

Using Eq. (7.25) and the properties of air at 70°C , we have

$$\begin{aligned} \Delta p &= \frac{1 \times 2.858^2}{1.029 \times 0.02} \left(21 + \frac{1750 \times 20.6 \times 10^{-6}}{2.858 \times 0.02} \right) \text{ N/m}^2 \\ &= 8585 \text{ N/m}^2 \\ &= 87.6 \text{ cm of water} \end{aligned}$$

This pressure drop is rather high and would not be acceptable in an actual application. In order to reduce it to an acceptable value, the air flow rate would have to be reduced by a factor of 4 or 5. This would also result in a reduction in the value of h_v . Consequently the rate at which energy is stored in the solid would also reduce (see problem 5).

The solutions just given are valid for the situation in which the solid is initially at a uniform temperature T_i and the fluid entering the bed is also at a constant temperature T_{fi} . If these conditions are not satisfied, it becomes difficult to obtain an analytical solution and recourse has to be taken to a numerical method. The governing differential equations (7.20) and (7.21) are expressed in a suitable finite-difference form by considering the bed to consist of a finite

number of slices of width Δx and considering finite time intervals of Δt . One then obtains sets of simultaneous linear equations at each instant of time and these are solved in order to obtain the temperature distributions.

7.2.5 Testing Procedures

Certain standard procedures suggested for the testing of thermal storage devices* are now considered. The set-ups used are similar to those described earlier for liquid flat-plate collectors (Section 4.12) and solar air heaters (Section 5.4), with the liquid flat-plate collector or solar air heater being replaced by the thermal storage device under test using either a liquid or air as the transfer fluid. The tests to be performed are the heat loss test and two charge-discharge tests for determining the storage capacity.

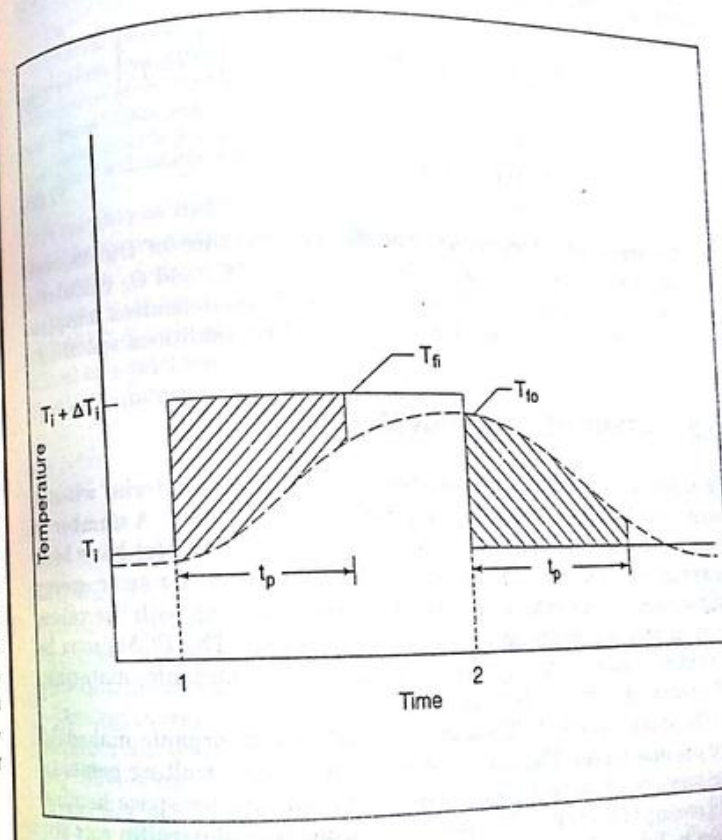
In the heat loss test, the transfer fluid is passed through the storage device at a fixed mass flow rate (\dot{m}) and at an inlet temperature (T_{fi}) 25°C above the ambient air temperature (T_a). After steady state conditions are achieved, the difference between the inlet and outlet fluid temperature is measured. The heat loss factor (UA) is calculated from the expression

$$(UA)_i = \frac{\dot{m}C_p(T_{fi} - T_{fo})}{(T_{fi} - T_a)} \quad (7.21)$$

where C_p is the specific heat of the transfer fluid.

In the charge-discharge test, the transfer fluid at a constant temperature is first passed through the device and the device brought to a uniform initial temperature T_i . Then the flow is adjusted to the test flow rate (\dot{m}) and the temperature of the transfer fluid is suddenly increased in a step-wise manner to $T_i + \Delta T_i$. The difference between the temperature of the transfer fluid entering and leaving the device is continuously recorded over a specified time period t_p as charging takes place. The temperature of the transfer fluid is maintained at $(T_i + \Delta T_i)$ until the exit temperature of the transfer fluid reaches a steady value. Thereafter with the same mass flow rate, the temperature of the transfer fluid is suddenly decreased in a step-wise manner

back to the initial value T_i . The difference between the temperature of the transfer fluid entering and leaving the device is again continuously recorded over the same time period t_p as discharging takes place. The charge-discharge cycle is performed for two test conditions. If the transfer fluid is a liquid, the value of ΔT_i is taken as 15°C for both test conditions, while the values of t_p are taken to be 2 and 4 hours. If the transfer fluid is air, the corresponding values are $\Delta T_i = 35^\circ\text{C}$, and $t_p = 2$ and 4 hours. The variation of the inlet and exit temperature of the transfer fluid during a typical charge-discharge cycle is shown in Fig. 7.9.



The value of T_i , the initial temperature of the storage device, is chosen by considering the intended temperature range of the device during use, while the value of the mass flow rate maintained during charging and discharging is calculated from the expression

$$\dot{m} = \frac{\text{TSC}}{t_p C_p \Delta T_i} \quad (7.29)$$

where,
 TSC = theoretical storage capacity of the device for a temperature change from T_i to $(T_i + \Delta T_i)$.

From the data recorded, the charge and discharge capacities of the device are obtained by integration as follows,

$$C_c = \dot{m} C_p \int_0^{t_p} (T_{fi} - T_{fo}) dt - (UA) t_p \left[\frac{T_{fi} + \bar{T}_{fo}}{2} - T_a \right] \quad (7.29)$$

$$C_d = \dot{m} C_p \int_0^{t_p} (T_{fo} - T_{fi}) dt \quad (7.30)$$

The standard recommends that the performance of the thermal storage device should be judged by the values of C_c and C_d calculated from Eqs (7.29) and (7.30) along with plots of dimensionless temperature $(T_{fo} - T_{fi})/\Delta T_i$ vs. time obtained for the two conditions specified.

7.3 LATENT HEAT STORAGE

In a latent heat storage system, heat is stored in a material when it melts and extracted from the material when it freezes. A number of such materials (called 'phase change materials' or PCMs) have been investigated from the point of view of their suitability for solar energy applications. Some of them are listed in Table 7.5 along with the values of their melting points and latent heats of fusion. The PCMs may be considered under the following groupings: (1) Organic materials, (2) Hydrated salts, (3) Inorganic materials.

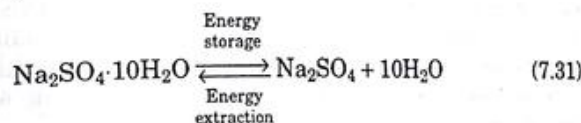
The most suitable PCMs under the category of 'organic materials' are paraffin waxes. They are readily available with melting points in the range of 40° to 60°C. This makes them suitable for space heating and cooling applications. The properties of one typical paraffin wax are given in Table 7.5. It will be noted that it does not have a well-defined melting point.

Table 7.5 Phase Change Materials

Substance	Formula	Melting point °C	Heat of fusion kJ/kg
Organic materials: Paraffin wax P116E	—	42-50	209
Hydrated salts: Calcium chloride hexahydrate Sodium sulphate decahydrate Magnesium nitrate hexahydrate	CaCl ₂ ·6H ₂ O Na ₂ SO ₄ ·10H ₂ O Mg(NO ₃) ₂ ·6H ₂ O	30 32 89	168 241 167
Inorganic materials: Ice Sodium nitrate Sodium hydroxide	H ₂ O NaNO ₃ NaOH	0 310 320	335 173 159

N.B. Some PCMs (sodium sulphate decahydrate and calcium chloride hexahydrate) are commercially available in encapsulated forms in various configurations like tubes, cans, wall panels, etc.

A number of hydrated salts have been developed as PCMs. Most of them have transition temperatures in the range of 10° to 100°C. The properties of three of them, viz. calcium chloride hexahydrate, sodium sulphate decahydrate and magnesium nitrate hexahydrate are listed in Table 7.5. It is of interest to note that sodium sulphate decahydrate (Glauber's salt) was the first PCM to be studied for solar applications. This salt undergoes the hydration-dehydration reaction at 32°C.



It was studied by Telkes* for a space-heating application. The main difficulty encountered with hydrated salts is that their thermal performance degrades with repeated cycling due to phase segregation. This difficulty is generally overcome by mixing certain additives.

Among inorganic materials, ice is a good PCM if the energy is to be stored/extracted at 0°C. A number of inorganic compounds and eutectics have been considered for high temperature applications. The properties of two of them, viz. sodium nitrate and sodium hydroxide are given in Table 7.5.

The properties required for a phase change material are as follows:

- (1) a melting point in the temperature range of the application for which it is being considered.
- (2) a high value of the latent heat of fusion.
- (3) a small volume change during the phase change, and
- (4) negligible supercooling or superheating for the phase change to occur.

In addition, it is desirable that the thermal conductivity of the material should be high in both phases, that it should have a low vapour pressure at the temperature of use, and that it should be non-corrosive.

An advantage associated with a latent heat storage system is that it is more compact than a sensible heat system. However, the heat exchange system for transferring energy between the working fluid (which is usually a gas) and the storage material is always more complex. This is due to the fact that during the heat extraction process, the storage material first solidifies at the heat transfer surface. Hence, the thermal resistance to the flow of heat keeps on increasing as heat is extracted from the storage. In order to prevent the thermal resistance from becoming too large, the storage material is placed in long thin containers and the gas is passed through narrow spaces between the tubes. Alternatively the storage material is in the spaces between the tubes and the gas is passed through the tubes. Both these arrangements are shown in Fig. 7.10.

Some novel arrangements have also been proposed or tried. In one system, the phase change material is contained in a bundle of long cylindrical tubes which is rotated at a low speed. This helps to keep the storage material mixed and it is claimed that solidification begins at a number of nuclei inside the liquid and not on the tube walls alone.

In another arrangement, a mixture of Glauber's salt, fused silica and some other chemicals has been encapsulated in a polymer concrete shell shaped in the form of a standard ceiling tile. The mixture has a melting point of 23°C and has been tried out for a passive space-heating system.

7.4 THERMOCHEMICAL STORAGE

In a thermochemical storage system, the solar energy to be stored is used to produce a certain endothermic chemical reaction and the products of the reaction are stored. When the energy is required to be released, the reverse exothermic reaction is made to take place. Both reactions take place at different temperatures, the forward reaction occurring at a higher temperature than the reverse reaction. Thermochemical storage systems are suitable for medium or high temperature applications only.

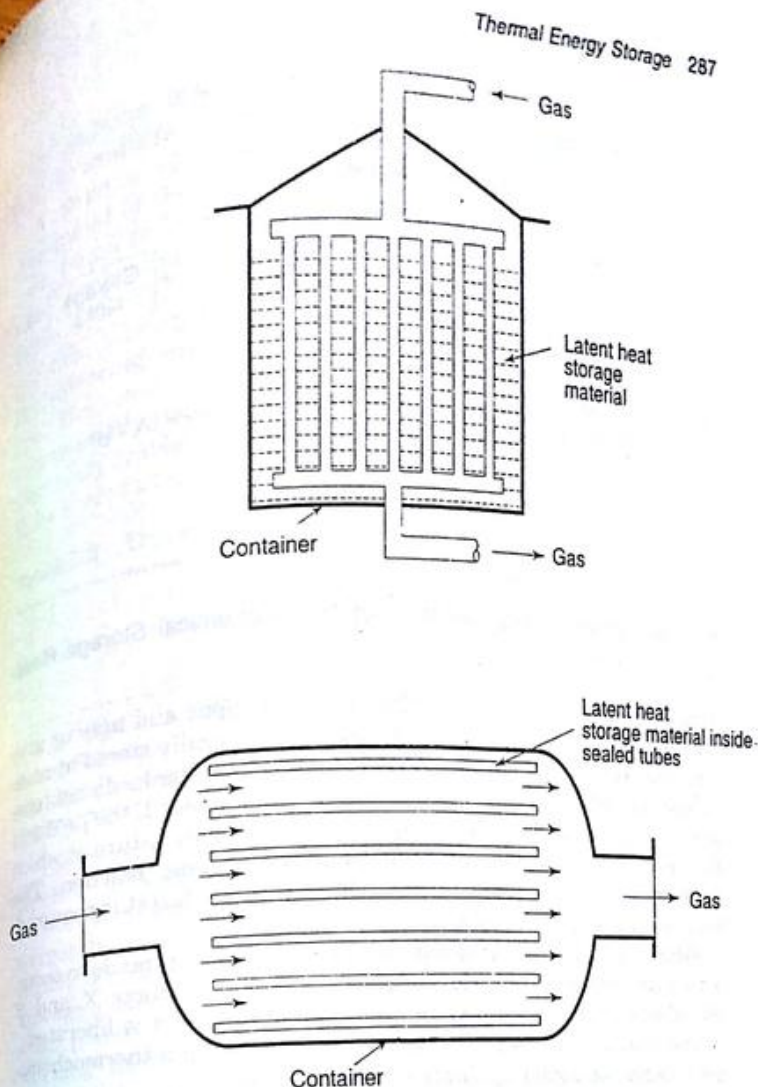


Fig. 7.10 Latent Heat Storage Arrangements

The reactions are shown schematically in Fig. 7.11. Chemicals A and B are converted through the forward reaction into products X and Y.*

*The number of chemicals involved may be more or less than two.

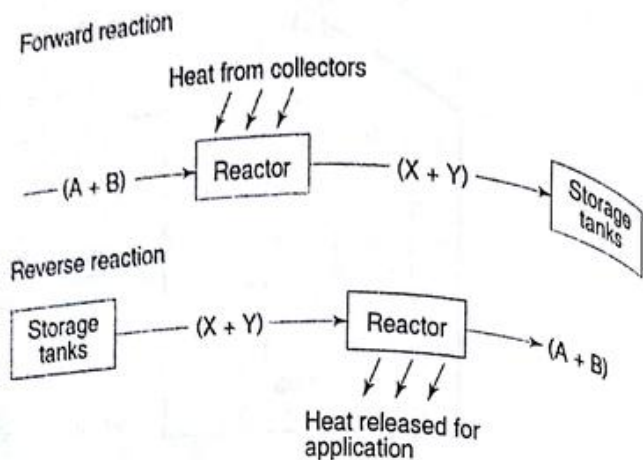


Fig. 7.11 Schematic Representation of Thermochemical Storage Reactions

This reaction occurs because of the solar heat input and may or may not need a catalyst. The products X and Y are generally stored at room temperature. This is an advantage since the storage tanks do not have to be insulated. However, in case a catalyst is not needed, the products of the forward reaction must be separated at the temperature at which the reaction occurs in order to prevent the reverse reaction. The products must then be stored separately. In case a catalyst is required, separation may not be required.

When energy is to be extracted, the reverse reaction is made to occur. This takes place at a lower temperature, with products X and Y recombining to form A and B. During the reaction, heat is liberated.

The criteria to be used for judging the suitability of a thermochemical reaction for a solar application are as follows:

- (1) The forward reaction should occur in the temperature range of the solar collectors used.
- (2) The reverse reaction should occur in the temperature range in which heat is to be extracted.
- (3) The two reactions should occur at temperatures which are close to each other. In this way, the collector temperature is minimized and its efficiency maximized.
- (4) In order to minimize the size of the storage tanks, the energy absorbed per unit volume of the products stored should be as large as possible and the products should be in the liquid form.
- (5) The reactions in both directions should be fast and completely reversible with no side reactions which may produce contaminants.

In addition, it is preferable that the chemicals required should be readily available at low cost and should be easy to handle. A number of chemical reactions have been examined from the standpoint of their suitability based on the above criteria. A few have been found to be suitable and have been proposed for future use in solar applications. The details of three such reactions are given in Table 7.6. The first reaction referred to as the methane-syngas reaction, takes place in the presence of a nickel catalyst. It has been the subject of interest because the technology required is available. In fact, the reverse reaction (called the methanation process) is being commercially used for the manufacture of methane on a large scale. The main problem is that the products CO and H₂ are gases and have to be stored at a pressure of about 100 bars.

Table 7.6 Thermochemical Storage Reactions

Reaction	Temperature of forward reaction (°C)	Temperature of reverse reaction (°C)	Energy stored per unit volume of storage material (kJ/m ³)
CH ₄ + H ₂ O \rightleftharpoons CO + 3H ₂	780	610	209.4 $\times 10^3$
SO ₃ \rightleftharpoons SO ₂ + $\frac{1}{2}$ O ₂	1025	590	460.6 $\times 10^3$
NH ₄ HSO ₄ \rightleftharpoons NH ₃ + H ₂ O + SO ₃	498	435	2143.7 $\times 10^3$

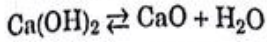
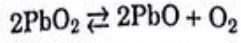
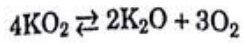
The second reaction in Table 7.6 involves the endothermic decomposition of sulphur trioxide to sulphur dioxide and oxygen in the forward step and the exothermic recombination of sulphur dioxide and oxygen to form sulphur trioxide in the reverse step, in the presence of a catalyst. After a detailed study* of various chemical reactions, this storage system has been suggested for use in a 100 MW central tower solar power plant operating on the Brayton cycle with helium as the working fluid. The system components have been sized and cost estimates have been given. A disadvantage associated with this system is that although SO₂ can be stored as a liquid, O₂ has to be stored as a gas under a pressure of about 100 bars. Problems of corrosion and safety may also require careful attention.

The third reaction involves the decomposition of ammonium hydrogen sulphate into ammonia, water and sulphur trioxide in the forward direction. The reaction does not require a catalyst. Wentworth and

*Electric Power Research Institute, "Technical and Economic Assessment of Phase Change and Thermochemical Advanced Thermal Energy Storage Systems", EPRI EM-256, Final Report, 1, Project 788-1 (Dec. 1976).

Chen* have selected this reaction after studying a number of thermal decomposition reactions since it satisfies most of the criteria mentioned earlier.

Some other reactions which have been suggested for energy storage are the thermal decomposition of various metal oxides† and of calcium hydroxide‡.



Despite the fact that the energy stored per unit volume in the proposed reactions is high, it is apparent that thermochemical storage systems would be too costly for short-term storage. It is possible that they may have a role to play only where long-term storage is required around the ambient temperature and the locations where the forward and reverse reactions occur are separated by some distance.

PROBLEMS

1. A well-mixed water storage unit contains 3000 kg of water and is provided with auxiliary heating of 3 kW as shown in Fig. 7.12. Data for the useful heat gain from the collectors, ambient temperature and rate of withdrawal to the load on a particular day from 0300 to 1200 h are as follows:

Hour	q_u (kJ/h)	T_a (°C)	m_{load} (kg/h)
0300-0400	0	16	200
0400-0500	0	16	200
0500-0600	0	18	200
0600-0700	0	20	220
0700-0800	4 000	22	250
0800-0900	15 000	24	260
0900-1000	30 000	26	260
1000-1100	50 000	28	230
1100-1200	70 000	30	220

Assume: (i) The auxiliary heater switches on when the temperature in the tank falls below 45°C. (ii) Make-up water at 24°C enters at the same rate as the rate of withdrawal to the load. (iii) $(UA)_t = 60 \text{ kJ/h}^{-\circ}\text{C}$.

*W.E. Wentworth and E. Chen, "Simple Thermal Decomposition Reactions for Storage of Solar Thermal Energy", *Solar Energy*, 18, 205 (1976).

†J.A. Simmons, "Reversible Oxidation of Metal Oxides for Thermal Energy Storage", *Proc ISES Meeting, Winnipeg*, 8, 219 (1976).

‡I. Fujii, K. Tsuchiya, Y. Shikakura and M.S. Murthy, "Thermal Decomposition of Calcium Hydroxide Pellets for Energy Storage", *Trans. ASME, J. Solar Energy Eng.* 111, 245 (1989).

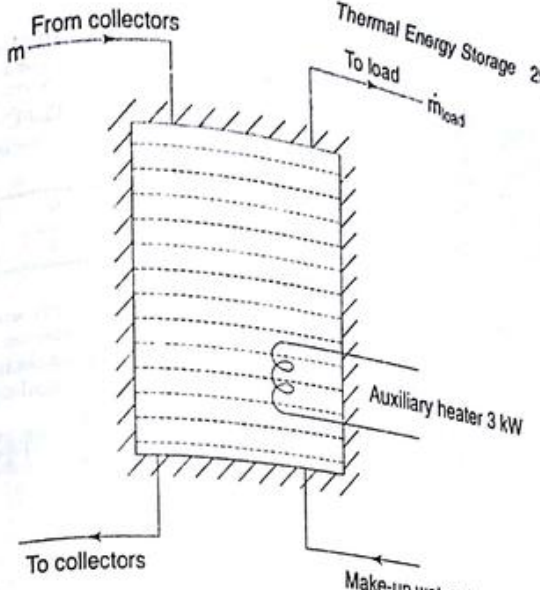


Fig. 7.12 Problem 1

Calculate the hourly variation of T_t from 0300 to 0800 h starting with the value of 49.5°C at 0300 h. At what time does the auxiliary heater switch on?

2. For a well-mixed liquid storage tank, it is given that (i) the useful heat gain rate can be approximated by a half-sine wave $q_u = A_1 \sin(\pi t/t_1)$ where A_1 and t_1 are constants, (ii) q_{load} = a constant, (iii) the ambient temperature T_a is constant, and (iv) at $t = 0$, the stored liquid is at a temperature T_{t1} . Show that the temperature variation in the tank is given by

$$(T_t - T_a) = \frac{\pi c_2 t_1}{(\pi^2 + c_1^2 t_1^2)} \left[\frac{c_1 t_1}{\pi} \sin \frac{\pi t}{t_1} - \cos \frac{\pi t}{t_1} + e^{-c_1 t} \right] + \left[T_{t1} - T_a + \frac{c_3}{c_1} \right] e^{-c_1 t} - \frac{c_3}{c_1}$$

$$\text{where } c_1 = \frac{(UA)_t}{(\rho V C_p)_t}; c_2 = \frac{A_1}{(\rho V C_p)_t}; c_3 = \frac{q_{load}}{(\rho V C_p)_t}$$

3. Write down the set of equations appropriate for a stratified water storage tank which is assumed to consist of three well-mixed sections.

4. Use the data of Example 7.2 with the assumption that the hot water tank consists of three equal well-mixed sections. Take $T_{t1} = 70^\circ\text{C}$, $T_{t2} = 67.5^\circ\text{C}$ and $T_{t3} = 65^\circ\text{C}$ at 1200 h and find their values at 1300 h.

5. Solve Example 7.3 by taking the air flow rate to be 0.22 kg/s.

6. (a) A cylindrical hot water storage tank has a diameter of 1.1 m and a height of 2.16 m. It is insulated on all faces with glass wool insulation 10 cm thick, having a thermal conductivity of 0.042 W/m·K. Calculate the heat loss factor $(UA)_t$ for the tank.

- (b) A heat loss test is conducted on the tank in which the flow rate of water is 0.11 kg/s, the inlet water temperature is 54.0°C and the ambient air temperature is 29.0°C. Under steady-state conditions, the average difference between the inlet and outlet water temperature is measured to be 0.32°C. Calculate the heat loss factor $(UA)_t$ from the experimental data. Compare the value obtained with the value calculated in part (a). Comment on possible reasons for the difference between the two values.

7. A hot water storage tank has a volume of 2.0 m^3 . For conducting a charge test according to the standard code, it is first brought to a uniform initial temperature of 53°C . Then the flow is adjusted to 0.272 kg/s and the temperature of the inlet water is increased stepwise by 15.3°C in 15.3°C steps. The temperature of the leaving water is measured at regular time intervals over a period of 2 hours and the following readings are recorded.

t (min)	0 to 78	84	90	96	102	108	114	120
T_f ($^\circ\text{C}$)	53.0	53.3	54.9	57.5	60.0	62.5	64.9	67.5

Plot the dimensionless temperature $(T_{f0} - T_{fi})/\Delta T$, against time and calculate the charge capacity of the device. Given that the heat loss factor (as obtained from a heat loss test) is 6.22 W/K and that the ambient air temperature is 24.5°C . Calculate also the ratio of the charge capacity to the theoretical storage capacity for the step change of 15.3°C .



Solar Pond

8.1 INTRODUCTION

In order to reduce the cost of large solar thermal installations, it is necessary to devise more economical ways of collecting and storing solar energy. In this context, attention has been focussed on the possibility of using large expanses of water of small depth for absorbing and storing solar radiation instead of using flat-plate collectors and hot water storage tanks. However, experience shows that the water in such a pond usually heats up only a few degrees, because of the natural convection currents which are set into motion as soon as heat is absorbed at the bottom. One would obtain a significant rise in the water temperature only if the convection could be prevented. An artificially constructed pond in which significant temperature rises are caused to occur in the lower regions by preventing convection is called a "solar pond".

The usual method adopted to prevent convection is to dissolve a salt in the water and to maintain a concentration gradient. For such ponds, the more specific term 'salt-gradient solar pond' is used. In this chapter, we will essentially discuss only the 'salt-gradient solar pond' since this concept has made good progress. Other concepts like the gel solar pond, the honeycomb solar pond and the equilibrium solar pond will only be described briefly.

In the last fifteen years, many salt-gradient solar ponds varying in size from a few hundred to a few thousand square metres of surface

area have been built in a number of countries, mostly on an experimental basis. The indications are that they appear to be economical for applications requiring low temperature process heat up to 70 or 80°C. It is therefore likely that they will be used more extensively in the future, as problems connected with their operation and maintenance are resolved.

The concept of a solar pond is derived from the observation that in some naturally occurring lakes, a significant temperature rise (of the order of 40 to 50°C) does occur in the lower regions. This is because of the fact that there is a natural salt concentration gradient in these lakes, whereby the water at the bottom remains denser even when it is hotter than the water at the top. Thus, convection does not occur and heat is lost from the hot water only by conduction. The salt concentration gradient in such lakes is maintained naturally because of the presence of salt deposits at the bottom of the lakes, which cause close to saturation concentrations in the lower regions and because of fresh water streams which flow across the top.

The working of a solar pond can be explained with reference to Fig. 8.1. Consider a pond of depth L having salts dissolved in the water.

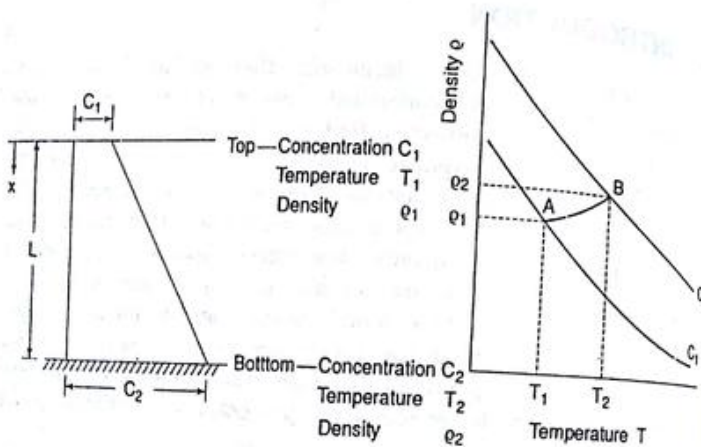


Fig. 8.1 Principle of Working of a Solar Pond

We assume that the concentration at the top (C_1) is less than that at the bottom (C_2) and that a concentration gradient exists from the top to the bottom. The variation of density with temperature for the two concentrations is as shown. Let T_1 and ρ_1 be the temperature and density of the top layer of water indicated by point A, and T_2 and ρ_2

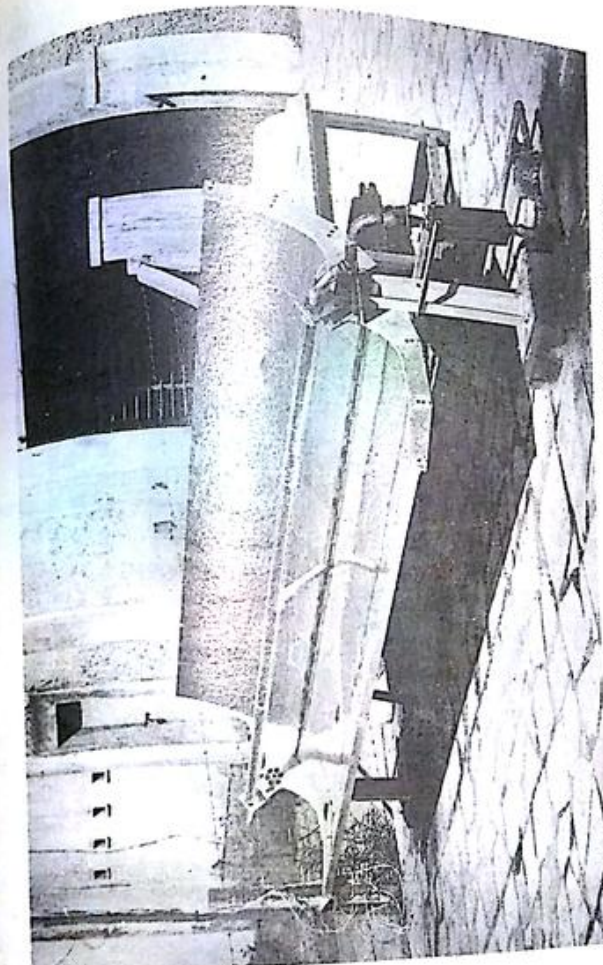


Photo 5
Cylindrical Parabolic Collector, Length 3.6 m, Aperture 1.25 m,
Concentration Ratio 9.6, Reflector Material: Electropolished
Anodized High Purity Aluminium Sheet, Location: Indian Institute
of Technology, Bombay

Plate 1

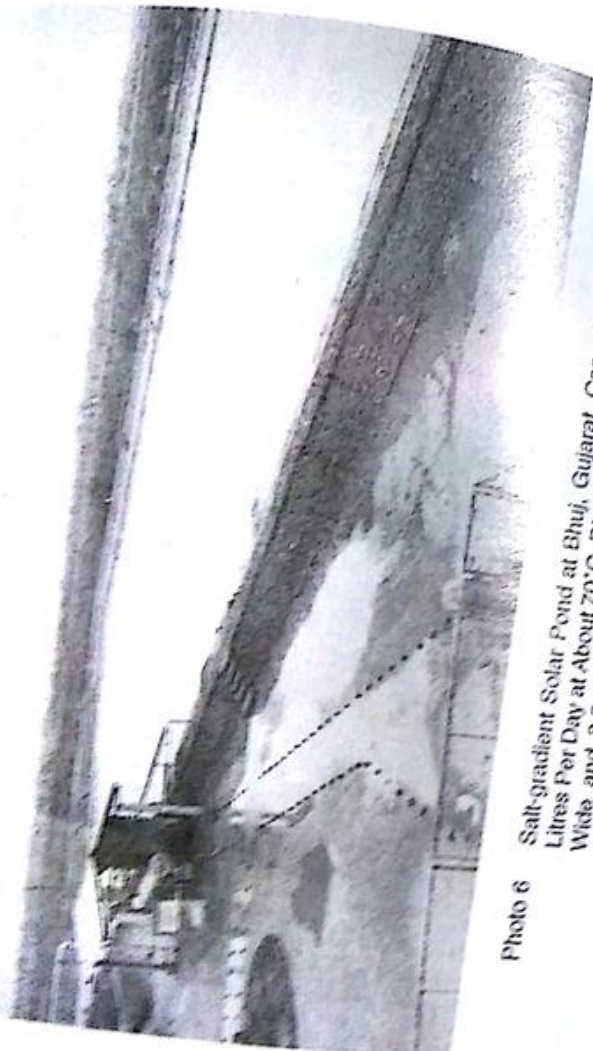


Photo 6

Salt-gradient Solar Pond at Bhuj, Gujarat. Capacity: 80 000 Litres Per Day at About 70°C. Dimensions: 100 m Long, 60 m Wide, and 3.5 m Deep (Courtesy: Tata Energy Research Institute, New Delhi)

be the temperature and density of the bottom layer indicated by point B . Similar points are located for the intermediate layers and the curve AB is drawn showing the variation of density as one moves downwards in the pond. It is obvious that no convection will occur so long as the slope of the curve AB is positive.

Mathematically, the condition that the lower layers remain denser than those above is given by

$$\frac{dp}{dx} > 0 \quad (8.1)$$

Since $\rho = \rho(C, T)$, it follows that the condition for stability is

$$\left[\frac{\partial \rho}{\partial C} \right]_T \left[\frac{dC}{dx} \right] + \left[\frac{\partial \rho}{\partial T} \right]_C \left[\frac{dT}{dx} \right] > 0$$

$$\frac{dC}{dx} > - \left\{ \left[\frac{\partial \rho}{\partial T} \right]_C \left(\frac{dT}{dx} \right) \right\} \left/ \left[\frac{\partial \rho}{\partial C} \right]_T \right\} \quad (8.2)$$

From a slightly more sophisticated analysis which considers the effect of small perturbations, it can be shown that

$$\frac{dC}{dx} > - \left\{ \frac{v + \alpha}{v + D} \right\} \left\{ \left[\frac{\partial \rho}{\partial T} \right]_C \left(\frac{dT}{dx} \right) \right\} \left/ \left[\frac{\partial \rho}{\partial C} \right]_T \right\} \quad (8.3)$$

where v = kinematic viscosity

α = thermal diffusivity

and D = diffusivity of salt in water

For solutions of salt in water under the conditions encountered in solar ponds, the value of the term $(v + \alpha)/(v + D)$ is about 1.15. Thus, the criterion for stability given by Eq. (8.3) is a little more stringent than the criterion given by Eq. (8.2). Equation (8.2) or (8.3) can be used for calculating the minimum concentration gradient required for maintaining a given temperature gradient at a particular level in a solar pond. In actual practice, a certain margin of safety is recommended and the actual concentration gradient is maintained at about twice the value given by Eq. (8.3).

The first experimental solar ponds were constructed in Israel in the early sixties by Tabor and his co-workers. Although the principle of working was demonstrated effectively and temperatures close to the maximum possible value of 100°C were obtained at the bottom, many practical difficulties were encountered and the work was abandoned. However, in the last few years, there has been a renewed interest in developing solar ponds. So far, about sixty solar ponds have been built all around the world and the heat energy stored in them has been used in a variety of applications. In USA, small ponds for research activities have been constructed at Ohio State University, University of New

Mexico and Los Alamos National Laboratory. Larger ponds include a pool and one of 3500 m^2 at El Paso, Texas to provide hot water for a swimming factory. The largest solar pond built so far is the $250\,000\text{ m}^2$ pond at Ha Arava in Israel. The heat collected in this pond has been used to generate 5 MW of electrical power using an organic fluid Rankine cycle.

In India, the first solar pond having an area of 1200 m^2 was built at the Central Salt and Marine Chemicals Research Institute, Bhavnagar in 1973. Experimental research ponds having areas of 100 m^2 and 240 m^2 respectively were operated for a few years at Pondicherry and at the Indian Institute of Science in Bangalore, while a 1600 m^2 pond was built in Bhavnagar again in the eighties. A solar pond having an area of 400 m^2 has been constructed at Masur (Karnataka) to meet the hot water needs of a rural community; and one having an area of 300 m^2 has been built to supply hot water for the students hostel of an engineering college at Hubli (Karnataka). The largest pond built in India so far is located at Bhuj (Gujarat). (Refer Photo No. 6.) The pond has an area of 6000 m^2 . It has been operating since September 1993 and supplies the process heat needs of a nearby dairy.

8.2 DESCRIPTION

A schematic diagram of a solar pond is shown in Fig. 8.2. As stated

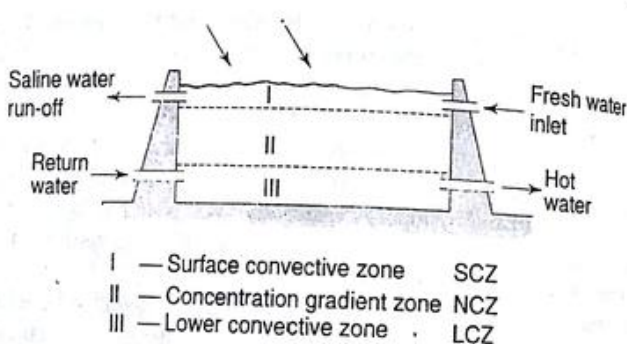


Fig. 8.2 Schematic Diagram of a Solar Pond

earlier, it combines the functions of heat collection with long-term storage and can provide sufficient heat for the entire year. Typically, it is about 1 or 2 metres deep with a thick durable plastic liner laid at the bottom. Materials used for the liner include low density polyethylene (LDPE), high density polyethylene (HDPE), woven polyester yarn (XB-5), and hypalon reinforced with nylon mesh. Salts

like magnesium chloride, sodium chloride or sodium nitrate are dissolved in the water, the concentration varying from 20 to 30 per cent at the bottom to almost zero at the top. Left to itself, the salt concentration gradient will disappear over a period of time because of upward diffusion of the salt. In order to maintain it, fresh water is added at the same time, concentrated brine is added at the bottom of the pond.* The amount of salt required for this purpose is about $50\text{ g/m}^2\text{-day}$, which is a large quantity when considered on an annual basis. For this reason the normal practice is to recycle the salt by evaporating the saline water run off from the surface in an adjacent evaporation pond. In order to extract the energy stored, hot water is removed continuously from the bottom, passed through a heat exchanger and returned to the bottom. Alternatively heat is extracted by water flowing through a heat exchanger coil submerged at the bottom. Because of movement and mixing of the fluid both at the top and the bottom, the solar pond is characterized by three zones: a surface convective zone, a non-convective concentration gradient zone, and a lower convective zone (Fig. 8.2). The surface convective zone (SCZ) usually has a small thickness, around 10 to 20 cm. It has a low, uniform concentration, which is close to zero, as well as a fairly uniform temperature, which is close to the ambient air temperature. The non-convective zone (NCZ) is much thicker and occupies more than half the depth of the pond. Both concentration and temperature increase with depth in this zone. It serves principally as an insulating layer and reduces heat losses in the upward direction. Some of the heat collection also takes place in this zone and it serves also as part of the thermal storage. The lower convective zone (LCZ) is comparable in thickness to the non-convective zone. Both the concentration and the temperature are nearly constant in this zone. It serves as the main heat-collection as well as thermal-storage medium. The lower convective zone is often referred to as the storage zone or as the bottom layer.

Typically, the temperature in the lower convective zone of a well designed large pond operating in India might fluctuate cyclically between a maximum value of 85° to 95°C in summer and a minimum of 50° to 60°C in winter. This is shown in Fig. 8.3, in which the variation of the ambient air temperature is also indicated. It will be noted that there is a phase difference of a month or two between the two curves. The annual collection efficiency generally ranges between 15 and 25 per cent. These values are lower than those obtained for a flat-plate

*In order to account for losses due to evaporation, the amount of liquid added at the top and bottom is greater than the amount withdrawn.

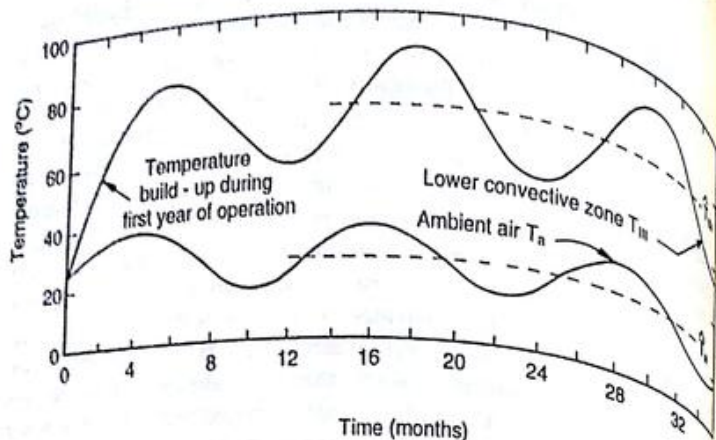


Fig. 8.3 Typical Annual Cyclic Variation of Daily Mean Temperature in a Solar Pond

collector. Nevertheless, solar ponds are more cost-effective, since their cost per square metre is much less than that for a liquid flat-plate collector system. This is particularly true when the area is of the order of 1000 m^2 or more.

8.3 PERFORMANCE ANALYSIS

In order to analyse the performance of a solar pond, the first task is to determine the manner in which the radiation incident upon the solar pond is reflected, absorbed and transmitted through the water.

8.3.1 Transmissivity Based on Reflection–Refraction at the Air–Water Interface

The transmissivity (τ_r) based on reflection and refraction at the air–water interface is calculated in a manner similar to that indicated in Sec. 4.3.1. Equations (4.5) to (4.9) are again valid with the refractive index for water relative to air being taken equal to 1.33. Values of τ_r obtained for different angles of incidence are given in Table 8.1. It is seen that for angles of incidence from 0 to 60° , the loss due to reflection is small and ranges from 2 to 6 per cent. For larger angles, the loss is large. From the point of view of energy collection in the pond, one is generally not interested in large angles of incidence because these are associated with low values of radiation.

Solar Pond 299
Table 8.1 Transmissivity Based on Reflection and Refraction at the Air–Water Interface of a Solar Pond

Angle of incidence θ_1 (degree)	Angle of refraction θ_2 (degree)	ρ_1 Eq. (4.6)	ρ_{11} Eq. (4.7)	$\rho = \frac{1}{2}(\rho_1 + \rho_{11})$	$\tau_r = (1 - \rho)$
0	0	0.020	0.020	0.020	0.980
15	11.32	0.022	0.018	0.020	0.980
30	22.08	0.030	0.012	0.021	0.979
45	32.12	0.052	0.003	0.027	0.973
60	40.63	0.114	0.004	0.059	0.941
75	46.57	0.312	0.111	0.211	0.789
90	48.75	1	1	1	0

8.3.2 Transmissivity Based on Absorption

In Sec. 4.3.2, the transmissivity (τ_a) based on absorption has been calculated by a single exponential given by Eq. (4.14). This description is adequate for glass but not for water, because for water experimental data indicate that the extinction coefficient K is a strong function of wavelength. Keeping this dependence in mind, Rabl and Nielsen* have modified Eq. (4.14) into the following form which is the sum of four exponentials.

$$\tau_a = \sum_{j=1}^4 A_j e^{-K_j x} \quad (8.4)$$

where x = depth of water. The constants A_j and K_j are found to have the following values after fitting the available experimental data,

$$\begin{aligned} A_1 &= 0.237, K_1 = 0.032 \text{ m}^{-1} \text{ for } 0.2 < \lambda < 0.6 \mu\text{m}, \\ A_2 &= 0.193, K_2 = 0.45 \text{ m}^{-1} \text{ for } 0.6 < \lambda < 0.75 \mu\text{m}, \\ A_3 &= 0.167, K_3 = 3 \text{ m}^{-1} \text{ for } 0.75 < \lambda < 0.9 \mu\text{m}, \\ A_4 &= 0.179, K_4 = 35 \text{ m}^{-1} \text{ for } 0.9 < \lambda < 1.2 \mu\text{m}. \end{aligned}$$

Equation (8.4) is stated to be accurate to within 3 per cent.

The four values of A in Eq. (8.4) correspond to the wavelength range 0.2 to 1.2 μm and add up to 0.776. Thus, only 77.6 per cent of the radiation is accounted for. The balance of 22.4 per cent corresponds to radiation of wavelengths greater than 1.2 μm , which is absorbed very near the surface within the first 1 or 2 cm. Thus, Eq. (8.4) is valid for all depths excepting the first 1 or 2 cm.

*A. Rabl and C.E. Nielsen, "Solar Ponds for Space Heating", *Solar Energy*, 17, 1 (1975).

An alternative and simple equation for calculating τ_a which was suggested by Bryant and Colbeck* is as follows.

$$\tau_a = 0.36 - 0.08 \ln x$$

where x = depth of water in metres. Equation (8.5) has the same accuracy as Eq. (8.4) and is also valid for $x > 0.01$ m. In case the radiation is not normally incident, it is recommended, for both Eqs (8.4) and (8.5), that x be replaced by $(x/\cos \theta_2)$, where θ_2 is the angle of refraction.

Example 8.1

A solar pond, 1.5 m deep, is built in Pondicherry ($11^{\circ}56'N$). The following values of global and diffuse radiation are measured by a horizontal pyranometer placed beside the pond on April 20 at 1300 h (LAT):

$$I_g = 0.964 \text{ kW/m}^2$$

$$I_d = 0.210 \text{ kW/m}^2$$

Calculate the variation of the solar radiation flux as it penetrates through the pond.

On April 20, $n = 110$

$$\delta = 23.45 \sin \left\{ \frac{360}{365} (284 + 110) \right\} = 11.23^\circ$$

From Eq. (3.5), the angle of incidence of the beam radiation is given by

$$\begin{aligned} \cos \theta_1 &= \sin 11.93^\circ \sin 11.23^\circ + \cos 11.93^\circ \cos 11.23^\circ \cos (-15^\circ) \\ &= 0.9672 \end{aligned}$$

$$\theta_1 = 14.71^\circ$$

Therefore, from Eq. (4.5),

$$\text{angle of refraction } \theta_2 = \sin^{-1} \left\{ \frac{\sin 14.71^\circ}{1.33} \right\} = 11.01^\circ$$

From Table 8.1, $\rho_b = 0.020$

For diffuse radiation, we take the angle of incidence to be 60° (see Sec. 4.3.3). Hence, from Table 8.1,

$$\text{angle of refraction} = 40.63^\circ$$

and

$$\rho_d = 0.059$$

Flux reflected from the water surface

$$\begin{aligned} &= I_b \rho_b + I_d \rho_d \\ &= (0.964 - 0.210) \times 0.020 + (0.210 \times 0.059) \\ &= 0.027 \text{ kW/m}^2 \end{aligned}$$

Therefore, flux entering the water

$$\begin{aligned} &= 0.964 - 0.027 \\ &= 0.937 \text{ kW/m}^2 \end{aligned}$$

Equation (8.5) is used for calculating the transmissivity based on absorption at depths of 0.01, 0.1, 0.5, 1.0 and 1.5 m.

At $x = 0.01$ m,

$$\tau_a \text{ for beam radiation } (\tau_{ab}) = 0.36 - 0.08 \ln (0.01/\cos 11.01^\circ)$$

$$= 0.7269$$

$$\tau_a \text{ for diffuse radiation } (\tau_{ad}) = 0.36 - 0.08 \ln (0.01/\cos 40.63^\circ)$$

$$= 0.7063$$

Hence, solar flux (I) at a depth of 0.01 m

$$\begin{aligned} &= I_b \tau_{rb} \tau_{ab} + I_d \tau_{rd} \tau_{ad} \\ &= (0.964 - 0.210) (1 - 0.020) \times 0.7269 \\ &\quad + 0.210 \times (1 - 0.059) \times 0.7063 \\ &= 0.677 \text{ kW/m}^2 \end{aligned}$$

Similarly, we obtain the following values of solar flux at the other depths:

Depth	0.1	0.5	1.0	1.5	m
Solar flux (I)	0.541	0.384	0.332	0.301	kW/m^2

The variation of solar radiation flux with depth is plotted in Fig. 8.4. The large amount of energy absorbed near the surface is clearly obvious. In the present case, assuming that the surface convective zone is 10 cm thick, it is seen that 0.396 kW/m^2 , amounting to 41 per cent of the incident energy, is absorbed in it*. This energy is almost entirely lost to the surroundings and is one of the main reasons accounting for the low collection efficiency of a solar pond. It is also seen from Fig. 8.4 that the flux penetrating to the bottom of the pond is 0.301 kW/m^2 , which amounts to 31 per cent of the incident energy.

Finally, it is worth noting that Eqs (8.4) and (8.5) for calculating the

*Most of the radiation absorbed in the surface convective layer has wavelengths

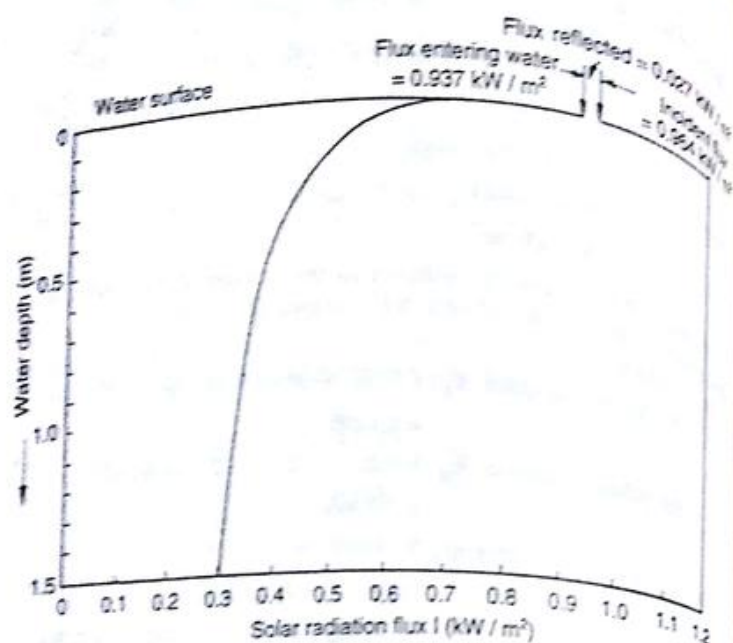


Fig. 8.4 Example 8.1—Reflection and Absorption of Solar Radiation in a Solar Pond

values of τ_s are valid for water. Some values for the salt solutions used in solar ponds are available. These are lower than the values for water alone.

8.3.3 Temperature Distribution and Collection Efficiency

The calculation of the temperature distribution in a solar pond is rather involved since the pond consists of three zones. For an exact solution, one has to solve the appropriate differential equation for each zone, use matching conditions at the interfaces between the zones and satisfy the boundary conditions at the top and bottom surfaces of the pond. Because of the complexity, the usual practice is to make some simplifications. We shall give here a formulation leading to one set of equations. In this formulation, the surface convective zone and the lower convective zone are assumed to be perfectly-mixed layers at uniform temperatures which change only with time.

Assuming that the lateral dimensions of the pond are large compared to its depth L (so that the temperature varies only in the vertical

direction) and that the properties are constant, the differential equation for the non-convective zone is the heat conduction equation of the form

$$\rho C_p \frac{\partial T_{II}}{\partial t} = k \frac{\partial^2 T_{II}}{\partial x^2} - \frac{dI}{dx} \quad (8.5)$$

$$\text{with } I = I_r \tau_{ab} \tau_{ad} + I_a \tau_{rd} \tau_{ad}.$$

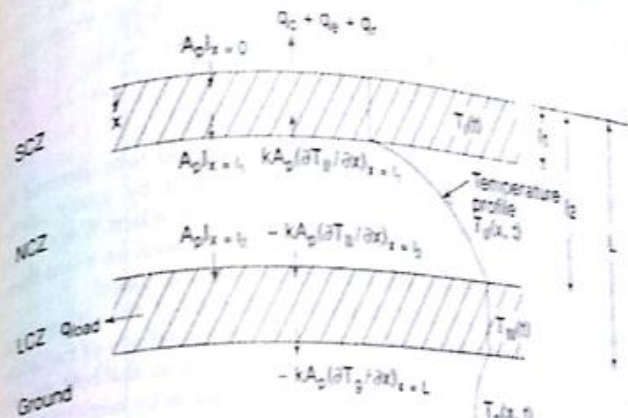


Fig. 8.5 Energy Flows In and Out of the Surface Convective Zone and the Lower Convective Zone

The term $(-dI/dx)$ accounts for the solar radiation absorbed in the pond.

The differential equations to be satisfied for the top and bottom layers of the pond are obtained by taking energy balances (Fig. 8.5).

For the Surface Convective Zone

Rate of change of energy contained in the surface convective zone of thickness l_1 :

$$\begin{aligned} &= (\text{Rate at which heat is conducted in from the non-convective zone}) \\ &+ (\text{Solar radiation absorbed in the thickness } l_1) \\ &- (\text{Rate at which heat is lost from the top surface by convection, evaporation and radiation}). \end{aligned}$$

Thus,

$$\rho l_1 C_p \left(\frac{dT_1}{dt} \right)_{z=l_1} = k \left(\frac{\partial T_{II}}{\partial x} \right)_{z=l_1} + [(I)_{z=0} - (I)_{z=l_1}] - \frac{1}{A_p} (Q_c + Q_e + Q_r) \quad (8.7)$$

For the Lower Convective Zone

Rate of change of energy contained in the lower convective zone of thickness $(L - l_2)$

- = (Rate at which heat is conducted in from the non-convective zone) + (Solar radiation absorbed in the thickness l_2) - (Rate at which heat is conducted out to the ground underneath) - (Rate of useful heat extraction).

Thus,

$$\rho(L - l_2)C_p \left(\frac{dT_{III}}{dt} \right)_{x=l_2} = -k \left(\frac{\partial T_{II}}{\partial x} \right)_{x=l_2} + (I)_{x=l_2} - \left[-k_g \left(\frac{\partial T_g}{\partial x} \right)_{x=L} - \frac{q_{load}}{A_p} \right]$$

Solutions to the set of Eqs (8.6) to (8.8) or similar sets (derived by making other simplifications) have been obtained by many investigators. They have been solved for the situation when there is no useful heat extraction from the pond ($q_{load} = 0$), as well as when there is a heat extraction. These solutions will now be discussed.

Weinberger* gave the first analytical solution of the differential Eq. (8.6) by a superposition technique in which the effects of radiation absorption at the surface, in the body of water and at the bottom, are considered separately. He also simplified the problem by neglecting the thicknesses of the convective zones and assuming the boundary condition that the temperature of the pond surface is equal to the ambient air-temperature. The need for correlations for calculating the losses q_c , q_e and q_r from the surface was thus eliminated. Weinberger used a sine-cosine series for the solar radiation falling on the pond surface and a sine series for the ambient temperature variation and gave the first estimates of the temperature rise which could be expected in a solar pond. For a pond one metre deep under typical conditions in Israel, he predicted a temperature rise of around 100°C if no heat was extracted. Starting in spring (April), it was estimated that this temperature would be attained in late summer (August) after about 120 days.

After the initial period in which the pond is allowed to heat up, the energy required for utilization is extracted and as a result, the temperature in the bottom layer does not keep on increasing. Weinberger obtained the interesting result that for a given mean extraction temperature there is a particular pond depth at which the rate of heat extraction is maximum. He further showed that this maximum rate of

energy withdrawal is equal to the solar radiation reaching the bottom of the pond. The results shown in Fig. 8.6 are for a location in Israel having a mean ambient temperature of 26°C and an annual average daily global radiation of 21 140 kJ/m²·day. For a given pond depth, the optimum mean extraction temperature and the corresponding annual collection efficiency can be obtained. Later investigations seem to indicate that Weinberger's analysis overestimates these values. Nevertheless, Fig. 8.6 can be used for approximately estimating solar pond behaviour in locations having similar annual values of ambient temperature and global radiation.

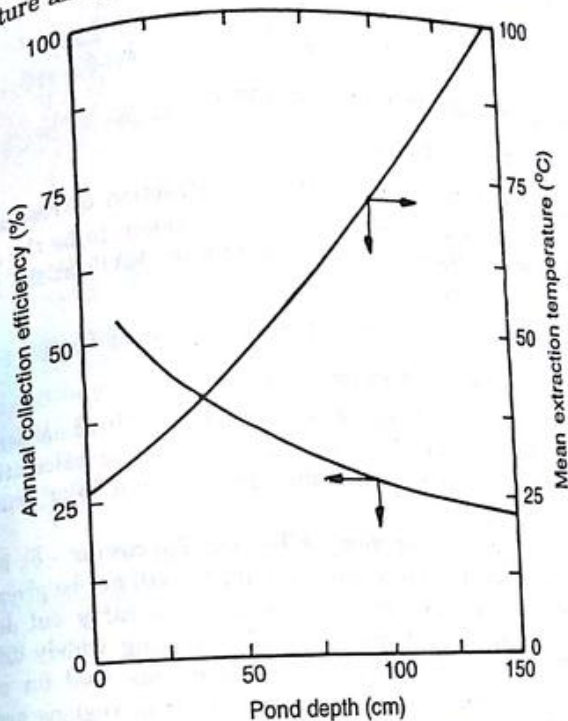


Fig. 8.6 Annual Collection Efficiency and Optimum Extraction Temperature as a Function of Pond Depth. From Weinberger. Used with Permission

Rabl and Nielsen* have also given an analytical solution for the annual temperature variation in a solar pond used for a space heating application. They have considered a pond several metres deep with a

lower convective zone of finite thickness, but a surface convective zone of negligible thickness. Diurnal variations are neglected and the temperature of the lower convective zone is obtained in the form

$$T_{III} = \hat{T}_{III} + \tilde{T}_{III} \cos(\omega t - \delta)$$

where \hat{T}_{III} = annual average temperature in the lower convective zone, \tilde{T}_{III} = amplitude, ω = frequency, and δ = phase lag with the variation of insolation. The annual average temperature T_{III} is time independent and is obtained quite easily by solving the heat conduction Eq. (8.6) in the steady state. The following solution is obtained,

$$\hat{T}_{III} - \hat{T}_a = \frac{\tau_r \hat{H}_g}{k} \sum_{j=1}^4 \frac{A_j}{K'_j} (1 - e^{-K'_j l_2}) - \frac{l_2}{k} \frac{\hat{q}_{load}}{A_p}$$

\hat{T}_a = annual average ambient temperature,

\hat{H}_g = annual average global radiation,

$K'_j = (K_j / \cos \theta_2)$, where θ_2 is the angle of refraction corresponding to an effective angle of incidence. This is taken to be the angle of incidence on the equinox day at 1400 h (LAT) at the location under consideration,

l_2 = depth of the pond at the bottom of the non-convective zone,

\hat{q}_{load} = annual average heat extraction rate.

The other symbols τ_r , k , A_j , K_j and A_p have been defined earlier.

Equation (8.9) is a simple and useful equation for calculating the average performance or for estimating the area of a solar pond for a given requirement.

The time dependent component of T_{III} , viz. $\hat{T}_{III} \cos(\omega t - \delta)$, is more difficult to calculate. The procedure for doing so will not be given here.

Rabl and Nielsen have used their solution to carry out detailed calculations for many locations in the USA having widely differing climates. They find that the solar pond performs well for all the locations and can supply adequate heating even in regions near the Arctic circle. For latitudes around 40° , they find that the pond should be approximately comparable in surface area and volume to the space it is to heat. Calculations also show that for a given location, heat load and annual mean extraction temperature, there is an optimum value of l_2 corresponding to which the pond area is a minimum.

Example 8.2

Estimate the area of a solar pond required for supplying 5×10^9 kJ of energy per year at an annual mean temperature of 70°C for an industrial process heat application. The pond is located in Nagpur

($21^\circ 06' \text{N}$, $79^\circ 03' \text{E}$) where the annual average daily global radiation is $19600 \text{ kJ/m}^2\text{-day}$ and the annual average ambient temperature is 26.3°C . Assume that the depth of the pond at the bottom of the non-convective zone is 0.95 m.

We first calculate the values of the effective angles of incidence and refraction. These are obtained on the equinox day ($\delta = 0^\circ$) at 1400 h (LAT). From Eq. (3.5),

$$\begin{aligned} \cos \theta_1 &= \cos \phi \cos \omega \\ &= \cos 21.1^\circ \cos (-30^\circ) = 0.8080 \\ \theta_1 &= 36.10^\circ \end{aligned}$$

Therefore, from Eq. (4.5),

$$\begin{aligned} \text{angle of refraction } \theta_2 &= \sin^{-1} \left(\frac{\sin 36.10^\circ}{1.33} \right) = 26.30^\circ \\ \cos \theta_2 &= 0.8965 \end{aligned}$$

$$K'_j = K_j / 0.8965$$

Hence,

From Table 8.1, the value of τ_r corresponding to an angle of incidence of 36.10° is 0.976. We will use a value of thermal conductivity of water corresponding to the approximate mean temperature in the whole pond. Assuming this temperature to be 50°C , we have $k = 0.648 \text{ W/m-K}$.

Now, annual average daily global radiation

$$\begin{aligned} \hat{H}_g &= 19600 \text{ kJ/m}^2\text{-day} \\ &= \frac{19600 \times 1000}{3600 \times 24} \\ &= 226.9 \text{ W/m}^2 \end{aligned}$$

Annual average heat extraction rate

$$\begin{aligned} \hat{q}_{load} &= 5 \times 10^9 \text{ kJ/year} \\ &= \frac{5 \times 10^9 \times 10^3}{365 \times 24 \times 3600} \text{ W} \\ &= 158549 \text{ W} \end{aligned}$$

Substituting into Eq. (8.9), we have

$$70 - 26.3 = \frac{0.976}{0.648} \times 226.9 \sum_{j=1}^4 \frac{0.8965 A_j}{K'_j} (1 - e^{-0.55 K'_j / 0.8965}) - \frac{0.95}{0.648} \times \frac{158549}{A_p}$$

Using the values of A_j and K'_j given in Eq. (8.4), we get

$$70 - 26.3 = 141.85 - \frac{232433}{A_p}$$

or

$$A_p = 2368 \text{ m}^2$$

$$\text{Annual collection efficiency} = \frac{158549}{226.9 \times 2368} \times 100 = 29.5\%$$

Kooi* has also analysed the solar pond as a steady state device and obtained solutions in terms of the annual average values which are time independent. For a steady state situation, Eq. (8.6) for the non-convective zone reduces to

$$k \frac{d^2 \hat{T}_{II}}{dx^2} = \frac{d}{dx} (\hat{H}_g \tau_r \tau_a) = \hat{H}_g \tau_r \frac{d \tau_a}{dx}$$

where the values of τ_r and τ_a are taken at the effective angle of incidence. Integrating twice, we get

$$\hat{T}_{II} = \hat{H}_g \tau_r \int_{l_1}^x \tau_a dx + c_1 x + c_2 \quad (8.10)$$

where c_1 and c_2 are constants of integration.

Substituting the conditions,

$$\text{at } x = l_1, \quad \hat{T}_{II} = \hat{T}_I \text{ (a constant)}$$

$$\text{at } x = l_2, \quad \hat{T}_{II} = \hat{T}_{III} \text{ (a constant)}$$

and solving for c_1 and c_2 , we obtain the following expressions for the temperature distribution and the temperature gradient distribution in the non-convective zone

$$k[\hat{T}_{II}(x) - \hat{T}_I] = \hat{H}_g \tau_r \int_{l_1}^x \tau_a dx + \frac{(x - l_1)}{(l_2 - l_1)} \left\{ k(\hat{T}_{III} - \hat{T}_I) - \hat{H}_g \tau_r \int_{l_1}^{l_2} \tau_a dx \right\} \quad (8.11)$$

$$k \frac{d \hat{T}_{II}}{dx} = \hat{H}_g \tau_r \tau_a + \left[\frac{k[\hat{T}_{III} - \hat{T}_I] - \hat{H}_g \tau_r \int_{l_1}^{l_2} \tau_a dx}{(l_2 - l_1)} \right] \quad (8.12)$$

The rate at which energy flows at the interface $x = l_2$ into the lower convective zone

$$= A_p \left[\hat{H}_g \tau_r (\tau_a)_{x=l_2} + \left\{ -k \left(\frac{d \hat{T}_{II}}{dx} \right)_{x=l_2} \right\} \right] \quad (8.14)$$

Substituting Eq. (8.13) with $x = l_2$ into Eq. (8.14) and recognizing

that for a steady state situation, the rate at which energy flows at the interface $x = l_2$ into the lower convective zone is equal to the annual average heat extraction rate from the pond, we have

$$\hat{q}_{\text{load}} = A_p \left[\left\{ \frac{\hat{H}_g \tau_r}{(l_2 - l_1)} \int_{l_1}^{l_2} \tau_a dx \right\} - \frac{k}{(l_2 - l_1)} [\hat{T}_{III} - \hat{T}_I] \right] \quad (8.15)$$

The annual average efficiency of the solar pond is obtained by dividing both sides of Eq. (8.15) by $\hat{H}_g A_p$. We get,

$$\hat{\eta} = \left\{ \frac{\tau_r}{(l_2 - l_1)} \int_{l_1}^{l_2} \tau_a dx \right\} - \frac{k}{(l_2 - l_1)} \left[\frac{\hat{T}_{III} - \hat{T}_I}{\hat{H}_g} \right] \quad (8.16)$$

It is useful to compare Eq. (8.16) with Eq. (4.67) which yields the efficiency of a flat-plate collector. We see that the expression $\left(\int_{l_1}^{l_2} \tau_a dx \right) / (l_2 - l_1)$ in Eq. (8.16) is equivalent to the transmissivity-absorptivity term $[F_R(\tau\alpha)_{\text{av}} A_p / A_c]$ in Eq. (4.67), while the expression $k(l_2 - l_1)$ in Eq. (8.16) is equivalent to the loss term $[F_R U_l A_p / A_c]$ in Eq. (4.67).

Using Rabl and Nielsen's equation (8.4) for τ_a and substituting K'_j for K_j , we get

$$\int_{l_1}^{l_2} \tau_a dx = \sum_{j=1}^4 \frac{A_j}{K'_j} (e^{-K'_j l_1} - e^{-K'_j l_2}) \quad (8.17)$$

Thus Eqs (8.15) and (8.16) become

$$\hat{q}_{\text{load}} = A_p \left[\left\{ \frac{\hat{H}_g \tau_r}{(l_2 - l_1)} \sum_{j=1}^4 \frac{A_j}{K'_j} (e^{-K'_j l_1} - e^{-K'_j l_2}) \right\} - \frac{k}{(l_2 - l_1)} [\hat{T}_{III} - \hat{T}_I] \right] \quad (8.18)$$

and

$$\hat{\eta} = \left\{ \frac{\tau_r}{(l_2 - l_1)} \sum_{j=1}^4 \frac{A_j}{K'_j} (e^{-K'_j l_1} - e^{-K'_j l_2}) \right\} - \frac{k}{(l_2 - l_1)} \left[\frac{\hat{T}_{III} - \hat{T}_I}{\hat{H}_g} \right] \quad (8.19)$$

Equation (8.18) is similar in structure to Eq. (8.9). Like Eq. (8.9), it can also be used for calculating the average performance of a solar pond or for estimating the area of a pond for a given requirement. It should be noted that Eq. (8.18) reduces to Eq. (8.9), if one neglects the thickness of the surface convective zone ($l_1 = 0$) and assumes that the temperature difference between the pond surface and the ambient is zero, i.e. $\hat{T}_I = \hat{T}_a$.

*C.F. Kooi, "The Steady State Salt Gradient Solar Pond", *Solar Energy*, 23, 37 (1973).

Example 8.3

Use Eq. (8.18) based on Kooi's analysis for calculating the area of a solar pond working under the same conditions as in Example 8.2. Take the depth of the surface convective zone to be 0.10 m and assume that the temperature of this zone is equal to the ambient air temperature.

Substituting into Eq. (8.18), we get

$$158549 = A_p \left[\left\{ \frac{226.9 \times 0.976}{(0.95 - 0.10)} \sum_{j=1}^4 \frac{0.8965 A_j}{K_j} \times (e^{-K_j \times 0.10/0.8965} - e^{-K_j \times 0.95/0.8965}) \right\} - \frac{0.648}{(0.95 - 0.10)} \times (70 - 26.3) \right]$$

Using the values of A_j and K_j given in Eq. (8.4), we get,

$$158549 = A_p [226.9 \times 0.412 - 0.76 \times 43.7]$$

Therefore

$$A_p = 2639 \text{ m}^2. \quad (8.20)$$

This value is slightly higher than the value of 2368 m^2 obtained by using the Rabl and Nielsen formula. It is likely to be a better estimate because the finite thickness of the surface convective zone has been considered.

From Eq. (8.20), it is seen that for the solar pond under consideration, the equivalent transmissivity-absorptivity term is only 0.412. Fortunately the value of the equivalent loss term is also low, viz. $0.76 \text{ W/m}^2\text{-K}$.

Analytical treatments like those due to Weinberger or Rabl and Nielsen require a number of simplifying assumptions, and are useful only for obtaining reasonably good estimates of pond performance. In order to obtain more correct answers, it becomes necessary to solve the basic equations numerically, using finite difference procedures. Numerical methods give greater freedom to incorporate appropriate initial and boundary conditions and permit a more realistic representation of climatic conditions as well as load variations.

Eliseev *et al.** obtained finite difference solutions for the temperature distribution in ponds varying in depth from 10 to 80 cm. The climatic data of Tashkent was used for the purpose. They neglected the presence of the surface convective zone and therefore used the following boundary condition at the surface instead of Eq. (8.7),

$$k \left(\frac{\partial T}{\partial x} \right)_{x=0} = \frac{1}{A_p} (q_c + q_e + q_r) \quad (8.21)$$

However, they considered the variation of properties like density and

specific heat with the concentration. Results were obtained for the increase in temperature in the bottom layer of the pond during the initial heating up with no heat extraction. It is seen from the results that the highest temperature attained in the bottom layer increases with the depth. It is predicted that a 20 cm deep pond would heat up to a temperature around 80°C in only 6 or 8 days, while an 80 cm deep pond would heat up to a temperature of 140°C in about 50 days. In reality the latter temperature would of course not occur because boiling would commence at a lower temperature. It is also seen that the diurnal fluctuation in temperature occurring because of the day-night cycle is about 6°C for the 80 cm deep pond, and that this amplitude decreases with increasing depth.

In a recent study, Hawlader and Brinkworth* have made performance predictions for a solar pond which might be located in England. They have solved the set of Eqs (8.6) to (8.8). While calculating the penetration of solar radiation in the pond, they have assumed that 40 per cent of the radiation corresponding to wavelengths above $0.9 \mu\text{m}$ is completely absorbed in the first 6 cm, while the remaining 60 per cent of shorter wavelengths is absorbed according to a single exponential decay term. The value of the extinction coefficient for this single term representation is found to vary from 0.32 m^{-1} to 1.0 m^{-1} when fitted to various data for fresh and salt water.

The initial temperature build-up in a 2.5 m deep pond ($l_1 = 0.1 \text{ m}$, $l_2 = 1.5 \text{ m}$) with no load is shown in Fig. 8.7 for two values of the extinction coefficient. It is seen that a maximum temperature of 63°C is reached with a reasonable value of $K = 1.0 \text{ m}^{-1}$. However, if it were possible to have a value of $K = 0.32 \text{ m}^{-1}$, the maximum temperature in the lower convective zone would approach 100°C .

The effect of varying only the thickness of the lower convective zone on the maximum temperature is shown in Fig. 8.8. As expected, it is seen that higher temperatures are attained in a shorter time with smaller thicknesses. A different trend is observed when the thickness of the non-convective zone is varied from 0.5 to 2.3 m. In this case, the maximum temperature obtained at first increases and then begins to decrease as less of the solar radiation reaches the bottom of the pond. Optimum values of l_2 seem to range from 1 to 1.5 m. Variations of temperature under various load conditions have also been studied. Overall, the investigation shows that useful temperatures can be obtained in a solar pond even in the unpromising climate of England where the mean annual global radiation is only about $10000 \text{ kJ/m}^2\text{-day}$.

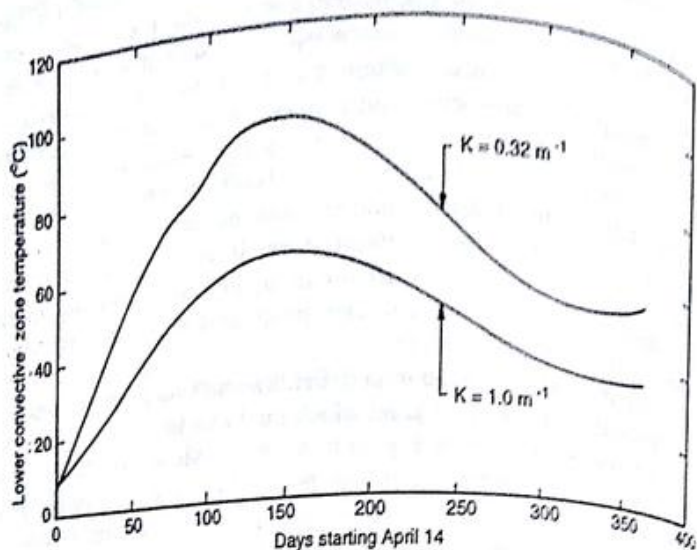
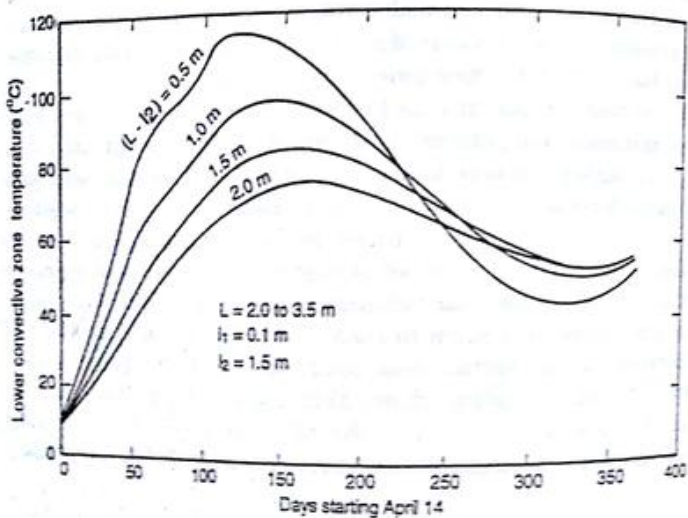


Fig. 8.7 Variation in Temperature of Lower Convective Zone with Extinction Coefficient. From Hawlader and Brinkworth. Used with Permission



6.4 EXPERIMENTAL STUDIES

We will now describe a number of experimental investigations on solar ponds in Israel, the USA and India.

Tabor and Matz* have given an account of the early pioneering investigations carried out from 1959 to 1964 on three solar ponds in Israel. The first pond at Sdom was 25×25 m and 1 m deep. The method of filling was to lay down a layer of concentrated brine about 5–10 cm thick, then to add a less concentrated layer on top and so on. By the time the filling was completed, the concentration steps had disappeared and a smooth linear concentration gradient was obtained. A peak temperature of 96°C was recorded in the pond. However, experiments had to be eventually discontinued because of decay of the walls.

A second pond with reinforced walls was constructed adjacent to the first pond. This pond was of the same size. It was also not ideal because of a porous bottom resulting in a loss or gain of water. Nevertheless, some useful measurements were made. The diffusivity of the mixture of MgCl_2 and KCl used in the pond was measured and found to be $2.5 \times 10^{-9} \text{ m}^2/\text{s}$ over the 30 – 60°C range.

The third pond at Atlit was 25×55 m and 1.50 m deep. It was constructed at ground level by building up the walls. Extensive instrumentation was incorporated in the design. This included thermocouples in the ground and walls to permit calculation of temperature gradients and hence heat flows; fixed sampling pipettes for withdrawing samples of solution at various depths; thermocouples at various depths of the solution; radiometers for measuring solar radiation at the surface and at various depths; evaporation pans for estimating evaporation rates; a wind velocity indicator and a meteorological station.

Pumps were installed to permit solutions to be added or withdrawn from the pond at different levels. Based on the experiences with the first pond, it had been expected that the pond would heat up to about 90°C at the bottom and that heat could be extracted by removing the lower layer. However, this could not be done because bubbles began to appear at a bottom temperature of 65°C . When the temperature reached 74°C , the effects of these bubbles became quite serious, because they disturbed the concentration gradient. Initially, it was believed that the bubbles were being formed due to anaerobic decomposition of organic material under the pond. However, subsequently, it was found that the gassing was due to dissolved air being released from nearby underground water.

Despite the fact that the pond could not be made fully operative, some information was obtained. Prior to the onset of bubbling, a temperature rise of 1.8°C per day was obtained. From this, it was calculated that about 12.5 per cent of the solar radiation was being collected at a bottom temperature of 70°C even though the pond was not clear.

The work in Israel was restarted in 1974 and two demonstration units were constructed. Details are not available, but it is known that a 1500 m^2 pond built in Yavne was used for operating a 6 kW turbo-generator, while a 7000 m^2 pond built at Ein Bokek provided 150 kW of peak power. Operating temperatures in both the units were around 90°C .

Nielsen* has supervised the construction and operation of a solar pond in Ohio, USA and has given details about its working. The pond was 2.5 m in depth and had an estimated effective area of 200 m^2 . It was planned as a prototype pond for space heating and was constructed at a minimum cost of \$ 7500 compatible with reliability. The pond was calculated to provide about $1.8 \times 10^8\text{ kJ}$ of thermal energy per year while operating between a maximum temperature of 90°C in autumn and a minimum temperature of 35°C in winter. The heat energy cost was estimated to be \$ 0.015 per kWh thermal. This value is much lower than what would be obtained in a conventional flat-plate collector and storage system.

Zangrando† has described the working of a solar pond at the University of New Mexico. The pond had the following dimensions: top diameter, 15 m ; depth, 2.5 m ; bank angle, 34° with horizontal; and surface area, 175 m^2 . Since the walls were sloping, all the radiation falling on the surface did not reach the bottom. The average collecting area was, therefore, less than the surface area and was estimated to be 105 m^2 . Sodium chloride was used as the salt. During operation, the concentration gradient zone extended for about 1 m , while the lower convective zone was about 1.4 m deep. The convective layer at the surface was much smaller, being only a few centimetres in thickness.

Extensive measurements of temperature, insolation, heat extraction and density distribution were made and analysed. The pond was first filled in November 1975 with water at 20°C . Figure 8.9 shows several temperature profiles taken between January 1976 and August 1977. The temperature of 93°C attained on August 8, 1977 represents the

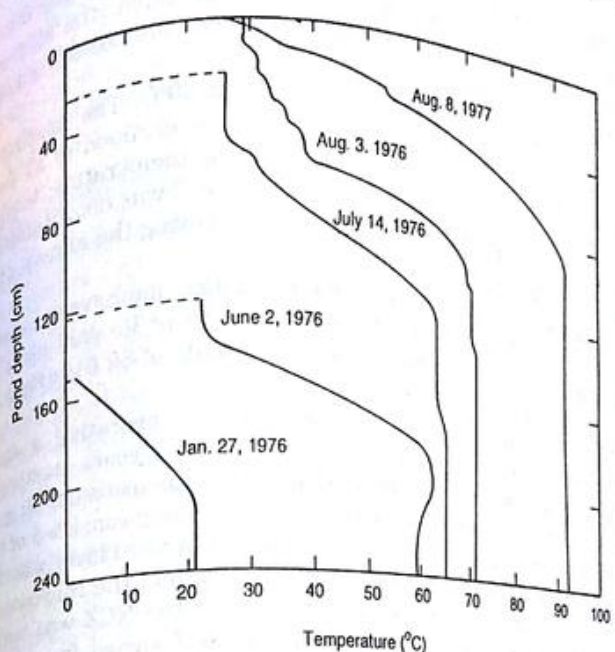


Fig. 8.9 Temperature Profiles in a Solar Pond. From Zangrando

highest value attained in 1977. This value was obtained with no heat extraction.

Heat extraction began on November 4, 1977 and continued through 1978. The pond supplied the full heating and hot water load of a 185 m^2 house from 1977 to 1979. This load was approximately 10^8 kJ per year. Measurements also indicated that the annual collection efficiency of the pond was about 9 per cent.

Patel and Gupta* constructed and operated a small solar pond in Pondicherry in 1980. The pond had a diameter of 11.5 metres and a depth of 2 m , thus giving an effective area of 100 m^2 . The floor of the pond was reinforced concrete, while the wall was brick. In order to ensure a water-tight surface, both the floor and the wall were plastered with a water-proofing compound mixed into the mortar. The pond floor was also blackened by adding black cement colour to the mortar during plastering and the side wall was painted white with a cement paint.

All these steps were undertaken with the intention of avoiding the use of a liner. However, after a few months of operation, the side walls developed cracks in a number of places and it became necessary to use a liner of high-density black polyethylene.

The pond was initially filled with water at 30°C. The heating-up was quite rapid and a temperature of 70°C was attained in 87 days. Because of the leakage which began when the temperature touched 70°C, the maximum expected temperature of 80°C was not attained in the summer of 1980. The lowest temperature during the annual cycle was 50°C in December.

The authors have made an economic evaluation and have calculated that the cost of heat delivered by the pond is about Re 0.20 per kWh (thermal). This is a little more than the estimate of \$0.015 (Re 0.14) made by Nielsen five years earlier.

Srinivasan* has discussed his experience of operating a small 240 m² solar pond in Bangalore over a period of 5 years starting in 1984. The pond was rectangular in shape with dimensions of 30 m by 8 m at the bottom, and a side slope of 45°. The lining consisted of two layers of 0.3 mm thick low density polyethylene. A third layer was also used on the side walls. During the experimentation, the thickness of the LCZ was limited to 0.4 m, the thickness of the NCZ was varied from 0.2 to 1.0 m, and the thickness of the SCZ varied from 0.3 to 0.6 m. Through the five year period, the temperatures attained in the storage zone ranged from a minimum of 50°C to a maximum of 75°C. Based on his studies, Srinivasan obtained a number of useful results. From the point of view of heat extraction, he showed that it was best to use an immersed copper heat exchanger in preference to an external heat exchanger. For maintaining the salt concentration gradient, a simple passive method was found to be adequate for a small pond, a polyvinyl chloride pipe (25 cm in dia and 4 m long) was suspended vertically at the centre of the pond. The bottom of the pipe was 10 cm from the bottom of the pond. 8 holes (5 cm diameter) were drilled around the circumference about 30 cm from the bottom. About 100 kg of salt was dumped into the tube daily. This salt dissolved within a day and measurements showed that it helped to maintain the required salt concentration gradient without causing any local problems.

Srinivasan also developed a simple two-zone model for predicting the seasonal temperature variations in the pond. The predictions of the model agreed well with the measurements made and showed that in small ponds, maximum temperatures in excess of about 70°C would

not be attained because of high side wall heat losses. Srinivasan also showed that a circular shape was preferable in comparison to a rectangular shape. He argued that notwithstanding the lower temperatures attained in small ponds, they had an important role to play in meeting the process heat needs of a number of small industries.

8.5 OPERATIONAL PROBLEMS

Some important problems associated with the operation and maintenance of solar ponds are now considered. We will describe methods adopted for obtaining the salt concentration gradient in a pond and consider the effect of diffusion on the salt concentration profile. The effect of the flow occurring in the upper and lower convective zones will be described. We will also describe the effect of wind-induced waves and rain, biological growth, fouling due to dirt and leaves falling in the water, and the effect of bottom reflectivity on the performance of a solar pond. Measures taken to counteract these problems will also be mentioned.

Establishing the Salt Concentration Gradient

In order to obtain the salt concentration gradient initially in a pond, the practice followed is to fill up the pond successively with layers of salt solution, one on top of the other. Each layer is 10 to 20 cm thick and has a concentration lower than its predecessor. Although this method is probably adequate for establishing the gradient in a small pond, it is time consuming and expensive for a large pond, and requires the provision of an external mixing tank. Zangrand* has described a simpler method which was first tried out at the University of New Mexico pond and subsequently applied successfully to establish the gradient at the 2000 m² solar pond at Miamisburg. The procedure consists of filling the pond partially with water (having a salt concentration equal to that desired in the LCZ), to a depth approximately equal to that of the LCZ plus half the NCZ. Fresh water is then pumped through a horizontal diffuser which is immersed in the upper portion of the existing solution. The diffuser is gradually raised as the water surface level rises in such a way that it reaches the surface at the predetermined final level of the pond. The upward motion of the diffuser may be continuous or in small discrete steps of a few cm.

Effect of Diffusion on Concentration Profile

As stated earlier, one of the methods used for producing a nearly linear

concentration gradient in a solar pond is to fill the pond with several layers of salt solutions, each successive layer having a decreasing concentration. Thus, immediately after filling, a step-like concentration profile is obtained. Because of diffusion of salt, this step-like profile is gradually converted into a linear profile. An obvious question which arises is the time required for the profile to acquire a nearly linear shape. A second question which arises is the time required for the profile to become uniform, if diffusion continues and no effort is made to control the values of the concentration at the upper and lower edges of the non-convective zone. Clearly one would like the first time to be small and the second to be as large as possible. Chepurniy and Savage have obtained a solution for the concentration profile by solving the one-dimensional unsteady state diffusion equation

$$\frac{\partial C}{\partial t} = D \frac{\partial^2 C}{\partial x^2} \quad (8.22)$$

in which D = diffusivity of salt in water.

Equation (8.22) is solved subject to the boundary conditions $(\partial C / \partial x) = 0$ both at $x = 0$ and $x = L$, i.e. there is no transfer of mass across the top and bottom surfaces of the non-convective zone. The initial condition assumed is a step-like concentration profile with M steps, $C = C_1$ at $x = 0$ and $C = C_2$ at $x = L$. The following solution is obtained

$$\frac{C - C_1}{C_2 - C_1} = \frac{1}{2} + \frac{2}{\pi(M-1)} \sum_{m=1}^{\infty} \frac{\cot \left[\frac{(2m-1)\pi}{2M} \right]}{(2m-1)} \cos \left[\frac{(2m-1)\pi x}{L} \right] \times \exp \left[-(2m-1)^2 \pi^2 D t / L^2 \right] \quad (8.23)$$

Results showing the development of concentration profiles with time have been plotted for various values of M . A typical plot obtained for $M = 10$ is shown in Fig. 8.10. Profiles are shown only for the upper half of the pond since there is symmetry about $x = L/2$. In all cases, it is seen that the step-like profile disappears with the passage of time and a nearly linear profile is obtained over the whole depth of the non-convective zone excepting the regions near the top and bottom. For the case of $M = 10$, a smooth linear profile is obtained for $(Dt/L^2) = 0.01$. Substituting typical values of $1.5 \times 10^{-9} \text{ m}^2/\text{s}$ and 1 m for D and L respectively, we get $t = 77$ days. This value is on the higher side and indicates the need for a larger value of M . With $M = 20$, one obtains $(Dt/L^2) = 0.001$ and $t = 8$ days, which is quite satisfactory.

*N. Chepurniy and S.B. Savage, "Effect of Diffusion on Concentration Profiles in a Solar Pond", *Solar Energy*, 17, 203 (1975).

[†]The value substituted is the diffusivity of sodium chloride in water at 25°C.

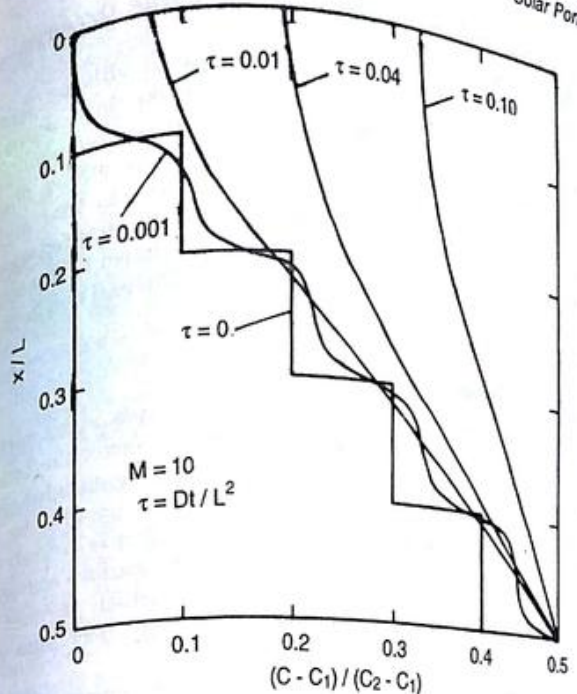


Fig. 8.10 Development of Salt Concentration Profile in a Solar Pond. From Chepurniy and Savage. Used with Permission

A measure of the time required for the profile to become uniform is obtained by finding out the time for the concentration $(C - C_1)/(C_2 - C_1)$ at the top to reach half the value at the mid-level ($x = L/2$). Referring again to Fig. 8.10, we see that the corresponding value of (Dt/L^2) is around 0.05, which gives $t = 406$ days. This time is sufficiently large. One therefore arrives at the important conclusion that it is not necessary to control the concentration values at the top and bottom continuously from day-to-day. Measures like passing fresh water across the top and removing saline water, or injecting salt at the bottom need to be carried out only at intervals of a few days in order to maintain the concentration gradient.

Surface Layer Flow and Lower Layer Flow

In Sec. 8.2, it has been stated that in order to maintain a zero or close to zero concentration at the top, fresh water is flushed across the top while slightly saline water formed by upward diffusion of salt is run off. Similarly in order to maintain the required concentration at the bottom and to extract the stored heat, hot water is pumped out from the bottom and returned with salt added to it after heat is removed in

an external heat exchanger. In both these situations, the direction of flow is horizontal and the velocities are small. Experimental investigations have been conducted with the object of ascertaining if it is possible to cause these layer-like flows across the surface and the bottom of the pond without disturbing the stability of the non-convective zone in between. Experiments on surface flow, in the presence of a concentration gradient, have shown that surface washing is indeed possible up to distances of several hundred metres. Similarly, experiments on lower layer flows have shown that a steady horizontal flow at the bottom of the pond is possible and can be made to extend to any length.

Wind-induced Waves

The winds blowing over a solar pond generate waves at its surface. These cause mixing because of which a surface convective zone is created. Thus, the presence of this zone cannot be avoided. It is desirable however to keep its thickness as small as possible for two reasons. Firstly, solar radiation absorbed in this zone is entirely lost to the surrounding air and secondly, the thicker the surface convective zone, the smaller will be the non-convective zone which provides the insulating effect. Hence, the efficiency of the pond decreases with increasing thickness of the surface convective zone.

In practice, keeping in mind the usual depths of solar ponds which range from 1 to 2 m, it is found to be desirable to restrict the surface convective zone to a thickness of 10 to 20 cm. Experiments show that waves having amplitudes of 2 cm can cause mixing up to a depth of 20 cm. Hence, efforts are generally made to see that the wave amplitudes do not exceed this value. The usual technique adopted is to float wind-wave breakers on the surface of the pond. Small diameter plastic pipes spaced a few metres apart and making a square grid have been used. The spacing depends upon the location of the solar pond and ranges between 5 and 10 m.

Effect of Rain

The effect of rain falling on a solar pond depends upon the nature of the rain. Light rain helps to maintain the salt concentration at the pond surface at a very low level and removes the need for flushing with fresh water across the top. On the other hand, heavy rain has a penetrating effect and causes an increase in the thickness of the SCZ. It has therefore been suggested that the SCZ be maintained at a higher thickness of 40 to 50 cm during the rainy season.

Biological Growth

Growth of algae is observed in most solar ponds because the water is

essentially stagnant or moves with a slow velocity. The growth gives the water a greenish colour and severely decreases the transmissivity. Prevention of the growth is therefore essential. The usual practice is to subject the water to some form of chemical treatment. Chlorination of the water and the addition of small amounts of copper sulphate have been found to be very effective in this respect.

Fouling Due to Dirt and Leaves

The transmissivity of the water is also decreased by the presence of unsettled dirt or leaves which are blown into the pond from the surroundings. With the passage of time, such materials usually settle to the bottom where the effect on performance is negligible. However, it is desirable to remove such debris by skimming it off from the surface before it begins to settle.

Effect of Bottom Reflectivity

The effect of the reflectivity of the bottom of a solar pond on the performance of the pond has been studied by Srinivasan and Guha*. They find that an increase in the bottom reflectivity (on account of accumulation of dirt or excess undissolved salt) can lead to a deterioration in pond performance. In the case of dirt, the increase in reflectivity is not very high. As a result, the performance of the pond is not affected significantly. However in the case of undissolved salt, the increase in reflectivity is quite high leading to a substantial deterioration in the performance of the pond.

8.6 OTHER SOLAR POND CONCEPTS

As stated earlier, a number of other concepts have also been suggested for building solar ponds. Some of these will now be described.

The Solar Gel Pond

The concept of any solar pond hinges on the presence of a non-convective zone to trap the solar energy collected in the lower convective zone. In a solar gel pond, a thick layer of a polymer gel floats on the lower convective zone and acts as the non-convective zone. The gel has good optical and thermal insulating properties. Wilkins† has demonstrated

*J. Srinivasan and A. Guha, "The Effect of Bottom Reflectivity on the Performance of a Solar Pond", *Solar Energy*, 39, 361 (1987).

†E. Wilkins, "Operation of a Commercial Solar Gel Pond", *Solar Energy*, 46, 3 (1991).

the feasibility of the concept by constructing a gel pond on a commercial scale in Albuquerque, New Mexico. The pond constructed had a surface area of 400 m^2 and was 5 m deep. The lower convective (storage) zone was made up of 2 to 7 per cent salt solution and was 3.5 m deep. The small salt concentration was necessary in order that the gel would float on top. The composition of the gel was 98.3 per cent water and 1.7 per cent polyacrylamid. It was kept in thin transparent plastic bags made from Tedlar and floated on the salt solution. The thickness of the gel layer was 0.6 m. The pond was designed to supply a minimum of 1 GJ of energy per day at a temperature of 70°C . However, the temperature actually obtained was 60°C .

In comparison with a salt-gradient solar pond, the advantages of a gel pond are as follows:

- (1) Evaporation losses from the surface are eliminated, while heat losses are smaller in magnitude.
- (2) Since salt water is used only to float the gel, a salt concentration gradient is not required to be maintained. Thus maintenance requirements are reduced.
- (3) The environmental hazards associated with handling salt are eliminated.

The main disadvantage with constructing a gel pond is the high cost of the chemicals required for making the gel.

The Honeycomb Solar Pond

The concept of a honeycomb solar pond is similar to that of the honeycomb collector described earlier in Sec. 4.13.2. In the case of a pond, an air-filled plastic honeycomb structure is floated on top of the water in the lower convective zone. No salt is required. The honeycomb is designed to have good transmission characteristics for incoming solar radiation, along with good insulating properties to reduce heat losses. Schaefer and Lowrey* have recommended an optimized honeycomb 6–9 cm thick having 1.25–1.5 cm diameter cells. Once again, like the gel pond, the main disadvantage is the cost of the honeycomb panels.

The Equilibrium Solar Pond†

The equilibrium solar pond is a special type of salt-gradient pond. It uses salts whose solubility in water increases strongly with tempera-

*R. Schaefer and P. Lowrey, "The Optimum Design of Honeycomb Solar Ponds and a Comparison with Salt Gradient Ponds", *Solar Energy*, 48, 69 (1992).

†Z. Harel, J. Tanny and A. Tsinober, "The Equilibrium Solar Pond: A Laboratory Model for the Gradient Layer", *J. of Solar Energy Engg.*, *Trans. ASME*, 115, 32 (1993).

ture. In such salt solutions, thermal diffusion of salt occurs from lower to higher temperature zones in the fluid. This is called the negative Soret effect. In the solar pond, the direction of this movement is downward and opposite to that of the mass diffusion occurring in the pond, the two mass fluxes are made to balance each other so that the net salt flux is zero. Thus the need for having regular operational procedures for maintaining the salt concentration gradient (as in a salt-gradient pond) is eliminated. Harel *et al.* have proved the concept of an equilibrium solar pond by conducting some experiments with potassium nitrate solution.

PROBLEMS

1. Sodium chloride is used as the salt in a solar pond. Estimate the minimum concentration (kg of salt per kg of water) required at the bottom if the concentration at the top is 0.02 and a temperature difference of 65°C is to be maintained. Assume that the concentration and temperature profiles are straight lines and take the average values of $(\partial p/\partial T)$ and $(\partial p/\partial C)$ to be $-0.5 \text{ kg/m}^3\text{ }^\circ\text{C}$ and 650 kg/m^3 respectively.
2. A solar pond, 2.5 m deep, is proposed to be built in Bhavanagar ($21^\circ 45' \text{ N}$, $72^\circ 11' \text{ E}$). Calculate the solar flux which would be received at the bottom of the pond on March 15 for which the following radiation data is available:

Time (h LAT)	0730	0930	1130	1330	1530	1730
$I_g (\text{kW/m}^2)$	0.308	0.721	0.921	0.840	0.496	0.070
$I_d (\text{kW/m}^2)$	0.111	0.157	0.183	0.165	0.140	0.040
3. Consider the radiation falling at 1200 h (LAT) on a solar pond 2.2 m deep located in New Delhi ($28^\circ 35' \text{ N}$, $77^\circ 12' \text{ E}$). Calculate (i) the percentage radiation reflected at the surface, (ii) the percentage radiation absorbed in the first 10 cm, and (iii) the percentage radiation reaching the bottom. Do the calculations for the following dates: January 15, May 15 and September 15, and use the monthly mean values of global and diffuse radiation given in Appendix III.
4. A solar pond located in New Delhi ($28^\circ 35' \text{ N}$, $77^\circ 12' \text{ E}$) is to be used for supplying the heat energy input for a low temperature Rankine cycle power unit using R-11 as the working fluid. The unit develops an output of 20 kW, has an energy conversion efficiency of 9.0 per cent, and requires its energy input at an annual mean temperature of 85°C . Use the Rabl and Nielsen analysis to calculate the pond area for values of the depth l_2 varying from 1 to 3 m. Show that the area is a minimum for a particular value of l_2 . The following data is given for New Delhi:

Annual average daily global radiation = $19690 \text{ kJ/m}^2\text{-day}$
 Annual average ambient temperature = 25.1°C .
5. Use the data of problem 4 and the analysis due to Kooi, to calculate the area of a solar pond for a situation in which $l_1 = 0.25 \text{ m}$, $l_2 = 1.75 \text{ m}$ and $L = 2.50 \text{ m}$. Assume that the temperature in the SCZ is equal to the ambient air temperature. Calculate also the quantities equivalent to the transmissivity-absorptivity term and the loss term for this pond.

In order to reduce the initial cost, a number of promotional incentives have been offered. Solar devices and systems are exempted from excise duty by the Central Government. In addition, most state governments have exempted them from sales tax. Financial subsidies are also available for purchasing some solar energy systems.

Annual Cost

The annual cost of a solar system installed by an individual or an organisation is the sum of a number of factors. These include the cost of the fuel consumed by the auxiliary energy source, repayment on the loan taken to install the system, maintenance of the system, electrical energy consumed by subsidiary equipment like pumps and blowers, local taxes, etc. Certain types of tax deductions are also available as incentives for installing the system. The tax deductions are of benefit in a particular year only if the individual or the organization has to pay taxes in that year. They are of various kinds. For example, they may be related to the interest payable on the loan taken or to the annual depreciation permitted on the system. In order to encourage the use of solar systems, loans at lower interest rates are offered by financial institutions. Further, the Central Government permits depreciation at a higher rate. Thus, the annual cost of a solar system may be stated as follows:

$$\begin{aligned} \text{Annual cost} = & \text{Fuel expense} + \text{Repayment on loan} \\ & + \text{Maintenance charges} + \text{Electrical energy bill} \\ & + \text{Local taxes} - \text{Tax deductions} \end{aligned} \quad (9.2)$$

Usually fuel expense, repayment on loan and tax deductions are the major items. Eq. (9.2) has been stated by keeping a solar thermal energy system in mind. However, it is a general equation applicable to any system using a conventional or a non-conventional energy source.

Economic Analysis



The value of a solar thermal application must ultimately be judged on the basis of its economy. In this chapter, we define some economic quantities and describe some of the methods used for making economic evaluations. As is evident by now, solar thermal devices and systems are characterised by high initial costs. However they bring long term benefits in the form of lower annual operating costs. An economic evaluation of a solar system has to consider both these aspects.

9.1 INITIAL AND ANNUAL COSTS

Initial Cost

The initial cost of a solar thermal system is the cost of buying the equipment and installing it. Solar collectors contribute significantly to the initial cost. Thus from the point of view of optimization, it is useful to recognize that the initial cost (C) is the sum of two components, one component being proportional to the total collector area and the other being independent of the collector area. We have,

$$\begin{aligned} C &= C_c + C_o \\ &= kA_c + C_o \end{aligned} \quad (9.1)$$

where C_c = component of cost proportional to collector area (Rs),
 C_o = component independent of collector area (Rs),
 k = proportionality constant (Rs/m²),
 A_c = collector area (m²).

9.2 DEFINITIONS

Consider a solar thermal energy system installed for an application like water heating, space heating, etc. In order to evaluate the economic viability of the system, we are interested in calculating the savings which will accrue annually and on a long term basis as a result of installing the solar system. An examination of the terms on the right hand side of Eq. (9.2) shows that on an annual basis, the solar system would help in saving conventional energy in the form of fuel or electricity. Tax deductions would also be permissible on the solar system. On the other hand, annual payments would be due for repaying the loan taken for installing the system, for maintenance, for paying

small electrical energy bills for running equipments like pumps, blowers, etc., and for local taxes. Thus we define:

$$\text{Annual solar savings* (ASS)} = \text{Fuel savings} - \text{Payment on loan} - \text{Maintenance charges} - \text{Electrical energy bill} - \text{Local taxes} + \text{Tax deductions} \quad (9.3)$$

Cumulative solar savings (CSS) over a certain number of years (n_t) is the sum of the annual solar savings over the period minus the initial down payment made at the time of installation of the solar system.

Life cycle savings (LCS) is the cumulative solar savings calculated over the life time (n_t) of a system plus the resale value of the system at the end of its life time. Thus,

$$\text{CSS} = \sum_{j=1}^{n_t} (\text{ASS})_j - (\text{Initial down payment}) \quad (9.4)$$

$$\text{LCS} = (\text{CSS})_{n_t} + (\text{Resale value})$$

$$= \sum_{j=1}^{n_t} (\text{ASS})_j - (\text{Initial down payment}) + (\text{Resale value}) \quad (9.5)$$

Since the value of money keeps changing with time, the usual practice is to obtain the sum of the annual solar savings in Eqs (9.4) and (9.5) in terms of money value at the present instant of time. This practice is referred to as discounting. The present worth of money required sometime in the future is obtained by calculating how much would have to be invested at the market interest (discount) rate today in order that the required money would be available when required in the future.

The term 'net present worth' or 'net present value' (NPV) is also used very often in place of cumulative solar savings or life cycle savings.

It is obvious that if a solar system is to be economically beneficial, the value of CSS over a reasonable period of time or the value of LCS must be positive. It is also obvious that in a given situation these values will decrease as the market discount rate increases. The discount rate for which the value of CSS or LCS is zero is called the rate of *return on investment* (ROI).

Another term which is used frequently for judging the economic

*Annual solar savings may be thought of as the difference between the annual cost of an imaginary conventional energy system performing the same function as the solar energy system and the annual cost of the given solar energy system.

ability of a solar system is the *payback period*. Unfortunately it is defined in a number of ways and this creates confusion. The most common definition is as follows:

Payback period is the time needed for the cumulative fuel savings to become equal to the total initial investment on the system. Two other definitions which are also used occasionally for payback period are the time needed for the cumulative solar savings to become zero and the time needed for the annual solar savings to become positive.

Because of the large number of definitions, it is necessary to ascertain which definition has been used when a value of payback period is quoted in a given situation. It is also necessary to know whether the value has been determined by using actual savings from year to year or by using the discounted value of money.

9.3 PRESENT WORTH CALCULATION

The present worth of a rupee needed n years from today is given by $\frac{1}{(1+d)^n}$ where d = interest (discount) rate. Assume that payments A_1, A_2, \dots, A_n are due after 1, 2, ..., n years. The present worth of these payments is $A_1/(1+d), A_2/(1+d)^2, \dots, A_n/(1+d)^n$ respectively. The sum (S) of these present worths is given by

$$S = \sum_{j=1}^n A_j/(1+d)^j \quad (9.6)$$

Frequently the payments A_1, A_2 , etc. are related and increase at a constant rate i . Thus $A_2 = A_1(1+i), A_3 = A_1(1+i)^2$, etc. Eq. (9.6) then becomes

$$S = A_1 \sum_{j=1}^n (1+i)^{j-1}/(1+d)^j \\ = \frac{A_1}{(d-i)} \left[1 - \left(\frac{1+i}{1+d} \right)^n \right], \quad \text{if } i \neq d. \\ = [A_1 n / (1+i)], \quad \text{if } i = d. \quad (9.7)$$

9.4 REPAYMENT OF LOAN IN EQUAL ANNUAL INSTALMENTS

We now derive an expression for the annual instalment due in repayment of a loan. Assume that the initial investment required for a given situation is C and that a fraction f_i of this amount is taken as a loan. Assume further that the lending institution charges an interest

rate d_l and that the agreement made is that the loan is to be paid back in equal annual instalments of A over a period of n_l years. By taking the present worth of each of the annual repayments, it follows that

$$f_l C = \sum_{j=1}^{n_l} A / (1 + d_l)^j$$

$$= \frac{A}{d_l} [1 - \{1 / (1 + d_l)^{n_l}\}]$$

Therefore

$$A = \frac{d_l f_l C}{[1 - \{1 / (1 + d_l)^{n_l}\}]} \quad (9.8)$$

Every annual repayment consists of two components—a part repayment on the loan and a payment of interest on the outstanding loan. The first component increases from year to year, while the second component decreases. Since tax deductions are generally permissible on the interest component, it is useful to put down an expression for the interest component. It can be shown that after j years, the interest component

$$= \left[1 - \frac{(1 + d_l)^{j-1} - 1}{(1 + d_l)^{n_l} - 1} \right] d_l f_l C \quad (9.9)$$

9.5 ANNUAL SOLAR SAVINGS

Statement of the Problem

Consider a solar energy system.

(i) Assume that the system requires a total investment C of which a fraction f_l is taken as a loan. As in Sec. 9.4, assume that the interest rate on the loan is d_l and that it is to be paid back in equal annual instalments over a period of n_l years.

(ii) Let the annual energy load to be met be E and assume that the solar system supplies a fraction F of this load. This would result in an annual savings of FE units of conventional energy. Assume that the cost of this energy is c_f per unit of energy and that it increases at the rate of i_f every year.

(iii) The solar system will normally require some annual expenditure by way of maintenance, electrical energy for running subsidiary equipments and local taxes. We assume that the extra cost associated with these minor items of expenditure is M in the first year of operation and that it increases at the rate of i_m every year. The rates i_m and i_f are related to inflation.

(iv) Finally we assume that tax deductions are allowed both on the interest component of the annual loan repayment instalment as well

as on depreciation of the system. The depreciation is assumed to be at a uniform rate r_d per year. The income tax rate is r_t . Derive an expression for the annual solar savings. Expressions for each of the quantities occurring on the right hand side of Eq. (9.3) are first noted down. In any year j ,

$$\text{Fuel savings} = c_f (1 + i_f)^{j-1} FE$$

From Eq. (9.8),

$$\text{Annual repayment on loan} = \frac{d_l f_l C}{[1 - \{1 / (1 + d_l)^{n_l}\}]} \quad \begin{cases} \text{if } j \leq n_l \\ = 0 \quad \text{if } j > n_l \end{cases}$$

$$\left. \begin{array}{l} \text{Maintenance charges} \\ + \text{Electrical energy bill for} \\ \text{subsidiary equipment} \\ + \text{Local taxes} \end{array} \right\} = (1 + i_m)^{j-1} M$$

From Eq. (9.9),

$$\left. \begin{array}{l} \text{Tax deduction on the interest} \\ \text{component of loan repayment} \end{array} \right\} = \left[1 - \frac{(1 + d_l)^{j-1} - 1}{(1 + d_l)^{n_l} - 1} \right] r_d d_l f_l C \quad \begin{cases} \text{if } j \leq n_l \\ = 0 \quad \text{if } j > n_l \end{cases}$$

$$\text{Tax deduction on depreciation} = r_t r_d C \quad \begin{cases} \text{if } j \leq (1/r_d) \\ = 0 \quad \text{if } j > (1/r_d) \end{cases}$$

Thus annual solar savings in the year j

$$= c_f (1 + i_f)^{j-1} FE - \frac{d_l f_l C}{[1 - \{1 / (1 + d_l)^{n_l}\}]} - (1 + i_m)^{j-1} M$$

$$+ \left[1 - \frac{(1 + d_l)^{j-1} - 1}{(1 + d_l)^{n_l} - 1} \right] r_d d_l f_l C + r_d r_t C \quad (9.10)$$

Eq. (9.10) is valid for $j \leq n_l$ and $j \leq (1/r_d)$.

If $j > n_l$, the second and fourth terms on the right hand side of Eq. (9.10) are zero, while if $j > (1/r_d)$, the fifth term is zero.

The present worth of the annual solar savings is obtained by dividing the right hand side by $(1 + d)^j$, where d is the discount rate.

9.6 CUMULATIVE SOLAR SAVINGS AND LIFE CYCLE SAVINGS

The cumulative solar savings over a period of n years for the system data given in Sec. 9.5 is obtained by summing the present worth of the annual solar savings and considering the initial down payment. Thus

$$\begin{aligned}
 \text{CSS} = & -(1-f_l)C + c_f FE \sum_{j=1}^n \frac{(1+i_f)^{j-1}}{(1+d)^j} - \frac{d_l f_l C}{[1 - \{1/(1+d_l)^{n_l}\}]} \sum_{j=1}^{n_l} \frac{1}{(1+d)^j} \\
 & - M \sum_{j=1}^n \frac{(1+i_m)^{j-1}}{(1+d)^j} \\
 & + r_t d_l f_l C \sum_{j=1}^{n_l} \frac{1}{(1+d)^j} \left[1 - \frac{(1+d_l)^{j-1} - 1}{(1+d_l)^{n_l} - 1} \right] \\
 & + r_t r_d C \sum_{j=1}^{1/r_d} \frac{1}{(1+d)^j}
 \end{aligned} \tag{9.11}$$

On summing the progressions, we get

$$\begin{aligned}
 \text{CSS} = & -(1-f_l)C + \frac{c_f FE}{(d-i_f)} \left[1 - \left(\frac{1+i_f}{1+d} \right)^n \right] \\
 & - \frac{d_l f_l C}{[1 - \{1/(1+d_l)^{n_l}\}]} \frac{1}{d} \left[1 - \frac{1}{(1+d)^{n_l}} \right] \\
 & - \frac{M}{(d-i_m)} \left[1 - \left(\frac{1+i_m}{1+d} \right)^n \right] \\
 & + r_t d_l f_l C \left[\frac{(1+d_l)^{n_l}}{(1+d)^{n_l}} \frac{1}{d} \left(\frac{(1+d)^{n_l} - 1}{(1+d_l)^{n_l} - 1} \right) \right. \\
 & \left. - \frac{1}{((1+d_l)^{n_l} - 1)} \frac{1}{(d-d_l)} \left\{ 1 - \left(\frac{1+d_l}{1+d} \right)^{n_l} \right\} \right] \\
 & + \frac{r_t r_d C}{d} \left[1 - \frac{1}{(1+d)^{1/r_d}} \right]
 \end{aligned} \tag{9.12}$$

Eqs (9.11) and (9.12) are valid for $n \geq n_l$, $n \geq (1/r_d)$, $d \neq i_f$, $d \neq i_m$ and $d \neq d_l$. If $n < n_l$, the summations for loan repayment (third term) and for tax deduction on interest component of loan repayment (fifth term) will be from $j = 1$ to $j = n$. The third term then becomes

$$\frac{d_l f_l C}{[1 - \{1/(1+d_l)^{n_l}\}]} \frac{1}{d} \left[1 - \frac{1}{(1+d)^n} \right]$$

and the fifth term becomes

$$\begin{aligned}
 & r_t d_l f_l C \left[\frac{(1+d_l)^{n_l}}{(1+d)^n} \frac{1}{d} \left(\frac{(1+d)^n - 1}{(1+d_l)^{n_l} - 1} \right) \right. \\
 & \left. - \frac{1}{((1+d_l)^{n_l} - 1)} \frac{1}{(d-d_l)} \left\{ 1 - \left(\frac{1+d_l}{1+d} \right)^n \right\} \right]
 \end{aligned}$$

Similarly if $n < (1/r_d)$, the summation for tax deduction on depreciation will be from $j = 1$ to $j = n$, and the sixth term on the right hand side in Eqs (9.11) and (9.12) becomes

$$\frac{r_t r_d C}{d} \left[1 - \frac{1}{(1+d)^n} \right]$$

Finally it should be noted that situations corresponding to $d = i_f$, $d = i_m$ or $d = d_l$ are special cases, for which summations can be readily done and the second, fourth and fifth terms in Eq. (9.12) suitably modified (Chapter 9, Problem 1).

Example 9.1

A solar hot water system having an array of flat-plate collectors with an area of 30 m^2 is installed in a factory. It costs Rs 150 000 and is set up with an initial down payment of 20 per cent of the investment, the balance 80 per cent being taken as a loan to be repaid in equal annual instalments over a 10 year period at an interest rate of 16 per cent. The cost of conventional fuel saved in the first year is Rs 21 000 and this cost increases at the rate of 4 per cent every year.

The annual expenditure required by way of maintenance, electrical energy for running subsidiary equipments, local taxes, insurance, etc. is Rs 6600 in the first year, and this expense increases at the rate of 5 per cent every year.

Tax deductions are permissible only on depreciation, which is allowed at the rate of 25 per cent each year, and the company income tax rate is 55 per cent.

Assuming that the market discount rate is 10 per cent, calculate the CSS over a period of 15 years.

In the present case, $n_l = 10$ years, $(1/r_d) = 4$ years and $n = 15$ years. Thus $n > n_l$ and $n > (1/r_d)$. Also $d = 0.10$, $d_l = 0.16$, $i_f = 0.04$ and $i_m = 0.05$. Thus $d \neq i_f$, $d \neq i_m$ and $d \neq d_l$. Consequently Eq. (9.12) is valid. The values of the other quantities are

$$C = \text{Rs. } 150\,000$$

$$f_l = 0.8$$

$$\text{Initial down payment} = \text{Rs. } (1 - 0.8) \times 150\,000 = \text{Rs. } 30\,000$$

$$\text{Loan} = \text{Rs. } 120\,000$$

$$c_f FE = \text{Rs. } 21\,000$$

$$M = \text{Rs. } 6600$$

$$r_t = 0.55$$

Substituting into Eq. (9.12), we get

$$\begin{aligned}
 \text{CSS} &= -30000 + \frac{21000}{(0.10 - 0.04)} \left[1 - \left(\frac{1.04}{1.10} \right)^{15} \right] \\
 &\quad - \frac{0.16 \times 120000}{0.10[1 - (1/1.16^{10})]} \left[1 - \frac{1}{1.16^{10}} \right] \\
 &\quad - \frac{6600}{(0.10 - 0.05)} \left[1 - \left(\frac{1.05}{1.10} \right)^{15} \right] \\
 &\quad + \frac{0.55 \times 0.25 \times 150000}{0.10} \left[1 - \frac{1}{1.10^4} \right] \\
 &= -30000 + 199104 - 152558 - 66306 + 65378 \\
 &= \text{Rs } 15618
 \end{aligned}$$

The result indicates that by investing in the given solar system, one would save Rs 15618 (in today's rupees) over a time period of 15 years. This is a reasonable saving.

It is instructive to calculate the value of CSS from one year to the next. This is done by substituting values of n ranging from 1 to 15 in Eq. (9.12) or its equivalent applicable form. The variation of CSS with the number of years is plotted in Fig. 9.1. It is seen that for the first four years, the CSS increases rapidly because of the high rate of depreciation and becomes positive at the end of four years. Thereafter till $n = 10$, it decreases because the fuel savings are offset by the loan repayment and annual expenditure on maintenance and other items. However, once the loan is paid off, the CSS increases rapidly again and attains the value of Rs 15618 after 15 years.

Example 9.2

An industrial solar energy system is installed at a cost of Rs 400000 for pre-heating boiler feed water. Assume:

- The cost of fuel saved in the first year is Rs 56000. This cost increases at the rate of 10 per cent in subsequent years.
- The entire initial cost of Rs 400000 is financed through a loan borrowed at the rate of 12.5 per cent.
- In order to encourage the use of solar energy, the Government permits depreciation at the high rate of 75 per cent in the first year and the remaining 25 per cent in the second year. The corresponding tax rate is 60 per cent.
- The annual repayment of the loan is not in equal instalments, but is adjusted every year to such a value that the annual solar savings are zero. This is done until the loan is fully paid.

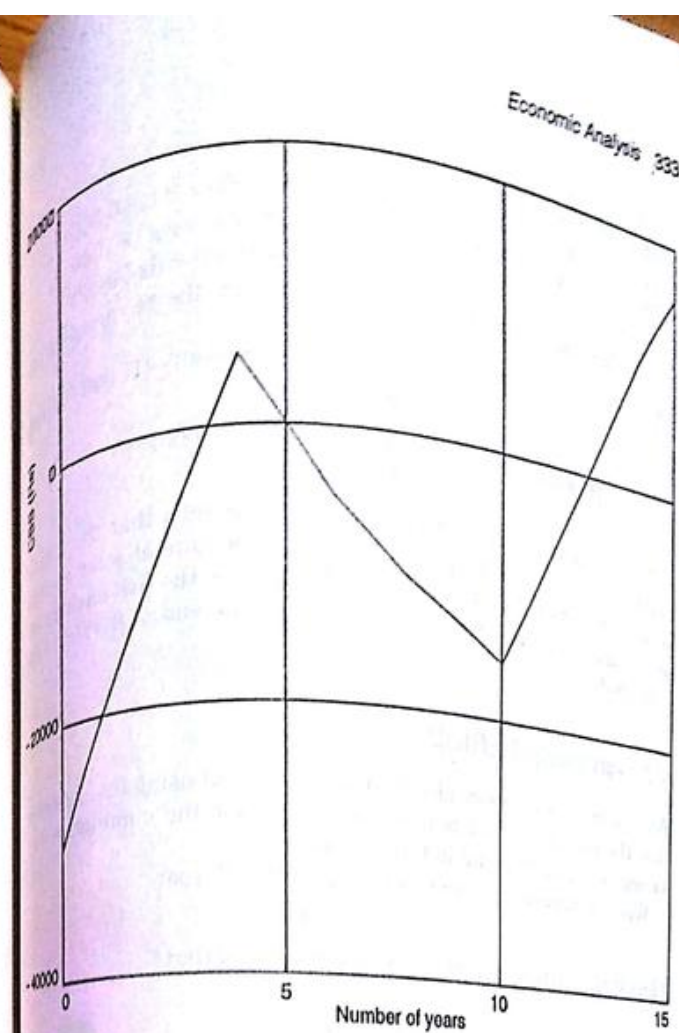


Fig. 9.1 Example 9.1—Variation of Cumulative Solar Savings with Time

(v) No tax saving is allowed on the interest component of the loan payment.

(vi) The annual expense associated with maintenance and other recurring items is Rs 11000 in the first year. This expense increases at the rate of 6 per cent every year.

Calculate the cumulative solar savings over a period of 8 years assuming a discount rate of 10 per cent.

Since the loan is not repaid in equal instalments and depreciation is not at a uniform rate, it is not possible to use Eq. (9.12). The present problem is more conveniently done on an year-wise basis by proceeding from one year to the next. Considering year 1,

Fuel saving	= Rs 56 000
Maintenance expenditure	= Rs 11 000
Depreciation	= Rs 0.75 × 400 000 = Rs 300 000
Tax savings on depreciation	= Rs 0.60 × 300 000 = Rs 180 000
Interest on loan	= Rs 0.125 × 400 000 = Rs 50 000
In order that the annual solar saving is zero, the payment on the loan	= Rs (56 000 + 180 000) - (11 000 + 50 000) = Rs 175 000 Thus loan remaining = Rs (400 000 - 175 000) = Rs 225 000

The calculations are given in Table 9.1. It is seen that the loan is entirely paid back after 5 years. Thereafter the annual solar savings is positive and the CSS increases rapidly because the fuel savings are much larger than the maintenance costs. At the end of 8 years, CSS = Rs 130 847.

9.7 PAYBACK PERIOD

We now derive expressions for the payback period using the definition that the payback period is the time needed for the cumulative fuel savings to equal the total initial investment.

Without discounting, the fuel saving in the j^{th} year

$$= c_f (1 + i_f)^{j-1} FE$$

Thus if the payback period = n_p years, it follows that

$$\sum_{j=1}^{n_p} c_f (1 + i_f)^{j-1} FE = C$$

$$\text{or } \frac{c_f FE}{i_f} [(1 + i_f)^{n_p} - 1] = C$$

$$\text{or } n_p = \ln \left(\frac{i_f C}{c_f FE} + 1 \right) \Bigg/ \ln (1 + i_f) \quad (9.13)$$

With discounting,

$$\sum_{j=1}^{n_p} c_f \frac{(1 + i_f)^{j-1}}{(1 + d)^j} FE = C$$

$$n_p = \ln \left[1 - \frac{C(d - i_f)}{c_f FE} \right] \Bigg/ \ln \left[\frac{1 + i_f}{1 + d} \right] \quad \text{for } i_f \neq d$$

and

$$n_p = \frac{C(1 + i_f)}{c_f FE} \quad \text{for } i_f = d \quad (9.14)$$

Table 9.1 Calculations of Example 9.2

Year	Fuel savings	Maintenance cost	Tax savings on depreciation	Interest on loan	Part payment on loan	Loan remaining	ASS	PVN of ASS	PVN of CSS
1	56 000	-11 000	180 000	-50 000	-175 000	225 000	0	0	0
2	61 600	-11 660	60 000	-28 125	-81 815	143 185	0	0	0
3	67 760	-12 360	-	-17 898	-37 502	105 683	0	0	0
4	74 536	-13 101	-	-13 210	-48 225	57 458	0	0	0
5	81 990	-13 887	-	-7 182	-57 458	0	3463	2150	2150
6	90 189	-14 720	-	-	-	75 469	42 600	44 750	
7	99 208	-15 603	-	-	-	83 605	42 903	87 653	
8	109 129	-16 539	-	-	-	92 590	43 194	130 847	

Example 9.3

Calculate the payback period, with and without discounting, for the data of the solar hot water system of Example 9.1.

Without discounting, from Eq. (9.13)

$$n_p = \ln \left(\frac{0.04 \times 150000}{21000} + 1 \right) / \ln (1 + 0.04)$$

= 6.4 years

With discounting, from Eq. (9.14)

$$n_p = \ln \left[1 - \frac{150000(0.10 - 0.04)}{21000} \right] / \ln \left[\frac{1 + 0.04}{1 + 0.10} \right]$$

= 10.0 years

Example 9.4

A solar pond is to be built in Delhi for supplying hot water at 70°C . The area of the pond is 5000 m^2 . The total initial cost of the pond, including associated heat exchange equipment is Rs 5 500 000. Assuming an annual collection efficiency of 20 per cent, calculate the energy collected in the pond in one year.

If a conventional system using oil is used for the same purpose, calculate the amount of oil required per year. Assume a heating value of 35 000 kJ/litre and an efficiency of 80 per cent for the equipment.

Calculate also the payback period for the pond assuming a fuel cost of Rs 5.50 per litre and a fuel inflation rate of 6 per cent. Assume a discount rate of 9 per cent.

From the radiation data available for Delhi (Appendix III, Table A3.1), global radiation incident on the pond surface in one year

$$\begin{aligned} &= (3.987 \times 31) + (5.001 \times 28) + (6.138 \times 31) + (6.935 \times 30) \\ &+ (7.287 \times 31) + (6.544 \times 30) + (5.334 \times 31) + (5.053 \times 31) \\ &+ (5.602 \times 30) + (5.355 \times 31) + (4.523 \times 30) + (3.843 \times 31) \\ &= 1995.1 \text{ kWh/m}^2 \end{aligned}$$

Thus energy collected in the pond in one year

$$\begin{aligned} &= 1995.1 \times 0.20 \times 3600 \times 5000 \\ &= 7.1824 \times 10^9 \text{ kJ} \end{aligned}$$

Equivalent amount of oil saved

$$\frac{7.1824 \times 10^9}{35000 \times 0.8} = 256513 \text{ litres}$$

Saving in the first year

$$\begin{aligned} &= \text{Rs } 256513 \times 5.50 \\ &= \text{Rs } 1410821 \end{aligned}$$

Economic Analysis 27

from Eq. (9.13), payback period without discounting

$$= \ln \left(\frac{0.06 \times 5500000}{1410821} + 1 \right) / \ln (1 + 0.06)$$

= 3.6 years.

from Eq. (9.14), payback period with discounting

$$= \ln \left[1 - \frac{5500000(0.09 - 0.06)}{1410821} \right] / \ln \left[\frac{1 + 0.06}{1 + 0.09} \right]$$

= 4.5 years

The values of payback period obtained for the solar pond of this example are less than the values obtained for the solar water heating system in Example 9.3. This will generally be the case and shows that the solar pond is an attractive proposition for providing process heat up to about 70°C in many parts of India.

9.8 CONCLUDING REMARKS

Two methods—one based on the solar savings approach and the other on the calculation of payback period—have been described in this chapter. Of these, the first obviously gives a more realistic cost-benefit picture and is to be preferred. This is because it takes account of many relevant factors like fuel costs, loan repayments, maintenance costs, tax deductions, inflation rates, etc. On the other hand, the commonly used definition of payback period takes a limited view and is concerned only with the fuel savings vis-a-vis the initial cost of the system.

PROBLEMS

1. Consider the special situations in which $d = i_f$, $d = i_m$ or $d = d_f$ and determine modified expressions for the second, fourth and fifth terms in Eq. (9.12).
2. Calculate the life cycle savings for the solar system of Example 9.1 if the life time of the system is taken to be 20 years and the resale value is Rs 42 000.
3. Use the data given for the solar hot water system of Example 9.1 and calculate the CSS for discount rates of 15, 17.5 and 20 per cent. Plot the values of CSS against the discount rate and hence obtain the rate of return on investment.
4. Consider the solar pond of Example 9.4. Assume that the pond has been built with an initial loan of Rs 4 000 000 to be paid back in equal annual instalments over a period of 8 years and that the interest on the loan is 10.5 per cent. The annual recurring expenditure on the pond is Rs 200 000 and this expense increases at the rate of 6 per cent per year. Depreciation is allowed at the rate of 30 per cent in the first 3 years and 10 per cent in the fourth year. Tax savings are permissible only on the depreciation and the income tax rate is 60 per cent. The company owning the pond is making profits and is liable for income tax. Calculate the present worth of the annual solar savings over a 5 year period.

